





ADA 036766

Department of AERONAUTICS and ASTRONAUTICS STANFORD UNIVERSITY

AR NO 501

SUDAAR NO. 501

THREE CONTRIBUTIONS TO MINIMUM WEIGHT STRUCTURAL OPTIMIZATION WITH DYNAMIC AND AEROELASTIC CONSTRAINTS

by

Solly A. Segenreich Erwin H. Johnson Paulo Rizzi



August 1976

This research was supported by the Air Force Office of Scientific Research under Contract No. AFOSR-74-2712 and by
National Aeronautics and Space Administration under Grant No. NASA 243

Approved for public release; distribution unlimited.

AIR FORCE OFFICE OF SCIENTIFIC RESEARCH (AFSC)

NOTICE OF TRANSMITTAL TO DDC

This technical report has been reviewed and is approved for public release IAW AFR 190-12 (7b).

A. D. BLOSE

Technical Information Officer

Department of Aeronautics and Astronautics Stanford University Stanford, California

THREE CONTRIBUTIONS TO MINIMUM WEIGHT STRUCTURAL OPTIMIZATION WITH DYNAMIC AND AEROELASTIC CONSTRAINTS

9 Joctural these ;
by

Solly And Segenreich,
Erwin H. Johnson
Paulo/Rizzi

(18) AFOSR) 19) TR-77-0127

SUDAAR 501

August 1976

VAF-AFOSR-2712-74

This research was supported by the Air Force Office of Scientific Research under Contract No. AFOSR-74-2712 and by National Aeronautics and Space Administration under Grant No. NASA 243.

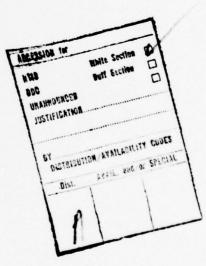
DISTRIBUTION STATEMENT A

Approved for public release; Distribution Unlimited

332560

GENERAL TABLE OF CONTENTS:

(General Preface	iii
77	Weight Optimization Under a Flutter Constraint	A-i
7	Optimization of Structures Undergoing Harmonic or Stochastic Excitation	B-i
>	The Optimization of Structures with Complex Constraints via a General Optimality Criteria Method	C-i



GENERAL PREFACE

Design of optimal structures with specified dynamic and aeroelastic performance has, for almost ten years, constituted a principal
interest of the small research group at Stanford led and advised by
former Assistant Professor Samuel C. McIntosh, Jr., and myself. The
products appear in some seven doctoral dissertations as well as in
numerous archival publications and contributions to the "sub-literature."
The last three of these dissertations have not hitherto been widely
circulated in extenso. Each contains several original discoveries, and
requests for copies are regularly received. Accordingly, it seems both
desirable and economical that they be combined and distributed as a
single large SUDAAR.

The investigations described herein are quite distinct and are the work of three individualists: Drs. Solly A. Segenreich, Erwin H. Johnson, and Paulo Rizzi. Except for minor proof corrections, their dissertations are reproduced without modification as parts A, B and C of this report. My decision to proceed in this manner accounts for the differences in format, notation, organization and style that a careful reader will detect. The curious scheme of page numbering is another consequence, for which no apology need be made.

These documents speak so well for themselves that no elaborate effort to tie them together seems necessary. They are linked by more than just close personal and professional bonds that existed among their authors and others in the group during their periods of gestation.

The reader will find certain continuities in both the subjects addressed and in the methods of problem formulation and optimal search. Segenreich and Johnson adapted search procedures that fall in the category known as mathematical programming. Building on the less efficient efforts of predecessors, Segenreich brought to a high degree of sophistication the process of practically designing the minimum-weight structure for a lifting surface whose flutter speed is constrained to exceed some prescribed value.

By contrast to constraints on structural-dynamic eigenvalues,

Johnson chose to examine designs where forced dynamic excitation constituted the environment to be satisfactorily withstood. His results

cover both simplified and more practical structures, as well as harmonic

and random sources of forcing. As a very rich diversion, he began the

analysis of a continuous, one-dimensional structure under sinusoidal

excitation at one end and constrained as to allowable stress amplitude.

This same problem was picked up by Rizzi, generalized and extended.

The focus of Rizzi's dissertation is the development and application of search methods based directly on properties of the optimal design — the so-called "optimality criteria." His examples include certain statically-loaded structures, but these were chosen to permit direct comparison with previous solutions by mathematical programming methods. The more demanding cases among those he successfully analyzed again involve flutter and forced dynamic constraints. Quite an elegant effort, his dissertation strikes me as a fitting final product of all our activity, which now goes temporarily into abeyance because of changing interests among my students.

One message appears repeatedly in this report: our expression of appreciation for continuing, enlightened research support from AFOSR and NASA. Without both of them, neither these contributions to knowledge nor the education achieved during their creation would have been possible.

Holt Ashley Professor

WEIGHT OPTIMIZATION UNDER FLUTTER CONSTRAINT

A DISSERTATION SUBMITTED TO THE DEPARTMENT OF AERONAUTICS AND ASTRONAUTICS AND THE COMMITTEE ON GRADUATE STUDIES OF STANFORD UNIVERSITY IN PARTIAL FULFILLMENT OF THE REQUIREMENTS FOR THE DEGREE OF DOCTOR OF PHILOSOPHY

by

Solly Andy Segenreich January 1975

ABSTRACT

A new approach to the weight minimization of wings subjected to a flutter speed constraint is the main topic of this dissertation.

The use of the flutter speed directly as a constraint is replaced by the vanishing of the damping factor condition. Besides the computational advantages of such an approach, especially in the treatment of compressible aerodynamic models, relatively simple optimality condition equations valid for both incompressible and compressible flows can be easily derived.

A second topic of the dissertation is the implementation of a hybrid structural optimization algorithm which attempts to combine the simplicity of the optimality criteria methods with the monotonic weight decrease behavior of the direct descent methods. Encouraging results are presented.

Finally, the viability of using assumed modes in static optimization is briefly discussed and one comparative example is given.

ACKNOWLEDGEMENTS

I wish to express my deepest gratitude to Dr. Samuel C. McIntosh, Jr., who acted as my advisor in the initial stages of the research and whose orientation throughout the whole work was invaluable.

I also wish to thank Professor Holt Ashley under whose leadership the work was concluded and with whom I shared most fruitful discussions, as well as Professor Douglas Wilde for his careful reading and constructive comments and Mr. Ranjan Vepa for his suggestions.

My gratitude is also directed to the Coordenação de Aperfeiçoamento de Pessoal de Nível Superior (CAPES-MEC) for their financial support through a scholarship and to the National Aeronautics and Space Administration (Contracts NGL-05-020-498 and NGL-05-020-243) for partially funding the computational work.

Finally, my appreciation is directed to my family and Stella for their continued encouragements as well as to Miss Andrea Dinsmore for typing the manuscript.

TABLE OF CONTENTS

LIST OF	ILLUS	STRATIONS	•	•			vi
LIST OF	SYMB	ols					ix
Chapter							Page
1	INTF	RODUCTION					1
2	А НУ	BRID OPTIMIZATION ALGORITHM					7
	2.1	Optimality Conditions and Direct Descent Methods					7
	2. 2 2. 3	Optimality Criteria Approach	е	•		•	8
		Recursive					16
	2.4	The Basic Weight Reduction Algorithm					19
	2.5	Numerical Examples	•	٠	٠	٠	23
3	OPT	IMIZATION UNDER FLUTTER CONSTRAINT					31
	3. 1	The V-g Method for Flutter Speed Determination					31
	3.2	The $g = 0$ Constraint Surface and the Optimality					
		Condition Equations					33
	3.3	Flutter Optimization Algorithm					39
	3.4	Numerical Examples					49
4	THE	VIABILITY OF MODAL ANALYSIS FOR STATIC					
	OPT	IMIZATION PROBLEMS					58
	4.1	Reduction of the Number of Degrees of Freedom					
		by Modal Decomposition					58
	4. 2	Numerical Example	•	•	•	•	61
5	CON	CLUSION					64
	5.1	Discussion of the Results					64
	5. 2	Summary					65
APPENDI	IX A:	NECESSARY AND SUFFICIENT CONDITIONS FOR					
	$\mathbf{M} = \mu$	β_1^2/β_2					67
APPENDI	IX B:	MINIMUM-GAGE OPTIMALITY CONDITION					69
REFERE	NCES						71

LIST OF ILLUSTRATIONS

Figure		P	age
1	Fixed-free rod in axial free-vibration		76
2	Plot of γ ratio as a function of the non-dimensional frequency		
	eta for the fixed-free rod		76
3	Plot of γ ratio as a function of the number of iterations for the		
	fixed-free rod		77
4	Comparison between the cross sectional area distribution of the		
	optimum rod as given by a ten-element approximation using the		
	hybrid algorithm and Turner's analytic solution (the analytic		
	solution is given by the smooth line)		77
5	Fixed-free bending torsion box in free-vibration		78
6	Optimization history diagram for the bending torsion box in		
	free-vibration		79
7	Fixed-free bending torsion box with an applied load		78
8	Optimization history diagram for the bending torsion box with		
	static compliance constraint		80
9	30-bar plane truss with applied loads		81
10	Optimization history diagram for the 30-bar truss with static		
	compliance constraint		82
11	V-g diagram for an aeroelastic system		83
12	Plot of critical speeds versus Mach number showing the		
	consistent matched point		83
13	Plot of U _i for each design variable i on a complex plane		
	when optimality condition is satisfied		84
14	V-g diagram. Regular type		84

Figure		Pa	ige
15	V-g diagram. Tangent type		85
16	V-g diagram. "Hump" type		85
17	Block-diagram of Step 1		40
18	Block diagram of Step 2		41
19	Variation of the reduced frequency along a branch		45
20	27-design variable rectangular wing. Dimensions		86
21	27-design variable rectangular wing. Design variable definition		87
22	27-design variable rectangular wing. Finite element sub-	•	87
23	Cross section of rectangular wing at station x, showing vertical displacement and rotational degrees of freedom	•	88
24	V-g diagram. Rectangular wing		89
25	V-g diagram. Rectangular wing		90
26	Optimization history for 27-design variable rectangular wing		
	under flutter constraint		91
27	90-design variable swept wing. Dimensions		92
28	90-design variable swept wing. Design variables definition		93
29	V-g diagram for initial design of swept wing. Mach = 0.50		95
30	V-g diagram for initial design of swept wing. Mach = 0.80		96
31	V-g diagram for initial design of swept wing. Mach = 0.86		97
32	V-g diagram for initial design of swept wing. Mach = 0.90		98
33	Diagram for matched flutter speed		99

Figure		Page
34	V-g diagrams for initial, intermediate and final designs	. 100
35	Optimization history diagram for 90-design variable swept	
	wing under flutter constraint	101

LIST OF SYMBOLS

[A]	aerodynamic matrix
[A']	aerodynamic matrix in modified form
A _i	cross sectional area of i-th element
a ij	coefficients of the 2-dimensional polynomial fit for the free-vibration modes
a _∞	freestream speed of sound
b	reference length
[C]	aeroelastic matrix, $[C] = [K]^{-1}([\Pi + [A])$
$C_i^{(\nu)}$	resizing factor associated with the i-th design variable at iteration $ \nu $
c _{ijr}	coefficient of $^{r-1}$ in the polynomial representation of $^{A}_{ij}$. $^{A}_{ij}$ are the elements of the aerodynamic matrix [A]
E	Young modulus
$\overset{\mathbf{F}}{\sim}$	external load vector
f	shape function associated with the generalized displacement $\textbf{q}_{i}^{}$
₹	external load vector in transformed coordinates
g	damping parameter
$\mathbf{g}_{j}(\overset{x)}{\sim})$	j-th inequality constraint function
$^{h}_{j}\overset{(x)}{\sim}$	j-th equality constraint function
[]]	inertia matrix associated with nonstructural mass
[1]	inertia matrix
$\bar{\Pi}_{i}$	inertia matrix associated with the i-th design variable
[Ī]	inertia matrix in transformed coordinate system
[K]	stiffness matrix
$[\overline{K}]_i$	stiffness matrix associated with the i-th design variable

k reduced frequency length of i-th element Li proportionality factor between the i-th design variable and the mass ℓ_i associated with it. $\ell_i = m_i/x_i$ 2 Lagrangian function mass associated with i-th design variable m, total mass of the design defined by the design vector x M(x)freestream Mach number p adjoint eigenvector 6 potential energy external pressure on the elastic system Q_{i} i-th generalized force \overline{Q}_{i} amplitude of i-th generalized force generalized displacements vector q q generalized displacement amplitudes vector [T] matrix of coordinate transformation $\{\overline{\mathbf{p}}\}^T \left(\frac{\partial [\mathbf{K}]}{\partial \mathbf{m_i}} - \omega^2 \ \frac{\partial [\mathbf{I}]}{\partial \mathbf{m_i}} \right) \{\overline{\mathbf{q}}\}$ $U_{\mathbf{i}}$ V airstream speed $V_{\mathbf{F}}$ flutter speed of the aeroelastic system given and constrained value of the flutter speed v_{FO} pseudo harmonic oscillation frequency r

stiffness matrix in transformed coordinate system

(K)

W

×

work

design variable vector

 $\hat{\mathbf{x}}$ optimum design variable vector

x, y, z cartesian coordinates

 α relaxation factor

 β non-dimensional frequency, $\beta = \omega L \sqrt{\frac{\rho}{E}}$

 $\beta_1 \qquad \qquad \sum_{i=1}^m \ (\frac{\partial h}{\partial m_i})_{\nu} m_i^{\nu}$

 β_2 $\sum_{i=1}^{m} \left(\frac{\partial h}{\partial m_i}\right)^2_{\nu} m_i^{\nu}$

 γ ratio between final and initial structural masses, $\gamma = \frac{M_f}{M_i}$

 $\lambda, \overline{\lambda}$ Lagrange multipliers

 μ dynamic pressure

ν Poisson's ratio or iteration number

 $ho_{f i}$ specific mass of element i

 $\rho_{\mathbf{a}}$ specific mass of air

arphi generalized displacements in the transformed coordinate system

 ω circular frequency

 Ω complex frequency, $\Omega = \frac{1+ig}{\omega^2}$

1. INTRODUCTION

Structural synthesis in general and structural optimization in particular are new fields in applied mechanics as opposed to structural analysis, which is relatively old. The principal reason for this is that synthesis is much more complex and actually encompasses the analysis. Structural design has always been guided by intuition and aesthetic factors, whereas structural analysis was used only to check whether the design would resist the prescribed loading system.

More recently, however, as weight and economic factors became increasingly important and as large computational facilities became accessible, new trends toward synthesis and optimization became apparent.

Surprisingly enough, one of the most important theoretical papers was written in 1904 by Michell (Ref. 1), who considered the optimum configuration of trusses. His work, which for a long time was not considered applicable in practice, is again receiving great attention as a basis for configuration optimization.

From the very beginning, the objective function in structural optimization has been mass (weight) or volume of the structure. This type of objective function has many attractive features. For instance, it is simple to understand, is almost directly related to the cost and is often linear in the design variables. The last feature renders the problem mathematically easier.

While the objective function is usually the mass, the constraints imposed on the behavior of the structure assume a variety of forms. Common constraint conditions involve limits placed upon static compliance (in the sense of work done by the external loading system), buckling loads, fundamental frequency of free-vibration, dynamic response, divergence and flutter speeds. References 2 and 3 present a thorough review of the work done in structural optimization before 1968.

Since the beginning of the 1960's, two important trends can be distinguished in structural optimization. One involved research into the basic principles governing optimum structures; references 4-10 exemplify this trend. The other

emphasized the investigation of methods and algorithms for optimizing realistic structures. Although the problems associated with the latter understanding were difficult, mathematical programming techniques led to highly encouraging results. References 11-16 exemplify the application of relatively standard concepts of mathematical programming to structural optimization. Although these techniques showed clearly how to handle practical structures, a weakness became apparent by the late 1960's. For configurations with increasingly many design variables, computation times grew so fast that 150 design variables were considered in 1970 as an upper limit for practicality.

In an effort to reduce computational effort and simultaneously accommodate a large number of design variables, optimality criteria methods, which represent a departure from the classical mathematical programming techniques, began to be investigated. The initial inspiration came from the fully-stressed design concept (Ref. 17). Later work by Berke (Refs. 18, 19), Gellatly (Refs. 20, 21) and Venkayya (Refs. 22, 23) brought out the full advantages of the method.

The central idea of optimality criteria methods is to perform the redesign step with the aid of simple recursion formulas, derived from properties of the final optimal solution, rather than to use more complicated and therefore time-consuming strategies. Kiusalaas (Refs. 24, 25) advanced the original concept by introducing a modified parameter-dependent resizing formula, with the aim of improving the rate of convergence of the redesign algorithm. In the field of optimization with constraints on aeroelastic eigenvalues, early work was published in the 1950's by MacDonough (Ref. 26) and Head (Ref. 27). More recently, the papers by Ashley and McIntosh (Refs. 28,5) applied newer concepts of structural optimization to the aeroelastic-constraint case.

Methods carried over from optimal control theory were used for aeroelastic optimization by Armand and Vitte (Ref. 29) and Weisshaar (Ref. 30). These methods have the advantage of being useful for finding exact solutions to simple problems, but they are not efficient for most practical structures, which are too complex for this type of approach. The first attempt to obtain a numerical solution for a flutter optimization of a fairly complex structure was made by Turner (Ref. 31).

His work was followed by that of Rudisill and Bhatia (Ref. 32); Fox, Miura and Rao (Ref. 33); Gwin and Taylor (Ref. 34).

A simplified optimality criterion method, which uses an approximate optimality condition as a basis for the derivation of a redesign formula, was developed in 1972 by Siegel (Ref. 35). A method that solves the optimality condition equations in an iterative way was presented by Pines and Newman (Ref. 36). Haftka, Starnes and Barton (Ref. 37) compare flutter optimization results using diverse methods. An assessment of the state-of-the-art as of mid-1974 was given by Stroud (Ref. 38).

The research that led to the present dissertation started in early 1973, with the aim of applying an optimality criterion method to the flutter problem using rigorous optimality conditions. It was believed that a successful application of this method might significantly improve the efficiency of aero-elastic optimization of large scale structures, while at the same time advancing the general state-of-the-art in this field. In an attempt to establish rigorous optimality conditions for a flutter constraint, a new concept of constraint evaluation was developed. Since most optimization algorithm work iteratively, several reanalysis steps are necessary as the optimization proceeds. In the case of flutter speed constraint, such reanalysis (i. e., the evaluation of the current flutter speed) calls for considerable computation and is therefore slow. One way to overcome this difficulty is to make an approximation in order to estimate the flutter speed of the modified structure from its value known for a previous design. Since several evaluations are needed, a significant error may build up during the process.

The concept proposed here involves the notion that there is no reason to use the flutter speed directly as the constraint. The same design problem can be properly posed by regarding the vanishing of the damping factor as the constraint, where the aerodynamic forces are calculated at an airstream velocity equal to the required flutter speed. Throughout the rest of the work, g will be viewed as the damping factor in a standard V-g analysis (Ref. 39). In other words, the fact that a given structure flutters at a given airstream velocity V_{FO} is

equivalent to the vanishing of $\, g \,$ when the aerodynamic matrix is calculated for this same $\, V_{\rm FO} \,$ and equal values of other governing parameters.

The primary advantage of the suggested approach is that it is not necessary to evaluate, either in an exact or in an approximate way, the flutter speed of each successive design. Rather, for the aerodynamic matrix calculated at a known and fixed speed V_{FO} , the current value of g is determined. This is an easy and exact calculation since g is nothing but the ratio of the imaginary to the real parts of the complex eigenvalue of the flutter eigensystem (Ref. 39). The aerodynamic matrix also depends on the fluttering frequency and this frequency will, in general, be changing as the optimization progresses. The way in which this change is accounted for will be fully discussed in Chapter 3. However, we may anticipate that this will be done by means of an auxiliary iterative procedure (in all examples one iteration per design step proved sufficiently accurate), where the initial point is given by the first-order approximation of a Taylor expansion in the frequency.

Another advantage of the present approach becomes apparent when flight Mach numbers are so high that compressible-flow aerodynamics must be used. In this case, the aerodynamic matrix depends on the Mach number, and the determination of the flutter speed derivatives as well as the evaluation of a current flutter speed must reflect this dependence. This added complication requires further computational effort besides introducing a new source for potential imprecisions. In case g is used as primary constraint, the dependence of the aerodynamic matrix on airstream velocity (and hence on Mach number) is completely elminiated along with all the troubles that this may cause.

Another cause for concern in the early stages of this research was associated with the convergence characteristics of the optimization procedure to be used. Although it is known that optimality criteria methods have demonstrated very good convergence when applied to static structural problems and even conservative dynamic problems, nothing can be said with respect to complex non-conservative situations like the flutter constraint. As a matter of

fact there is no formal proof of convergence even for static conservative problems with the remarkable exception of statically determinate structures, where convergence to the optimum structure is obtained in a single step. All that is known is the "experimental" fact that the method converges satisfactorily to what seems to be the desired optimum design.

Enforcing convergence characteristics for a general constraint was recognized as highly desirable. The following possible solution was proposed by the author: Instead of using a fixed recursion formula as a means for proceeding from one design step to the next, the formula should vary from iteration to iteration in such a way that monotomic weight decrease would be assured. In that way, if the problem were properly posed, convergence to a local stationary point would be enforced no matter how complex the constraint. In order to achieve this extra flexibility in the redesigning formula, a parameter-dependent formula was needed. The one developed by Kiusalaas (Ref. 24) was selected.

A numerical algorithm, called "hybrid" in the sense that it combines a monotonically decreasing characteristic of the objective function typical of "direct descent methods" with a simple resizing formula peculiar to the "optimality criterion" approach, was implemented.

In the second Chapter, the main concepts of optimality criteria methods and direct descent methods are briefly reviewed and contrasted. The hybrid method is then fully developed and numerical examples are given.

Fluter optimization is treated in Chapter 3. After a review of the V-g method rigorous optimality conditions are derived. The concept of $g\equiv 0$ constraint serves as basis for this derivation and later is tested with the hybrid algorithm of Chapter 2 in two numerical examples. The first is a 27-design variable rectangular wing (for incompressible aerodynamics). The second is a 90-design variable swept wing (for compressible aerodynamics).

The fourth chapter, which is relatively unrelated to the others, deals with the concept of using assumed modes in static optimization problems with the aim of reducing the order of the linear system one has to solve during the analysis step. An example is performed and the error in relation to the full order analysis is computed.

Concluding remarks as well as a discussion of the results are given in Chapter 5.

2. A HYBRID OPTIMIZATION ALGORITHM

2. 1 OPTIMALITY CONDITIONS AND DIRECT DESCENT METHODS

Most of the optimization problems that occur in structural design can be formulated in the following form:

Find Min
$$M(x)$$
 (2.1.1)

subject to,

where x is a (n×1) design variable vector.

The problem stated above is very general in its form and most of the actual problems solved up to now are, in fact, sub-problems of this general formulation.

The necessary conditions for local minimum are the well known Kuhn-Tucker conditions (Ref. 40) and are given by,

$$\nabla \mathbf{M}(\hat{\mathbf{x}}) + \sum_{j=1}^{m} \lambda_{j} \nabla h_{j}(\hat{\mathbf{x}}) + \sum_{j=1}^{k} \overline{\lambda_{j}} \nabla \mathbf{g}_{j}(\hat{\mathbf{x}}) = 0$$
 (2.1.3)

$$\overline{\lambda}_{j} \ge 0$$
 $(j = 1, 2, ... k)$ (2.1.4)

$$\sum_{j=1}^{k} \overline{\lambda}_{j} \mathbf{g}_{j}(\hat{\mathbf{x}}) = 0$$
 (2.1.5)

$$g_{j}(\hat{x}) \ge 0$$
 $(j = 1, 2, ... k)$ $(2.1.6)$

A and $\overline{\lambda}$ represent Lagrange multipliers and \hat{x} represents the point of minimum.

In order to illustrate the difficulties underlying such a minimization problem, let us consider the problem with equality constraints only, which is simpler than the one with inequality constraints. We immediately discover that

we face a n+m system of equations which in general are highly nonlinear and whose solution, even approximate, is very difficult to obtain. There are even more complicated situations, for instance, in the case of a flutter speed constraint, where we cannot even write the constraint equations in an analytic form.

To overcome this unhappy situation, certain researchers involved with optimization started to approach the problem from a different viewpoint. Instead of trying to locate the solution point by directly satisfying the necessary conditions, they proposed to locate this point by a step-by-step search. This search is terminated according to some criterion by which the final point is declared the solution.

Among the diverse search methods currently in use, the so-called "direct descent methods" are most popular. Their very common characteristic is that they proceed in a step-by-step search in such a way that the algorithm enforces a monotonically decreasing objective M(x). A broader discussion of these methods can be found in Refs. 40 and 41.

One of the primary advantages of all direct descent methods is their logical simplicity and the fact that they are convergent, in principle at least, by virtue of their own definition. On the other hand, however, the high dimensionality of any practical problem increases dramatically the amount of computation necessary to locate the optimum and is a strong limiting factor. Actually, multidimensional problems present an intrinsically more complicated structure to which Bellman (Ref. 42) refers as "the curse of dimensionality."

2.2 OPTIMALITY CRITERIA APPROACH

Unless the reader is deeply familiar with the history of structural optimization in recent years, he will be puzzled by the names "mathematical programming" and "optimality criteria" as they are used today in numerical structural optimization. His confusion will grow when he discovers that under the name mathematical programming technique he may find such different methods as feasible directions, penality functions, sequence of linear programs, etc. The confusion is legitimate and as so often happens in a quickly developing

discipline, the consistency of the nomenclature trails behind the scientific achievement itself.

The name "mathematical programming" had its origin in operation research. The word "programming" was used in the context of scheduling, since the initial task was to find efficient and even optimum schedules for operations in industrial organizations. In a short time, the concept of optimization grew as an independent and quite general discipline, and hence the name "mathematical programming" for any mathematically based optimization algorithm. In order to characterize better some specific problem, names like linear programming, integer programming, etc., were introduced. In any event, mathematical programming still retains its original meaning, and any optimization algorithm can be considered as being a mathematical programming algorithm.

The fruitful combination of mathematical programming techniques, already in an advanced state of development, and computer oriented structural analysis, mainly finite element methods, extended the concept of optimization to the field of structural design, and mathematical programming techniques became familiar as related to numerical procedures for finding optimum structures.

As was pointed out in Chapter 1, the initial enthusiasm caused by the straightforward application of existing optimization techniques in structural optimization began to decrease by the end of the 1960's due to the increase of computational effort as more realistic structures were considered. It is in this context that Berke (Ref. 18) suggested a new philosophical approach to the structural optimization problem by introducing the concept of redesigning by means of simple recursion formulas derived from the optimality conditions, which were known to work very well for fully-stressed designs. Berke argued that the lack of mathematical rigor and any proof of convergence was fully compensated for by the experimental fact that the method worked very well. Since the recursion formulas for the redesign are derived from the optimality conditions, it is natural that the name "optimality criteria" became associated with such an approach.

However, it is evident that optimality criteria methods are in a broad sense mathematical programming techniques, since after all they have the same goal, namely, the optimization of a structural system. At the same time as optimality criteria methods began to be studied, a parallel interest arose in discovering what physical properties distinguish optimum structures from others, and determining to what extent these properties serve as a basis for obtaining analytical solutions or as a basis for further development of numerical algorithms. In this context, the term "optimality criteria" also characterizes the work by Prager (Ref. 43). By means of a dual development, he has shown that when the structural problem is governed by a minimum principle, sufficient conditions for global optimality can be obtained. In addition to the theoretical implications of such results, they have the practical effect of ensuring that the designs obtained by a numerical algorithm are in fact global minima when such duality is valid.

For completeness, the optimality criteria recursion formulas will be rederived since they are used in our later development. The work of Berke (Ref. 18) is loosely followed for the derivation.

Consider a structural system having m design variables and subjected to a single constraint equation $h = h_0$. Note that h may have any general physical connotation, such as static compliance, fundamental free vibration frequency, flutter speed, etc.

The problem is to minimize the total mass $\,M$. Assuming that $\,m_{i}^{}$ is the mass associated with each design variable and that the design vector is given by $\,x$, the optimality conditions reduce to

$$\frac{\partial \mathbf{m}_{i}}{\partial \mathbf{x}_{i}} + \lambda \frac{\partial \mathbf{h}}{\partial \mathbf{x}_{i}} = 0 \qquad (i = 1, 2, \dots m) \qquad (2.2.1)$$

Equations (2.2.1) can be rewritten as,

$$\frac{\partial m_{i}}{\partial x_{i}} + \lambda (\frac{\partial h}{\partial m_{i}})(\frac{\partial m_{i}}{\partial x_{i}}) = 0$$

or

$$\frac{\partial \mathbf{h}}{\partial \mathbf{m}_{i}} = -\frac{1}{\lambda} \tag{i = 1, 2, ... m}$$

The main idea in the optimality criteria methods is the use of simple recursion formulas, based on the optimality conditions, for the resizing process.

In general, the resizing formula can be written as

$$\mathbf{x}_{i}^{(\nu+1)} = C_{i}^{(\nu)} \mathbf{x}_{i}^{(\nu)}$$
 (i = 1, 2, ... m) (2.2.3)

where $C_i^{(\nu)}$ is the resizing factor.

The problem is how to choose $C_i^{(\nu)}$. Berke has suggested using $-\lambda(\partial h/\partial m_i)$ as the resizing factor. His justification was that for a statically determinate structure, the optimum would be obtained in a single step. In order to show this, consider two sets of external loads F^P and F^Q . The problem is to minimize the mass of the structure subject to the condition that the work done by the loads F^P in the displacements caused by the loads F^Q remains constant.

Define S_i^Q and S_i^P as the generalized internal forces in member i due to the load systems Q and P respectively. The constraint equation can be written as

$$h = \sum_{i=1}^{m} \frac{s_{i}^{P} s_{i}^{Q}}{A_{i} E_{i}} L_{i}^{-h}$$
 (2. 2. 4)

where

 E_{i} = Young modulus of element i.

 A_{i} = cross sectional area of element i.

L; = length of element i.

 h_{o} = fixed value for the constraint

Differentiating equation (2.2.4) yields

$$\frac{\partial h}{\partial m_j} \; = \; \frac{\partial h}{\partial A_j} \; \frac{\partial A_j}{\partial m_j} \label{eq:deltah}$$

or

$$\frac{\partial h}{\partial m_{j}} = \frac{\partial A_{j}}{\partial m_{j}} \left[-\frac{s_{j}^{P} s_{j}^{Q}}{A_{j}^{2} E_{j}} L_{j} + \sum_{i=1}^{m} \frac{\frac{\partial s_{i}^{P}}{\partial A_{j}} s_{i}^{Q}}{A_{i}^{E} E_{i}} L_{i} + \sum_{i=1}^{m} \frac{s_{i}^{P} \frac{\partial s_{i}^{Q}}{\partial A_{j}}}{A_{i}^{E} E_{i}} L_{i} \right] (2.2.5)$$

Since the external loads are fixed, $\partial s_i^P/\partial A_j$ and $\partial s_i^Q/\partial A_j$ are self-equilibrating stress systems, and by virtue of the principle of virtual work, their work is zero in any virtual displacement. Hence, equation (2.2.5) is reduced to

$$\frac{\partial h}{\partial m_{j}} = -\frac{\partial A_{j}}{\partial m_{j}} \cdot \frac{S_{j}^{P} S_{j}^{Q}}{A_{j}^{2} E_{j}} L_{j}$$
(2. 2. 6)

We further assume that,

$$\mathbf{m}_{\mathbf{j}} = \mathbf{A}_{\mathbf{j}} \rho_{\mathbf{j}} \mathbf{L}_{\mathbf{j}} . \tag{2.2.7}$$

where $\rho_{\mathbf{j}}$ is the specific mass of element \mathbf{j} .

In view of eq. (2.2.7) we can write eq. (2.2.6) as

$$\frac{\partial h}{\partial m_{j}} = -\frac{S_{j}^{Q}S_{j}^{P}}{A_{j}^{2}\rho_{j}E_{j}}$$
(2. 2. 8)

Substituting $\partial h/\partial m_i$ into the optimality condition (2.2.2), we get

$$\frac{S_{j}^{P}S_{j}^{Q}}{A_{j}^{\rho}\rho_{j}E_{j}} = \frac{1}{\lambda}$$
 (j = 1, 2, ... m) (2. 2. 9)

Equation (2.2.9) states that the ratio of the energy in each element to its mass has a constant value for the optimum structure. Besides this interesting conclusion, we can actually obtain the unknown A from the relations (2.2.9) as follows.

$$A_{j} = \sqrt{\lambda \cdot \frac{s_{j}^{P} s_{j}^{Q}}{\rho_{j} E_{j}}}$$
(2. 2. 10)

The multiplier λ is determined in such a way that the constraint condition is satisfied:

$$h_{o} = \sum_{i=1}^{m} \frac{S_{i}^{P} S_{i}^{Q} L_{i}}{\sqrt{\lambda} \sqrt{\frac{S_{i}^{P} S_{i}^{Q}}{\rho_{i}^{E_{i}}}} E_{i}}$$
(2. 2. 11)

Hence,

$$A_{j} = \left(\frac{1}{h_{o}} \sum_{i=1}^{m} \frac{\sqrt{S_{i}^{P} S_{i}^{Q} \rho_{i}}}{\sqrt{E_{j}}} L_{i}\right) \sqrt{\frac{S_{j}^{P} S_{j}^{Q}}{\rho_{j}^{E} j}}$$
(2. 2. 12)

If the system is statically determinate, S_j^P and S_j^Q do not depend on the areas A_j and can be obtained from static considerations, so that relations (2.2.12) give the optimum structure at once.

In order to see how this concept is extended to statically indeterminate structures, recall eq. (2.2.10). In order to emphasize that the internal loads correspond to the unknown structure, we write

$$A_{j}^{(\nu+1)} = \sqrt{\lambda} \sqrt{\frac{(S_{j}^{P} S_{j}^{Q})_{\nu+1}}{\rho_{j}^{E}_{j}}}$$
 (2. 2. 13)

where, again, λ is such that the design $(\nu+1)$ meets the constraint condition. We can rewrite equations (2.2.13) as

$$A_{j}^{(\nu+1)} = \sqrt{\lambda} \sqrt{\frac{(S_{j}^{P} S_{j}^{Q})_{\nu+1}}{A_{j}^{(\nu)} \rho_{j} E_{j}}} A_{j}^{(\nu)}$$
(2. 2. 14)

We recognize that if there is no internal force redistribution, equation (2.2.14) can be written as

$$A_{j}^{(\nu+1)} = \sqrt{-\lambda (\frac{\partial h}{\partial m_{j}})_{\nu}} A_{j}^{(\nu)}$$
(2. 2. 15)

Berke suggested that this equation could be used as a recursive resizing formula for statically indeterminate structures that would lead to the optimum structure when applied iteratively.

For relation (2. 2. 15) be meaningful as a recursion formula, it is important to show that if at the step ν we have the optimum structure, the structure will not change when the recursion formula is applied.

The multiplier λ is given from eq. (2.2.11) as

$$\sqrt{\lambda} = \frac{1}{h_0} \sum_{i=1}^{m} \sqrt{\frac{(S_i^P S_i^Q)_{\nu} \rho_i}{E_i}} L_i$$

or

$$\sqrt{\lambda} = \frac{1}{h_o} \sum_{i=1}^{m} \left(\frac{\sqrt{(S_i^P S_i^Q)}_{\nu}}{A_i \sqrt{\rho_i E_i}} \right) A_i \rho_i L_i$$
(2. 2. 16)

For the optimum structure, the quantity in parentheses [which is $-(\partial h/\partial m_1)$] is known to be constant. Therefore, we can write (2.2.16) as

$$\lambda = \frac{M^2}{h_0^2} \frac{(S_j^P S_j^Q)_{\nu}}{A_i^2 \rho_j E_j}$$
 (2. 2. 17)

Substituting (2. 2. 17) into the recursion formula (2. 2. 15), we have

$$A_{j}^{(\nu+1)} = \left[\frac{M}{h_{o}} \cdot \frac{(s_{j}^{P} s_{j}^{Q})_{\nu}}{A_{j}^{2} \rho_{j} E_{j}} \right] A_{j}^{(\nu)}$$
(2. 2. 18)

Recalling that

$$h_{o} = \sum_{i=1}^{m} \frac{(S_{i}^{P} S_{i}^{Q})_{\nu}}{A_{i}^{E} i} L_{i}$$

or

$$h_{o} = \sum_{i=1}^{m} \left[\frac{(S_{i}^{P} S_{i}^{Q})_{\nu}}{A_{i}^{2} E_{i} \rho_{i}} \right] A_{i}^{\rho}{}_{i} L_{i}$$
 (2. 2. 19)

and, again, using the fact that for the optimum structure the term in the brackets is constant, we have

$$\mathbf{h}_{\mathbf{O}} = \frac{(\mathbf{S}_{\mathbf{j}}^{\mathbf{P}} \mathbf{S}_{\mathbf{j}}^{\mathbf{Q}})_{\nu}}{\mathbf{A}_{\mathbf{j}}^{2} \mathbf{E}_{\mathbf{j}} \rho_{\mathbf{j}}} \cdot \mathbf{M}$$
 (2. 2. 20)

Combining eqs. (2.2.20) and (2.2.18) we finally obtain

$$A_{j}^{(\nu+1)} = A_{j}^{(\nu)}$$

Although the recursion formula is only approximate, as has been seen, it is known to converge quite rapidly.

Venkayya (Refs. 22 and 23) has used a similar recursion formula and extended its use to different types of constraints.

In order to obtain greater flexibility, Kiusalaas (Ref. 24) proposed a recursion formula containing a relaxation factor α :

$$C_{i}^{(\nu)} = \alpha + (1-\alpha)\lambda^{(\nu)} \left(\frac{\partial h}{\partial m_{i}}\right)_{\nu}$$
 (2. 2. 21)

The idea here is that a good choice of $\,\alpha\,$ could improve the convergence. Again, for the optimum structure all the derivatives $\,\partial h/\partial m_{\hat{i}}\,$ are equal and have the value $\,1/\lambda\,$. Therefore, for the optimum structure

$$C_i^{(\nu)} = \alpha + (1 - \alpha) = 1$$
 (2. 2. 22)

which implies that for the optimum structure, the design remains unchanged no matter what α is chosen.

As has been shown, optimality criteria methods have the advantage of redesigning by means of simple recursion formulas and their name comes from the fact that they are derived directly from the optimality conditions. Their major weakness is that a rigorous proof of convergence does not exist.

The concept of changing dynamically the resursion formula from step to step in order to achieve a monotonic weight decrease is introduced next in an attempt to overcome this weakness. The hybrid character is related to the combination of the concept of monotonic decrease and the concept of redesigning by means of recursion formulas derived from the optimality conditions.

2.3 A MODIFICATION OF THE OPTIMALITY CRITERIA RECURSIVE RELATION

Consider the problem of minimizing the mass M of a structural system subject to a constraint $h = h_0$, where h is any type of behavioral constraint (compliance, natural frequency, buckling load, etc.).

Let

$$M = \sum_{i=1}^{m} m_{i}$$
 (2.3.1)

and consider the iterative resizing process given by

$$x_i^{(\nu+1)} = C_i^{(\nu)} x_i^{(\nu)}$$
 (2.3.2)

Now, we take for the resizing factor the same expression adopted by Kiusalaas (Ref. 24):

$$C_{i}^{(\nu)} = \alpha + (1-\alpha)\lambda^{(\nu)} \left(\frac{\partial \mathbf{h}}{\partial \mathbf{m}_{i}}\right)_{\nu}$$
 (2.3.3)

We further assume (although it is not essential) that the mass m_i associated with each design variable is linearly related to the design variable itself. So,

$$\mathbf{m}_{\mathbf{i}} = \mathbf{x}_{\mathbf{i}} \mathcal{L}_{\mathbf{i}} \tag{2.3.4}$$

where ℓ_i is constant.

From eq. (2.3.2) we have,

$$\mathbf{x}_{i}^{(\nu+1)} - \mathbf{x}_{i}^{(\nu)} = \Delta \mathbf{x}_{i} = [C_{i}^{(\nu)} - 1] \mathbf{x}_{i}^{(\nu)}$$
 (2. 3. 5)

and in view of eq. (2.3.4)

$$\Delta m_{i} = [C_{i}^{(\nu)} - 1] m_{i}^{(\nu)}$$
 (2. 3. 6)

Substituting for $C_i^{(\nu)}$ in (2.3,6), we obtain

$$\Delta m_{i} = [\alpha - 1 - (\alpha - 1)\lambda^{(\nu)} (\frac{\partial h}{\partial m_{i}})_{\nu}] m_{i}^{(\nu)}$$

or

$$\Delta m_{i} = (\alpha - 1) \left[1 - \lambda^{(\nu)} \left(\frac{\partial h}{\partial m_{i}} \right)_{\nu} \right] m_{i}^{(\nu)}$$
(2. 3. 7)

The value of $\lambda^{(\nu)}$ is chosen, at each step, so that the new design still satisfies the constraint. To first order, the change in the constraint is

$$\mathbf{h}^{(\nu+1)} - \mathbf{h}^{(\nu)} = \sum_{i=1}^{m} \left(\frac{\partial \mathbf{h}}{\partial \mathbf{m}_{i}} \right) \Delta \mathbf{m}_{i}$$
 (2.3.8)

If we substitute the values for Δm_i as given by relation (2.3.7) we obtain

$$\mathbf{h}^{(\nu+1)} - \mathbf{h}^{(\nu)} = (\alpha - 1) \sum_{i=1}^{m} \left[1 - \lambda^{(\nu)} \left(\frac{\partial \mathbf{h}}{\partial \mathbf{m}_{i}} \right)_{\nu} \right] \left(\frac{\partial \mathbf{h}}{\partial \mathbf{m}_{i}} \right)_{\nu} \mathbf{m}_{i}^{(\nu)}$$
(2.3.9)

Solving for $\lambda^{(\nu)}$ from eq. (2.3.9) yields

$$\lambda^{(\nu)} = \frac{\sum_{i=1}^{m} \left(\frac{\partial h}{\partial m_{i}}\right)_{\nu} m_{i}^{(\nu)} - \frac{h^{(\nu+1)} - h^{(\nu)}}{\alpha - 1}}{\sum_{i=1}^{m} \left(\frac{\partial h}{\partial m_{i}}\right)_{\nu}^{2} m_{i}^{(\nu)}}$$
(2. 3. 10)

Since we want the design $\nu+1$ to be as close to the constraint as possible, and since $h^{(\nu)}$ will in general be different from h_0 because of the first order approximation used above, we make $h^{(\nu+1)} = h_0$ and rewrite relation (2.3.11) as

$$\lambda^{(\nu)} = \frac{\sum_{i=1}^{m} \left(\frac{\partial h}{\partial m_{i}}\right)_{\nu} m_{i}^{(\nu)} - \frac{h_{o} - h^{(\nu)}}{\alpha - 1}}{\sum_{i=1}^{m} \left(\frac{\partial h}{\partial m_{i}}\right)_{\nu}^{2} m_{i}^{(\nu)}}$$
(2. 3. 11)

Substituting this relation for $\lambda^{(\nu)}$ in eq. (2.3.7), we have

$$\Delta m_{i} = (\alpha-1) \left[1 - \frac{\sum_{i=1}^{m} (\frac{\partial h}{\partial m_{i}})_{\nu} m_{i}^{(\nu)} - \frac{h_{o} - h^{(\nu)}}{\alpha-1}}{\sum_{i=1}^{m} (\frac{\partial h}{\partial m_{i}})_{\nu} m_{i}^{(\nu)}} (\frac{\partial h}{\partial m_{i}})_{\nu} \right] m_{i}^{(\nu)}$$
(2. 3. 12)

In order to simplify the notation, we write

$$\beta_1 = \sum_{i=1}^m \left(\frac{\partial h}{\partial m_i}\right)_{\nu} m_i^{(\nu)}$$

$$\beta_2 = \sum_{i=1}^{m} \left(\frac{\partial h}{\partial m_i}\right)^2_{\nu} m_i^{(\nu)}$$

The total change of mass of the system will be

$$\Delta \mathbf{M} = \sum_{i=1}^{m} \Delta \mathbf{m}_{i} \tag{2.3.13}$$

or,

$$\Delta M = (\alpha - 1)M - \frac{(\alpha - 1)\beta_1^2 - [h_0 - h^{(\nu)}]\beta_1}{\beta_2}$$
 (2. 3. 14)

Solving eq. (2.3.14) for α gives

$$\alpha = 1 + \frac{\Delta M - \frac{[h_o - h^{(\nu)}]\beta_1}{\beta_2}}{M - \frac{\beta_1^2}{\beta_2}}$$
(2. 3. 15)

Relation (2.3.15) is of central importance in our development. It relates the overall change in mass in one iteration to the value of the parameter α . We can use this fact to our advantage by choosing α in each iteration in such a way that it will cause a certain reduction of mass.

Since at the beginning of each iteration $h^{(\nu)}$, M, β_1 and β_2 are fixed and known, we see from eq. (2.3.15) that α depends linear and uniquely on the

intended mass reduction ΔM and can always be determined with the only exception when $M=(\beta_1^2/\beta_2)$. Recalling the definition of β_1 and β_2 and taking into account that all m_1 are non-negative, it is seen (Appendix A) that $M=(\beta_1^2/\beta_2)$ if and only if all the constraint derivatives are equal. But that is exactly the stationary condition so that we may state that unless we are at a stationary point, given an intended ΔM , the parameter α can be obtained from eq. (2.3.15).

It now becomes clear that a good strategy would be to use the redesigning formula (2.3.2), with α being dynamically updated at each iteration in order to achieve some mass reduction. In that way, we can enforce a monotomic mass decrease and consequently ensure convergence independently of the nature of the constraint. Note that the continuous updating of α is equivalent to a feedback procedure, since α is controlled by the intended output ΔM .

Looking at expression (2.3.15), one could argue that any amount of mass reduction could be achieved in a single step and therefore that some inconsistency does exist. The inconsistency is removed by recalling that expression (2.3.15) was derived by assuming a first-order approximation for $h_0^-h^{(\nu)}$. This in turn implies that (2.3.15) is only valid for relatively small Δm_1^- and hence the overall mass reduction at each step cannot be made to large.

2.4 THE BASIC WEIGHT REDUCTION ALGORITHM

We present in this section the basic logic and flow chart of the weight reduction algorithm based on the dynamic updating concept developed in Section 2.3.

Besides the primary equality constraint, the algorithm also handles minimum-gage constraints by holding a design variable fixed at its minimum value if this condition is reached during the optimization.

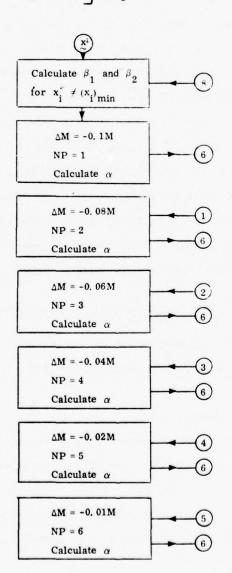
As a result of this simple way of treating minimum-gage constraints, the final design may not be optimum in the sense that Kuhn-Tucker conditions may not be satisfied for some design variables that reached their minimum-gage constraints

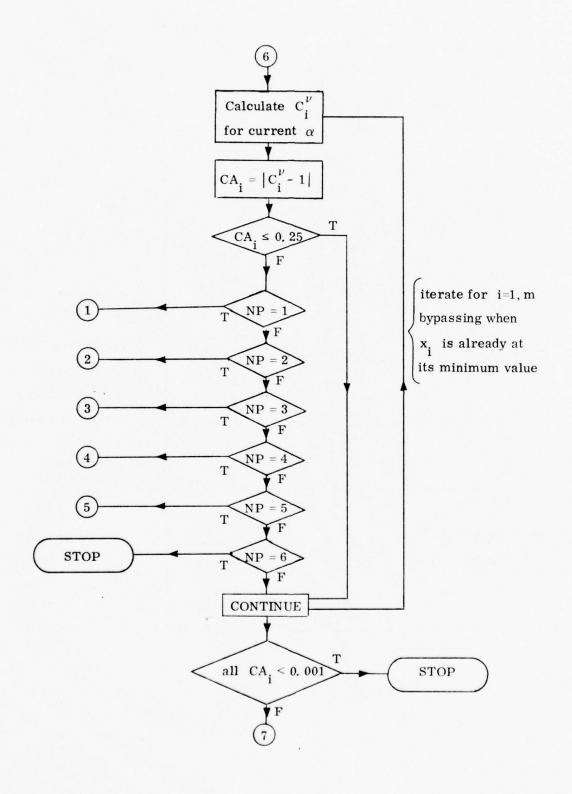
during the design process. Described in Appendix B is the action that may be taken when these conditions are not satisfied.

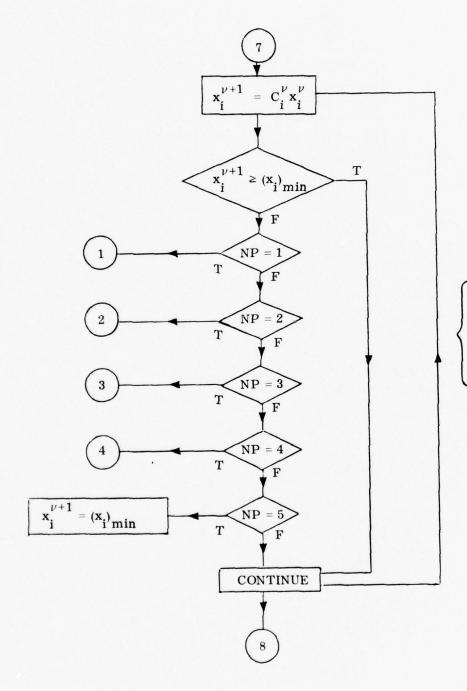
In the flow chart presented below, the nomenclature is the same as in the previous discussion, and α is calculated according to expression (2.3.15).

From Eqs. (2.3.11) and (2.3.3) $C_{i}^{(\nu)}$ is given by

$$C_{i}^{(\nu)} = \alpha + \left[\frac{(h_{o}^{-h^{\nu}}) - (\alpha - 1)\beta_{1}}{\beta_{2}}\right] \left(\frac{\partial h}{\partial m_{i}}\right)_{\nu}$$
(2. 4. 1)







iterate for i=1, m
bypassing when
x
i is already at
its minimum value

In summary, the algorithm works by choosing α at each step in such a way that a predetermined proportion (10%, 8%, 6%, 4%, 2%, or 1%) of the total current mass is reduced. It uses the highest possible reduction that will not cause any design variable to change by more than 25% or to fall below its minimum-gage value.

Two possible situations arise:

- i) A % reduction is not possible without at least one design variable dropping below its minimum value. In this case, the minimum value is assigned to this variable and a new iteration starts.
- ii) A 1% reduction is not possible without at least one design variable having to change more than 10%. In this case the procedure stops and the last design is declared optimum within the present framework.

2.5 NUMERICAL EXAMPLES

The four numerical examples that are presented in this section were selected from among the problems used in the debugging and development stages of the algorithm. Because of this, mass-reduction sequences different from the one shown in the flow chart have been used. The actual sequences are given with the code explained below:

$$[10. \ 0, \ 8. \ 0, \ 6. \ 0, \ 4. \ 0, \ 2. \ 0, \ 1. \ 0 - 10. \ 0]$$

 $\Delta M = 10.0\% \text{ of total } M$

$$\Delta M = 8.0\%$$
 of total M

$$\Delta M = 6.0\%$$
 of total M

$$\Delta M = 4.0\%$$
 of total M

$$\Delta M = 2.0\%$$
 of total M

$$\Delta M = 1.0\%$$
 of total M

Maximum variation of a design variable in a single step = 10% of its current value.

(a) Rod in Axial Free-Vibration (Fig. 1)

Sequence = [5. 0, 4. 0, 3. 0, 2. 0, 1. 0, 0. 5, 0. 3, 0. 2, 0. 1-5. 0]

Number of design variables = 4

Number of degrees of freedom = 4 (nodal).

The stiffness matrix is given by

[K] =
$$\sum_{i=1}^{4} A_i[\overline{K}]_i$$
 (2.5.1)

and the inertia matrix by

$$[I] = \sum_{i=1}^{4} A_{i}[\overline{I}]_{i} + [\overline{I}]_{tip}$$
 (2. 5. 2)

where

$$\overline{\left[K\right]}_{2} = \begin{bmatrix} 0 & 0 & 0 & 0 \\ 0 & 1 & -1 & 0 \\ 0 & -1 & 1 & 0 \\ 0 & 0 & 0 & 0 \end{bmatrix} \underbrace{^{E}_{2}}_{L_{2}} \qquad \overline{\left[I\right]}_{2} = \begin{bmatrix} 0 & 0 & 0 & 0 \\ 0 & 2 & 1 & 0 \\ 0 & 1 & 2 & 0 \\ 0 & 0 & 0 & 0 \end{bmatrix} \underbrace{^{\rho_{2}L_{2}}_{2}}_{6}$$

$$L_{i} = 1.0$$

$$(i = 1, 2, 3, 4)$$

$$\rho_i = 0.6$$

$$(i = 1, 2, 3, 4)$$

$$E_{i} = 1000.0$$

$$(i = 1, 2, 3, 4)$$

The free-vibration frequencies are given by the solution of the eigensystem

$$[K] \{\overline{\mathbf{q}}\} = \omega^2 [\eta \{\overline{\mathbf{q}}\}]$$

(2.5.3)

Rewrite eq. (2.5.3) as

$$([K] - \omega^2[\Pi)\{\overline{q}\} = 0$$

(2.5.4)

Differentiating eq. (2.5.4) with respect to m, one has

$$\left(\frac{\partial}{\partial m_i} [K] - \frac{\partial \omega^2}{\partial m_i} [I] - \omega^2 \frac{\partial [I]}{\partial m_i}\right) \{\overline{q}\} + ([K] - \omega^2 [I]) \{\frac{\partial \overline{q}}{\partial m_i}\} = 0 \qquad (2.5.5)$$

By pre-multiplying eq. (2.5.5) by $\left\{\overline{\mathbf{q}}\right\}^{\mathrm{T}}$ and taking into account that [K] and [I] are symmetric matrices, the second term of eq. (2.5.5) vanishes and we find for the constraint derivatives

$$\frac{\partial \omega^{2}}{\partial \mathbf{m}_{i}} = \frac{\{\overline{\mathbf{q}}\}^{\mathrm{T}} \left(\frac{\partial}{\partial \mathbf{m}_{i}} [K] - \omega^{2} \frac{\partial}{\partial \mathbf{m}_{i}} [I]\right) \{\overline{\mathbf{q}}\}}{\{\overline{\mathbf{q}}\}^{\mathrm{T}} [I] \{\mathbf{q}\}}$$
(2. 5. 6)

Since $\rho_i L_i$ is the same for all four design variables we can substitute $\partial \omega^2/\partial A_i$ for $\partial \omega^2/\partial m_i$ in the redesigning formulas. Using expressions (2, 5, 1) and (2, 5, 2) to evaluate derivatives of [K] and [I], we finally have

$$\frac{\partial \omega^{2}}{\partial \mathbf{A}_{i}} = \frac{\{\overline{\mathbf{q}}\}^{T}([\overline{\mathbf{K}}]_{i} - \omega^{2}[\overline{\mathbf{I}}]_{i})\{\overline{\mathbf{q}}\}}{\{\overline{\mathbf{q}}\}^{T}[\mathbf{I}]\{\overline{\mathbf{q}}\}}$$
(2. 5. 7)

In order to compare the numerical results with known analytical solution, we define two non-dimensional parameters

$$\beta = \omega L \sqrt{\frac{\rho}{E}}$$
 (2.5.8)

$$\gamma = \frac{M_f}{M_i} \tag{2.5.9}$$

where \mathbf{M}_{f} and \mathbf{M}_{i} are respectively the final and initial total masses of the structural system. In order to be able to vary the fundamental frequency and also to avoid meaningless optimal solutions, a controlling tip mass was introduced.

The optimization results are shown below:

Table 1. Results for Axial Rod Optimization Under Fundamental Free-Vibration Frequency Constraint.

m _{tip}	ω	β	γ	number of iterations
5. 00	6.55	. 642	.982	3
3.00	8. 05	. 791	.958	4
1.00	11.52	1, 132	. 809	9
0.50	13. 33	1, 309	. 620	16
0. 25	14.61	1, 430	. 409	23

Figure 2 shows a plot of γ versus β for the example above and it compares very well with the analytical result by Turner (Ref. 9). Figure 3 shows a plot of γ versus the number of iterations. Its roughly linear behavior pattern reveals that as the starting point becomes more distant from the optimum, the number of iterations grows in a proportional way which is a positive quality of the procedure.

In a later step, in order to obtain a better graphical comparison between the optimum thickness distribution given by the algorithm and the analytic solution, the rod was divided into ten elements and Fig. 4 shows this comparison.

(b) Built-Up Bending-Torsion Box in Free-Vibration (Fig. 5)

Sequence = [10.0, 8.0, 6.0, 4.0, 2.0, 1.0, 0.6, 0.4, 0.2-25.0].

Number of design variables = 27

Number of degrees of freedom = 72 (nodal)

A full description of the dimensions, structural constants, finite element definition, design variable definition, etc. is given in Chapter 3 where this same structure is optimized for the flutter speed constraint.

In the optimization procedure, only the first nine free vibration modes of the initial structure were retained as modal degrees of freedom.

The final design has all the design variables at their minimum values with the following exceptions:

 $t_{\rm r}(7) = 0.02645$ in.

 $t_{\mathbf{f}}(8) = 0.02645 \text{ in.}$

Additional optimization results for this problem are given below:

 $\omega_i = 48.8 \text{ rd/sec}$ (initial design)

 $\omega_{\mathbf{f}} = 48.8 \text{ rd/sec}$ (final design)

number of iterations = 29

 $M_i = 195 lb$

 $M_f = 49 lb$

CPU time per iteration = 0.075 min/iter.

The final design satisfies Kuhn-Tucker conditions in the sense of Appendix B. Figure 6 shows a plot of the optimization history and reveals that the optimum was basically reached after only thirteen iterations. Further comments on the results will be given in the final chapter.

(c) Built-Up Bending Torsion Box for Static Compliance (Fig. 7)

Sequence = [10.0, 8.0, 6.0, 4.0, 2.0, 1.0-25.0]

Number of design variables = 27

Number of degrees of freedom = 72

The static compliance constraint is enforced by requiring that the work done by the applied force is constant.

The initial structure is the same as in the previous example.

The final design has all the design variables at their minimum values with the following exceptions:

$$t_f(7) = 0.147$$
 in.

$$t_{f}(8) = 0.410 in.$$

$$t_{c}(9) = 0.091 \text{ in.}$$

$$t_{c}(10) = 0.197$$
 in.

$$t_f(11) = 0.021$$
 in.

$$t_f(12) = 0.048$$
 in.

Additional results are give below:

$$(Comp.)_f = 3571 lb-in$$
 (final design)

Number of iterations = 24

 $M_i = 195 lb$

 $M_f = 69 lb$

CPU time per iteration = 0.042 min/iter.

The final design satisfies Kuhn-Tucker condition in the sense of Appendix B. Figure 8 shows the plot of the optimization history and reveals that the optimum was practically reached in 14 iterations.

(d) 30-Bar Plane Truss (Fig. 9)

Sequence = [10.0, 8.0, 6.0, 4.0, 2.0, 1.0, 0.6, 0.4, 0.2-25.0]

Number of design variables = 30

Number of degrees of freedom = 24

 $E = 10.0 \times 10^6 \text{ psi}$

The optimization results are given below:

Table 2. Cross sectional areas of the design variables.

Design Variable	$t_{i}^{(in^2)}$	t _f (in ²)	t _{min} (in ²)
1	1.000	1.806	0.600
2	1.000	1.260	0.600
3	1.000	0.800	0.600
4	1.000	0.600	0.600
5	1.000	0.600	0.600
6	1.000	0.600	0.600
7	1.000	1.862	0.600
8	1.000	1.287	0.600
9	1.000	0.831	0.600
10	1.000	0.600	0.600
11	1.000	0.600	0.600
12	1.000	0.600	0.600
13	1.000	0.622	0.600
14	1.000	0.600	0.600
15	1.000	0.600	0,600
16	1,000	0,600	0.600
17	1.000	0.600	0.600

Table 2 - continued

Design Variable	t _i (in ²)	t _f (in ²)	t _{min} (in ²)	
18	1, 000	0,600	0,600	
19	1, 000	0.600	0.600	
20	1, 000	0.600	0.600	
21	1, 000	0.600	0.600	
22	1,000	0.600	0.600	
23	1,000	0.600	0.600	
24	1,000	0.600	0.600	
25	1.000	0.747	0.600	
26	1,000	0.600	0.600	
27	1,000	0.600	0.600	
28	1.000	0.600	0.600	
29	1.000	0.600	0.600	
30	1.000	0.600	0.600	

 $(Comp)_i = 2478 lb-in$

(initial design)

 $(Comp)_f = 2478 lb-in$

(final design)

Number of iterations = 54

 $M_i = 308 lb$

 $M_f = 212 lb$

CPU time per iteration = 0.011 min/iter.

The static compliance is enforced in the same sense as in the previous example. The final design satisfies Kuhn-Tucker conditions and Fig. 10, showing the optimization history, reveals that the optimum was basically reached in 4 iterations which is an excellent result in view of the change in total mass.

The relatively high number of iterations used to reach the final structure was due to a minor error in the computer code at this time. Its only effect was to slow convergence; the final design was unaffected.

3. OPTIMIZATION UNDER FLUTTER CONSTRAINT

3.1 THE V-g METHOD FOR FLUTTER SPEED DETERMINATION

For completeness we present the V-g method for flutter speed determination although it is standard and well known. A deeper discussion and additional references are given in Ref. 39.

Consider an aeroelastic system with a finite number n of degrees of freedom. We say that the system is "fluttering" if it presents steady state harmonic oscillations. Namely

$$\{\mathbf{q}\} \approx \operatorname{Re}\left\{\{\overline{\mathbf{q}}\}e^{i\omega t}\right\} \tag{3.1.1}$$

where

{q} = vector of generalized displacements

 $\{\overline{q}\}\ \approx\ vector\ of\ complex\ amplitudes$

It can be shown (39) that the linearized equations of motion are given in matrix form as

$$([\Pi - \Omega[K] + [A])\{\overline{q}\} = 0$$
 (3.1.2)

where

[K] = stiffness matrix

[I] = inertia matrix

 $\Omega = \frac{1+ig}{2} \quad \text{complex frequency}$

[A] = aerodynamic matrix

Equation (3.1.2) may be rewritten as

$$[C]\{\overline{q}\} = \Omega\{\overline{q}\} \tag{3.1.3}$$

where

$$[C] = [K]^{-1}([I]+[A])$$

Since [A] is, in general, a complex non-hermitian matrix, so will [C] be and consequently the solution of the eigensystem (3. 1. 3) give rise to complex eigenvalues and eigenvectors.

For the sake of simplicity, we will introduce the V-g method for the incompressible case, and then, we will extend it to the compressible case.

Let an aeroelastic system, a cantilever wing, for instance, be subjected to an airstream with velocity V.

The aerodynamic matrix will be only a function of the reduced frequency k. For a given value of k, the eigensystem (3.1.3) can be solved and one gets n complex eigenvalues Ω and n complex eigenvectors $\{\overline{q}\}$.

Recalling the definition of the complex eigenvalues, we obtain

$$\omega = \sqrt{\frac{1}{\text{Re}[\Omega]}}$$
 (3. 1. 4)

$$\mathbf{g} = \frac{\mathrm{Im}[\Omega]}{\mathrm{Re}[\Omega]} \tag{3.1.5}$$

$$V = \frac{\omega b}{k} \tag{3.1.6}$$

If we plot on a V-g plane the n (V,g) pairs corresponding to the given k and repeat the calculation for several different values of k, we end up with a so-called V-g diagram as shown in Fig. 11.

It is clear that there are n such curves, each one corresponding to a possible steady-state harmonic oscillation mode, which can occur under the associated (V,g) pair of conditions. It is also shown in Ref. 39 that the imaginary part g of the complex eigenvalue can be interpreted as a structural damping factor. Since actual structures exhibit positive damping, but yet the factor g is relatively small (0.01 to 0.04 for metallic structures), it is usually assumed that the flutter phenomenon exists when g = 0. As a consequence, the critical flutter speed is the one associated with the first crossing of the g = 0 axis.

Now we turn to the situation where the flutter speed is high enough so that compressibility effects cannot be neglected. In this case, the aerodynamic matrix will depend on both reduced frequency and Mach number, and a simple way for finding the flutter speed is as follows:

- i) Plot V-g diagrams for different Mach numbers at fixed altitude.
- ii) Find the critical speed for each diagram and plot it versus Mach number as shown in Fig. 12.
- iii) Then, find the "matched point," which represents the flutter speed consistent with the altitude and Mach number.

3.2 THE g = 0 CONSTRAINT SURFACE AND THE OPTIMALITY CONDITION EQUATIONS

In this section, we derive the optimality condition equations for the flutter optimization problems and introduce a new approach which will serve as a basis for our algorithm.

Consider an aeroelastic system and recall the equations of motion in the form

$$([\Pi - \Omega | K] + [A]) \{\overline{\mathbf{q}}\} = 0$$
 (3. 2. 1)

The aerodynamic matrix, as already discussed, depends on reduced frequency and Mach number.

Consider, now, that the airstream velocity is fixed. We are interested in changes in the solution of the eigensystem when structural elements are slightly changed. In order to make our statement more precise, we consider that design variables are defined over the structure and we are asking for the derivatives of the eigenvalues of (3.2.1) with respect to the design variables, holding V fixed.

Differentiating (3. 2. 1) with respect to the mass associated with the i-th design variable, we have

$$\left(\frac{\partial}{\partial \mathbf{m_i}}\left[\mathbf{I}\right] - \frac{\partial\Omega}{\partial \mathbf{m_i}}\left[\mathbf{K}\right] - \Omega\frac{\partial}{\partial \mathbf{m_i}}\left[\mathbf{K}\right] + \frac{\partial}{\partial \mathbf{m_i}}\left[\mathbf{A}\right]\right)\left\{\overline{\mathbf{q}}\right\} + (\left[\mathbf{I}\right] - \Omega\left[\mathbf{K}\right] + \left[\mathbf{A}\right])\left\{\frac{\partial\overline{\mathbf{q}}}{\partial \mathbf{m_i}}\right\} = 0 \tag{3.2.2}$$

Consider the adjoint eigenproblem

$$([\Pi - \Omega[K] + [A])^{T} \{\overline{p}\} = 0$$
 (3.2.3)

We pre-multiply eq. (3.2.2) by $\{\overline{p}\}^T$ and since transposing does not affect the eigenvalues, the second term of (3.2.2) vanishes. We can thus write,

$$\left\{\overline{p}\right\}^{T} \left(\frac{\partial [\Pi]}{\partial m_{i}} - \frac{\partial \Omega}{\partial m_{i}} [K] - \Omega \frac{\partial [K]}{\partial m_{i}} + \frac{\partial [A]}{\partial m_{i}}\right) \left\{\overline{q}\right\} = 0 \tag{3.2.4}$$

Since the airstream velocity and the altitude are fixed, so will the Mach number be, and we have

$$\frac{\partial [A]}{\partial m_{i}} = \frac{d}{dk} [A] \frac{\partial k}{\partial m_{i}}$$
 (3.2.5)

But,

$$k = \frac{\omega b}{V}$$

Then,

$$\frac{\partial [A]}{\partial m_i} = \frac{b}{V} \frac{\partial \omega}{\partial m_i} \frac{d[A]}{dk}$$
 (3.2.6)

From this result and the definition of Ω we can write eq. (3.2.4) as,

$$\{\overline{p}\}^T \left[\frac{\partial [\Pi]}{\partial m_i} - \frac{i\omega \frac{\partial g}{\partial m_i} - 2(1+ig) \frac{\partial \omega}{\partial m_i}}{\omega^3} [K] - \frac{1+ig}{\omega^2} \frac{\partial [K]}{\partial m_i} + \frac{d[A]}{dk} (\frac{b}{V}) \frac{\partial \omega}{\partial m_i} \right] \{\overline{q}\} = 0$$

$$(3. 2. 7)$$

Equation (3.2.7) represents for each design variable a complex scalar equation which can be decomposed into two real scalar equations.

Define,

$$\begin{split} \mathbf{R}_1 &= \mathrm{Re}\left[\{\overline{\mathbf{p}}\}^T \frac{\partial [\Pi]}{\partial \mathbf{m}_i} \{\overline{\mathbf{q}}\}\right] & \mathbf{I}_1 &= \mathrm{Im}\left[\{\overline{\mathbf{p}}\}^T \frac{\partial [\Pi]}{\partial \mathbf{m}_i} \{\overline{\mathbf{q}}\}\right] \\ \\ \mathbf{R}_2 &= \mathrm{Re}\left[\{\overline{\mathbf{p}}\}^T \frac{\partial [K]}{\partial \mathbf{m}_i} \{\overline{\mathbf{q}}\}\right] & \mathbf{I}_2 &= \mathrm{Im}\left[\{\overline{\mathbf{p}}\}^T \frac{\partial [K]}{\partial \mathbf{m}_i} \{\overline{\mathbf{q}}\}\right] \\ \\ \mathbf{R}_3 &= \mathrm{Re}\left[\{\overline{\mathbf{p}}\}^T [K] \{\overline{\mathbf{q}}\}\right] & \mathbf{I}_3 &= \mathrm{Im}\left[\{\overline{\mathbf{p}}\}^T [K] \{\overline{\mathbf{q}}\}\right] \end{split}$$

$$\boldsymbol{R}_{4} = \operatorname{Re}\left[\left\{\overline{\boldsymbol{p}}\right\}^{T} \frac{d[A]}{dk} \left\{\overline{\boldsymbol{q}}\right\}\right] \qquad \quad \boldsymbol{I}_{4} = \operatorname{Im}\left[\left\{\overline{\boldsymbol{p}}\right\}^{T} \frac{d[A]}{dk} \left\{\overline{\boldsymbol{q}}\right\}\right]$$

The two real scalar equations can be written as

$$\begin{cases} R_1 + \frac{2}{\omega^3} (\frac{\partial \omega}{\partial m_i}) R_3 - \frac{1}{\omega^2} R_2 + \left(\frac{1}{\omega^2} \frac{\partial g}{\partial m_i} - \frac{2g}{\omega^3} \frac{\partial \omega}{\partial m_i}\right) I_3 + \frac{g}{\omega^2} I_2 + (\frac{b}{V}) \frac{\partial \omega}{\partial m_i} R_4 = 0 \\ I_1 + \frac{2}{\omega^3} \frac{\partial \omega}{\partial m_i} I_3 - \frac{1}{\omega^2} I_2 + \left(-\frac{1}{\omega^2} \frac{\partial g}{\partial m_i} + \frac{2g}{\omega^3} \frac{\partial \omega}{\partial m_i}\right) R_3 - \frac{g}{\omega^2} R_2 + \\ + (\frac{b}{V}) \frac{\partial \omega}{\partial m_i} I_4 = 0 \end{cases}$$
(3.2.9)

or

$$\begin{cases} \left(\frac{2}{\omega^3} R_3 - \frac{2g}{\omega^3} I_3 + \frac{b}{V} R_4\right) \frac{\partial \omega}{\partial m_i} + \left(\frac{I_3}{\omega^2}\right) \left(\frac{\partial g}{\partial m_i}\right) = \frac{R_2}{\omega^2} - R_1 - \frac{g}{\omega^2} I_2 \\ \left(\frac{2g}{\omega^3} R_3 + \frac{2}{\omega^3} I_3 + \frac{b}{V} I_4\right) \frac{\partial \omega}{\partial m_i} + \left(-\frac{R_3}{\omega^2}\right) \left(\frac{\partial g}{\partial m_i}\right) = \frac{I_2}{\omega^2} - I_1 + \frac{g}{\omega^2} R_2 \end{cases}$$

$$(3. 2. 11)$$

These two equations form a linear system in $\partial \omega/\partial m_i$ and $\partial g/\partial m_i$. Solving the system yields

$$\frac{\partial \omega}{\partial \mathbf{m_i}} = \frac{\left(\frac{R_2}{\omega^2} - R_1 - \frac{\mathbf{g}}{\omega^2} I_2\right) \frac{R_3}{\omega^2} + \left(\frac{I_2}{\omega^2} - I_1 + \frac{\mathbf{g}}{\omega^2} R_2\right) \frac{I_3}{\omega^2}}{D}$$
(3. 2. 12)

$$\frac{\partial \mathbf{g}}{\partial \mathbf{m}_{i}} = \left[\left(\frac{\mathbf{R}_{2}}{\omega^{2}} - \mathbf{R}_{1} - \frac{\mathbf{g}}{\omega^{2}} \mathbf{I}_{2} \right) \left(\frac{2\mathbf{g}}{\omega^{3}} \mathbf{R}_{3} + \frac{2}{\omega^{3}} \mathbf{I}_{3} + \frac{\mathbf{b}}{\mathbf{V}} \mathbf{I}_{4} \right) - \left(\frac{2}{\omega^{3}} \mathbf{R}_{3} - \frac{2\mathbf{g}}{\omega^{3}} \mathbf{I}_{3} + \frac{\mathbf{b}}{\mathbf{V}} \mathbf{R}_{4} \right) \left(\frac{\mathbf{I}_{2}}{\omega^{2}} - \mathbf{I}_{1} + \frac{\mathbf{g}}{\omega^{2}} \mathbf{R}_{2} \right) \right] / \mathbf{D} \tag{3.2.13}$$

where

$$D = \left(\frac{2g}{\omega^3} R_3 + \frac{2}{\omega^3} I_3 + \frac{b}{V} I_4\right) \frac{I_3}{\omega^2} + \left(\frac{2}{\omega^3} R_3 - \frac{2g}{\omega^3} I_3 + \frac{b}{V} R_4\right) \frac{R_3}{\omega^2}.$$

The mass of the structure is given by

$$M = m_0 + \sum_{i=1}^{m} m_i$$
 (3.2.14)

According to Chapter 2, the necessary conditions for a local minimum with a fixed flutter speed $\,V_{\rm FO}\,$ as a constraint are given by

$$\frac{\partial M}{\partial m_i} + \lambda \frac{\partial}{\partial m_i} (V_F - V_{FO}) = 0 \qquad (i = 1, 2, ... m)$$
 (2.2.15)

where V_F is the actual flutter speed of the structure.

Combining eqs. (2, 3, 15) and (3, 2, 14) gives

$$\frac{\partial V_{\mathbf{F}}}{\partial m_{\mathbf{i}}} = -\frac{1}{\lambda} \qquad (\mathbf{i} = 1, 2, \dots m) \qquad (3.2.16)$$

Expressions (3. 2. 16) represent the optimality conditions for the problem. One disadvantage of using expressions (3. 2. 16) is that we have to derive $\partial V_F/\partial m_i$. Another disadvantage of formulating the problem in the form (3. 2. 15) appears when we actually perform the numerical optimization, since we have to calculate (or at least approximately predict) the flutter speed of the modified design at each iteration step.

An alternative approach, which avoids these difficulties, may be derived as follows.

Consider the structure subjected to an airstream with velocity $\rm V_{FO}$, which happens to be the flutter speed of the structure. To say that $\rm V_{FO}$ is actually the flutter speed of the structure is the same as saying that:

- a) The V-g diagram for the structure has a g = 0 crossing point at V_{FO} .
- b) This crossing point gives the lowest critical speed if there is more than one.

The requirement (a) implies that for $\ln_{\infty}=V_{FO}/a_{\infty}$ there is a value of k such that at least one eigenvalue has null imaginary part (g = 0), and its associated velocity V coincides in value with V_{FO} .

Let us drop, for the time being, the requirement (b), though we will return to it later.

If we reformulate our constraint condition, namely that the structure flutters at an airstream velocity V_{FO} , in terms of saying that g has to vanish for $V = V_{FO}$, we can write the optimality conditions as

$$\frac{\partial \mathbf{M}}{\partial \mathbf{m_i}} + \lambda \frac{\partial}{\partial \mathbf{m_i}} (\mathbf{g} - \mathbf{0}) = 0 \qquad (i = 1, 2, \dots \mathbf{m})$$
 (3. 2. 17)

for $V = V_{FO}$.

Taking into account relation (3.2.14), we obtain

$$\frac{\partial \mathbf{g}}{\partial \mathbf{m}_{\mathbf{i}}} = -\frac{1}{\lambda} \tag{i = 1, 2, ... m}$$

Equations (3.2.18) represent the optimality conditions for the alternate approach.

Upon substitution for $\partial g/\partial m_i$ from equations (3.2.13), with g=0 since the structure satisfies the constraint, the optimality condition equations become

$$\left(\frac{R_{2}}{\omega^{2}} - R_{1}\right) \left(\frac{2I_{3}}{\omega^{3}} + \frac{b}{V_{FO}}I_{4}\right) - \left(\frac{I_{2}}{\omega^{2}} - I_{1}\right) \left(\frac{2R_{3}}{\omega^{3}} + \frac{b}{V_{FO}}R_{4}\right) = -\frac{1}{\lambda} = \text{const.}$$
(i = 1, 2, ... m)
(3, 2, 19)

Since R_3 , R_4 , I_3 and I_4 are constant for any particular design, we have

$$(I_2 - \omega^2 I_1) = c_1(R_2 - \omega^2 R_1) + c_2$$
 (i=1, 2, ... m) (3.2.20)

Now, we define

$$U_{i} = \{\overline{p}\}^{T} \left(\frac{\partial}{\partial m_{i}}[K] - \omega^{2} \frac{\partial}{\partial m_{i}}[I]\right) \{\overline{q}\} \qquad (i = 1, 2, ... m) \qquad (3. 2. 21)$$

Thus, we can write eqs. (3.2.20) as

$$Im[U_i] = c_1 Re[U_i] + c_2$$
 (i = 1, 2, ... m) (3. 2. 22)

The optimality conditions in form (3.2.22) read that if we plot the quantities U_i in a complex plane, then for the optimal structure they will be aligned on a straight line. This interpretation is shown in Fig. 13.

Note that because eqs. (3.2.22) are necessary conditions, the dropping of requirement (b) does not change their validity.

It is beyond our knowledge at this time, what further theoretical implication may arise from the optimality conditions in the form of eqs. (3.2.22) and we recognize the particular importance of additional research in this direction.

An unhappy event that may occur in flutter optimization is due to the possibility of discontinuous behavior of the flutter speed as will be shown. According to the definition, the flutter speed is associated with the <u>first crossing</u> of the g=0 axis.

Now, if we make a small change Δm_i in the mass associated with the i-th design variable, we can plot a new V-g diagram for the altered structure (represented in Fig. 14 by the dotted line) and obtain the new flutter speed V_{Γ} .

The constraint derivatives, in terms of flutter speed, may be defined as

$$\frac{\partial V_{F}}{\partial m_{i}} = \lim_{\Delta m_{i} \to 0} \frac{V_{F}^{\prime} - V_{F}}{\Delta m_{i}}$$
(3. 2. 23)

and nothing abnormal is observed if the V-g diagram is of the normal type.

Unfortunately, abnormal situations shown in Figs. 15 and 16 may develop. In both cases, while the local behavior predicts V_F' as the new flutter speed, the most critical will be V_F'' . Since all practical optimization algorithms depend on local analysis, and ours is no exception, such potential problems should not be ignored, and periodic checks of the redesigned structure are vital in order to detect as soon as possible any abnormal behavior. Hence, the requirement of item (b) previously dropped, is handled by periodically plotting V-g diagrams and checking for any abnormality.

3.3 FLUTTER OPTIMIZATION ALGORITHM

In this section, we outline the optimization algorithm as it will be used in the numerical examples. Only the general features of the algorithm will be discussed here.

The task of the optimization algorithm can be stated as: Minimize the mass of a structural system holding fixed its initial flutter speed.

The algorithm as used in this work is subject to the following restrictions and conditions:

- a.) The geometry of the structural system is fixed so that the only design variables are cross sectional areas and thicknesses of structural components.
- b.) Except for minimum thickness (or area), no other constraints are imposed.
- c.) Inertias and stiffnesses associated with a design variable are assumed proportional to the associated mass m_i.
- d.) Non-structural mass can be accounted for.

According to our discussion in the last section, our constraint will be the hypersurface $g\equiv 0$ for the given V_{FO} rather than the hypersurface $V\equiv V_{FO}$ itself.

The principal steps of the numerical procedure are as follows:

- 1) Determination of the flutter speed of the initial design.
- 2) Redesigning by the algorithm developed in Chapter 2 using the flutter speed calculated in the first step as the constraint. When some design variable reaches its minimum value, the optimization proceeds holding the design variable at its minimum value for the rest of the procedure.

Next, we present the basic block-diagrams for step 1 and step 2 as well as a discussion of their working sub-steps.

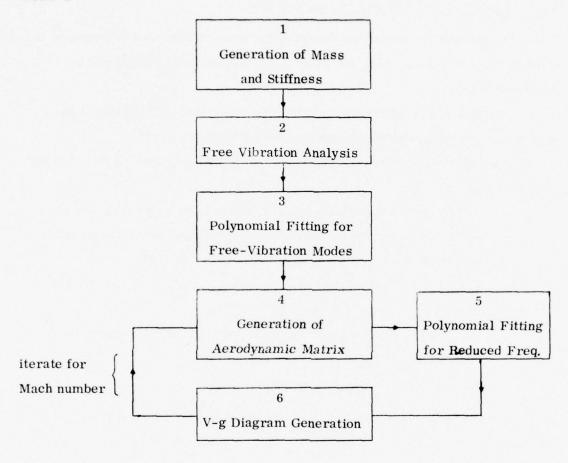


Fig. 17. Block-diagram of Step 1.

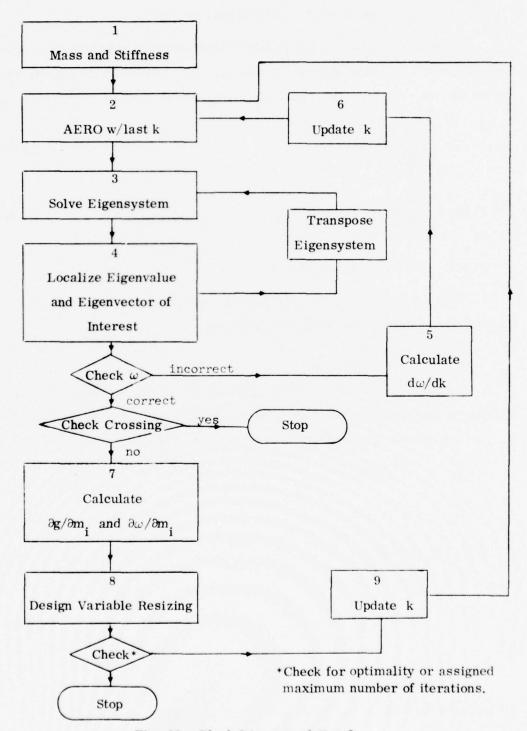


Fig. 18. Block Diagram of Step 2.

STEP 1:

1.1 Generation of Inertia and Stiffness Matrices

Generates by means of any standard finite-element technique the stiffness and the inertia associated with each design variable, as well as the non-structural inertia matrix. Namely, $\overline{[K]}_i$ and $\overline{[I]}_i$ are generated so that

$$[K] = \sum_{i=1}^{m} [\overline{K}]_{i}$$
 (3.3.1)

$$[I] = \sum_{i=1}^{m} [\overline{I}]_i + [\overline{I}]_o$$

$$(3.3.2)$$

1.2 Free-Vibration Analysis.

Uses the stiffness and inertia matrices generated in 1.1 and finds the free-vibration frequencies and modes by solving

$$[K] \{\overline{\mathbf{q}}\} = \omega^2 [\Pi \{\overline{\mathbf{q}}\}] \tag{3.3.3}$$

After solving the above real symmetric eigensystem, it transforms the stiffness and inertia matrices associated with each design variable from nodal to modal coordinates by means of

$$[\overline{K}]_{i} = [T]^{T}[\overline{K}]_{i}[T]$$

$$[\overline{I}]_{i} = [T]^{T}[\overline{I}]_{i}[T] \qquad (3.3.4)$$

$$[\overline{I}]_{o} = [T]^{T}[\overline{I}]_{o}[T] \qquad (*)$$

where

[T] =
$$[\overline{\mathbf{q}}_1, \overline{\mathbf{q}}_2, \dots \overline{\mathbf{q}}_\ell]$$

and

^{*}We retained the same symbols for both coordinate systems.

 \mathbf{q}_{i} are the eigenmodes (i = 1, 2, ... ℓ)

 ℓ is the number of degrees of freedom of the transformed problem.

We also assume that in all the cases to be studied $[K]_i$ and $[\Pi]_i$ are proportional to their associated design variable so that,

$$\{\overline{K}\}_{i} = [\overline{K}]_{i}^{*} x_{i}$$

$$[\overline{\Pi}_{i} = [\overline{\Pi}_{i}^{*} x_{i}]$$

where $[\overline{K}]_{i}^{*}$ and $[\overline{I}]_{i}^{*}$ are constants.

1.3 Polynomial Fitting for Free-Vibration Modes

In order to calculate three-dimensional unsteady generalized aerodynamic forces it is necessary to represent the vertical displacement $\, z \,$ of each mode as a two-dimensional polynomial in $\, x \,$ and $\, y \colon$

$$\frac{z(x,y)}{b} = \sum_{i=1}^{p} \sum_{j=1}^{r} a_{ij} (\frac{x}{b})^{i-1} (\frac{y}{b})^{j-1}$$
(3.3.5)

Here b is the same reference length used in the definition of reduced frequency. The present sub-step finds the coefficients a of the polynomial fit.

In the case where incompressible strip-theory aerodynamics (Ref. 44) is used for the aerodynamic forces, the polynomial fitting is uncessary and the sub-step is replaced by a numerical integration of the eigenmodes so that coefficients f_{ij} can be obtained:

$$f_{ij} = \iint_{\mathbf{x}} z_i z_j dxdy \qquad (i, j = 1, 2, \dots \ell)$$
 (3.3.6)

These coefficients are used as input to generate the incompressible striptheory aerodynamic matrix,

1.4 Generation of the Aerodynamic Matrix

Using the output of the previous sub-step, the aerodynamic matrix [A] is generated. Further details will be presented with the examples.

1.5 Polynomial Fitting for Reduced Frequency

When three-dimensional unsteady aerodynamic theory is being used, a polynomial fit is made for a given Mach number in terms of powers of the reduced frequency, so that the elements of the aerodynamic matrix are represented by

$$A_{ij} = \sum_{r=1}^{n} c_{ijr} k^{r-1}$$
 (3.3.7)

where n is chosen by the user.

When incompressible strip-theory aerodynamics is assumed, the above polynomial fit is already embodied in the previous sub-step.

1.6 V-g Diagram Generation

For a given Mach number and reduced frequency, the complex eigensystem

$$[C]\{\overline{q}\} = \Omega\{\overline{q}\} \tag{3.3.8}$$

is solved, where

$$[C] = [K]^{-1}([I] + [A]).$$

Then, for each complex eigenvalue $\,\Omega\,,\,\,\,V\,,\,\,g\,$ and $\,\omega\,$ are found from the relations

$$\omega = \sqrt{\frac{1}{\text{Re}[\Omega]}}$$
 (3.3.9)

$$\mathbf{g} = \frac{\mathrm{Im}[\Omega]}{\mathrm{Re}[\Omega]} \tag{3.3.10}$$

$$V = \frac{\omega b}{k} \tag{3.3.11}$$

At this point, an important observation has to be made. From eq. (3.3.9) it can be seen that if $\operatorname{Re}[\Omega] < 0$, ω will become imaginary, which contradicts our assumption of real ω .

In order to properly interpret this occurrence, we recall that in a V-g diagram the dependence of a certain branch on the reduced frequency is as shown in Fig. 19. As $V \to 0$, we approach the free-vibration case which has a finite and nonzero frequency. Therefore, as $V \to 0$ we have $k \to \infty$.

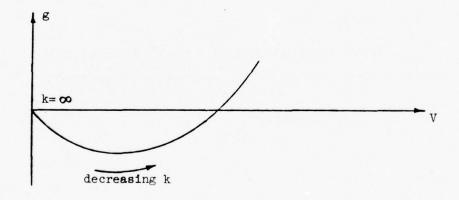


Fig. 19. Variation of the reduced frequency along a branch.

Rewriting eqs. (3.3.9) and (3.3.11) we have

$$\operatorname{Re}\left[\Omega\right] = \frac{1}{2} \tag{3.3.12}$$

$$\mathbf{k} = \frac{\omega \mathbf{b}}{\mathbf{V}} \tag{3.3.13}$$

Equation (3.3.12) shows that as $Re[\Omega]$ approaches zero, ω approaches ∞ and from eq. (3.3.13) we also see that V approaches ∞ , since k is decreasing. The primary conclusion is that the branches extend to infinity in the V direction as k approaches some critical value which causes a change in

the sign of $Re[\Omega]$. When that happens, we can safely ignore the imaginary frequency, since we know that the limit of this particular branch has already been reached.

STEP 2:

2, 1 Inertia and Stiffness Matrices

$$[\overline{\boldsymbol{\eta}}] = \sum_{i=1}^m \, \boldsymbol{x}_i[\overline{\boldsymbol{\eta}}_i^* + \, [\overline{\boldsymbol{\eta}}_o]$$

$$[K] = \sum_{i=1}^{m} x_{i}^{[K]}_{i}^{*}$$
 (3.3.14)

2.2 Aerodynamic Matrix

The flutter Mach number, the updated reduced frequency and the polynomial fit of (1.3) are used to generate the aerodynamic matrix [A]

2.3 Solution of the Eigensystem

The eigensystem

$$\{C\}\{\overline{q}\} = \Omega\{\overline{q}\}$$

is solved.

2.4 Identification of Critical Eigenvector

This sub-step identifies, among the ℓ eigenvalues-eigenvector pairs generated in the last sub-step, the one corresponding to the desired flutter speed and therefore the one being monitored. This is done in the following way.

Consider a reduced frequency k* defined as

$$\mathbf{k}^* = \frac{\sqrt{\frac{1}{\text{Re}[\Omega]}} \cdot \mathbf{b}}{V_{\text{FO}}}$$
(3.3.16)

Since V_{FO} is the constant flutter speed, k^* will depend only on the eigenvalue Ω . For the critical Ω , we will have k^* approximately equal to k. Therefore, if we define an error ϵ given by

$$\epsilon = |\mathbf{k}^* - \mathbf{k}| \tag{3.3.17}$$

The critical eigenvalue will be the one that gives the smallest value for ϵ .

2.5 Reduced Frequency Matching

Consider the reduced frequency k used in the generation of the aerodynamic matrix [A].

If the reduced frequency is correctly matched (which means that the current flutter frequency is the actual one), then for the critical k^* we have,

$$\epsilon = |\mathbf{k}^* - \mathbf{k}| = 0 \tag{3.3.18}$$

However, it might happen that the reduced frequency k* calculated from the critical eigenvalue is different from the reduced frequency k used in the aerodynamic matrix, and a reevaluation of the flutter frequency is necessary. This is accomplished as follows.

Consider the eigensystem for the current design:

$$([I] + [A] - \Omega[K])\{\overline{q}\} = 0$$
 (3. 3. 19)

Since the design, the Mach number and the airstream velocity are fixed, the eigenvalues of the eigensystem (3. 3. 19) will ultimately depend on the frequency chosen in the definition of k. Let this frequency be r. Then,

$$\mathbf{k} = \frac{\mathbf{rb}}{\mathbf{V}_{\mathbf{FO}}} \tag{3.3.20}$$

Differentiating eq. (3.3.19) with respect to r, we obtain

$$\left(\frac{d[A]}{dr} - \frac{d\Omega}{dr}[K]\right)\left\{\overline{q}\right\} + ([\Pi + [A] - \Omega[K])\left\{\frac{d\overline{q}}{dr}\right\} = 0$$
(3. 3. 21)

Upon pre-multiplying by $\{\overline{p}\}^T$, the second term on the left hand side of (3, 3, 21) vanishes and

$$\{\overline{p}\}^{T} \frac{d[A]}{dr} \{\overline{q}\} = \frac{d\Omega}{dr} \{\overline{p}\}^{T} [K] \{\overline{q}\}$$
 (3. 3. 22)

But,

$$\frac{d}{dr}[A] = \frac{dk}{dr} \frac{d}{dk}[A]$$
 (3. 3. 23)

Thus,

$$\frac{d\Omega}{d\mathbf{r}} = \frac{\frac{\mathbf{b}}{\mathbf{V}_{FO}} \{\overline{\mathbf{p}}\}^{T} \frac{\mathbf{d}}{d\mathbf{k}} [\mathbf{A}] \{\overline{\mathbf{q}}\}}{\{\overline{\mathbf{p}}\}^{T} [\mathbf{K}] \{\overline{\mathbf{q}}\}} = \frac{i\omega \frac{d\mathbf{g}}{d\mathbf{r}} - 2(1+i\mathbf{g}) \frac{d\omega}{d\mathbf{r}}}{\omega^{3}}$$
(3.3.24)

From the above equation,

$$\operatorname{Re}\left[\frac{\mathrm{d}\Omega}{\mathrm{d}\mathbf{r}}\right] = -\frac{2}{\omega^3} \frac{\mathrm{d}\omega}{\mathrm{d}\mathbf{r}} \tag{3.3.25}$$

Combining eqs. (3.3.25) and (3.3.22), we finally obtain

$$\frac{d\omega}{d\mathbf{r}} = -\frac{\omega^3 \mathbf{b}}{2V_{FO}} \operatorname{Re} \left[\frac{\{\overline{\mathbf{p}}\}^T \frac{d}{d\mathbf{k}} [A] \{\overline{\mathbf{q}}\}}{\{\overline{\mathbf{p}}\}^T [K] \{\overline{\mathbf{q}}\}} \right]$$
(3. 3. 26)

To first order approximation we can write

$$\omega_2 - \omega_1 = (\mathbf{r}_2 - \mathbf{r}_1) \frac{d\omega}{d\mathbf{r}} |_{\mathbf{r}_1}$$
 (3. 3. 27)

Now, if we enforce point 2 to be the matched point, we have

$$\omega_2 = \mathbf{r}_2 \tag{3.3.28}$$

Thus,

$$\left(1 - \frac{d\omega}{d\mathbf{r}}\Big|_{\mathbf{r}_{1}}\right)\mathbf{r}_{2} = \omega_{1} - \mathbf{r}_{1} \frac{d\omega}{d\mathbf{r}}\Big|_{\mathbf{r}_{1}}$$
(3. 3. 29)

or in general,

$$\mathbf{r_{i+1}} = \frac{\omega_{i} - \mathbf{r_{i}} \frac{d\omega}{d\mathbf{r}}|_{\mathbf{r_{i}}}}{1 - \frac{d\omega}{d\mathbf{r}}|_{\mathbf{r_{i}}}}$$
(3.3.30)

A - 48

Relation (3, 3, 30) can be used iteratively until $\,\omega_{\,i}^{\,\,\simeq\,} r_{\,i}^{\,\,}$ and hence the matching is completed.

For numerical purposes, the matching was considered completed when $(k^*-k) \le 0.01k$.

2.6 Updating of Reduced Frequency

See discussion of sub-step (2.5).

2.7 Calculation of Design Variable Derivatives

This sub-step calculates $\partial \omega/\partial m_i$ and $\partial g/\partial m_i$ using formulas (3. 2. 12) and (3. 2. 13) respectively.

2.8 Design Variable Resizing

The optimization algorithm as described in Chapter 2 is used. The constraint condition is g=0 and $\partial g/\partial m_{\hat{1}}$ derivatives calculated in the last substep are used.

2.9 Updating of Reduced-Frequency

Use the $\partial \omega/\partial m_i$ derivatives and updates the flutter frequency for the new design by means of a first-order expansion

$$\omega_{\text{new}} = \omega_{\text{old}} + \sum_{j=1}^{m} \left(\frac{\partial \omega}{\partial m_{j}}\right) \Delta m_{j}$$
 (3.3.31)

The new reduced frequency will be

$$k_{new} = \frac{\omega_{new}^b}{V_{FO}}$$

3.4 NUMERICAL EXAMPLES

In this section, we present two numerical examples used for debugging as well as to check both the validity of the concepts discussed earlier and the stability of the algorithm when applied to relatively complex structures.

The first example is a 27-design variable rectangular wing, with incompressible strip-theory aerodynamics (Ref. 44). The initial design is similar to the one used by Rudisill and Bhatia (Ref. 32).

The second example consists of a swept wing modeled with 90 design variables and three-dimensional subsonic compressible aerodynamics.

All the computational work has been done on an IBM 360/67.

3.4.1 27-Design Variable Rectangular Wings

- (a) Dimensions Fig. 20
- (b) Design variable definition Fig. 21
- (c) Finite-element sub-division Fig. 22

$$E = 10.5 \times 10^6 \text{ psi}$$

$$\nu = 0.3$$

$$\rho_{\text{S}} = 0.262 \times 10^{-3} \frac{\text{lb-sec}^3}{\text{in}^4} \qquad \text{speicific mass of structural material}$$

n = 72 nodal degrees of freedom

The inertia and stiffness matrices were generated by a standard finiteelement program. Details concerning element geometry, displacement functions and strain energy functionals are described in Refs. 45-47.

(d) Aerodynamic matrix

As mentioned earlier, incompressible strip-theory aerodynamics was used for this first example.

Consider a cross section of the wing as shown in Fig. 23. The coordinates $\alpha(x)$ and z(x) are respectively torsion and bending displacements at a station x measured from the root of the wing.

Now, we represent z(x) and $\alpha(x)$ as a superposition of given uncoupled bending and torsion modes. Thus,

$$z(\mathbf{x}) = z_1 f_1(\mathbf{x}) + z_2 f_2(\mathbf{x}) + \dots + z_{\ell} f_{\ell}(\mathbf{x})$$

$$\alpha(\mathbf{x}) = \alpha_1 f_{\ell+1}(\mathbf{x}) + \alpha_2 f_{\ell+2}(\mathbf{x}) + \dots + \alpha_r f_{\ell+r}$$

$$A-50$$
(3.4.1)

Using the above representation, the aerodynamic matrix can be written as (Ref. 44)

$$A_{ij} = \pi \rho_a b^3 [G_{ij}^f f_{ij}]$$
 (i, j = 1, 2, ... \(\ell + r\)) (3.4.2)

where

$$f_{ij} = \int_{0}^{L} f_{i}(x) f_{j}(x) dx$$
 (3.4.3)

$$G_{ij} = \frac{L_h}{b}$$
 — if i is a bending mode and j is a bending mode

$$G_{ij} = L_{\alpha} - (\frac{1}{2} + a)L_{h}$$
 — if i is a bending mode and j is a torsion mode

$$G_{ij} = \frac{1}{2} - (\frac{1}{2} + a)L_h$$
 — if i is a torsion mode and j is a bending mode

$$G_{ij} = b[M_{\alpha} - (\frac{1}{2} + a)(\frac{1}{2} + L_{\alpha}) + (\frac{1}{2} + a)^2 L_h] - if i is a torsion mode and j is a torsion mode$$

 L_h , L_α and M_α can be expressed further in terms of reduced frequency and Theodorsen's function C(k) (Ref. 44),

$$L_h = 1 - 2i \frac{1}{k} C(k)$$
 (3. 4. 4)

$$L_{\alpha} = \frac{1}{2} - i(\frac{1}{k})[1 + 2C(k)] - 2(\frac{1}{k})^{2}C(k)$$
(3.4.5)

$$M_{\alpha} = \frac{3}{8} - i(\frac{1}{k})$$
 (3.4.6)

Finally, we represent the Theodorsen's function C(k) as a ratio of second-degree polynomials in k (Ref. 47).

$$C(k) = \frac{k^2 - 1.5ik - 0.375}{2k^2 - 2.5ik - 0.375}$$
(3.4.7)

Relation (3. 4. 7) enables us to represent [A] and d[A]/dk in an analytic form.

In the present example, the elastic axis coincides with the axis of the center of mass, so the free vibration modes will be uncoupled and can be directly used in eqs. (3.4.1). The only concern is to eliminate in-plane and breathing modes which are easily recognized. The integrations in formula (3.4.3) were done numerically using the trapeziodal rule and are represented in the block-diagram by sub-step 1.3.

(e) Results

The flutter speed determination and the following optimization procedure were calculated for the constants shown below:

$$\ell = 9$$
 number of free-vibration modes*

$$\rho_{\rm a} = 1.0 \times 10^{-7} \frac{\rm lb. sec}{\rm in}^2$$
 specific mass of air

From the V-g analysis we obtain

$$V_{FO} = 715 \text{ fps}$$
 $k = 0.276$

The optimization results are given below.

^{*}The 4th mode is neither a bending nor a torsional one.

Table 3. Optimization Results*

Design Variables	Туре	Measure	${ m i}\atop { m in~or~in}^2$	t _f in or in ²	t min in or in ²
	- 77				
1	Q	T	0.040	0. 011	0.010
2	Q	Т	0.040	0.011	0.010
3	Q	T	0.040	0.012	0.010
4	Q	T	0.040	0.012	0.010
5	Q	T	0.040	0.010	0.010
6	Q	T	0.040	0.010	0. 010
7	Q	T	0.080	0.010	0.010
8	Q	T	0.080	0.050	0.010
9	Q	Т	0.080	0.022	0.010
10	Q	Т	0.080	0.019	0.010
11	Q	Т	0.080	0.025	0.010
12	Q	Т	0.080	0.013	0.010
13	R	A	2.000	0.512	0,500
14	R	A	2.000	0.500	0.500
15	R	A	2.000	0.500	0.500
16	R	A	2.000	0.512	0.500
17	R	A	2.000	0.500	0.500
18	R	A	2.000	0.514	0.500
19	R	A	2.000	0.514	0.500
20	R	A	2.000	0.500	0.500
21	R	A	2.000	0.500	0.500
22	R	A	2.000	0. 591	0.500
23	R	A	2.000	0.591	0.500
24	R	A	2.000	0.500	0.500
25	Q	Т	0.040	0.040	0.040
26	Q	Т	0.040	0.040	0.040
27	Q	Т	0.040	0.040	0.040

^{*}Q stands for quadrangular membrane, R for axial rod, T for thickness and A for cross sectional area.

Sequence = [10. 0, 8. 0, 6. 0, 4. 0, 2. 0, 1. 0, 0. 6, 0. 4, 0. 2-25. 0]

Number of iterations = 25

$$M_i = 195 \text{ lb}$$

$$M_{f} = 52.5 \text{ lb}$$

CPU time per iteration = 0.088 min/iter.

Figures 24 and 25 show the V-g diagram at several stages of the redesigning process and reveal that the present approach is very stable in the sense of keeping the flutter speed unchanged. The optimization was interrupted after 25 iterations because the critical mode became tangent (Fig. 25). Figure 26 shows the optimization history diagram and it is seen that after ten iterations the mass of the structure was already close to its final value.

3. 4. 2 90-Design Variable Swept Wings

- (a) Dimensions Fig. 27
- (b) Design variable definition Fig. 28
- (c) Finite-element sub-division

The finite-element sub-division coincides with the design variables.

$$E = 10.0 \times 10^6 \text{ psi}$$

$$\rho_{\rm S} = 0.262 \times 10^{-3} \frac{\text{lb-sec}^2}{\text{in}^4}$$

$$\nu = 0.3$$

n = 108 nodal degrees of freedom

A mass of 378 lb. was evenly distributed among the last six nodes on the tip of the wing as shown in Fig. 28.

(d) Aerodynamic matrix

In contrast to the previous example, three-dimensional subsonic compressible aerodynamic theory was used here. The particular computational technique employed was the doublet-lattice method (Ref. 48). In order to obtain the aerodynamic matrix [A], the output matrix [D] of the program has to be

scaled as shown:

[A] =
$$\frac{1}{2} \rho_a \text{Sb}^3 \frac{1}{k^2}$$
 [D] (3. 4. 8)

where

S = planform area of the wing

b = reference length

 ρ_{a} = specific mass of air

Furthermore, the elements of [D] were fitted at the flutter Mach number by a fourth degree polynomial using 5 distinct values of k. Thus,

$$[D] = [\psi_1] + [\psi_2]k + [\psi_3]k^2 + [\psi_4]k^3 + [\psi_8]k^4$$
(3. 4. 9)

or

$$[A] = \frac{1}{2} \rho_{a} Sb^{3} (\frac{1}{k^{2}} [\psi_{1}] + \frac{1}{k} [\psi_{2}] + [\psi_{3}] + k [\psi_{4}] + k^{2} [\psi_{5}])$$
 (3. 4. 10)

and

$$\frac{\mathrm{d}}{\mathrm{d}\mathbf{k}}[\mathbf{A}] = \frac{1}{2} \rho_{\mathbf{a}} \mathrm{Sb}^{3} \left(-\frac{2}{\mathbf{k}^{3}} [\psi_{1}] - \frac{1}{\mathbf{k}^{2}} [\psi_{2}] + [\psi_{4}] + 2\mathbf{k} [\psi_{5}]\right) \tag{3.4.11}$$

Further details on the generation of the [D] matrix are found in Refs. (45-47.)

(e) Results

The initial design is given in Table 4. The flutter speed determination and the following optimization results were calculated for the constants shown below:

& = 11 number of free vibration assumed modes

$$\rho_{\mathbf{a}} = 1.0 \times 10^{-7} \frac{\text{lb-sec}^2}{\text{in}^4}$$
 specific mass of air

The fluttering condition is

$$V_{FO} = 915 \text{ fps}$$

m = 0.84

k = 0.34

Table 4. Definition of Initial Design and Minimum-Gage Conditions.
Q, R, T and A are defined in Table 3.

Design Variable	Туре	Measure	t in or in ²	t min in or in ²
1 : : 42	Q	Т	0.080	0. 020 : : 0. 020
43 : : 78	R	0. 250 A	0. 250 : : 0. 250	0. 050 : : 0. 050
79 : : 90	Q	Т	0. 080 : : 0. 080	0. 080 ; 0. 080

The optimum structure had all the design variables at their minimum values with the exception of those listed below:

Table 5. Final Design. Design Variables Which Are Not at Their Minimum Values.

Design Variables	${}^{ m t_f}_{ m f}$ in or in 2	
3	0. 0231	
11	0. 2015	
15	0. 0228	
23	0. 2032	
25	0, 0556	

Table 5. (continued)

Design Variables	${ m t_f} { m in~or~in}^2$
25	0. 0556
26	0. 1769
27	0. 2314
28	0. 0405
30	0. 0550

Sequence = [10.0, 8.0, 6.0, 4.0, 2.0, 1.0-25.0]

 $M_{i} = 2130 lb$ (excluding tip mass)

 $M_f = 894 lb$ (excluding tip mass)

Number of iteration = 41

CPU time per iteration \approx 0.368 ($\frac{\text{min}}{\text{iter}}$)

Figures 29-32 show V-g diagrams of the initial design for different Mach numbers while Fig. 33 is the matching diagram from which the consistent flutter speed and Mach number are obtained. The V-g diagrams of the initial, intermediate and final designs are shown in Fig. 34. Again, it is seen that the method is very stable and the flutter speed of the final design is practically the same as of the initial. The optimization was interrupted after 41 iterations when the slope of the critical branch became negative. The optimization history is shown in Fig. 35 and it is seen that most of the mass reduction has been achieved after approximately 15 iterations.

4. THE VIABILITY OF MODAL ANALYSIS FOR STATIC OPTIMIZATION PROBLEMS

4. 1 REDUCTION OF THE NUMBER OF DEGREES OF FREEDOM BY MODAL DECOMPOSITION

As already pointed out, structural optimization of practical structures requires iterative techniques and with the present state-of-the-art the number of analysis is likely to vary between ten and one hundred. For most static problems, an analysis step is equivalent to the solution of a linear system with order equal to the number of degrees of freedom of the structural model.

On the other hand, the number of degrees of freedom (understood as generalized displacements at nodal points) may become relatively large for complex structures and consequently the computational effort spent in each analysis may rapidly reach very high levels. Based on these considerations, an optimization problem of a large scale structure may become fantastically time consuming and usually that will be a limiting factor.

One way of trying to overcome this problem is to perform an "approximate" analysis with the aim of saving computational effort. Storaasli and Sobieszczanski (Ref. 49) considered the response of the modified structure as given by a first order Taylor approximation. Bhatia (Ref. 50) extended the concept and also studied dynamical problems. Fox and Miura (Ref. 51) considered the response of a current design as given by a linear superposition of some basic responses (obtained as responses to some basic designs) with the aim of reducing the order of the linear system. Noor and Lowder (Ref. 52) proposed to use response derivatives as generalized coordinates for the reduced basis and present some comparative results.

In the present Chapter, we investigate the viability of using modal analysis with the objective of reducing the order of the linear system and comparing the results with those obtained using standard finite-element analysis. It should be noted that the use of modal decomposition as a mean for static analysis was standard before digitial computers made possible the use of finite-element

techniques and hence, the idea is not new in itself.

Consider a structure with linear behavior, subjected to a given set of loads. The displacements are obtained from the matrix equation

$$[K] \{q\} = \{F\} \tag{4.1.1}$$

where

 $\{q\}$ = is a vector of generalized displacements

{F} = is a vector of applied generalized forces

[K] = stiffness matrix

As is usual in finite-element analysis, linear and rotational displacements measured at pre-assigned points over the structure, are defined as degrees of freedom and let their number be n.

Consider now a linear transformation of variables given by

$$\{\mathbf{q}\} = [\mathbf{T}]\{\varphi\} \tag{4.1.2}$$

where [T] is the transformation matrix.

Substituting $\{q\}$ from eq. (4,1,2) into eq. (4,1,1) yields

$$[K][T]{q} = {F}$$
 (4.1.3)

Premultiplying eq. (4.1.3) by $[T]^T$, we obtain

$$[T]^{T}[K][T]\{\varphi\} = [T]^{T}\{F\}$$

or

$$[\overline{K}]\{\varphi\} = \{\mathfrak{F}\} \tag{4.1.4}$$

where

$$[\overline{K}] = [T]^T [K][T]$$

and

$$\{\mathfrak{F}\} = [T]^T \{F\}$$

The columns of matrix [T] are recognized to be the assumed modes and [T] is also called modal matrix. The advantage of such a transformation of variables is that if [T] is a $n \times \ell$ matrix with $\ell < n$, we are in fact reducing

the order of our system.

Let us partition the vector $\{\varphi\}$ into two parts. $\{\varphi_{\mathbf{R}}\}$ represents the first ℓ components of $\{\varphi\}$ and $\{\varphi_{\mathbf{T}}\}$ the remaining n- ℓ components.

$$\{\varphi\} = \left\{\frac{\varphi_{\mathbf{R}}}{\varphi_{\mathbf{T}}}\right\} \tag{4.1.5}$$

Substituting representation (4.1.5) into eq. (4.1.4) yields

$$\begin{bmatrix}
K_{RR} & K_{RT} \\
--- & K_{TR}
\end{bmatrix}
\begin{pmatrix}
\varphi_{R} \\
--- \\
\varphi_{T}
\end{pmatrix} = \begin{pmatrix}
\mathfrak{F}_{R} \\
--- \\
\mathfrak{F}_{T}
\end{pmatrix}$$
(4. 1. 6)

From eq. (4.1.6) we can write

$$[\mathbf{K}_{\mathbf{R}\mathbf{R}}]\{\boldsymbol{\varphi}_{\mathbf{R}}\} + [\mathbf{K}_{\mathbf{R}\mathbf{T}}]\{\boldsymbol{\varphi}_{\mathbf{T}}\} \ = \ \{\boldsymbol{\mathfrak{F}}_{\mathbf{R}}\}$$

or

$$\{\varphi_{\mathbf{R}}\} = [\overline{\mathbf{K}}_{\mathbf{R}\mathbf{R}}]^{-1} \{\mathfrak{F}_{\mathbf{R}}\} - [\overline{\mathbf{K}}_{\mathbf{R}\mathbf{R}}]^{-1} [\overline{\mathbf{K}}_{\mathbf{R}\mathbf{T}}] \{\varphi_{\mathbf{T}}\}$$
(4. 1. 7)

If we assume that the components of $\{\varphi_T^{}\}$ are small enough so that the second term of the r.h.s. of (4.1.7) can be neglected in the presence of the other, $\{\varphi_R^{}\}$ can be approximated by

$$\{\varphi_{\mathbf{R}}\} = [\overline{\mathbf{K}}_{\mathbf{R}\mathbf{R}}]^{-1}\{\mathfrak{F}_{\mathbf{R}}\}$$
(4. 1. 8)

On the other hand, if the modes are suitably chosen, it is possible to the actual displacements of a modified structure be approximated by the same modes used to approximate the actual displacements of the initial structure and hence, all the analysis would be made on matrices of order $\ell \times \ell$. This corresponds to say that for the modified structure, $\{\varphi_T\}$ continues to be small enough so that $[\overline{K}_{RR}]^{-1}[\overline{K}_{RT}]\{\varphi_T\}$ can be neglected.

A major problem is to generate a suitable modal matrix in an efficient way. This problem has not been solved yet and calls for further research.

4.2 NUMERICAL EXAMPLE

In order to access the applicability of the procedure outlined in Section 4.1 and to obtain an estimate of the error involved in using an approximate analysis, a numerical example was carried out. The example is identical to the one used in 2.5-c and hence will not be restated here.

The assumed modes were chosen as the eigenvectors of the eigensystem

$$[K]\{x\} = \lambda\{x\} \tag{4.2.1}$$

There is no special justification for choosing these vectors as assumed modes, though their orthogonality property in relation to the matrix [K] simplifies the computation of the respective components. In general, however, this approach is not attractive since it requires the solution of an eigensystem of the same order as of the initial problem and that may involve a very large computational effort.

The solution of the problem using assumed modes proceeded as follows:

- a) Solution of the eigensystem $[K]\{x\} = \lambda\{x\}$ and construction of the transformation matrix [T] using these eigenvectors. Note that [K] is in the original 72×72 nodal system.
- b) Generation of the n+n transformed stiffness matrix and the $n\times 1$ transformed force vector

$$[\overline{K}] = [T]^{T}[K][T] \tag{4. 2. 2}$$

$$\{\mathfrak{F}\} = [T]^{\mathsf{T}}\{F\} \tag{4.2.3}$$

Note that since [T] is obtained using eigenvectors, [K] is diagonal and the triple matrix product is not actually carried out.

c) Solution of the static problem in the transformed system

$$\{\varphi\} = [\overline{K}]^{-1}\{\mathfrak{F}\} \tag{4.2.4}$$

and reordering of the components of $\{\varphi\}$ in decreasing order of absolute values,

- d) Reduction of the order of the system from 72 to 15 by retaining the 15 components of $\{\varphi\}$ in decreasing order of absolute values.
- e) Optimization using the algorithm of Chapter 2.

The optimization results are as follows:

Sequence = [10.0, 8.0, 6.0, 4.0, 2.0, 1.0-25.0]

Number of iterations = 22

 $M_i = 195 lb$

 $M_f = 69 lb$

CPU time per iteration = 0.148 min./iter.

The final design has all the variables at their minimum thickness with the following expections:

 $t_{f}(7) = 0.163 \text{ in}$

 $t_{f}(8) = 0.411 \text{ in}$

 $t_{\mathbf{f}}(9) = 0.087 \text{ in}$

 $t_f(10) = 0.163 \text{ in}$

 $t_{\rm f}(11) = 0.017 \text{ in}$

 $t_{f}(12) = 0.039$

error = 4.3%

The above error is in the sense of approximate compliance in relation to exact compliance.

Table 6. First Fifteen Modal Coordinates in Order of Decreasing Absolute Values

k	φ _k (in)
1	9.6055
2	-0.6534
3	0. 1813
4	-0.0690
5	-0.0201
6	0.0172
7	-0.0103
8	-0.0052
9	0. 0046
10	-0. 0015
11	-0. 0011
12	-0, 0005
13	0.0004
14	-0.0004
15	0.0003

Table 7. Compliances Using Full and Reduced Analysis

	Reduced Space Analysis (lb. in)	Full Space Analysis (lb. in)	
initial design	3571. 1	3571.5	
final design 3571.4		3727. 1	

5. CONCLUSION

5.1 DISCUSSION OF THE RESULTS

5.1.1 Optimization Algorithm

The optimization algorithm developed in Chapter 2 has shown the following characteristics:

- a) Very high stability. The constraint was always satisfied at the optimum within less than 1%.
- b) The main characteristic associated with optimality criteria, namely, the fact that the computation effort does not increase very sharply increasing the number of design variables, was preserved as seen by comparing both flutter optimizations.
- c) In all the examples (except in the 90-design variable wing) 80% of the total weight reduction was achieved in less than ten iterations. For the 90-design variable wing, this figure was reached after 14 iterations.
- d) Except for the flutter optimization problems, all final structures satisfied Kuhn-Tucker conditions although the algorithm does not enforce them. In the case of flutter optimization, the procedure was terminated due to abnormalities in the V-g diagram rather than satisfaction of optimality conditions.

On the other hand, the relatively slow convergence near the final design is mainly due to an over-conservative treatment of the minimum-gage conditions and that should be improved.

5.1.2 Flutter Optimization

The utilization of g = 0 as a constraint for flutter optimization revealed:

- a) A new expression for the flutter optimality condition as given in eq. (3.2.22) and shown in Fig. 13.
- b) Very high stability in the constrained flutter speed.
- Relatively low computation time considering the high number of modes and design variables used.

5.1.3 Assumed Modes for Static Optimization

With respect to this problem, the relatively low error of less than 5% in comparing the approximate analysis with the full finite-element analysis, indicate that the method may be attractive. However, the overall efficiency was low.

5.2 SUMMARY

Although the principal subject of this dissertation is structural optimization under a flutter constraint, two other concepts have also been studied with very encouraging results.

With regard to the flutter optimization problem, this work advances the idea of using as a constraint the condition g=0 rather than using directly $V_F = V_{FO}$. The advantage of this approach is that it eliminates the need to calculate either an exact current flutter speed, which is time consuming, or an approximate flutter speed, which after several iterations may introduce appreciable error. In this respect, the results of having the flutter speed within 1% of the specified value exceeded all expections. Another advantage of this approach is that it is simpler to calculate ∇g than ∇V_F specially when compressible aerodynamics is used.

It is strongly believed that this is a sound way to handle flutter optimization problems, no matter what specific optimization algorithm is being used. This conclusion should be equally valid for multiple constraints.

Because there is a possibility for other modes to become flutter critical or even for the intial flutter mode to produce instability at a lower speed as the redesign progresses, there is the need to perform an accurate reanalysis from time to time, to make sure that no abnormality is occurring. In the present work, this has been done by stopping the redesign at a given number of iteration cycles, performing a V-g analysis and, finally, plotting the results by hand. A future improvement in flutter optimization would be to improve the software so that at a given number of iterations, the redesigning would stop and a V-g plot for the current structure would be performed and displayed on a CRT scope.

This would enable the investigator to decide, almost in real time, whether to continue the redesigning process or not. In other words, the process would be interactive to a large degree.

A second concept developed during this research was the idea of a hybrid algorithm, which aims to combine the monotomic weight-decrease property of the "descent methods" with the simplicity of redesigning by means of recursion formulas of the "optimality criteria" methods. This was accomplished by using a parameter-dependent recursion formula, with the parameter being constantly readjusted in order to obtain this monotomic weight decrease.

Finally, the use of assumed modes for the analysis of static problems is discussed in light of optimization and the necessity of repeating the analysis step several times. The relatively low error of this approximate approach suggests that the concept is viable and further research in this area should prove fruitful.

APPENDIX A

NECESSARY AND SUFFICIENT CONDITIONS FOR $M = \beta_1^2/\beta_2$

We know, by definition, that

$$\beta_1 = \sum_{i=1}^{m} \left(\frac{\partial h}{\partial m_i} \right) m_i \tag{A. 1}$$

$$\beta_2 = \sum_{i=1}^{m} \left(\frac{\partial h}{\partial m_i} \right)^2 m_i \tag{A. 2}$$

For simplicity of notation, let $(\partial h/\partial m_i) = a_i$. Hence

$$\beta_1 = \sum_{i=1}^m a_i m_i \tag{A.3}$$

$$\beta_2 = \sum_{i=1}^m a_i^2 m_i$$
 (A. 4)

But

$$M = m_1 + m_2 + \dots + m_m$$
 (A.5)

Thus

$$M\beta_2 = (m_1 + m_2 + ... + m_m)(a_1^2 m_1 + a_2^2 m_2 + ... + a_m^2 m_m)$$
 (A.6)

$$\begin{split} \mathbf{M}\beta_{2} &= \mathbf{a}_{1}^{2}\mathbf{m}_{1}^{2} + \mathbf{a}_{2}^{2}\mathbf{m}_{2}^{2} + \dots + \mathbf{a}_{m}^{2}\mathbf{m}_{m}^{2} + \mathbf{m}_{1}\mathbf{m}_{2}(\mathbf{a}_{1}^{2} + \mathbf{a}_{2}^{2}) + \mathbf{m}_{1}\mathbf{m}_{3}(\mathbf{a}_{1}^{2} + \mathbf{a}_{3}^{2}) + \\ &+ \dots + \mathbf{m}_{m-1}\mathbf{m}_{m}(\mathbf{a}_{m-1}^{2} + \mathbf{a}_{m}^{2}) \end{split} \tag{A.7}$$

On the other hand

$$\beta_1^2 = a_1^2 m_1^2 + a_2^2 m_2^2 + \dots + a_m^2 m_m^2 + 2(a_1 a_2 m_1 m_2 + a_1 a_3 m_1 m_3 + \dots + a_{m-1} a_m m_{m-1} m_m)$$
(A. 8)

From eq. (A, 7) and eq. (A, 8) we have

$$M\beta_{2}^{-\beta_{1}^{2}} = m_{1}^{m_{2}(a_{1}^{-a_{2}})^{2} + m_{1}^{m_{3}(a_{1}^{-a_{3}})^{2} + \dots + m_{m-1}^{m_{m-1}^{m}(a_{m-1}^{-a_{m}})^{2}}$$
(A. 9)

Since all m are non-negative, we conclude that $M\beta_2 - \beta_1^2 = 0$ if and only if all the derivatives have the same value.

APPENDIX B

MINIMUM-GAGE OPTIMALITY CONDITION

Consider that some design variable is at its minimum value.

$$x_i = (x_i)_{min}$$

If we further assume the linear relation $m_i = x_i \ell_i$ we have that

$$m_{i} = (m_{i})_{min}$$
 (B. 1)

Let Θ be the value of the constraint derivatives with respect to those variables that <u>are not</u> at their minimum value. We know that a necessary condition for optimality is to have this value equal for all those variables.

Consider, now, a small change in Δm_i . From eq. (B. 1) it is required that $\Delta m_i > 0$. There are two possibilities, $\Theta > 0$ or $\Theta < 0$. ($\Theta = 0$ is a pathological case which we do not consider)

i) $\Theta > 0$

Let h = 0 be the constraint equation. We can write,

$$\Delta \mathbf{h} = \frac{\partial \mathbf{h}}{\partial \mathbf{m}_{i}} \Delta \mathbf{m}_{i} + \Theta \sum_{\mathbf{j} \in \Gamma} \Delta \mathbf{m}_{j}$$
 (B. 2)

Here Γ is the set of non-minimum-gage variables. But $\Delta h = 0$ in order to meet the constraint condition. Thus,

$$\frac{-\frac{\partial \mathbf{h}}{\partial \mathbf{m}_{\mathbf{i}}}}{\Theta} = \frac{\sum_{\mathbf{j} \in \Gamma} \Delta \mathbf{m}_{\mathbf{j}}}{\Delta \mathbf{m}_{\mathbf{i}}}$$
(B. 3)

or

$$\frac{\Theta - \frac{\partial \mathbf{h}}{\partial \mathbf{m_i}}}{\Theta} = \frac{\Delta \mathbf{m_i} + \sum_{\mathbf{j} \in \Gamma} \Delta \mathbf{m_j}}{\Delta \mathbf{m_i}}$$
(B. 4)

Recalling that $\Theta>0$ and $\Delta m_{\hat{1}}>0$ we obtain from eq. (B.4) that a mass reduction is <u>not possible</u> if and only if

$$\Theta > \frac{\partial \mathbf{h}}{\partial \mathbf{m}_{i}}$$
 (B. 5)

ii) $\Theta < 0$

Using the same procedure as in (i) we obtain,

$$\frac{\Theta - \frac{\partial \mathbf{h}}{\partial \mathbf{m}_{i}}}{\Theta} = \frac{\Delta \mathbf{m}_{i} + \sum_{j \in \Gamma} \Delta \mathbf{m}_{i}}{\Delta \mathbf{m}_{i}}$$
(B. 6)

Now, $\,\, \Theta < 0 \,\,$ and $\,\, \Delta m_{\, \hat{1}} > 0. \,\,$ In view of eq. (B.6) the condition for impossibility in mass reduction is

$$\Theta < \frac{\partial \mathbf{h}}{\partial \mathbf{m}_{i}}$$
(B. 7)

The optimality condition (B. 5) and (B. 7) can be used to check the final design for optimality. If the final design is not optimum in terms of these conditions and additional mass decrease is desired, a small increase in the critical variable may be given and the algorithm may be restarted.

REFERENCES

- Michell, A. G., "The Limit of Economy of Material in Frame Structures," Phil. Mag. 8, (4), 1904.
- 2. Wasiutynski, Z. and Brandt, A., "The Present State of Knowledge in the Field of Optimum Design of Structures," Appl. Mech. Reviews, Vol. 16, No. 5, May 1963, pp. 341-350.
- 3. Sheu, C. Y. and Prager, W., "Recent Developments in Optimal Structural Design," Appl. Mech. Reviews, Vol. 21, No. 10, October 1968, pp. 985-992.
- 4. Prager, W., "Optimality Criteria in Structural Design," Proc. Natl. Acad. Sci. 61, (794-796), 1968.
- 5. Ashley, H. and McIntosh, S. C., Jr., "Application of Aeroelastic Constratin in Structural Optimization," <u>Proceedings of the 12th International</u> Congress of Applied Mechanics, Stanford University, August 1968.
- 6. McIntosh, S. C., Jr., and Eastep, F. E., "Design of Minimum Mass Structures with Specified Stiffness Properties," <u>AIAA Journal</u>, Vol. 6, No. 5, May 1968, pp. 962-964.
- Keller, J. B., "The Shape of the Strongest Column," Archive for Rational Mechanics and Analysis, Vol. 5, 1960, pp. 275-285.
- 8. Prager, W. and Taylor, F. E., "Problems of Optimal Structural Design,"

 J. Appl. Mech., Vol. 35, No. 1, March 1968, pp. 102-106.
- Turner, M. J., "Design of Minimum Mass Structures with Specified Natural Frequencies," AIAA Journal, Vol. 5, No. 3, March 1967, pp. 406-412.
- 10. Hamp, W.S., Optimum Structures, Clarendon Press, Oxford, 1973.
- Gellatly, R. A., Gallagher, R. H., and Luberacki, W. A., "Development of a Procedure for Automated Synthesis of Minimum Weight Structures," AFFDL-TR-64-141, 1964.

- Schmit, L. A., "Structural Design by Systematic Synthesis," <u>Proceedings</u>
 of the Second National Conference on Electronic Computation, ASCE, 1960,
 pp. 105-132.
- 13. Fox, R. L. and Schmit, L. A., "Advances in the Integrated Approach to the Structural Synthesis," <u>J. of Spacecraft and Rockets</u>, Vol. 3, No. 6, June 1966, pp. 858-866.
- 14. Gellatly, R. A., "Developments of Procedures for Large Scale Automated Minimum Weight Design," AFFDL-TR-66-180, 1966.
- 15. Vanderplaats, G. and Moses, F., "Structural Optimization by Methods of Feasible Directions," <u>Computers and Structures</u>, Vol. 3, No. 4, July 1973, pp. 739-755.
- 16. Pope, G. G. and Schmit, L. A., (Ed.), "Structural Design Applications of Mathematical Programming Techniques," AGARDograph 149, February 1971.
- 17. Razani, R., "Behavior of Fully Stressed Design of Structures and Its Relationship to Minimum Weight Design," <u>AIAA Journal</u>, Vol. 3, No. 12, December 1965, pp. 2262-2268.
- 18. Berke, L., "An Efficient Approach to the Minimum Weight Design of Deflection Limited Structures," AFFDL-TM-70-4-FDTR, May 1970.
- 19. Berke, L., "Convergence Behavior of Optimality Criteria Based Iterative Procedures," AFFDL-TM-72-1-FBR, January 1972.
- 20. Gellatly, R.A., Berke, L., and Gibson, W., "The Use of Optimality
 Criteria in Automated Structural Design," <u>Proceedings of the 3rd Air</u>
 Force Conference on Matrix Methods in Structural Mechanics, October 1971.
- 21. Gellatly, R. A. and Berke, L., "Optimal Structural Design," AFFDL-TR-70-169, February 1971.
- 22. Venkayya, V. B., "Design of Optimum Structures," J. of Computers and Structures, Vol. 1, No. 1/2, August 1971, pp. 265-309.

- 23. Venkayya, V. B., Khot, N. S., and Berke, L., "Application of Optimality Criteria Approaches to Automated Design of Large Practical Structures," Second Symposium on Structural Optimization, AGARD CP-123, Milan, April 1973.
- 24. Kiusalaas, J., "Minimum Weight Design of Structures via Optimality Criteria," NASA TN-D-7115, December 1972.
- Kiusalaas, J., "Optimum Design of Structures with Buckling Constraint,"
 Int. Journal of Solids and Structures, Vol. 9, No. 7, July 1973, pp. 863-878.
- 26. MacDonough, E. P., "The Minimum Weight Design of Wings for Flutter Conditions," J. Aeron. Sci., Vol. 20, No. 8, August 1953, pp. 573-574.
- 27. Head, A. L., Jr., "A Philosophy of Design for Flutter," <u>Proceedings AIAA National Specialists Meeting on Dynamics and Aeroelasticity</u>, Ft. Worth, Texas, November 1958.
- 28. Ashley, H. and McIntosh, S. C., Jr., "Expanding the Consciousness of the Aeroelastician," Fluid Solid Interaction, ASME 1967, pp. 120-143.
- 29. Armand, J.-L. and Vitte, W.J., "Foundations of Aeroelastic Optimization and Some Applications to Continuous Systems," Department of Aeronautics and Astronautics SUDAAR No. 390, Stanford University, January 1970.
- 30. Weisshaar, T.A., "An Application of Control Theory Methods to the Optimization of Structures Having Dynamic or Aeroelastic Constraints," Department of Aeronautics and Astronautics SUDAAR No. 412, Stanford University, October 1970.
- 31. Turner, M. J., "Optimization of Structures to Satisfy Flutter Requirements," AIAA Journal, Vol. 7, No. 5, May 1969, pp. 945-951.
- 32. RudisiII, C.S. and Bhatía, K.G., "Optimization of Complex Structures to Satisfy Flutter Requirements," <u>AIAA Journal</u>, Vol. 9, No. 8, August 1971, pp. 1487-1491.

- 33. Fox, R. L., Miura, H., and Rao, S. S., "Automated Design Optimization of Supersonic Airplane Wing Structures under Dynamic Constraints,"

 Proc. AIAA/ASME 13th Structures, Structural Dynamics and Materials
 Conference, San Antonio Texas, Paper 72-333, April 1972.
- 34. Gwin, L. B. and Taylor, R. F., "A General Method for Flutter Optimization," AIAA Journal, Vol. 11, No. 12, December 1973, pp. 1613-1617.
- 35. Siegel, S., "A Flutter Optimization Program for Aircraft Structural Design," AIAA 4th Aircraft Design, Flight Test and Operations Meeting, Los Angeles, California, Paper 72-795, August 1972.
- 36. Pines, S. and Newman, M., "Constrained Structural Optimization for Aeroelastic Requirements," <u>Journal of Aircraft</u>, Vol. 11, No. 6, June 1974, pp. 313-320.
- 37. Haftka, R. T., Starnes, J. H., Jr., and Barton, F. W., "A Comparison of Two Types of Structural Optimization Procedures for Satisfying Flutter Requriements," AIAA/ASME/SAE 15th Structures, Structural Dynamics and Materials Conference, Los Vegas, California, Paper 46-405, April 1974.
- 38. Stroud, J.W., "Automated Structural Design with Aeroelastic Constraints:
 A Review and Assessment of the State of the Art," Proc. ASME Winter
 Annual Meeting, New York, November 1974.
- 39. Bisplinghoff, R. L., Ashley, H., and Halfman, R. L., <u>Aeroelasticity</u>, Addison-Wesley, Massachusetts, 1955.
- 40. Jacoby, S. L., Kowalik, J. S., and Pizzo, J. T., <u>Iterative Methods for Nonlinear Optimization Problems</u>, Prentice-Hall, 1972.
- 41. Wilde, D. J., and Beightler, C.S., <u>Foundations of Optimization</u>, Prentice-Hall Inc., Englewood Cliffs, 1967.
- Bellman, R., <u>Dynamic Programming</u>, Princeton University Press, Princeton, NJ, 1967.

- 43. Prager, W., Optimality Criteria in Structural Design, "AGARD-R-589-71, December 1971.
- 44. Scanlan, R. H. and Rosenbaum, R., <u>Introduction to the Study of Aircraft</u>
 Vibration and Flutter, MacMillan Co., New York, 1951.
- 45. Gwin, L. and McIntosh, S. C., Jr., "A Method of Minimum Weight Synthesis for Flutter Requirements," AFFDL-TR-72-22, Part I and II, June 1972.
- 46. Gwin, L. and McIntosh, S. C., Jr., "Large Scale Flutter Optimization of Lifting Surfaces," AFFDL-TR-73-91, Part I and II, January 1974.
- 47. Vepa, R., "Finite State Modeling of Aeroelastic Systems," Ph. D. Dissertation, Department of Applied Mechanics, Stanford University, (to be published in 1975).
- 48. Albano, E. and Rodden, W. P., "A Doublet-Lattice Method for Calculating Lift Distributions on Oscillating Surfaces in Subsonic Flow," AIAA Journal, Vol. 7, No. 2, February 1969, pp. 279-285.
- 49. Soraasli, O. O. and Sobieszczanski, J., "Design Oriented Structural Analysis," AIAA/ASME/SAE 14th Structures, Structural Dynamics and Materials Conference, Williamsburg, Virginia, March 1973.
- 50. Bhatia, K. G., "Rapid Iterative Reanalysis for Automated Design," NASA TN D-4353, 1971.
- 51. Fox, R. L. and Miura, H., "An Approximate Analysis Technique for Design Calculation," AIAA Journal, Vol. 9, No. 1, January 1971, pp. 177-179.
- 52. Noor, A. K. and Lowder, H. E., "Approximate Techniques of Structural Reanalysis," <u>Computers and Structures</u>, Vol. 4, No. 4, August 1974, pp. 801-812.

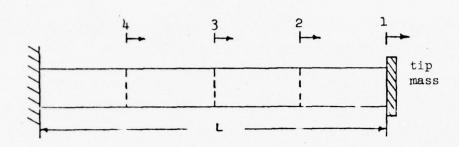


Fig. 1. Fixed-free rod in axial free-vibration

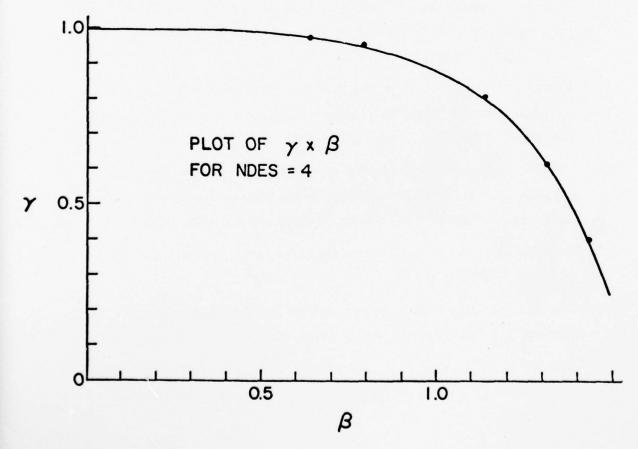


Fig. 2. Plot of γ ratio as a function of the non-dimensional frequency β for the fixed-free rod.

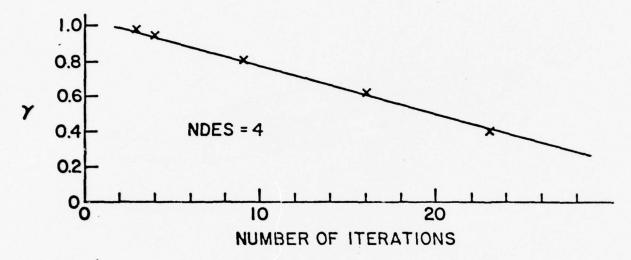


Fig. 3. Plot of γ ratio as a function of the number of iterations for the fixed-free rod.

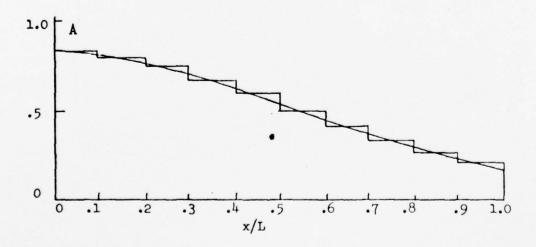


Fig. 4. Comparison between the cross sectional area distribution of the optimum rod as given by a ten-element approximation using the hybrid algorithm and Turner's analytic solution (the analytic solution is given by the smooth line).

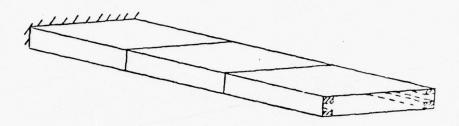


Fig. 5. Fixed-free bending torsion box in free-vibration.

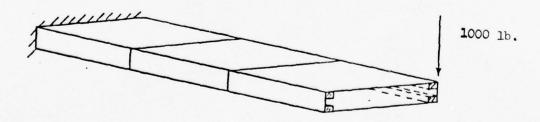


Fig. 7. Fixed-free bending torsion box with an applied load.

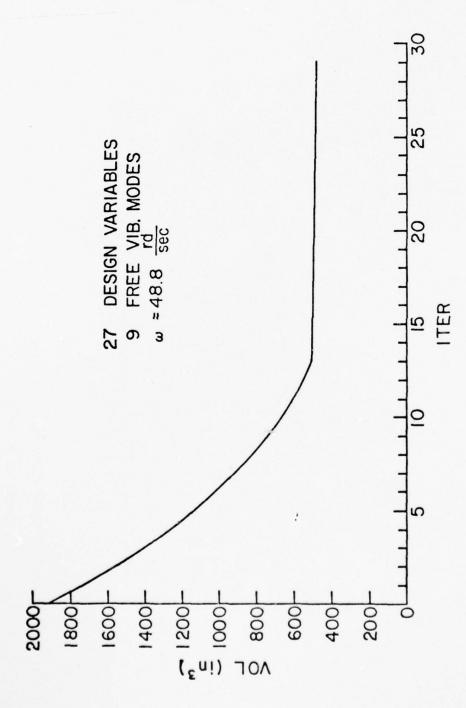
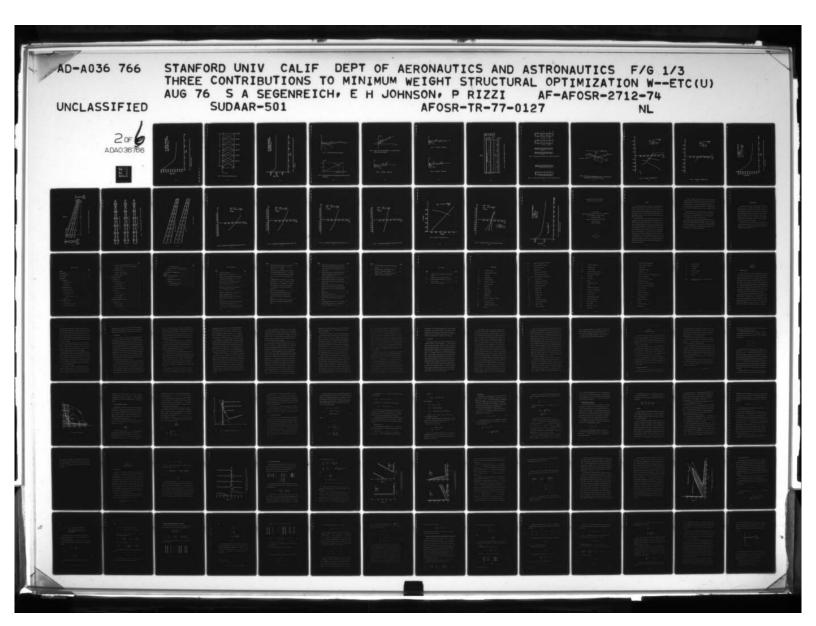


Fig. 6. Optimization history diagram for the bending torsion box in free-vibration.



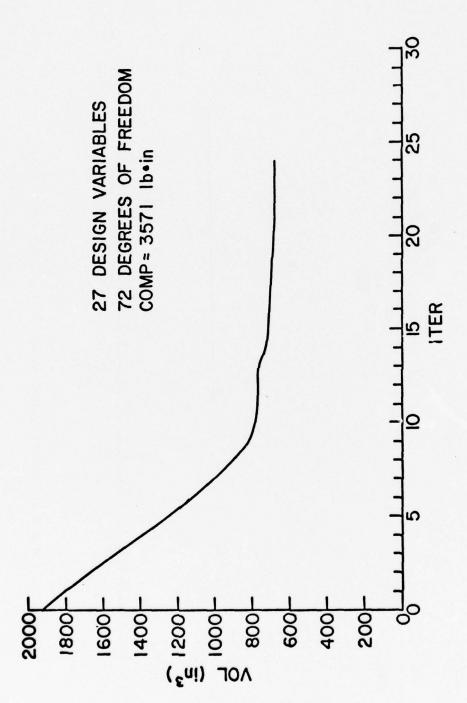


Fig. 8. Optimization history diagram for the bending torsion box with static compliance constraint,

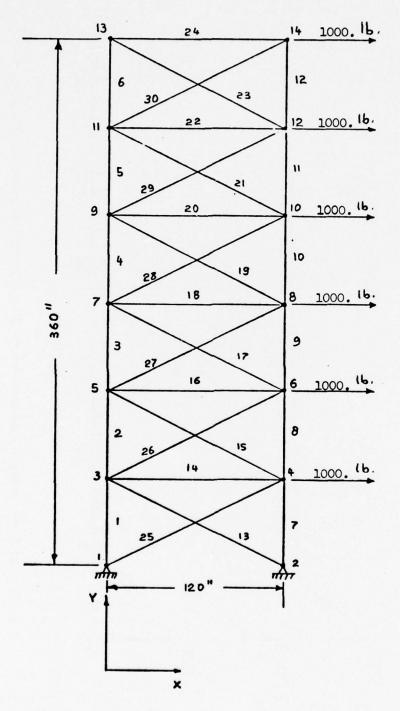


Fig. 9. 30-bar plane truss with applied loads.

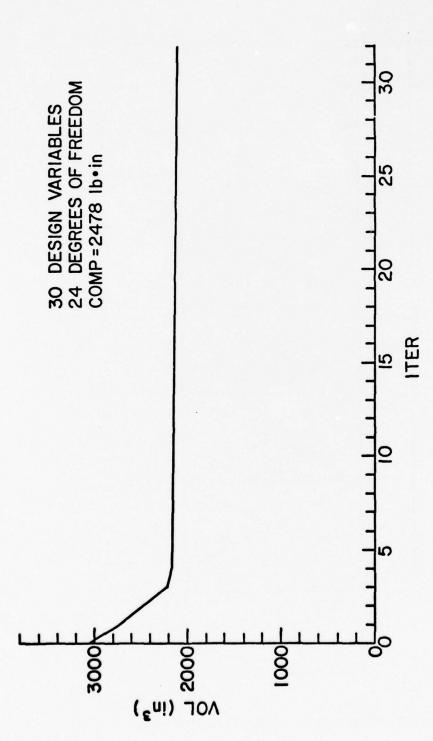


Fig. 10. Optimization history diagram for the 30-bar truss with static compliance constraint

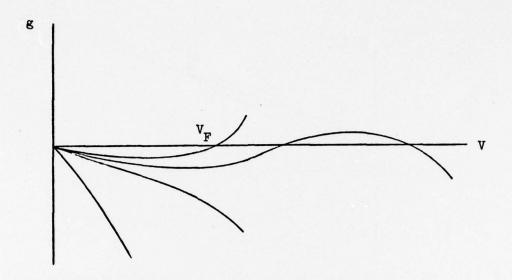


Fig. 11. V-g diagram for an aeroelastic system.

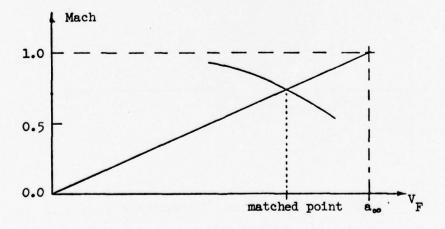


Fig. 12. Plot of critical speeds versus Mach number showing the consistent matched point.

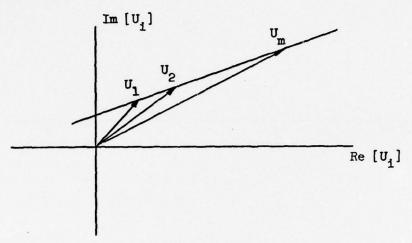


Fig. 13. Plot of U_{i} for each design variable i on a complex plane when optimality condition is satisfied.

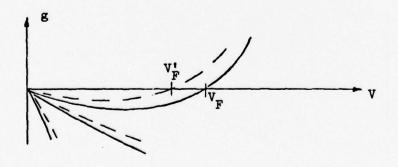


Fig. 14. V-g diagram. Regular type.

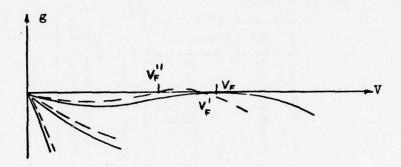


Fig. 15. V-g diagram. Tangent type.

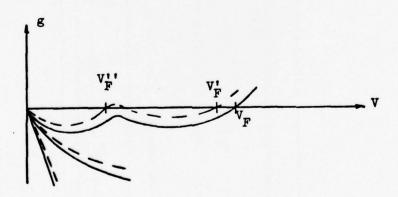


Fig. 16. V-g diagram. "Hump" type.

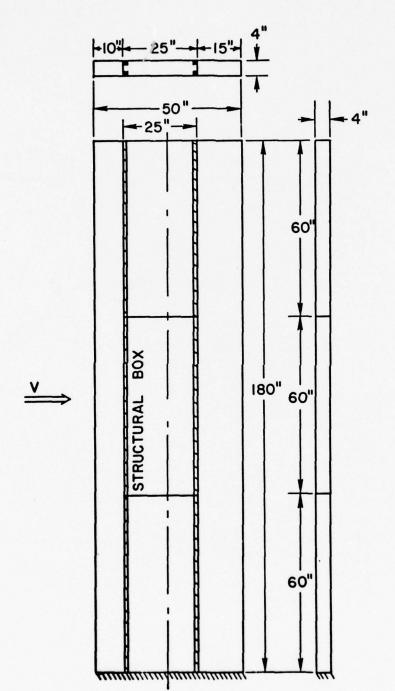


Fig. 20. 27-design variable rectangular wing. Dimensions.

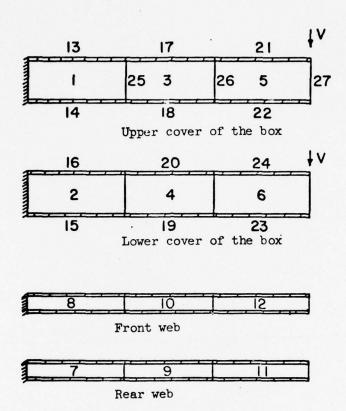


Fig. 21. 27-design variable rectangular wing. Design variable definition.

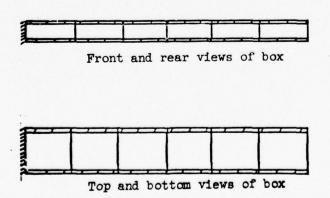


Fig. 22. 27-design variable rectangular wing. Finite element sub-division.

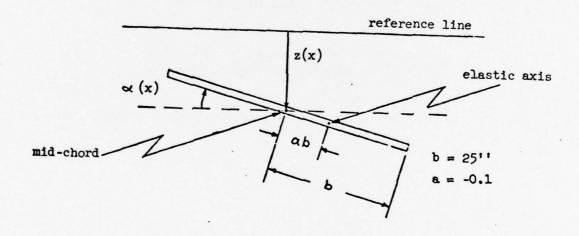


Fig. 23. Cross section of rectangular wing at station x, showing vertical displacement and rotational degrees of freedom.

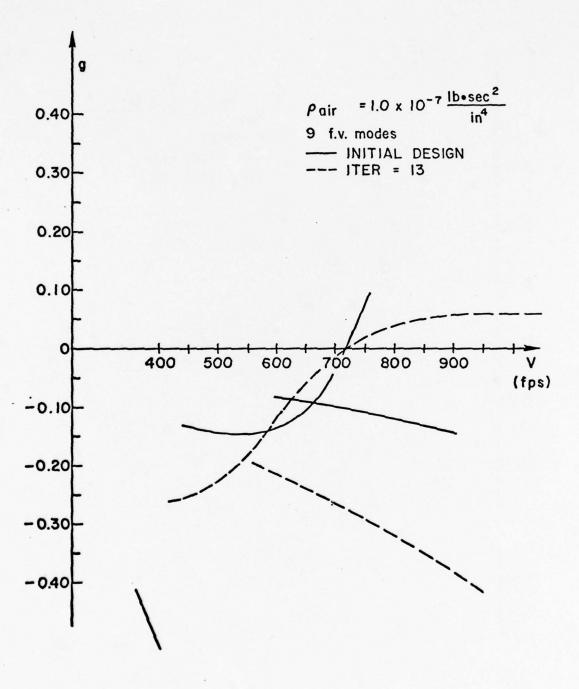


Fig. 24. V-g diagram. Rectangular wing.

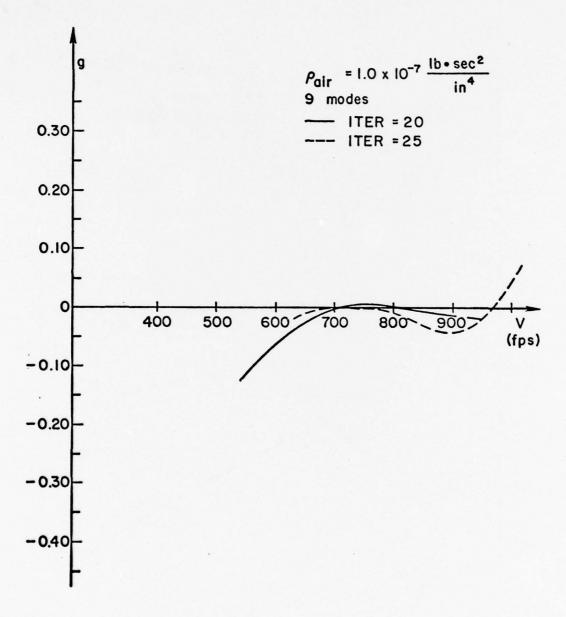


Fig. 25. V-g diagram. Rectangular wing.

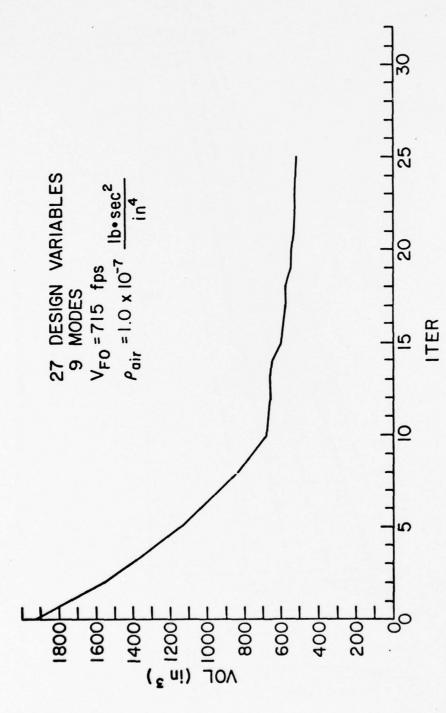


Fig. 26. Optimization history for 27-design variable rectangular wing under flutter constraint.

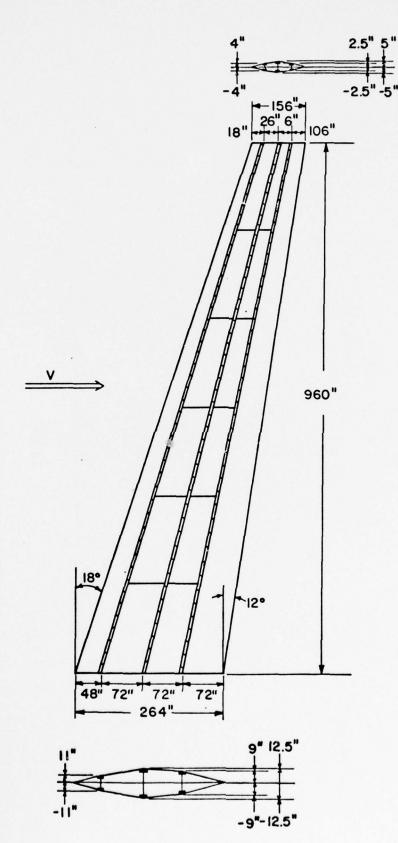
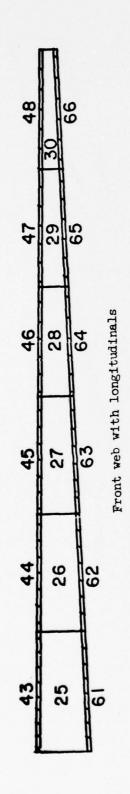
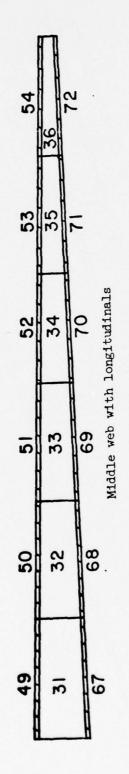


Fig. 27. 90-design variable swept wing. Dimensions.





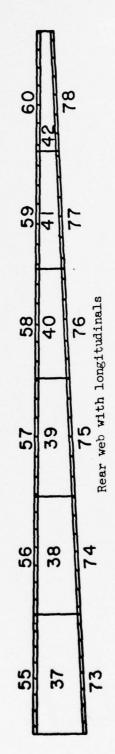


Fig. 28. 90-design variable swept wing. Design variables definition.

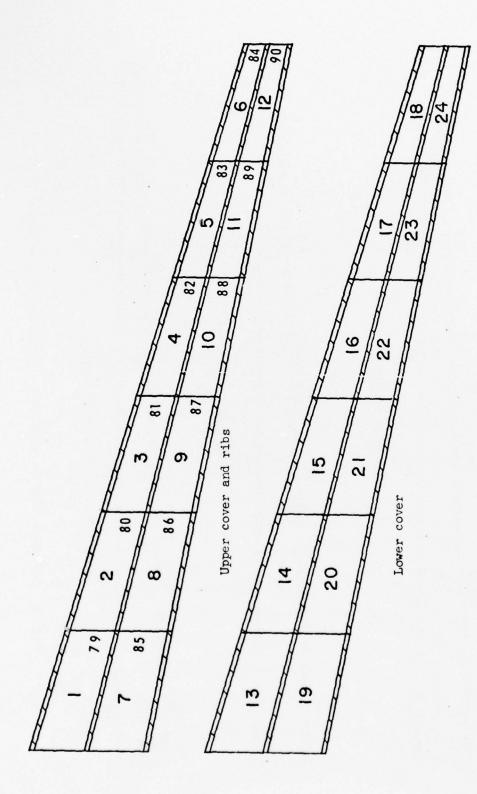


Fig. 28. (Continued)

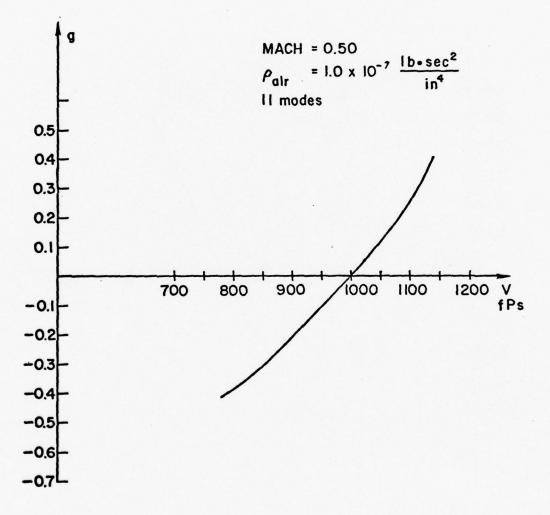


Fig. 29. V-g diagram for initial design of swept wing. Mach = 0.50.

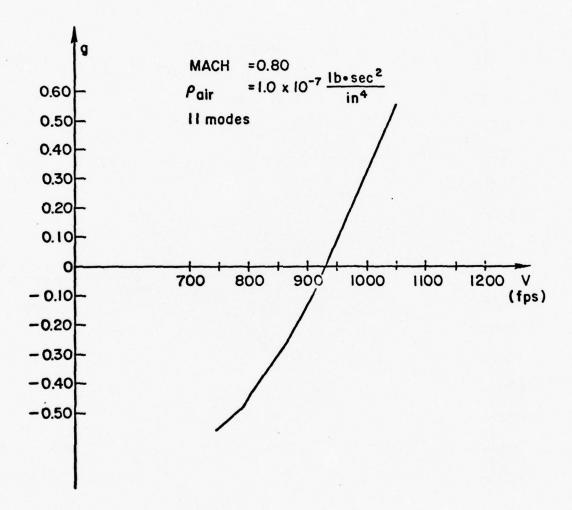


Fig. 30. V-g diagram for initial design of swept wing. Mach = 0.80.

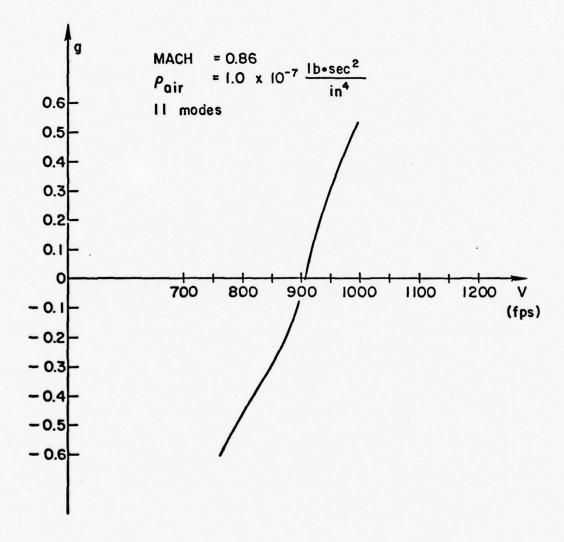


Fig. 31. V-g diagram for initial design of swept wing. Mach = 0.86.

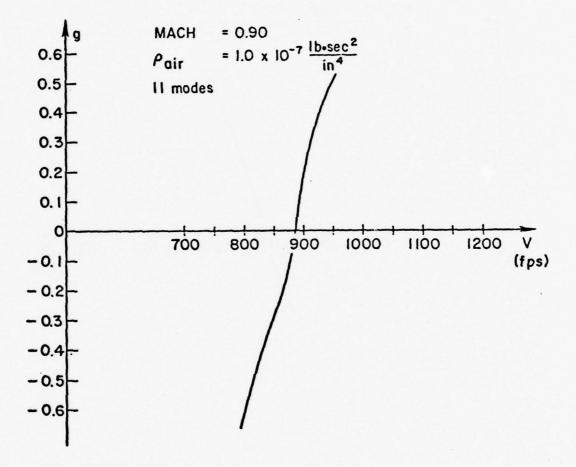


Fig. 32. V-g diagram for initial design of swept wing. Mach = 0.90. A- 98

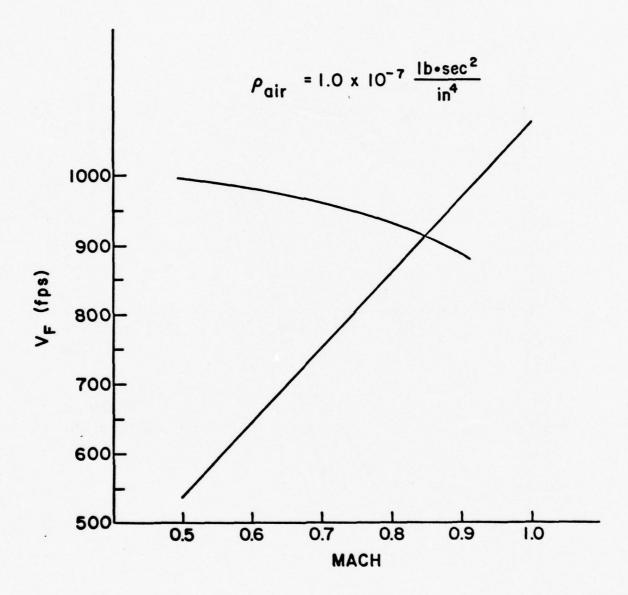


Fig. 33. Diagram for matched flutter speed.

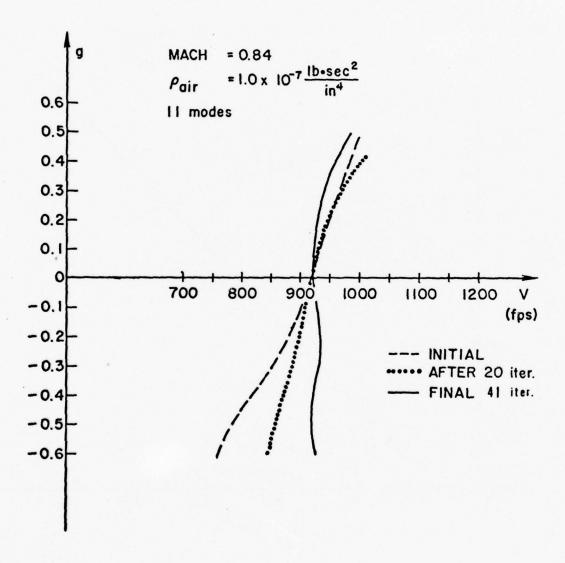


Fig. 34. V-g diagrams for initial, intermediate and final designs.

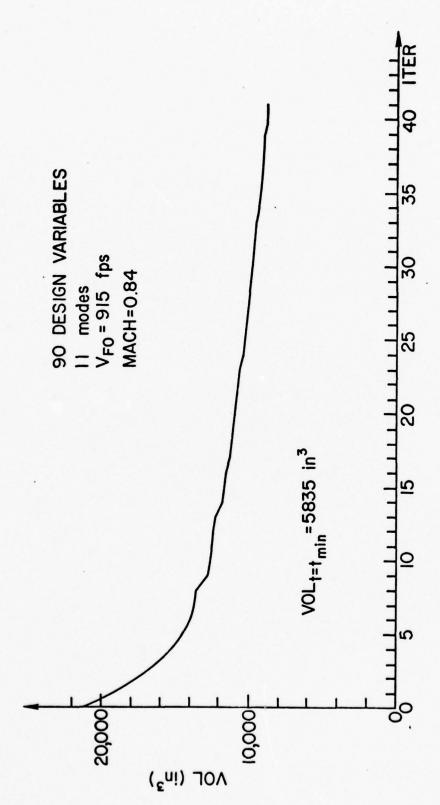


Fig. 35. Optimization history diagram for 90-design variable swept wing under flutter constraint.

OPTIMIZATION OF STRUCTURES UNDERGOING HARMONIC OR STOCHASTIC EXCITATION

A DISSERTATION

SUBMITTED TO THE DEPARTMENT OF AERONAUTICS AND ASTRONAUTICS

AND THE COMMITTEE ON GRADUATE STUDIES

OF STANFORD UNIVERSITY

IN PARTIAL FULFILLMENT OF THE REQUIREMENTS

FOR THE DEGREE OF

DOCTOR OF PHILOSOPHY

By

Erwin Harry Johnson

May 1975

ABSTRACT

This study investigates the optimal design of simple structures subjected to dynamic loads, with constraints on the structures' responses. Previous studies have mainly dealt with static loads, and their methodology has been extended here to time dependent cases. The contributions of this work are in the formulation and satisfaction of the complicated dynamic constraints and in the insights gained into the nature of these problems.

Three separate analyses search for the optimal design of: (1) one-dimensional structures excited by harmonically oscillating loads, (2) similar structures excited by white noise and (3) a wing in the presence of continuous atmospheric turbulence. The first problem has constraints on the maximum allowable stress while the last two place bounds on the probability of failure of the structure. In all of these problems, approximations are made in order to replace the time parameter with a frequency parameter. For the first, this involves the simple assumption that the steady state response is the area of interest. In the remaining cases, power spectral techniques are employed to find the root mean square values of the responses. The primary means of search for the optimal solutions is through the use of computer algorithms that combine finite element methods with optimization techniques based on mathematical programming.

A general conclusion is that the inertial loads for these dynamic problems can result in optimal structures that are radically different from those obtained for structures loaded statically by forces of comparable magnitude. In the case of the harmonically loaded structure, it is found that the design space can be disjoint. This makes the task of finding the global optimum difficult for even the simplest of problems.

An interesting feature of the optimal designs for cantilevered structures with a white noise excitation is that there is a tendency for some mass to be concentrated near the tip. The inertial forces from this mass tend to relieve the inboard stress.

The wing in a turbulent gust environment demonstrates a possible practical application of the methods developed in the study. The model used contains a fuselage and nacelle and permits rigid body plunging as well as transverse bending. It is felt that the preliminary techniques developed are of practical value towards the design of aircraft that have fatigue life as an important design factor.

ACKNOWLEDGMENTS

The author wishes to express his appreciation to Dr. Samuel C. McIntosh, Jr. who, in the capacity of thesis adviser, aided in the original definition and development of the thesis. Professor Holt Ashley assumed the adviser duties, and his enthusiasm and physical understanding helped bring this work to completion. Valuable assistance was obtained from fellow students Paulo Rizzi and Solly Segenreich and from Dr. Garrett N. Vanderplaats of the NASA Ames Research Center. Suzanne Bennett expertly typed the final manuscript while under a tight time schedule.

The Fannie and John Hertz Foundation provided generous fellowship aid during the last two years of the author's doctoral studies. Additional funds for computer expenses were partially supplied by NASA under Contract NASA NGL 05-020-243.

TABLE OF CONTENTS

<u>Pe</u>	ge
ABSTRACT	ii
ACKNOWLEDGMENTS	v
LIST OF ILLUSTRATIONS	ix
LIST OF TABLES	ii
NOMENCLATURE	iv
I. INTRODUCTION	1
A. Problem Motivation	1
B. Related Work	3
C. Scope of Work	9
II. OPTIMIZATION TECHNIQUES	13
A. Concepts of Optimization	13
B. Interior Penalty Function	17
C. Variable Metric Method	
1. Interpolation	24
2. Minimum Thickness Constraints	26
D. Comments	27
III. HARMONIC EXCITATION	31
A. Introduction	31
B. Two Design Variable Example	34
C. Function Space Solutions	43

		<u>Pa</u>	ge
		1. Example: Cantilevered Beam With a Static Load	46
		2. Example: Torsional Rod Excited by a Harmonically	
		Varying End Load	51
	D.	Finite Element Solutions	59
		1. Example: Cantilevered Rod	60
		2. Example: Cantilevered Beam	67
	Ε.	Concluding Comments	70
IV.	WHI	TE NOISE LOADING	74
	Α.	Introduction	74
	В.	Failure Criteria	76
		1. First Excursion Failure	78
		2. Fatigue Failure	82
	C.	Response to White Noise	86
		1. Derivative Calculations	97
	D.	Examples	02
		1. Torsion Rod	04
		2. Effects of Tip Mass	08
		3. Cantilevered Beam	12
	Ε.	Concluding Comments	16
v.	CON	TINUOUS ATMOSPHERIC TURBULENCE	18
	Α.	Introduction	18
	В.	Computational Models	19
		1. Structural Model	19
		2. Turbulence Model	22

	<u>Pa</u>	gε
	3. Aerodynamic Operators	23
С.	Response Quantities and Gradient Evaluation 12	28
D.	Results	35
VI. CON	CLUSIONS AND RECOMMENDATIONS	+5
REFERENCE	s	50
APPENDIX:	FINITE ELEMENT MODELS	57
Α.	Torsion Rod	57
В.	Cantilevered Beam in Bending 16	1
С.	Tapered Wing	56
	1. Mass and Stiffness Matrices 16	57
	2. Aerodynamic Matrices	59

LIST OF ILLUSTRATIONS

Figure		Page
2.1	Concepts of Optimization	16
2.2	Extended Interior Penalty Function	19
3.1	Response of the Tip of a Uniform Rod Excited by a	
	Uniformly Distributed Harmonic Load as a Function	
	of the Frequency of Excitation	33
3.2	Design Space for a Cantilevered Rod Excited in	
	Torsion at Nondimensional Frequency $\boldsymbol{\lambda}_{\boldsymbol{e}}$.	
	(a) $\lambda_{e} = 0.0$; (b) $\lambda_{e} = 1/24$	36
3.3	Design Space for a Cantilevered Rod Excited in	
	Torsion at Nondimensional Frequency $\boldsymbol{\lambda}_{e}$.	
	(a) $\lambda_{e} = 1/6$; (b) $\lambda_{e} = 3$	37
3.4	Comparison of Two-Dimensional Design Spaces for	
	Damped and Undamped Solutions, $\lambda_e = 1/6$	42
3.5	Optimal Thickness Distribution for a Cantilevered	
	Rod Using Ten Finite Elements. (a) $\overline{\omega}_{\mathbf{e}}^2 = 0.0$;	
	(b) $\overline{\omega}_{\mathbf{e}}^2 = 1.0$	63
3.6	Two Solutions for the Optimal Thickness Distribution	
	of a Cantilevered Rod Excited at $\frac{1}{100} = 4.0$.	
	(a) Structure's First Natural Frequency Greater Than	
	$\omega_{\mathbf{e}}$; (b) Structure's First Natural Frequency Less	
	Than ω_{e}	65

Figure	<u>I</u>	Page
3.7	Optimal Thickness Distribution for a Cantilevered	
	Beam Using Five Finite Elements. (a) $\omega_e = 42.5$	
	rad/sec; (b) $\omega_e = 100 \text{ rad/sec} \dots \dots$	69
3.8	Two Solutions for the Optimal Thickness Distribution	
	of a Cantilevered Beam Excited at $\omega_e = 80 \text{ rad/sec}$.	
	(a) Structure's First Natural Frequency Greater Than	
	$\omega_{\mathbf{e}}$; (b) Structure's First Natural Frequency Less	
	Than $\omega_{\mathbf{e}}$	71
3.9	$(a) \ \ \textbf{Optimal} \ \ \textbf{Thickness} \ \ \textbf{Distribution} \ \ \textbf{for} \ \ \textbf{a} \ \ \textbf{Cantilevered}$	
	Beam Excited at 170 rad/sec $(\omega_{ m e}>{ m Structure's}$ First	
	Natural Frequency). (b) Comparison of the Weights of	
	Local Optima as a Function of Excitation Frequency	
	$(\omega_1^{} \equiv$ the Structure's First Natural Frequency)	72
4.1	Exceedances of U	79
4.2	Peaks in a Record of Random Noise	84
4.3	Representative Power Spectral Density Shapes for	
	a Structural System with a White Noise Input.	
	(a) White Noise Excitation; (b) Representative	
	Response	103
4.4	Optimal Thickness Distributions for a Cantilevered	
	Rod Excited by a Uniformly Distributed White Noise	
	Torque	106

Figure		Page
4.5	Optimal Thickness Distribution for a Cantilevered	
	Rod Excited by a Uniformly Distributed White Noise	
	Torque - Comparison of Solutions Using Two and Four	
	Natural Modes	1 07
4.6	Root Mean Square Stress in a Uniform Cantilevered	
	Beam with a Concentrated Tip Mass Excited by Uni-	
	formly Distributed White Noise	110
4.7	Root Mean Square Stress Rate of the Beam of Fig. 4.6 .	111
4.8	Optimal Thickness Distribution of a Cantilevered	
	Beam Excited by a Uniformly Distributed White Noise	
	Transverse Load	114
4.9	Optimal Thickness Distribution for a Cantilevered	
	Beam Excited by a Uniformly Distributed White Noise	
	Transverse Load - Effect of the Number of Structural	
	Modes	115
5.1	Wing Planform	120
5.2	Comparison of Excitation Spectra	124
5.3	Optimal Thickness Distribution for a Wing Excited by	
	Continuous Atmospheric Turbulence (Three Finite	
	Elements)	138
5.4	Root Bending Moment Power Spectra of Initial Design	140
5.5	Optimal Thickness Distribution for a Wing Excited	
	by Continuous Atmospheric Turbulence	141

Figure		Page
5.6	Root Bending Moment Power Spectrum of the Optimal	
	Design	. 143
A.1	Cantilevered Rod. (a) Representation Using n	
	Elements; (b) Individual Rod Element	. 158
A.2	Cantilevered Beam. (a) Representation Using n	
	Elements; (b) Individual Beam Element	162

LIST OF TABLES

<u>Table</u>		Page
3.1	Properties of the Two Thickness Distributions of	
	Figure 3.6	66
4.1	Comparison of Two and Four Mode Solutions	105
4.2	Cantilevered Beam: Comparison of Two and Four	
	Mode Solutions	113
5.1	Wing in a Turbulent Atmosphere	142

NOMENCLATURE

[A]	Aerodynamic matrix
a _i	Modal participation factor
Ъ	Beam width
b(y)	Wing semichord
b _{ref}	Reference semichord
C(k)	Theodorsen's function
c(y)	Wing chord length
d	Beam depth
DR	Damage rate
E	Young's modulus
E()	Expected value
G	Shear modulus
g _i	Equality or inequality constraint
{G}	Vector of gust loads
{ GG }	Generalized gust loads
[GA]	Generalized aerodynamic forces
Н	Hamiltonian

[H]	Matrix in variable metric algorithm
\mathbf{I}_{α}	Mass polar moment of inertia
I	Area moment of inertia
$\mathfrak{Im}(\mathbf{z})$	Imaginary part
J	cost function or functional
J	Area polar moment of inertia
J _O ()& J ₁ ()	Bessel functions of the first kind
[K]	Stiffness matrix
[K]	Generalized stiffness matrix
k	Reduced frequency $(= \omega b_{ref}/U)$
L	Structural span length
l	Element length
L _F	Fatigue life
L _S	Strength life
$^{\rm L}_{ m T}$	Turbulence scale
[M]	Mass matrix
[m]	Generalized mass matrix
m _O	Structural mass/thickness
mn	Number of modes
n	Number of elements

nc	Number of constraints
P	Transverse load
$\{p_i\}$	I th mode shape
$\boldsymbol{p}_{\mathbf{x}}(\mathbf{x})$	Probability density function of x
r	Penalty function parameter
R	Rod radius
$\Re e(z)$	Real part of z
S	Stress
s	Nondimensional length
t	Time
t _i	Thickness design variable
Ŧ	Amplitude of a torsional load
υ	Free stream velocity
u _s	Ultimate stress
^u i	Transformed design variable
w	Transverse displacement
w _g	Vertical gust velocity
× _i	State variable
X _{ab}	Covariance of a and b

Complex number

α	One-dimensional search parameter
α	Structural damping parameter
Γ()	Gamma function
r	Nondimensional frequency
Δ()	Incremental value
ϵ	Transition point for the extended penalty function
θ	Rotational displacement
$\lambda_{\mathbf{i}}$	Adjoint variable of the states
λ	Nondimensional frequency
$^{\lambda}e$	Nondimensional excitation frequency
μ	Adjoint variable of the constraints
$\rho_{\mathbf{a}}$	Atmospheric density
°s	Structural density
σ _{xx}	Root mean square value of x
Φ	Augmented cost function
$\Phi^{\mathbf{x}\mathbf{x}}(\omega)$	Power spectrum of x
Ω	Spatial frequency $(=\omega/U)$
ω	Frequency
© _e	Excitation frequency
©i	Modal frequency

∇() Gradient operator

()' Differentiation

()^T Transpose

() Complex conjugate

{ } Column vector

[] Matrix

Note: Additional nomenclature is explicitly defined in the text

CHAPTER I

INTRODUCTION

A. PROBLEM MOTIVATION

The goal of the field of structural optimization can be succinctly described as one of finding the structure of least weight that satisfies certain specified constraints. The combination of more efficient algorithms with modern computers has expanded the capabilities of this field rapidly and to the extent that techniques have been developed that routinely optimize practical, statically loaded structures. Similar results for dynamically loaded structures have lagged behind due to the complications introduced by inertial loads and the time parameter. This thesis attempts a partial remedy of this situation by investigating a series of dynamic response problems in order to find the least weight structure that can withstand the dynamic loads.

The design of many engineering structures is influenced by the dynamic loads that act on the structure so that the search for optimal structures is a legitimate exercise. Landing impacts, gust excitation, rotating machinery and acoustic noise create loads on aeronautical vehicles that are dynamic in nature and that are of primary importance in the design of aircraft substructures. Similarly, for astronautical vehicles, rocket exhausts and atmospheric turbulence

B - 1 -

are important design loads. These aerospace applications were the ones that were kept in mind while the methods of analysis used in this thesis were developed. However, other disciplines could benefit from the methods presented here. Specifically, for architectural structures, earthquakes and winds create loads that are dynamic in nature, and these loads are playing an increasingly important role in building design. Further examples could be drawn from naval architecture and from mechanical design.

Many of the examples mentioned above include loads that are stochastic, or random, in nature. Coupled with the fact that a large proportion of in-service failure of metal structures are due to fatigue, this provides a powerful motivation for studying the optimal design of structures under stochastic loading conditions.

While no claim is made as to the direct applicability of the techniques developed in this work to practical problems in engineering design, techniques are developed and results achieved that could be a useful starting point for the more practical problems. The usefulness is enhanced by the use of constraints in the examples worked that are of practical interest in actual designs. For instance, constraints are placed on the maximum stress in the structure or on the fatigue life in the case of random loads.

Due to the paucity of studies dealing with the optimization of dynamically loaded structures, it is felt that this work makes significant contributions to the basic understanding of these types of problems. The inertial loads present in these problems can have an important effect on the loads a structure is required to withstand.

The results obtained show that the optimal structure can be radically different from one obtained based on static strength considerations.

B. RELATED WORK

This section presents a survey of studies that have been done that relate to the present one, pointing out their characteristics and how they compare with the present study. The thesis uses elements from a number of disciplines, but the unique portion of this work is the use of structural optimization and it is in this area that the survey will concern itself. Even in this specialized field, it would be impractical to give a comprehensive survey; instead, only the most relevant works are described. A more general view of the structural optimization field can be obtained from a survey article by Sheu and Prager (Ref. 1) while a text by Fox (Ref. 2) serves as an excellent introduction to the computational aspects of optimal design. Two recent conferences (Ref. 3 and Ref. 4) provide "state of the art" descriptions of various portions of the field.

Structural optimization with constraints on the dynamic behavior is a more specific area that includes the present study. A survey by Pierson (Ref. 5) on this subject divided it further into two subdivisions: (1) problems with eigenvalue constraints, and (2) problems with constraints on the response. The present investigation clearly falls into the latter category, but problems of the first kind played an important role in the development of the methodology used in this

report. In particular, references 6 through 10 are works that place constraints on the natural frequency or the flutter speed of the systems to be optimized and that provided a basis from which to attack the response problem. In fact, as Pierson pointed out, one of the dynamic response problems solved by Icerman (Ref. 11) has results identical to a problem with a natural frequency constraint that was first solved by Turner (Ref. 9).

It is to be understood that the five references cited above for the eigenvalue constraint studies are in no way inclusive of the contributions made to these problems. An attempt is made below to include all the significant studies that have been conducted with constraints on dynamic response quantities. These papers are a small, but rapidly increasing, part of the literature.

The relative youth of the field presents difficulties when one tries to classify the types of problems that have been studied. The ideal procedure would be to describe the problem that was studied, the method of solution and a discussion of results. Unfortunately, and unlike the more developed field of optimization with static loads, each paper treats a unique problem, usually in a unique way and, of course, obtains a unique result. Therefore, only the features of the studies that are relevant to the present work will be stressed in what follows.

The youthfulness of the field is indicated by the fact that the earliest papers of this type known to the author were published in 1968. This work, published by Brach in two papers (Ref. 12 and Ref. 13),

found approximate optimal solutions for some one-dimensional structures loaded by impulsive or step forces. The problem formulation for these studies was in terms of finding the structure of fixed weight that minimized a specified deflection. This is a transformation of the formulation used in this work: finding the structure of least weight with a constraint on the size of the maximum deflection.

Fox and Kapoor (Ref. 14) published another "early" work that developed a mathematical programming algorithm for finding the optimal design of truss-frame structures subjected to a half-cycle sine pulse. The response was estimated by using shock spectral techniques that gave conservative upper bound limits on the deflection and stress. A previous work by Fox and Kapoor (Ref. 15) made the important contribution of developing a simple technique for finding the derivatives of the eigenvalues and eigenvectors with respect to the system parameters.

Levy and Wolf (Ref. 16 and Ref. 17) provide a means of finding the fully stressed design for one-dimensional structures under dynamic loading. A fully stressed design is one where all structural elements exactly satisfy the stress constraints imposed on them. The motivation for their study comes from the fact that for determinate, statically loaded structures with constraints on the stress, the fully stressed design is optimal. For the impulsive loading conditions and the finite element representations used, the solutions shown in these references are found to be optimal. However, fully stressed designs are usually not optimal in cases where more general dynamic loads are considered.

A series of related papers by Venkayya, et al. (Ref. 18 and Ref. 19) describes an optimality criterion that is used to find approximate optimal solutions for various types of dynamic loading. The criterion was developed specifically for problems with constraints on the natural frequency, so that it is exact for that case. When more general dynamic conditions are considered, the results obtained have to be considered as preliminary, qualitative designs.

A specific area of practical interest that can benefit from the methods of optimization with dynamic constraints is that of the optimal design of structures to withstand earthquake loads. The 5th World Conference on Earthquake Engineering held in Rome in June, 1973 included four short papers on this topic. One of these, by Solnes and Holst (Ref. 20), replaced the dynamic load by an equivalent static load, so that it is not a dynamic response problem, strictly speaking. However, inertial effects are artificially included in the statically equivalent load. Another paper from the conference, by Nigam and Narayanan (Ref. 21), considered the excitation to be either a specified acceleration or a probabilistic acceleration with a given power spectrum. The techniques employed in the paper and in another paper by Nigam (Ref. 22) to deal with the probabilistic nature of the excitation come closest to the techniques employed in Chapters IV and V of the present work to treat similar loadings. Another work of optimization for earthquake type of loads is given by Kato, et al. (Ref. 23). The loads in this case are approximated by shock spectra in a manner similar to that of Ref. 14. The diversity of models and

techniques used to study the optimization problem for civil engineering structures indicates that it is a fertile ground for further research and systemization.

A study that is more general in scope, but that has application to the earthquake problem, is contained in a recent report by Cassis (Ref. 24). In this case, the load is modelled as a half-cycle sine pulse and the response is obtained by performing a time integration of the equations of motion. The constraints considered include integrals of the time history of the response. This is one of the few papers dealing with dynamic response that retain the time parameter in an explicit form. It is also the first report known to the author that includes mention of the fact that the feasible design space can be disjoint for certain types of dynamic excitations. This feature of such problems is one of the more exciting. The disjoint design space receives extensive treatment in Chapter III of this report.

Chapter III deals with the optimization of structures excited by harmonically varying loads. In one sense, this is the simplest of the dynamic response problems since the time parameter can be removed by assuming that the steady state response is the only response of interest. By the use of energy methods, Icerman (Ref. 11) was able to develop an optimality criterion for one-dimensional structures excited by a point load with an equality constraint on the displacement directly under the load. In order to develop the optimality criterion, it was necessary to add the further constraint that the excitation frequency be less than the first natural frequency of the structure. Plaut

(Ref. 25) made a similar investigation but allowed the loading to be more general. While several examples were analyzed, and their optimality criteria obtained, no explicit solutions were shown in this second study. Mroz (Ref. 26) conducted a mathematically more rigorous study, which replaced the displacement constraints by one on the dynamic compliance of the structure. This is defined as the integral, over the entire structure, of the product of the magnitude of the load times the magnitude of the displacement under it. Despite the successes reported in these studies, the author knows of no effort that was made to expand on the results. An obvious, although difficult, extension would be to find an energy method that allowed the sinusoidal excitation to be applied at a frequency greater than the structures' first natural frequency.

Finally, a series of papers that deal with static loads should be mentioned because of their relevance to the problem investigated in Chapters IV and V. They include some relatively early papers that sought optimal structures with constraints on their reliability (Ref. 27 and Ref. 28). Moses and Kinser (Ref. 29) extended these results and used mathematical programming to find the optima. Araslanov (Ref. 29) developed an optimality criterion that is applicable to simple beam structures loaded statically by forces whose properties are known only probabilistically. To do this, he defined the optimal structure to be the one where all cross sections have the same specified probability of failure. These problems are the counterpart of the present study in that they assume that the structure and the load distributions

are described in some probabilistic manner but the loads are assumed independent of time. In the present work, the structural properties are assumed to be given and the loads are constant in the space co-ordinate but vary in a probabilistic fashion with time. Perhaps an enterprising investigator will integrate these two problems.

C. SCOPE OF WORK

The preceding literature survey omitted a few papers that were considered redundant or of little importance. It is quite likely that other papers were inadvertently overlooked. However, the survey attempted to demonstrate the full scope of the field of structural optimization with dynamic excitation and to indicate that this scope is still quite narrow. In addition, few of the papers cited were published, or, if published, were known to the author when this research began. For these reasons, the work reported on here does not build on the results of previous investigations to any major extent but rather attacks new problems. Of course, the tools needed for the analyses are gathered from existing disciplines, such as structural optimization, structural dynamics, aeroelasticity and probability.

The core of the thesis is contained in three chapters that deal with three distinct optimization problems. In addition, a separate chapter describes the optimization algorithm used for the majority of the examples studied and an appendix details the finite element models that feed into each of the three problems.

The first problem is that of the structural optimization of onedimensional structures excited by harmonically oscillating loads. This is similar to the cases dealt with in references 11, 25, and 26, but a different approach is used that provides added insight into the problem. In particular, the constraint that the first natural frequency of the optimal structure be greater than the excitation frequency, which was an integral part of developing the optimality criterion of the previous studies, is removed. Another change is that the equality constraints on the displacements or the dynamic compliance are replaced by inequality constraints on the allowable stress within the structure. It is felt that these innovations provide for solutions of greater physical interest. Another facet of the present formulation is that the feasible region is disjoint. This provides an interesting theoretical result and one that may be of physical usefulness as well. The major drawback of this formulation is that it is no longer possible to find an optimality criterion based on energy methods. This forces the investigator to deal with each problem on an ad hoc basis. One way of combatting this deficiency is the construction of analytical solutions to the optimization problems by the use of concepts from optimal control. This is a technique that met with some success when applied to problems with constraints only on the natural frequencies (Ref. 9). It is introduced, with limited success, in the present investigation because it holds the promise of providing solutions that analytically detail the effects of the various parameters.

Chapter IV deals with the second problem, which is the structural optimization of one-dimensional structures excited by white noise uniformly distributed along the span. A technical note by Nigam (Ref. 22) aided in developing the means for dealing with this type of problem, although the specific structures and constraints of Chapter IV differ substantially from those used by Nigam. Since the excitation is expressed in probabilistic terms, the constraints also have to be evaluated using probability theory. Much of the chapter is therefore devoted to defining the failure criteria used to evaluate a structure's lifetime. The methods ultimately used were obtained from Chapter 9 of a text by Lin (Ref. 31) and include both fatigue failure and first excursion failure. Further analysis in Chapter IV is devoted to outlining how the response quantities and their derivatives, which are needed in the optimization procedure, are obtained through the use of superposition of natural modes. Finally, some numerical results are given and comments are made on points of interest.

The methods of the earlier chapters are applied in Chapter V to a more practical problem, that of finding the optimal design for a wing excited by continuous atmospheric turbulence. The turbulence was represented by a power spectrum so that methods similar to those used in Chapter IV could be used to obtain the lifetime of the structure. A complicating factor is the translation of the atmospheric turbulence to the loads a wing experiences. A text by Bisplinghoff, et al. (Ref. 32, Chap. 5), provided the theory that permitted this. This

text also supplied the example (Ref. 32, Example 10.6) that was optimized, a tapered unswept wing that includes a nacelle and a fuselage and allows rigid body plunging in addition to wing bending.

Finally, the last chapter summarizes the results obtained from the research and indicates areas that merit further study.

CHAPTER II

OPTIMIZATION TECHNIQUES

This chapter provides a description of the optimization methods that were used for the majority of the examples studied in this work. It does not attempt to describe alternative methods or to compare them with the methods used here. As mentioned in the introductory chapter, references 2, 3, and 4 collectively provide a good survey of the current state of various methods.

Briefly stated, the methods used here involve coupling an interior penalty function technique with a variable metric algorithm.

These methods have been described elsewhere; in particular, Fox's text (Ref. 2) provides an excellent general presentation. Therefore, the present chapter gives only a brief outline of the method with emphasis on modifications developed during the use of the techniques.

The first section defines terms that are common to optimization studies and are needed when the actual procedures are described in the following sections. A final section offers some observations on the algorithm based on experience gained from exercising it for the problems of the thesis.

A. CONCEPTS OF OPTIMIZATION

The general process of optimization entails searching for the design that minimizes some specified function while satisfying all

the limitations applied to the design or its response. This section briefly outlines the concepts that put this general concept into quantifiable terms. Since finite elements are used for the majority of examples presented in this thesis, the development is presented in terms applicable to a finite element analysis.

The first term to be defined is the objective or cost function.

This is the function (or functional) to be minimized and is designated by J. For the problems of this thesis, the cost function is always simply the sum of the design variables.

The design variable is the second concept to be defined. This is an element of the system that may be changed in the process of seeking an optimum. The present study is concerned with one-dimensional thin walled structures whose design variables are the thicknesses of individual elements. The design variables are elements of a design vector that is notationally represented by $\{t\}$. A related concept is that of the design space, which is simply the space of all physically possible design variables.

Limitations on the design are termed constraints, and it is to the formulation and satisfaction of these constraints that the bulk of the effort of this work is directed. The constraints are designated by the requirement that

$$g_i \ge 0$$
 , $(i = 1, 2, ..., no. of constraints) , (2.1)$

where $\mathbf{g}_{\mathbf{i}}$ is a function (explicit or implicit) of the design variables and the time and space coordinates.

The simple two-dimensional example shown in Fig. 2.1 depicts these concepts plus some additional terms. This figure illustrates the problem of minimizing the cost function $J = t_1^2 + t_2^2$ subject to the constraints:

$$g_1 = t_1 - 1 \ge 0$$
,
 $g_2 = t_2 - 0.5 \ge 0$,
 $g_3 = t_1 t_2 - 1 \ge 0$

The circular arcs are lines along which J is constant. The design vector is $\{t_1,t_2\}^T$ and the design space is given by all real values of t_1 and t_2 . This design space is divided into two regions by the constraint conditions: the "feasible" and the "infeasible" region. The shaded, infeasible region is where the constraints are not satisfied, while the unshaded portion is the feasible region from which the optimal design must be found. While the optimal value of $t_1 = t_2 = 1.0$ can almost be found by inspection (or by methods of ordinary calculus) in this case, it should be obvious that problems involving a large number of design variables and more complicated constraints require considerable effort and ingenuity in the search for the optimum.

A further concept that can be demonstrated with this two-dimensional example is that of the active and the inactive constraint. At

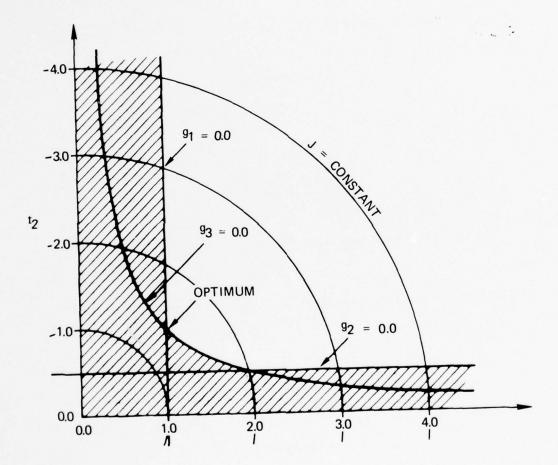


FIG. 2.1--Concepts of Optimization.

the optimum it is seen that constraints g_1 and g_3 are satisfied as equality constraints (i.e., $g_1=g_3=0.0$). These are therefore designated active constraints. Constraint g_2 is also satisfied, but the optimum does not lie on this constraint so that it is designated inactive.

B. THE INTERIOR PENALTY FUNCTION

When inequality constraints are imposed on the design, penalty function methods can be used to include the constraint in the objective function. This strategem converts the problem to one that can utilize the powerful methods used to solve the unconstrained minimization problem. Reference 2 contains a good description of these methods, and this presentation therefore focuses on the details of the particular penalty function used here.

An interior penalty function is one that forces the trial design always to be in the feasible region. The specific function used in this work was of the form:

$$\Phi = J - r \sum_{i=1}^{nc} \ell n (g_i) \qquad (2.2)$$

The modified objective function, Φ , is seen to become arbitrarily large as the design vector approaches the constraint $g_{\hat{\bf 1}}=0$. As mentioned, this has the effect of forcing the trial design to be in the feasible region. Note that the form used here requires that the constraint be in the range $0 \le g_{\hat{\bf 1}} \le 1$. This is accomplished by

redefining a given constraint so that it fits within these limits (e.g., the constraint $g_1=t_1-1.0$ of Fig. 2.1 can be cast into the equivalent form $g_1=1.0-1.0/t_1$. The r used in equation (2.2) is a specified scalar. The procedure followed is to minimize Φ for a chosen value of r and then to reduce r by some factor and repeat the optimization. In the limit as $r\to 0$, the optimal result for the modified problem is seen to be arbitrarily close to the optimum of the unmodified problem.

The extended interior penalty function method is a variation that was applied in reference 2^{l_1} to a similar penalty function method. Figure 2.2 depicts an optimization problem that aids in explaining this refinement. In this diagram the function J=ax is being minimized subject to the constraint that $x \ge b$ (or $g=1-(b/x) \ge 0$). While the modified cost function $\Phi=ax-r \ln (1.0-b/x)$ blows up as x approaches b, the extended penalty function remains finite. This is done by using the formulation:

$$\Phi = J - r \sum_{i=1}^{nc} G_i(g_i) , \qquad (2.3)$$

where:

$$G_{\mathbf{i}}(g_{\mathbf{i}}) = \begin{cases} \ln (g_{\mathbf{i}}) & g_{\mathbf{i}} \geq \epsilon \\ \\ \ln \epsilon + \frac{g_{\mathbf{i}} - \epsilon}{\epsilon} & g_{\mathbf{i}} < \epsilon \end{cases}$$

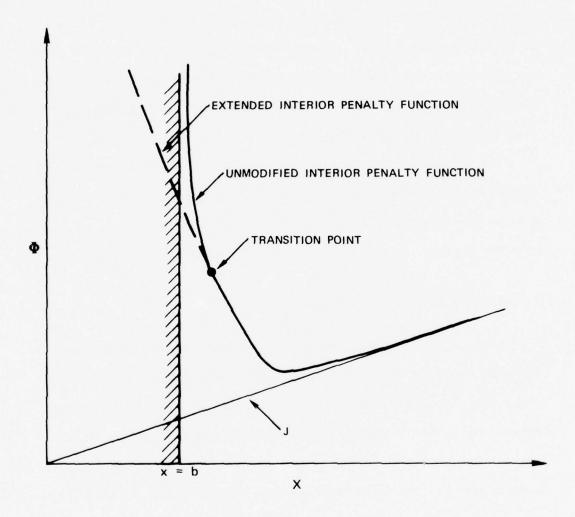


FIG. 2.2--Extended Interior Penalty Function,

The new expression is a Taylor series expansion of $\ln(g_i)$ about the point $\ln(g_i) = \epsilon$. The reason for this esoteric construction is that the optimization process can now deal with designs in the infeasible region. Analysis of designs that are infeasible may sometimes be inadvertently performed either during the one-dimensional minimization described in the next section or by starting from an initial design that is infeasible.

The value used for ϵ was selected by recourse to an argument similar to one used by Cassis (Ref. 24) for a different penalty function. For the present penalty function, this gives $\epsilon = \exp(-r/\Phi)$. More comments on this choice for ϵ are made at the end of this chapter.

C. THE VARIABLE METRIC METHOD

This section describes the particular mathematical programming algorithm used for the numerical optimizations of the thesis. When this study was in its early stages, a steepest descent algorithm was tried. The latter technique simply computes the gradient of the objective function with respect to the design vector at the design point. A new design is then found by taking an improving step in the direction of the gradient ("down the hill"). It is well known that the steepest descent method has very poor convergence properties but it was felt that it would suffice for the simple problems to be dealt with. For designs with more than three elements, this proved not to be the case.

Following an investigation of various alternative algorithms, the variable metric method (also referred to as the Davidon-Fletcher-Powell method, after its developers) was settled upon. Reference 2 contains an excellent description of this method, and what follows is essentially a summary of that description. The variable metric method can be motivated by looking at a Taylor series expansion, about design $\{t_0\}$, of an objective function:

$$\begin{split} \Phi(\mathbf{t}) &= \Phi(\mathbf{t}_{\bigcirc}) + \left\{ \nabla \Phi(\mathbf{t}_{\bigcirc}) \right\}^{T} \left\{ \Delta \mathbf{t} \right\} \\ &+ \frac{1}{2} \left\{ \Delta \mathbf{t} \right\}^{T} \left[\nabla^{2} \Phi(\mathbf{t}_{\bigcirc}) \right] \left\{ \Delta \mathbf{t} \right\} \\ &+ \text{ higher order terms} \qquad , \end{split} \tag{2.4}$$

where:

$$\{\Delta \mathbf{t}\} = \{\mathbf{t} - \mathbf{t}_0\}$$

$$= \{\nabla \Phi(\mathbf{t}_0)\} = \{\frac{\partial^{\Phi}}{\partial \mathbf{t}_i}\}_{\{\mathbf{t}\}} = \{\mathbf{t}_0\}$$

$$= \mathbf{n} \times \mathbf{n}$$

$$[\nabla^2 \Phi(\mathbf{t}_0)] = [\frac{\partial^2 \Phi}{\partial \mathbf{t}_i \partial \mathbf{t}_j}]_{\{\mathbf{t}\}} = \{\mathbf{t}_0\}$$

At the optimum $\{ \nabla\! \Phi \} \equiv \{0\}$, so that, to terms of second order, near the optimum

$$\{\nabla \Phi(\mathbf{t})\} = \{\nabla \Phi(\mathbf{t}_0)\} + [\nabla^2 \Phi(\mathbf{t}_0)] \{\Delta \mathbf{t}\} = \{0\} \qquad . \tag{2.5}$$

Starting from $\{t_0^{}\}$, the indicated correction step is:

$$\{\Delta \mathbf{t}\} = - \left[\nabla^2 \Phi(\mathbf{t}_0)\right]^{-1} \{\nabla \Phi(\mathbf{t}_0)\} \qquad (2.6)$$

If this were the actual procedure used to find the new design, it would be a second-order method. In practice, the $[\nabla^2 \Phi]$ matrix is often difficult to obtain. This is particularly true for problems dealt with here since the constraints used are very complex.

The variable metric method was developed to circumvent this problem by finding an approximation to the $[\nabla^2 \phi]^{-1}$ matrix. The method is outlined below and is followed by a brief justification of the algorithm.

Directly from Ref. 2:

- (1) Start with some initial design vector $\{t\}_{\bigcirc}$ and an initial positive definite matrix $[H]_{\bigcirc}$ (typically the identity matrix). Set $\{s\}_{\bigcirc} \equiv -[H]_{\bigcirc} \{ \nabla \Phi(t_{\bigcirc}) \}$.
- (2) Find $\{\Delta t\} = \alpha_q \{s\}_q$, picking α_q so as to minimize $\Phi(t_{q-1} + \alpha_q s_q)$. The q subscript refers to the iteration number.

(3) Compute:

$$[H]_{q+1} = [H]_q + [A]_q + [B]_q$$
 , (2.7)

where, designating

$$\begin{split} \left\{\mathbf{V}\right\}_{\mathbf{q}} & \equiv \left\{ \nabla \Phi\left(\mathbf{t}_{\mathbf{q}+\mathbf{1}}\right) - \nabla \Phi\left(\mathbf{t}_{\mathbf{q}}\right) \right\} \quad , \\ \\ \left\{\mathbf{A}\right\}_{\mathbf{q}} & \equiv \left[\alpha_{\mathbf{q}} \left\{\mathbf{S}\right\}_{\mathbf{q}}^{\mathbf{T}}\right] / \left(\left\{\mathbf{S}\right\}_{\mathbf{q}}^{\mathbf{T}} \left\{\mathbf{V}\right\}_{\mathbf{q}}\right) \\ \\ \left\{\mathbf{B}\right\}_{\mathbf{q}} & \equiv -\left[\left\{\left[\mathbf{H}\right]_{\mathbf{q}} \left\{\mathbf{V}\right\}_{\mathbf{q}}\right\} \left\{\left[\mathbf{H}\right]_{\mathbf{q}} \left\{\mathbf{V}\right\}_{\mathbf{q}}\right\}^{\mathbf{T}}\right] / \left(\left\{\mathbf{V}\right\}_{\mathbf{q}}^{\mathbf{T}} \left[\mathbf{H}\right]_{\mathbf{q}} \left\{\mathbf{V}\right\}_{\mathbf{q}}\right) \\ \end{split}$$

(4) Then set $\{s\}_{q+1} = -[H]_{q+1} \{ \nabla \Phi(t_{q+1}) \}$ and return to (2) until convergence is achieved.

This rather complicated procedure can be heuristically justified by the fact that, for a quadratic objective function with n design variables, the procedure yields $[\mathtt{H}]_n = [\nabla^2 \varphi]^{-1} \quad .$

That is, if Φ is of the form:

$$\Phi = \{t\}^{T}[M]\{t\} + [N]\{t\} + C$$
Then: $[H]_{n} = [M]^{-1}$ (2.8)

A proof of this statement can be found in Ref. 33. While the problems dealt with here are not quadratic in the design vector, the assumption is made that, close to the optimum, the objective can be approximated by a quadratic.

1. Interpolation

A remaining task is the elaboration of the rather innocent statement contained in step two of the algorithm: "picking $\alpha_{\bf q}$ so as to minimize $\Phi({\bf t_q}+\alpha_{\bf q}{\bf S_q})$ ". This entails performing a one-dimensional minimization at each iteration, and it proved to be the most difficult and time consuming aspect of the optimization. The procedure finally settled on to perform this 1-D search was a rather complex form of cubic interpolation that will be summarized here.

The goal is to find the value α^* that minimizes the scalar function $\Phi(\mathbf{t}+\alpha\mathbf{S})$. Assume that the objective function can be approximated by a cubic equation in α

$$\Phi = \mathbf{a} + \mathbf{b}\alpha + \mathbf{c}\alpha^2 + \mathbf{d}\alpha^3 \qquad . \tag{2.9}$$

If this approximation were exact, the minimum could be readily found by setting the derivative of $\,\Phi\,$ with respect to $\,\alpha\,$ equal to zero and then solving for $\,\alpha\,$:

$$\frac{\partial^{\Phi}}{\partial \alpha} = \mathbf{b} + 2\mathbf{c}\alpha + 3\mathbf{d}\alpha^2 = 0 \qquad , \tag{2.10}$$

$$\therefore \quad \alpha^* = \left(-c \pm \sqrt{c^2 - 3db}\right)/3d \quad .$$

The choice of sign is resolved by using the additional constraint that, at the minimum, the second derivative of the function is positive:

$$\frac{\partial^2 \Phi}{\partial \alpha^2} = 2\mathbf{c} + 6\mathbf{d}\alpha \ge 0 \qquad . \tag{2.11}$$

Substituting the solution for α^* from equation (2.10) into (2.11) gives:

$$2c + \frac{6d}{3d} \left(-c \pm \sqrt{c^2 - 3db} \right)$$

$$= \pm 2 \sqrt{c^2 - 3db} > 0 . (2.12)$$

Clearly, the positive sign must be chosen.

To complete the analysis, the values of the coefficients (a , b , c and d) must be obtained. The original design is the value of the objective function at $\alpha=0$. The slope of the objective in the α direction at $\alpha=0$ is given by $\{\nabla \!\!\!/ \!\!\!/ \!\!\!/ (t_0)\}^T \!\!\!\!/ \{s\}$. Immediately then, a = $\Phi(t_0)$ and b = $\{\nabla \!\!\!/ \!\!\!/ \!\!\!/ (t_0)\}^T \!\!\!\!/ \{s\}$. The remaining coefficients are determined by evaluating Φ at two different values of α . In order to assure convergence, these values were picked so that the minimum was bracketed by the three function evaluations.

Once α^* is obtained using the above procedure, a test is made to see if it indeed is at the minimum value of $\Phi(t+\alpha S)$. The test used was to compute $|\{\nabla \Phi(t+\alpha^*S)\}^T\{s\}|/(|\{\nabla \Phi(t+\alpha^*S)\}^T\}|\{s\}|\equiv c i$.

If α^* is exactly at the minimum, CI is zero. The criterion used was that if CI was less than some specified δ then the optimization would proceed. If not, then an additional interpolation must be made utilizing the new values of $\Phi(t + \alpha^*S)$ and $\{\nabla\Phi(t + \alpha^*S)\}^T\{S\}$ until the criterion is satisfied.

2. Minimum Thickness Constraints

Under certain design conditions, it is possible, in the absence of constraints on their size, that design variables may go to zero and even take on negative values. Since these design variables correspond to element thicknesses, it is physically and computationally undesirable for this to happen. Various methods have been constructed to deal with this problem, and this section describes a novel method used in Chapter III of this work. It is a method that worked quite well and is not well known in the structural optimization field.

The technique used is a transformation employed by Pierson (Ref. 10) for a continuous design variable. Modified to accept a discrete design vector, this transformation has the form:

$$\{t\} = \{t_{\min}\} + \frac{1}{2} \{u^2\}$$
 (2.12)

The t_{min} is a constant minimum thickness constraint while u is considered the new design variable. The beauty of this transformation is the $\{t\}$ remains positive even if $\{u\}$ inadvertently has some negative components.

A minor difficulty arises when derivatives are needed with respect to the new design vector $\{u\}$. The indicated procedure is to use the chain rule by first taking the derivative with respect to $\{t\}$ and then use

$$\left\{\frac{\partial\Phi}{\partial u}\right\} = \left\{\frac{\partial\Phi}{\partial t} \frac{\partial t}{\partial u}\right\} = \left\{u \frac{\partial\Phi}{\partial t}\right\}$$
(2.13)

D. COMMENTS

Despite the analytical underpinnings described above, optimization techniques remain very much an art. It is felt that some personal observation from one who began this work with a limited knowledge of optimization techniques might prove of value to others who are in a similar situation.

First, a disclaimer must be made to the effect that the use of the variable metric method coupled with an interior penalty function should not be considered a recommendation of either technique as the best method for solving a general problem. Each problem must be approached on an individual basis, with a consideration of the requirements and capabilities of each technique. The strong points of the method are that it is a sophisticated gradient method that proceeds to the optimum in a deliberate fashion. Other techniques, utilizing feasible directions (Ref. 34) or optimality criteria (Ref. 3), are more efficient for certain applications and may even be better suited

for the problems worked here. A further general comment is that computer centers are now likely to contain optimization routines in their libraries. The first step for anyone embarking on an optimization problem should then be to determine if these readily available routines are adequate or can be adapted for their needs.

Given these general comments, specific perceptions gained while exercising the programs are offered below.

The use of the - \ln (g_i) as a penalty function is an innovation with respect to structural optimization problems as far as the author knows. The more common interior penalty function is one of the form $1/g_i$. The log function seems to provide a smooth function with an easily calculated derivative. It would be interesting to hear of others' experience with different functions.

The values chosen for the penalty parameter r of equation (2.2) have to be selected in an arbitrary manner. For this thesis, values of r ranging from 10 to 10^{-5} were used. The reduction $r_{i+1} = r_i/10$ was always used until the minimum r was reached.

Texts on this method advocate iterating on each value of r until an optimum is reached before reducing it. This seems to be an unnecessarily strict requirement and an alternative was used that reduced r after it appeared that little improvement would be made at the present value. This was done by specifying that if $\Phi_q/\Phi_{q-1} \ge 1.0/(1.0+10~r)$, then r should be reduced by ten and the new optimization problem initiated. If not, iteration continued until the criterion was met. This

approach has the added benefit that the criterion is satisfied quickly for large values of $\, r \,$ and becomes increasingly more stringent as $\, r \,$ is reduced. For the final value of $\, r \,$, a convergence criterion was employed. The criterion used was obtained from Ref. 2 and entailed checking if

$$|\{\nabla\Phi\}^{\mathbf{T}}$$
 [H] $\{\nabla\Phi\}|/\Phi$ < 0.02

If the inequality was satisfied, the problem was considered solved; if not, the iteration continued.

The use of the extended interior penalty function described in Section II.B proved to be of marginal value. The main reason for this is that the values of ϵ were so small that the objective functions calculated using the extended penalty function were almost always too large to be of value in the interpolation procedure. This in turn was due to the way in which ϵ is calculated. In order to assure that the transition point (i.e., ϵ) is between the minimum point and the infeasible region it was found necessary to use $\epsilon = \exp(-r/\Phi)$. Without going into detail, it is recommended that, if the extended penalty function is to be used, further efforts be made to obtain a better transition point when using the log penalty function, or that the $1/g_1$ penalty function be used coupled with a transition point calculated by Cassis (Ref. 2^{l_1}): $\epsilon = r/\phi$.

A number of other "tricks" were employed in the optimization and particularly in the one-dimensional search. However, it seems of

little value to detail them here. The main thing to be kept in mind is the nature of the optimization process and the mechanics involved. Some of the calculations of the next three chapters may appear excessive unless it is remembered why the optimization algorithm makes them necessary.

CHAPTER III

HARMONIC EXCITATION

A. INTRODUCTION

Among the simplest dynamic response problems to formulate and solve are those of one-dimensional structures excited by harmonically oscillating loads. If only the steady state response is of interest, the time parameter can be removed from the equations of motion by assuming that the structure responds at the frequency of excitation. It was supposed, therefore, that this type of problem would be a logical beginning to a study of structural optimization in the presence of dynamic loading. The results of this chapter indicate that this supposition is essentially correct but that there are unanticipated difficulties related to the fact that the feasible region is disjoint. In order to demonstrate this difficulty, some extremely simple examples are presented in the following paragraphs.

Consider a uniform cantilevered rod excited by a uniformly distributed sinusoidal torque. The differential equation and related boundary conditions for this system are (Ref. 32, Chap. 3)

$$\frac{\partial}{\partial \mathbf{x}} \left(\mathbf{G} \mathbf{J} \frac{\partial \theta}{\partial \mathbf{x}} \right) - \mathbf{I}_{\alpha} \frac{\partial^{2} \theta}{\partial \mathbf{t}^{2}} = - \overline{\mathbf{T}} e^{\mathbf{i} \omega_{\mathbf{e}} \mathbf{t}} , \qquad (3.1)$$

and

$$\theta \mid_{\mathbf{x}=0} = 0$$
 and $GJ \frac{\partial \theta}{\partial \mathbf{x}} \mid_{\mathbf{x}=\mathbf{L}} = 0$.

Here, ω_{e} is the excitation frequency. The amplitude of the steady state solution of Eq. (3.1) is

$$\overline{\theta}(x) = \frac{\overline{T}}{GJ\lambda} \left[\cos \sqrt{\lambda} x - 1 + \tan \sqrt{\lambda} L \sin \sqrt{\lambda} x \right] , \quad (3.2)$$

where

$$\lambda = \frac{I_{\alpha} \omega^2}{GJ} .$$

A graphical representation of $\theta(L)$ is presented in Figure 3.1. The points to be made are that the magnitude of the deflection does not increase monotonically with the magnitude of the excitation frequency and that, given a specified deflection, there is not a unique value of the excitation frequency that results in that deflection. In fact, there are an infinite number of such excitation frequencies. This should provide an inkling of the problems to be encountered with a harmonic excitation. To make it more explicit, a further example is presented below that involves a structural optimization problem with only two design variables.

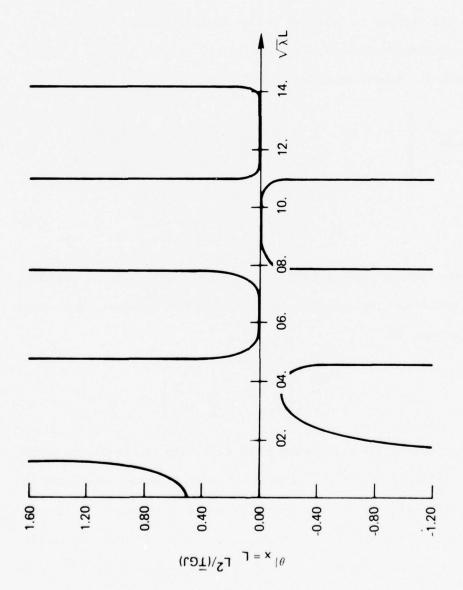


FIG. 5.1--Response of the Tip of a Uniform Rod Excited by a Uniformly Distributed Harmonic Load as a Function of the Frequency of Excitation.

B. TWO DESIGN VARIABLE EXAMPLE

This section seeks the optimal design of a thin walled cantilevered rod excited uniformly in torsion by a harmonically varying load. If this system is modelled by two finite elements of equal length, equations from Section A.1 can be specialized to the $\,n=2\,$ case to give the steady state equation of motion:

$$\left(-\frac{\omega_{\mathbf{e}}^{2}\mathbf{I}_{\infty}\mathbf{L}^{2}}{2^{4}\mathbf{G}\mathbf{J}_{0}}\begin{bmatrix}2(\mathbf{t}_{1}+\mathbf{t}_{2}) & \mathbf{t}_{2}\\ \mathbf{t}_{2} & 2\mathbf{t}_{2}\end{bmatrix} + \begin{bmatrix}\mathbf{t}_{1}+\mathbf{t}_{2} & \mathbf{t}_{2}\\ \mathbf{t}_{2} & \mathbf{t}_{2}\end{bmatrix}\right) \begin{pmatrix} \theta_{1}\\ \theta_{2} \end{pmatrix}$$

$$= \frac{\mathbf{T}\mathbf{L}^{2}}{8\mathbf{G}\mathbf{J}_{0}} \begin{cases} 2\\ 1 \end{cases} \qquad (3.3)$$

The constraints considered are that the magnitude of the stress be no greater than some specified value. From the Appendix, the stress can be expressed as:

$$\{S\} = \frac{2GR}{L} \begin{bmatrix} 1 & 0 \\ -1 & 1 \end{bmatrix} \begin{Bmatrix} \theta_1 \\ \theta_2 \end{Bmatrix} .$$

The motivation for representing the structure by two design variables is that it is possible to depict the results graphically, thereby gaining a qualitative description of what would be encountered with a more realistic representation containing many elements. In this particular case, an added benefit is that it is relatively easy to compute

the stress amplitudes explicitly:

$$\frac{s_1}{s_{\text{max}}} = \frac{2GR}{L} \theta_1 = \frac{3T_n t_2(1 - \lambda_e)}{DET} ,$$

$$\frac{s_2}{s_{\text{max}}} = \frac{2GR}{L} (\theta_2 - \theta_1) = \frac{T_n(3\lambda_e t_2 + t_1(1 - 2\lambda_e))}{DET} ,$$
(3.4)

where:

$$\lambda_{e} = \frac{\omega_{e}^{2} I_{\alpha O} L^{2}}{2^{4} G J_{O}} ,$$

$$T_{n} = \overline{T} L R / (^{4} J_{O} S_{max}) ,$$

$$DET = t_{2} \{ t_{1} (1 - 2\lambda_{e})^{2} - t_{2} (6\lambda_{e} - 3\lambda_{e}^{2}) \} .$$

The constraints for this problem are that the absolute values of $s_i/s_{max} \quad \text{must be less than unity.} \quad \text{In the notation of Chapter II, these are written as} \quad g_i = 1 - (s_i/s_{max})^2 \ge 0 \quad .$

Figures 3.2 and 3.3 show the feasible and infeasible regions for values of λ_e ranging from zero to three and for T_n equal to 0.085.

For the λ_e = 0 case (static loading), presented in Fig. 3.2(a), the constraints are seen to be two straight lines. The cost function is simply J = t_1 + t_2 so that the optimum is at the intersection of these two lines. Figure 3.2(b) shows the design space for λ_e = 1/24

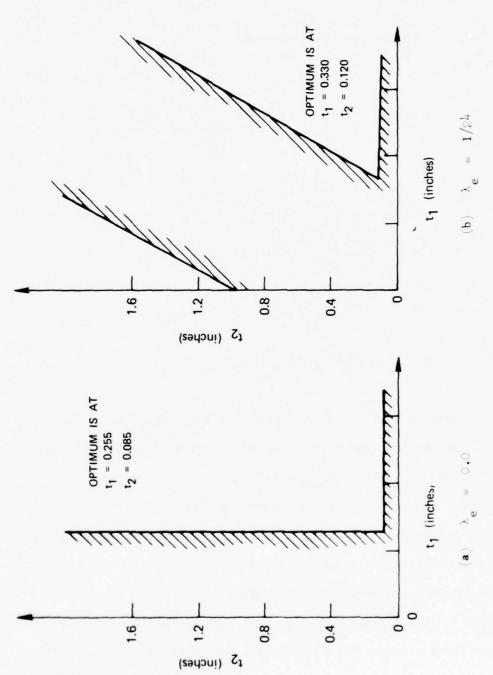


FIG. 3.2--Design Space for a Cantilevered Rod Excited in Torsion at Nondimensional Frequency λ .

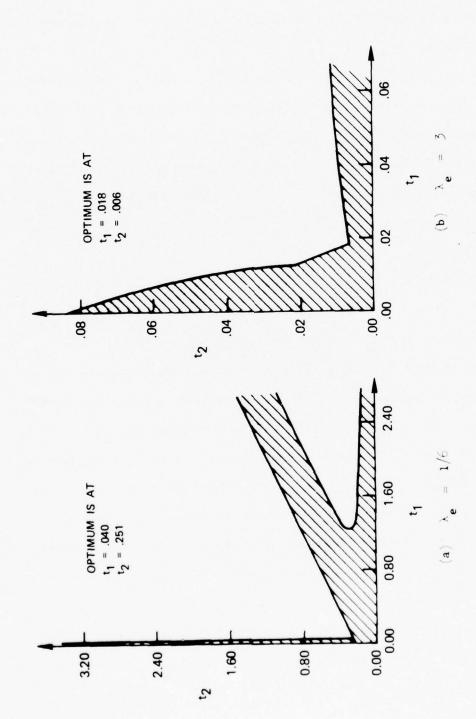


FIG. 3.3--Design Space for a Cantilevered Rod Excited in Torsion at Nondimensional Frequency $^{\lambda}_{\rm e}$.

and it is seen that there are two separate feasible regions. This is the difficulty that is illustrated by this example and is discussed further below.

Figure 3.3(a) shows the results for $\lambda_e=1/6$. The constraint at $t_1=0.04$ is a minimum thickness constraint that is included to eliminate the $t_1=0.0$ solutions that satisfy the stress constraints but are physically unrealistic. It is seen that the least weight solution is in the upper region at $t_1=0.04$ and $t_2=0.25$. Finally, Fig. 3.3(b) shows that for the $\lambda_e=3$ case there is again only one feasible region.

The explanation for this curious behavior is to be found by studying the eigenvalues of the system. Let λ_1 and λ_2 denote the non-dimensional values of the first and second eigenvalues. In Fig. 3.3(a), the designs with λ_1 equal to the excitation frequency are all on a straight line emanating from the origin with an equation given by $t_1 = 2.06 \ t_2$. This line proceeds directly through the middle of the infeasible region, dividing the design space into two distinct regions. Clearly designs that have $\lambda_e = \lambda_1$ are infeasible because this represents a resonance condition with an unbounded response. The region $t_1 \geq 2.06 \ t_2$ contains designs where $\lambda_1 > \lambda_e$ while the region $t_1 \leq 2.06 \ t_2$ contains designs where $\lambda_1 < \lambda_e$. Each of these regions has its own optimum, as is demonstrated by the figure.

Segenreich and Rizzi (Ref. 35) have shown that the eigenvalues of cantilevered rods modelled in the fashion described in the Appendix

have prescribed limits. For the specific case of two design variables of interest here, these limits are given by:

$$0 \le \lambda_1 \le 0.5$$
 , $0.5 \le \lambda_2 \le 2.0$. (3.5)

As a function of the excitation frequency, there are, therefore, either one or two distinct feasible regions. These regions are given by:

Excitation Frequency	No. of Regions	Eigenvalue Relationships
$\lambda_{\mathbf{e}} = 0$	1	$\lambda_2 > \lambda_1 > \lambda_e$
$0 < \lambda_{\mathbf{e}} \leq 0.5$	2	$\begin{cases} 1. & 0 < \lambda_{\mathbf{e}} < \lambda_{1} < \lambda_{2} \\ 2. & 0 \le \lambda_{1} < \lambda_{\mathbf{e}} < \lambda_{2} \end{cases}$
$0.5 < \lambda_{e} < 2.0$	2	$\begin{cases} 1. & \lambda_1 < \lambda_e < \lambda_2 \\ 2. & \lambda_1 < \lambda_2 < \lambda_e \end{cases}$
λ > 2.0	1	$\lambda_{e} > \lambda_{2} > \lambda_{1}$

The $\lambda_e>$ 2.0 case explains why Fig. 3.3(b) contains only one feasible region; the excitation frequency is greater than any possible eigenvalue of the system.

It should be clear why this disjoint property of the feasible region presents a difficult obstacle in the search for a global optimum. While it is possible to analyze the two design variable case graphically in a thorough fashion, this is not practical for designs with a greater number of elements. Figure 3.1 was presented to motivate the hypothesis that for the continuous case there are an infinite number of local optima corresponding to the infinite number of distinct regions where $\lambda_{\bf i}<\lambda_{\bf e}<\lambda_{\bf i+1}$, ${\bf i}=1,2,\ldots,\infty$.

For problems with an arbitrary number of elements, some method such as that described in Chapter II has to be utilized to search for an optimum. But such methods have the drawback that the search takes place inside one feasible region. Therefore, for a given problem, the global optimum is found by selecting the minimum of all the distinct local minima. Cassis (Ref. 24) encountered disjoint feasible design spaces while studying a different dynamic response problem and found it preferable to search for the optimum in the infeasible region by using an exterior penalty function method. His thought was that the solution would be more likely to proceed to the global optimum. But this technique provides no advantage here since an exterior penalty function technique still proceeds "downhill" and would not, therefore, cross over the infinitely high "ridge" where the excitation frequency equals an eigenfrequency in order to descend into the "valley" of the global optimum. More comments are offered on this problem in Section D.

It might be supposed that the disjoint nature of the feasible region is due to the omission of structural damping; in a sense, this is true. The addition of damping gets rid of the infinitely high ridges, since a damped structure excited at its resonant frequency has a finite response. A brief study that included damping was made, and a result from the study is presented in Fig. 3.4. The figure superimposes the $\lambda_e = 1/6$ case of Fig. 3.3(a) and the results from an identical problem except that the shear modulus was multiplied by $(1+i\alpha)$, where α is a small structural damping factor. This is a technique frequently used to take account of the fact that structures have damping present in them (Ref. 36, Chap. 12). The value of α used to obtain the results shown was 0.1 - an unrealistically high value, but one that depicts the damping effect clearly. It is seen that the damping reduces the infeasible region and prevents it from extending to infinity. The disjoint character of the design space has been eliminated, but two minima are still retained as pockets of the unified design space. The basic problem of finding the global optimum still remains. Note that the optimal solutions for the damped case do not differ greatly from the undamped case. Damping was not included in the analyses presented in the remainder of this chapter since it was felt that the benefits gained from added practicality or realism do not offset the complications introduced by complex variables.

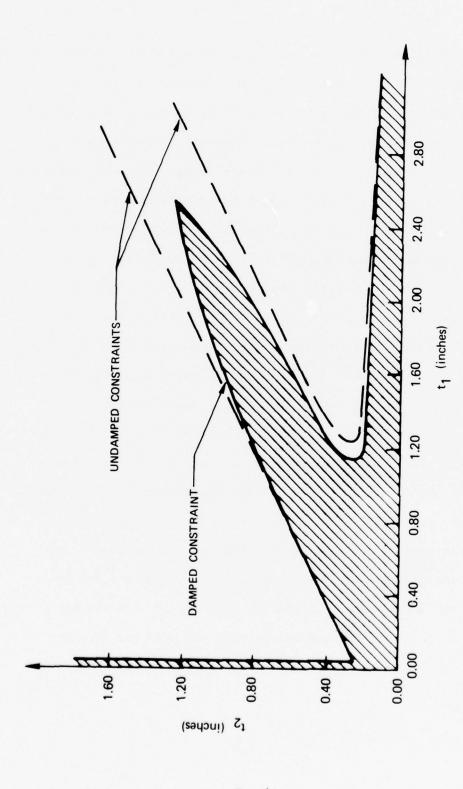


FIG. 3.4--Comparison of Two-Dimensional Design Spaces for Damped and Undamped Solutions, $\lambda_e=1/6$.

C. FUNCTION SPACE SOLUTIONS

Before proceeding to the finite element solutions, another procedure that is applicable to these sorts of problems is presented: that of solving optimization problems by dealing with the differential equations directly. The motivation for this section comes from the success others achieved while applying optimal control techniques to structural optimization problems. In particular, Weisshaar (Ref. 7) and Armand and Vitte (Ref. 8) were able to find optimal thickness distributions for a number of problems that had constraints on the system eigenvalues.

This section develops the criteria for an optimal solution for a harmonically loaded structure and solves some special cases.

Only one-dimensional structures are used in this study; therefore, the equations can be put into the first order form generally used in control theory:

$$\{x\}' = [F(t,s)]\{x\} + \{P\}$$
 (3.6)

With boundary conditions at s=0 and s=1 . The terms used are defined as:

$$\{x\} = \{x(s)\} = n \times 1$$
 vector of state variables
$$t = t(s) =$$
thickness distribution, the control variable of the problem

and

 $\{P\}$ = n × 1 vector of the load amplitude

()' = denotes a derivative with respect to s

s = the nondimensional coordinate and independent variable.

The analysis given below is an application of the methods described by Bryson and Ho (Ref. 37). Only the barest outline of the procedure is presented here.

The problem statement used in this thesis is that of minimizing the weight subject to constraints on the response. Mathematically, minimize

$$J = \int_{0}^{1} tds \qquad (3.7)$$

Subject to

$$\{g(x,s,t)\} \ge 0$$
 ,
 $q \times 1 \text{ vector}$. (3.8)

The Hamiltonian is constructed by using standard procedures of Ref. 37

$$H = t + {\lambda}^T ([F]{x} + {P}) + {\mu}^T {g},$$
 (3.9)

where

 $\{\lambda\}$ = $n \times 1$ vector of adjoint states

 $\left\{ \mu\right\} \ = \ q \, \times \, 1 \ \mbox{ adjoint vector for the constraints}$

The value of $~\mu_i~$ is zero when $~g_i^{}\neq 0~$ and is $\geq 0~$ when $~g_i^{}=0~$. The Euler-Lagrange equations are:

$$\{\lambda\}' = -\left\{\frac{\partial H}{\partial x}\right\} = -\{\lambda\}^T [F] - \{\mu\}^T \left\{\frac{\partial g}{\partial x}\right\}$$
 (3.10)

And the "control equation" is:

$$\frac{\partial H}{\partial t} = 0 = 1 + \{\lambda\}^{T} \left[\frac{\partial F}{\partial t}\right] \{x\} + \{\mu\}^{T} \left\{\frac{\partial g}{\partial t}\right\} \qquad . \quad (3.11)$$

The transversality condition provides the required boundary conditions:

$$\{\lambda\}^{\mathrm{T}} \{\delta \mathbf{x}\}\Big|_{0}^{1} = 0 \qquad . \tag{3.12}$$

It is felt that the method is best dealt with here by example. Hopefully, these examples also clarify the technique.

1. Example: Cantilevered Beam With a Static Load

A cantilevered beam acted upon by a uniform <u>static</u> load has a differential equation and associated boundary conditions given by

$$\frac{d^2}{dx^2} \left(EI \frac{d^2w}{dx^2} \right) = P \qquad , \qquad (3.13)$$

$$w\big|_{\mathbf{x}=0} = \frac{d\mathbf{w}}{d\mathbf{x}} \bigg|_{\mathbf{x}=0} = \mathbf{E}\mathbf{I} \frac{d^2\mathbf{w}}{d\mathbf{x}^2} \bigg|_{\mathbf{x}=\mathbf{L}} = \frac{d}{d\mathbf{x}} \left(\mathbf{E}\mathbf{I} \frac{d^2\mathbf{w}}{d\mathbf{x}^2} \right) \bigg|_{\mathbf{x}=\mathbf{L}} = 0 .$$

Using notation and assumptions given in Ref. 7, the first order form of this system is

$$\begin{cases} x_1 \\ x_2 \\ x_3 \\ x_{14} \end{cases} = \begin{bmatrix} 0 & 1 & 0 & 0 \\ 0 & 0 & \frac{1}{t} & 0 \\ 0 & 0 & 0 & 1 \\ 0 & 0 & 0 & 0 \end{bmatrix} \begin{cases} x_1 \\ x_2 \\ x_3 \\ x_{14} \end{cases} + \overline{P} \begin{cases} 0 \\ 0 \\ 0 \\ 1 \end{cases}$$

$$\mathbf{x}_{1}(0) = \mathbf{x}_{2}(0) = \mathbf{x}_{3}(1) = \mathbf{x}_{4}(1) = 0$$
 , (3.14)

where

$$x_1 = w/L$$
 ,

and

$$\mathbf{x}_{2} = \frac{1}{L} \frac{d\mathbf{w}}{d\mathbf{x}},$$

$$\mathbf{x}_{3} = \frac{\mathbf{t}}{L^{2}} \frac{d^{2}\mathbf{w}}{d\mathbf{x}^{2}},$$

$$\mathbf{x}_{4} = \frac{1}{L^{3}} \frac{d}{d\mathbf{x}} \left(\mathbf{t} \frac{d^{2}\mathbf{w}}{d\mathbf{x}^{2}} \right),$$

$$\overline{\mathbf{P}} = \frac{PL^{3}}{EI_{0}}.$$

The optimization problem is specified as that of finding the thickness distribution that minimizes the total weight while satisfying the constraint that the magnitude of the stress along the span of the beam is less than some specified S_{max} . By use of the familiar formula $S=(Ed/2)\,(d^2w/dx^2)$, this constraint can be put into the form:

$$g_1 = 1 - a|x_3|/t$$
 , (3.15)

where $a = EdL^2/2S_{max}$.

Equation (3.9) is then:

$$H = t + \lambda_1 x_2 + \frac{\lambda_2 x_3}{t} + \lambda_3 x_4 + \lambda_4 \overline{P} + \mu \left(1 - \frac{a |x_3|}{t} \right) . \quad (3.16)$$

Equations (3.10) and (3.11) are evaluated to give:

$$\begin{cases}
\lambda_{1} \\
\lambda_{2} \\
\lambda_{3} \\
\lambda_{4}
\end{cases} = \begin{bmatrix}
0 & 0 & 0 & 0 \\
-1 & 0 & 0 & 0 \\
0 & -1/t & 0 & 0 \\
0 & 0 & -1 & 0
\end{bmatrix}
\begin{cases}
\lambda_{1} \\
\lambda_{2} \\
\lambda_{3} \\
\lambda_{4}
\end{cases} - \frac{a\mu}{t} \begin{cases}
0 \\
sgn(x_{3}) \\
0
\end{cases}, (3.17)$$

$$\frac{\partial H}{\partial t} = 0 = 1 - \frac{\lambda_2 x_3}{t^2} + \frac{\mu a |x_3|}{t^2} = 1 - \frac{\lambda_2 x_3}{t^2} + \frac{\mu}{t} \qquad (3.18)$$

The last substitution is made because if $~\mu \neq 0$, [a(x_{_{3}})/t] = 1~ .

The notation sgn () designates that only the algebraic sign of the quantity is used.

The boundary conditions on the adjoint variables are

$$\lambda_{1}(1) = \lambda_{2}(1) = \lambda_{3}(0) = \lambda_{4}(0) = 0$$
.

The first order equations and the boundary conditions give immediately

$$\mathbf{x}_{1_{1}} = \overline{\mathbf{P}}(\mathbf{s} - 1) ,$$

$$\mathbf{x}_{3} = \overline{\mathbf{P}}(\mathbf{s}^{2} - 2\mathbf{s} + 1)/2 ,$$

$$\lambda_{1} = 0 ,$$

$$\lambda_{2} = 0 . \qquad (3.19)$$

These results can be placed in Eq. (3.15) to give:

$$1 + \frac{\mu}{t} = 0 \implies t = -\mu$$
 (3.20)

Since μ is zero only when $a|x_3|/t$ is less than unity, it is clear that $t \ge \frac{a\overline{P}}{2} (1. - 2s + s^2)$. Equation (3.20) states that if μ is zero, then t = 0 and the inequality on t is violated except at s = 1. Therefore, μ cannot equal zero, requiring $a|x_3|/t = 1.0$ across the span. Stated another way, this says that the optimal solution is the one that creates a fully stressed structure. This is a well known result for problems of this type with a static loading.

The entire solution can now be written down as:

$$t = -\mu = a\overline{P}(1 - 2s + s^2)/2$$
 $x_2 = s/a$
 $\lambda_3 = as$
 $x_1 = s^2/2a$
 $\lambda_4 = as^2/2$. (3.21)

The ease with which this analytical solution was obtained makes it appear that solutions with a harmonically oscillating load might also be tractable. The formulation for the same problem as above except that the excitation is harmonic with frequency $\frac{d}{e}$ can be written in terms of the static problem by adding several terms. The subscript ()_{st} in the following equations refers to the static case

and $\Gamma_{\rm e}$ is a nondimensional frequency equal to $\omega_{\rm e} \sqrt{m_{\rm o} L^3/EI_{\rm o}}$. With this notation, the changes in Eqs. (3.14)-(3.18) for the harmonically excited structure are:

$$\dot{x}_{1} = \Gamma_{e}^{2} t x_{1} + \overline{P} ,$$

$$H = H_{st} + \lambda_{1} \Gamma_{e}^{2} t x_{1} ,$$

$$\dot{\lambda}_{1} = -\Gamma_{e}^{2} t \lambda_{1} ,$$

$$\frac{\partial H}{\partial t} = \frac{\partial H_{st}}{\partial t} + \lambda_{1} \Gamma_{e}^{2} x_{1} = 0 .$$

$$(3.22)$$

These additions prevent determining that the optimal structure is fully stressed. Without this, it has been found impossible to treat these equations analytically. Numerical techniques that solve the two point boundary value problem and the associated control equation have been applied with little success. The main difficulty is in dealing with the stress constraint. The character of the solution changes at the value of s where the constraint changes from being inactive to being active. This requires patching together arcs as explained in Ref. 37, Chap. 3. If numerical techniques are to be used, it seems preferable to convert the problem to an unconstrained one by using the penalty function method as described in Section II.B.

If this is done, Eq. (3.7) becomes

$$J = \int_{0}^{1} [t - r \ln (g)] ds ,$$

and the difficulty in patching arcs is avoided, albeit the formulation becomes slightly more complex.

2. Example: Torsional Rod Excited by a Harmonically Varying End Load

Consider a torsional rod that is being excited at its tip by a harmonically oscillating load with frequency $\omega_{\rm e}$ and constant amplitude $\overline{\rm T}$. Pose the problem of finding the thickness distribution that minimizes the weight of the structure subject to the constraint that the tip rotational amplitude is equal to a specified value D . This problem was first solved by Icerman using energy considerations and with the additional constraint that the first natural frequency of the structure be greater than the excitation frequency. It is similar to a problem studied by Ashley and McIntosh (Ref. 6) and by Turner (Ref. 9) who found the minimum weight structure for a cantilevered torsional rod with a fixed tip mass and an equality constraint on the first natural frequency.

With the familiar assumptions that $GJ=GJ_0t$ and $I_{\alpha}=I_{\alpha 0}t$, the differential equations can be put into the form (Ref. 8):

And the associated boundary conditions are

$$x_1(0) = 0$$
 , $x_1(1) = D$, $x_2(1) = \overline{T}$,

where

$$\Gamma^2 \equiv \frac{\omega_e^2 I_{\infty} L^2}{GJ_0} .$$

Note that the equality constraint and the excitation are contained in the boundary conditions. The inertial loads appear in the - Γ^2 t term.

The Hamiltonian of Eq. (3.9) has the form:

$$H = t + \frac{\lambda_1 x_2}{t} - \lambda_2 r^2 t x_1 \qquad (3.24)$$

Equations (3.10) and (3.11) give the relations

$$\frac{\partial H}{\partial t} = 0 = 1 - \frac{\lambda_1 x_2}{t^2} - \lambda_2 r^2 x_1 \qquad , \qquad (3.26)$$

and the boundary condition $\lambda_2(0) = 0$.

A solution is found by noting that λ_2 and x_1 are equivalent in that they have the same differential equations and similar boundary conditions:

$$(t\lambda'_{2})' + \Gamma^{2}t\lambda_{2} = 0$$
 $\lambda_{2}(0) = 0$, $t\lambda'_{2}(1) = c_{1}$,

$$(tx'_1)' + \Gamma^2 tx_1 = 0$$
 $x_1(0) = 0$, $tx'_1(1) = \overline{T}$.

Since the differential equations are linear, this requires that

$$\lambda_2 = -c_1 x_1 / \overline{T} , \qquad (3.27)$$

where c_1 is an unspecified constant.

Similarly, it can be shown that

$$\lambda_1 = c_1 x_2 / \overline{T} \qquad . \tag{3.27a}$$

Substituting these relations into Eq. (3.26) gives

$$1 - \frac{x_2^2 c_1}{t^2 \overline{T}} + \frac{\Gamma^2 c_1 x_1^2}{\overline{T}} = 0 . (5.28)$$

Since $x_2 = tx_1'$, this can be written as

$$(x_1')^2 = B^2 + \Gamma^2 x_1^2$$
 (5.29)

where $B^2 = \overline{T}/c_1$.

Murphy (Ref. 38) lists three solutions to this differential equation, but they are essentially equivalent and can be expressed in the general form

$$x_1 = \pm \frac{B}{\Gamma} \sinh (C \pm \Gamma s)$$
 (3.30)

Here C is the undetermined constant of the differential equation. Applying the boundary conditions on \mathbf{x}_1 gives

$$x_1 = D \sinh \Gamma s / \sinh \Gamma$$
 . (3.31)

Note that this determines that $c_1 = \overline{T}/B^2 = \overline{T} \sinh^2 \Gamma/(D\Gamma)^2$.

Placing this value for \mathbf{x}_1 in the original differential equation gives

$$t'\Gamma D = \frac{\cosh \Gamma s}{\sinh \Gamma} + 2\Gamma^2 t = \frac{\sinh \Gamma s}{\sinh \Gamma} = \frac{dt}{t} = -2\Gamma \tanh \Gamma s ds . \quad (3.32)$$

Integrating both sides:

$$ln t = -2 ln cosh \Gamma s + c_2$$
,

or

$$t = c_2/\cosh^2 \Gamma s \qquad . \tag{3.33}$$

The relation $\mathsf{tx}_1'(1) = \overline{\mathsf{T}}$ provides a value for c_2 and hence for the optimal thickness distribution:

$$\frac{\overline{T}}{c_2} = \frac{-\cosh \Gamma \sinh \Gamma}{\Gamma D}$$

and

$$t = \frac{\overline{T} \cosh \Gamma \sinh \Gamma}{\Gamma D \cosh^2 \Gamma s} . \qquad (3.34)$$

This is the result found by Icerman while including the constraint that the first natural frequency must be greater than the excitation frequency. This constraint was not explicitly included in the present formulation, but it is clear that the constraint is satisfied since the solution is identical to Icerman's.

The question of whether additional solutions exist that do not satisfy the frequency constraint, and, if so, what they are, took up a large part of the time spent on the thesis. The answer to the question of existence is clearly "yes" and can be demonstrated by looking at the behavior of the solution as P becomes large. The total weight of the structure is proportional to:

$$J = \int_{0}^{1} tds = \overline{T} \sinh^{2} \Gamma / \Gamma^{2} D \qquad (3.35)$$

J increases monotonically and without limit as Γ increases. The curves of Fig. 3.1 show that a uniform rod can also satisfy the

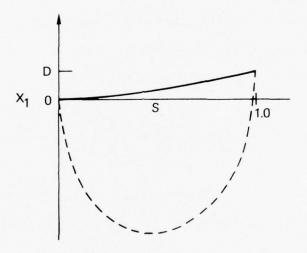
 $\mathbf{x}_1(1) = \mathbf{D}$ constraint at any number of excitation frequencies. Clearly then, the <u>uniform</u> rod at some frequency satisfies the constraint and has less weight than the "optimal" solution. This indicates that the solution of Eqs. (3.31) - (3.34) is not a global solution for all frequencies.

Once this fact is established, the unanswered question is: "What are the other optimal solutions?" At first, it was thought that additional solutions could be found for Eq. (3.29). After a long fruitless search for other solutions, it was determined that the problem was ill-posed, in a special sense.

The adjective ill-posed has generally been reserved for formulations that possess no solutions or no physically meaningful ones. A structural optimization example of such a problem is that of finding the minimum weight thickness distribution for a cantilevered rod with the constraint that the first natural frequency of the optimum rod have the same natural frequency as the uniform rod. If the rod is modelled in the same way as was done at the beginning of this section, it is relatively easy to show (Ref. 8) that this problem statement is satisfied by a uniform rod of vanishingly small thickness, a physically uninteresting solution.

Since Eq. (3.34) gives one solution to the problem at hand, it cannot be considered to be ill-posed in a strict sense. However, by modelling the rod with three equal length segments, each with constant thickness, it is possible to find analytical solutions that satisfy

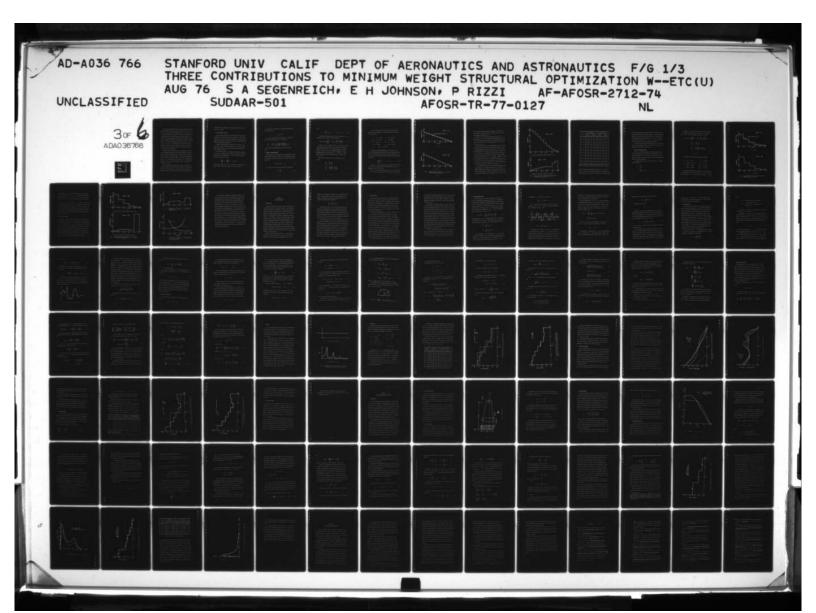
all the boundary conditions and constraints and that have a vanishingly small thickness distribution. The diagram below gives a qualitative comparison of the mode deflection shape given by Eq. (3.31) and the mode shape that this physically unrealistic thickness distribution would have.



As the thickness goes to zero for the second solution, the displacement is unbounded, except for finite values at the root and tip.

A physically meaningful problem statement must, therefore, have additional constraints on the response or involve changes in the system equations themselves. Possible modifications include:

- (1) Imposing a minimum allowable thickness constraint.
- (2) Additions of non-structural mass along the rod.
- (3) More constraints on the response quantities (e.g., inequality constraints on the stress or the displacement).



The first two modifications were successfully applied to the optimization problems with natural frequency constraints but have been unsuccessful for the forced case developed above. It is felt that, even with a minimum thickness constraint or a non-structural mass addition, an optimal structure with the frequency of excitation greater than a structural natural frequency has discontinuities in thickness. Specifically, it appears likely that the optimal structures have concentrated masses; i.e., thickness distributions that include terms of the form $t_c \delta(s-s_c) \ , \ \text{where} \ \delta \ \text{is the dirac delta}. \ \text{The motivation for this speculation comes from solutions obtained using finite element models}$ and piecewise constant continuous models. More comments on this are offered at the end of the chapter.

Inequality constraints, such as those mentioned above, can be included in the manner described in the original formulation. Unfortunately, the added complexity has made the problems so far insoluble by analytical means. As mentioned, there is no reason why the equations could not be solved by numerical means. However, once the decision is made to go to the computer, the most efficient means of attacking these problems is by the use of finite elements. The next sections detail how this can be done.

Before proceeding to this analysis, it should be stressed that finding additional function space solutions remains as a suitable goal. Variations on the example above are the only analytical solutions for harmonically excited structures, as far as is known. Additional analytic

solutions would aid tremendously in uncovering the special features of this type of problem.

D. FINITE ELEMENT SOLUTIONS

The frustration encountered while dealing with the function space formulation led to efforts utilizing finite elements. In any realistic problem, the use of finite elements is practically a necessity; but the generality and elegance of function space solutions makes them the first choice for preliminary investigations.

Examples are given below that extend the two element case of Section III.B to similar structures modelled by up to ten finite elements. Further examples deal with a cantilevered beam structure modelled by various numbers of elements.

The constraints used for these examples are inequality constraints on the stress. The Appendix indicates how the stress can be determined as a function of the displacements. With this formulation, the augmented cost function has the form:

$$\Phi = \sum_{i=1}^{n} t_i - r \sum_{i=1}^{n} \ln \left[1 - (s_i/s_{max})^2\right] \qquad . \tag{3.36}$$

Note that the constraint $|S_i| \le S_{max}$ is handled by squaring the stress values, thereby obviating the need for absolute value brackets.

The thickness is transformed by a technique motivated and described in Section II.C:

$$t_{j} = t_{min} + \frac{1}{2} u_{j}^{2}$$
 (2.11)

The \ensuremath{u}_{j} are considered the design variables. Derivatives of the cost function with respect to \ensuremath{u}_{j} are given by

$$\frac{\partial^{\Phi}}{\partial u_{j}} = u_{j} \left\{ 1 + \frac{r}{(s_{max})^{2}} \sum_{i=1}^{n} \frac{s_{i} \partial s_{i} / \partial t_{j}}{[1 - (s_{i} / s_{max})^{2}]} \right\} \qquad (3.37)$$

The specific examples given below develop the values for $\partial^S i^{\big/\partial t} j$.

1. Example: Cantilevered Rod

This section deals with a cantilevered rod excited by a uniformly distributed load in torsion. Figure A.1 aids in depicting the nature of the problem. The steady state equation of motion for the problem is given by:

$$(-\omega_{\mathbf{p}}^{2} [\mathbf{M}] + [\mathbf{K}])\{\theta\} = \{\mathbf{p}\}$$
 (3.38)

The stresses in the elements are developed in the Appendix:

$$s_1 = \frac{GRn}{I} \theta_1$$
, (Cont'd)

and

$$S_{i} = \frac{GRn}{L} [\theta_{i} - \theta_{i-1}]$$
 $i = 2,3,...,n$. (A.9)

By taking the derivative of Eq. (3.38) with respect to t_j , an expression for the $\{\partial\theta/\partial t_j\}$ vector is obtained:

$$(-\omega_{\mathbf{e}}^{2} [\mathbf{M}] + [\mathbf{K}]) \left\{ \frac{\partial \theta}{\partial \mathbf{t_{j}}} \right\} = -\left(-\omega_{\mathbf{e}}^{2} \frac{\partial [\mathbf{M}]}{\partial \mathbf{t_{j}}} + \frac{\partial [\mathbf{K}]}{\partial \mathbf{t_{j}}} \right) \{\theta\} \quad . (3.39)$$

Note that $\{\theta\}$ and $\{\partial\theta/\partial t_j\}$ in Eqs. (3.38) and (3.39) have the same coefficient matrix. This fact can be exploited by using a subroutine that solves $[A]\{x\}=\{b\}$ by decomposing the [A] matrix (Ref. 39). Since the [A] matrix remains unchanged, it has to be decomposed only once to solve for the n+1 systems of n simultaneous equations to find the separate vectors $\{\theta\}$ and $\{\partial\theta/\partial t_j\}$, $j=1,2,\ldots,n$.

With $\{\partial\theta/\partial t_{j}\}$ determined, the stress derivative is found directly:

$$\frac{\partial \mathbf{S}_{\mathbf{i}}}{\partial \mathbf{t}_{\mathbf{j}}} = \frac{\mathbf{GRn}}{\mathbf{L}} \frac{\partial \theta_{\mathbf{1}}}{\partial \mathbf{t}_{\mathbf{j}}},$$

$$\frac{\partial \mathbf{S}_{\mathbf{i}}}{\partial \mathbf{t}_{\mathbf{i}}} = \frac{\mathbf{GRn}}{\mathbf{L}} \left[\frac{\partial \theta_{\mathbf{i}}}{\partial \mathbf{t}_{\mathbf{i}}} - \frac{\partial \theta_{\mathbf{i}-1}}{\partial \mathbf{t}_{\mathbf{i}}} \right] . \tag{3.40}$$

All the tools necessary for a solution using the techniques of Chapter II are now assembled. The numerical values used in the computer program were

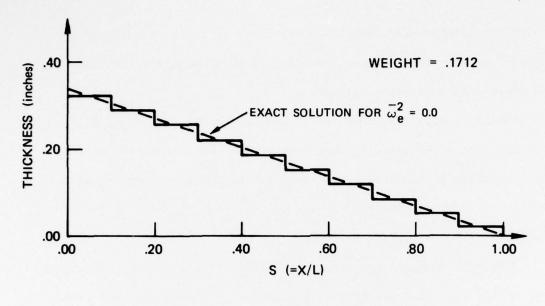
$$G = 3.75 \times 10^6 \text{ psi}$$
 $J_0 = 2\pi R^3 = 1352 \text{ in}^3$
 $S_{\text{max}} = 5.5 \times 10^4 \text{ psi}$ $\rho_s = 0.1 \text{ lbm/in}^3$
 $R = 6 \text{ inches}$ $I_{00} = J_0 = 4.2 \text{ slugs}$
 $L = 120 \text{ inches}$ $p_x = 35,200 \text{ in-lbs/in}$

A check on the algorithm was made by first solving the $\omega_{\rm e}=0$ case. By using the methods of Section III.C, an exact answer can be found for the optimal solution for this statically loaded case. With the values of the structural parameters given above, this solution can be written as

t =
$$\frac{P_x RL}{S_{max} J_0} (1 - s) = 0.34 (1 - s)$$
 (3.41)

Figure 3.5(a) shows a comparison of the optimal solution obtained using ten finite elements with the exact analytical solution. The agreement is seen to be excellent.

Figure 3.5(b) shows a ten element solution for $\overline{\omega}_e^2 \equiv \omega_e^2 I_{QQ} L^2/n^2 G J_Q$ = 1.0 . It is seen that the effect of the excitation is to make the



$$(\mathbf{a}) \quad \overline{\mathbf{a}}_{\mathbf{e}}^{2} = 0.0$$

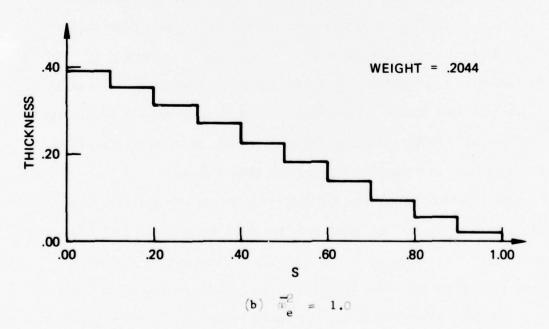


FIG. 3.5--Optimal Thickness Distribution for a Cantilevered Rod Using Ten Finite Elements.

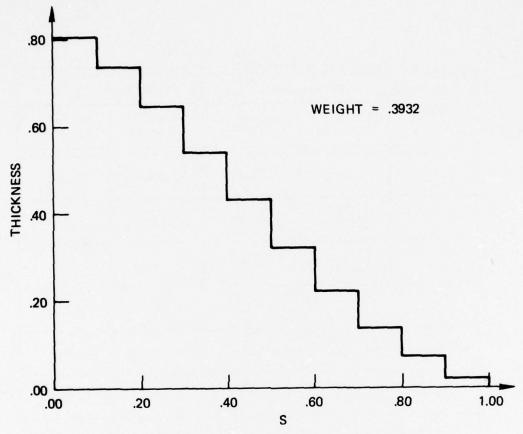
thickness greater all along the span, compared to the static case.

This is because the inertial loads act in phase with the excitation, necessitating a stronger structure.

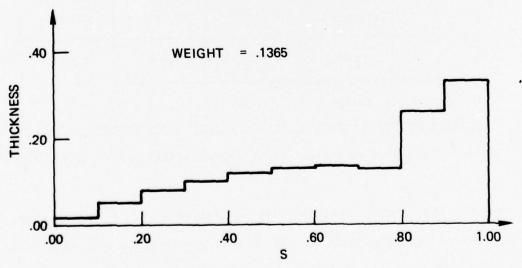
Finally, Fig. 3.6 shows two solutions for the case $\overline{\omega}_e^2 = 4.0$. The solution of Fig. 3.6(b) is an example where the fundamental frequency is less than the excitation frequency and is designated the second solution. This second solution is lighter than the first solution by a factor of 1.36 to 3.93.

Table 3.1 compares the rotational displacements and the constraint values for these two solutions. The two deflection shapes are seen to have similar magnitudes but the second solution is 180° out of phase from the excitation. This allows the inertial load to partially cancel the effects of the excitation, with the result that much less structure is required to satisfy the constraints. These constraints are presented in the form $g_i = [1.0 - (s_i/s_{max})^2]$ in Table 3.1. With the convergence criterion used for the particular example, a value of g_i that is less than 0.1 can be considered an active constraint. The root element of the second solution is at its minimum thickness and the constraint is clearly not tight for this element.

The constraints results for the first solution suggest an interesting question: "Is the first mode solution fully stressed?" The results presented here are ambiguous with the minimum thickness constraint clouding the issue further. One might suppose that it would be possible to hypothesize that the optimal solution is fully stressed



(a) Structure's First Natural Frequency Greater Than $\boldsymbol{x}_{\mathrm{e}}$.



(b) Structure's First Natural Frequency Less Than $\varpi_{\mbox{\sc e}}$.

FIG. 3.6--Two Solutions for the Optimal Thickness Distribution of a Cantilevered Rod Excited at $\overline{\omega}_e^2 = 1.0$.

Element	Displacement		Constraint (g_i)	
	First Solution	Second Solution	First Solution	Second Solution
1	0.029	- 0.027	0.024	0.150
2	0.058	- 0.056	0.012	0.030
3	0.088	- 0.085	0.010	0.016
4	0.117	- 0.115	0.006	0.008
5	0.146	- 0.144	0.006	0.002
6	0.176	- 0.173	0.006	0.014
7	0.205	- 0.202	0.004	0.041
8	0.234	- 0.231	0.006	0.018
9	0.264	- 0.242	0.006	0.851
10	0.293	- 0.246	0.006	0.987

TABLE 3.1--Properties of the Two Thickness Distributions of Figure 3.6.

and use the function space methods on Section III.C to test the hypothesis. However, even for this simple problem, the analytical complications make a closed form result impossible. A much simpler means

of testing the hypothesis is available, however. This is the two design variable example of Section III.B. Figure 3.3(a) shows an example where the first solution is not fully stressed. For this figure, the local optimum with the thickness values $\{t\} = \{1.27, 0.35\}$ has a constraint vector given by $\{0.24, 0.00\}$; i.e., the first element is not at the maximum allowable stress while the second is.

It should be admitted that the above demonstration is not a rigorous proof that the optimal continuous structure is not fully stressed and that the question merits further study.

2. Example: Cantilevered Beam

The second calculation examines the structural optimization of a beam excited transversely by a harmonically oscillating load. As in the previous example, a stress constraint is imposed, and it is first necessary to derive an expression for the derivative of the stress with respect to the design variables.

The Appendix shows that the stress at the center of the element can be expressed as:

$$S_1 = \frac{Edn}{2L} w_2$$
,
 $S_i = \frac{Edn}{2L} (w_{2i} - w_{2i-2})$ $i = 2,3,...,n$. (A.18)

Physically, this equation says that the stress is proportional to the change in the end slopes of the elements. The analysis of Eqs. (3.38)-(3.40) can be repeated almost directly to give:

$$(-\omega_{\mathbf{e}}^{2} [\mathbf{M}] + [\mathbf{K}]) \left\{ \frac{\partial \mathbf{w}}{\partial \mathbf{t}_{\mathbf{j}}} \right\} = -\left(-\omega_{\mathbf{e}}^{2} \frac{\partial [\mathbf{M}]}{\partial \mathbf{t}_{\mathbf{j}}} + \frac{\partial [\mathbf{K}]}{\partial \mathbf{t}_{\mathbf{j}}} \right) \left\{ \mathbf{w} \right\} , (3.42)$$

$$\frac{\partial \mathbf{s}_{\mathbf{i}}}{\partial \mathbf{t}_{\mathbf{j}}} = \frac{\mathbf{Edn}}{2\mathbf{L}} \frac{\partial \mathbf{w}_{2}}{\partial \mathbf{t}_{\mathbf{j}}} ,$$

$$\frac{\partial \mathbf{s}_{\mathbf{i}}}{\partial \mathbf{t}_{\mathbf{j}}} = \frac{\mathbf{Edn}}{2\mathbf{L}} \left(\frac{\partial \mathbf{w}_{2\mathbf{i}}}{\partial \mathbf{t}_{\mathbf{j}}} - \frac{\partial \mathbf{w}_{2\mathbf{i}-2}}{\partial \mathbf{t}_{\mathbf{j}}} \right) , (3.43)$$

$$(\mathbf{i} = 2, 3, ..., \mathbf{n}) .$$

The parameters chosen for the optimization program were

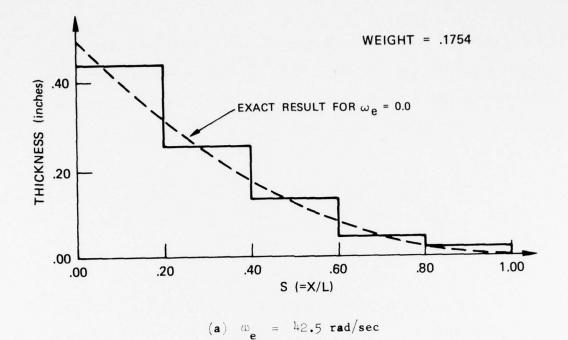
$$E = 10.5 \times 10^6 \text{ psi} \qquad \rho_s = 0.1 \text{ lbm/in}^3$$

$$L = \text{length} = 120 \text{ inches} \qquad p_x = 100 \text{ lbs/in}$$

$$d = \text{depth} = 4 \text{ inches} \qquad t_{min} = 0.02 \text{ inches}$$

$$b = \text{width} = 12 \text{ inches} \qquad S_{max} = 30,000 \text{ psi}$$

Solutions were found using five elements for excitation frequencies ranging from 42.5 rad/sec to 300 rad/sec. Figure 3.7 shows first type of solutions for ω_e = 42.5 rad/sec and 140 rad/sec . The line



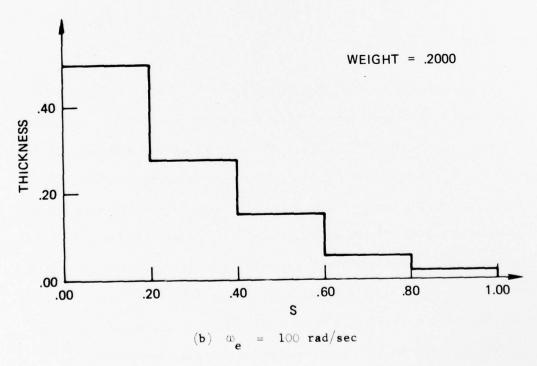


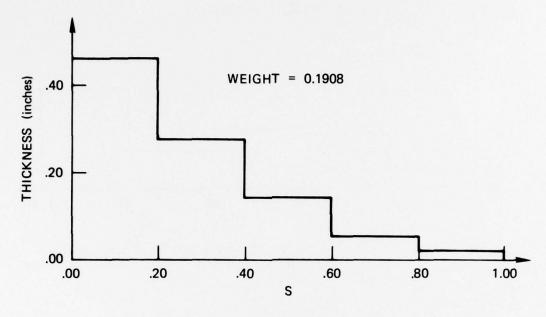
FIG. 3.7--Optimal Thickness Distribution for a Cantilevered Beam Using Five Finite Elements.

superimposed on Fig. 3.7(a) is the exact solution for the statically loaded structure given by Eq. (3.21). For the parameters given above, the exact solution is $t = 0.5 (1.0 - 2s + s^2)$. Even with the harmonic excitation, there is close correspondence between the two solutions.

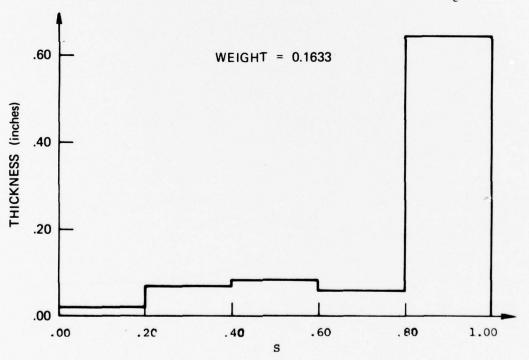
Figure 3.8 shows two solutions for $\omega_e = 80 \text{ rad/sec}$. The second solution is slightly lighter for this case. Another second type of solution is shown in Fig. 3.9(a), while Fig. 3.9(b) plots the weight of the two solutions as a function of frequency. It is seen that the first solution is the lighter for values of the excitation frequency less than 75 rad/sec and that the second solution becomes significantly lighter for higher excitation values.

E. CONCLUDING COMMENTS

Cassis (Ref. 24) reported on the existence of disjoint feasible design spaces in connection with problems dealing with truss structures excited by half-wave sine pulses. It is felt that the problems investigated in this chapter add a great deal to the understanding of this phenomenon, primarily because the simplicity of the formulation permits a minute examination of the behavior of the structure. The main conclusion from this investigation is that the natural frequencies play a central role in creating the many feasible regions. Structures respond vigorously when excited near a natural frequency, accordingly, the optimal designs try to stay away from these resonant conditions.



(a) Structure's First Natural Frequency Greater Than $\overset{\scriptscriptstyle(i)}{_{e}}$.



(b) Structure's First Natural Frequency Less Than $\overset{\text{\tiny (1)}}{=}$.

FIG. 3.8--Two Solutions for the Optimal Thickness Distribution of a Cantilevered Beam Excited at $\varpi_{e}=80$ rad/sec .

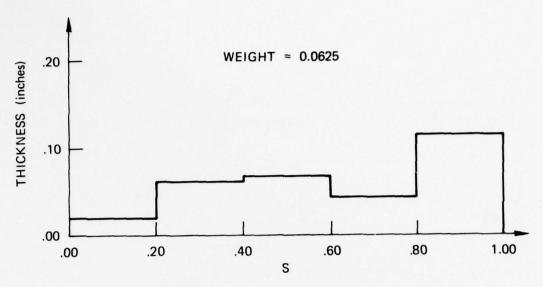


FIG. 3.9(a)--Optimal Thickness Distribution for a Cantilevered Beam Excited at 170 rad/sec (a) > Structure's First Natural Frequency).

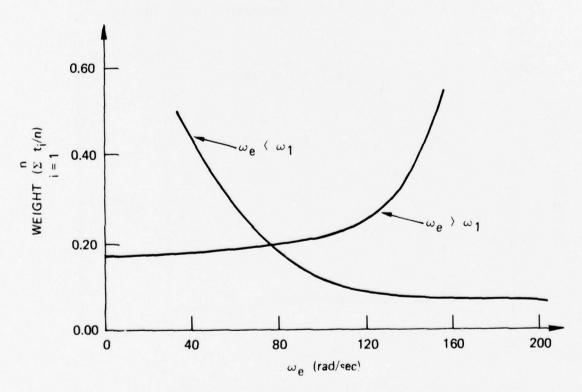


FIG. 3.9(b) --Comparison of the Weights of Local Optima as a Function of Excitation Frequency (ω_1 = the Structure's First Natural Frequency).

The construction of analytical solutions by the methods of Section III.C would further aid in the understanding of these types of problems because they show the role that various parameters of the problem (such as load, frequency and the constraints) play for a range of values rather than the specific values of a particular numerical solution. It is currently felt that much of the difficulty in attaining these analytical solutions is due to the fact that they often contain concentrated masses. At the present time, this is just a hypothesis that is partially based on the results shown in Figs. 3.5(b), 3.8(b) and 3.9(a). In these figures, it is seen that the elements at the tip are significantly larger than the other elements. Based on further studies that used more elements, it appears that in the limit as $n \to \infty$ the final element is discontinuous from the rest of the structure and, in fact, represents a concentrated mass. This is an area of current research and efforts to prove (or disprove) the hypothesis have so far been unsuccessful. It is mentioned here to indicate the quirks these problems can have and to hopefully aid in further research in this area.

CHAPTER IV

WHITE NOISE LOADING

A. INTRODUCTION

This chapter moves from the area of the previous chapter, where the structure was excited at a single frequency, to cases where the structure is excited at all frequencies. In particular, this chapter deals with excitations that possess a Gaussian probability density function and a power spectrum that has a constant value for all frequencies. The present analysis considers loads that are random in time only. It is possible to conceive of structures that are loaded randomly in space as well and of structures whose properties are described in a probabilistic fashion, but these complications are not considered here. The motivation for this type of formulation comes from the atmospheric turbulence example of the next chapter. The turbulence wavelengths are frequently so large that any variation in the turbulence magnitude across the span of the wing can be considered negligible compared with the time variation due to the aircraft's rapid penetration of the gust field.

The flat power spectrum mentioned above is a useful analytical concept and is frequently referred to as a "white noise" spectrum. Since the excitation is described in probabilistic terms, it is

necessary to use probabilistic estimates for the response quantities as well. The most useful of these, the mean square values of responses, are obtained by integrating the power spectrum of the response over the entire range of frequencies:

$$\sigma_{RR}^2 = \int_{-\infty}^{\infty} \Phi_{RR}(\omega) d\omega$$
 (4.1)

It has been shown (Ref. 40) that the quantities that are of interest here, the displacements and the stresses, have finite mean square values even though the excitation has a finite value over an infinite range of frequencies. This fact is very important since it allows the development of analyses using the attractively simple white noise model. It is, of course, necessary to include structural damping in the model in order to obtain a finite response.

It is not possible to have a disjoint feasible design space for this problem. The disjoint properties of the examples in the previous chapter arose because of the relationships between the excitation frequency and the natural frequencies of the structure. Since the white noise excites the structure at all frequencies, it is no longer possible to have these relationships and, in fact, the design space appears to be very well behaved for these problems. The next two sections develop the constraint criteria used for the study and the analysis needed to evaluate the constraints. These methods are then applied to beam and rod models, and optimizations are performed.

B. FAILURE CRITERIA

A difficulty intrinsic to the analysis of structures excited by random loads is that explicit values of the response quantities cannot be obtained. Instead, mean values or expected values are computed using principles from probability. A further complication is that it is often unclear what meaning these estimates have relative to the safe design of a structure. The aim of this section is to describe and evaluate methods that can be used to estimate the life of a structure subjected to random loads.

Cyclic loading, characteristic of white noise excitation, can cause a structure to fail even when the magnitude of the applied stress is well below the theoretical yield stress of the material used. These fatigue failures, which are a common source of failure in actual structures, are quite difficult to predict even empirically. This is an area of intensive active research that is generally designated fracture mechanics. Current efforts divide the fatigue process into three separate areas: (1) crack initiation, (2) crack propagation, and (3) strength degradation and failure. A recent summary of this type of analysis is given by Yang and Trapp (Ref. 41). These analyses require the definition of parameters relating to load time histories, crack size, material properties and other factors, in addition to involving lengthy calculations. While the reliability estimates obtained through the use of these methods should be quite good, it is felt that the complexity of the calculations involved makes them

ill-suited for the present preliminary analysis. Instead, assumptions were made that allowed relatively simple calculations and that required the definition of a minimum number of parameters. These assumptions were obtained from Lin (Ref. 31) with supporting material from Powell (Ref. 43).

With stochastic excitations, there are two logical failure criteria, corresponding to two separate modes of failure, that could be used in the optimization procedure. The first type is failure due to the stress exceeding some specified upper limit. This is commonly referred to as first passage or first excursion failure. The other type of failure mode treats the damage to the structure as a cumulative process resulting from the fluctuations in the load. When the accumulated damage becomes equal to some specified value, the structure is assumed to have failed. (It should be mentioned that while this analysis treats these types of failure separately, the more recent fracture mechanics studies combine these two modes by postulating that the random loading causes damage through crack initiation and growth which results in the reduction of the failure stress so that the final failure is of the first type.)

The reader's familiarity with certain concepts of probability theory is assumed in the following discussion. Papoulis (Ref. 44) was found to be a useful text for reviewing this theory and should aid in the understanding of the pertinent results described below.

1. First Excursion Failure

In order to determine an estimate of the time to the arrival of the first stress greater than some specified value, it is advantageous to make a number of assumptions regarding the nature of the excitation process. Basic assumptions are that the process is stationary, Gaussian and with a zero mean. If this process is denoted by $\mathbf{x}(t)$, then the time derivative of the process, $\dot{\mathbf{x}}(t)$, is also stationary, Gaussian, has a zero mean and is independent of $\mathbf{x}(t)$. The joint probability density function and $\mathbf{x}(t)$ and $\dot{\mathbf{x}}(t)$ is

$$p_{\mathbf{x}\dot{\mathbf{x}}}(\mathbf{x},\dot{\mathbf{x}}) = \frac{1}{2\pi\sigma_{\mathbf{x}}\sigma_{\dot{\mathbf{x}}}} \exp\left(-\frac{\mathbf{x}^2}{2\sigma_{\mathbf{x}}^2} - \frac{\dot{\mathbf{x}}^2}{2\sigma_{\dot{\mathbf{x}}}^2}\right) \qquad (4.2)$$

The parameters $\sigma_{\mathbf{x}}$ and $\sigma_{\dot{\mathbf{x}}}$ in the above equation are the root mean square values of $\mathbf{x}(t)$ and $\dot{\mathbf{x}}(t)$ respectively. These can be evaluated from the power spectrum of $\Phi_{\mathbf{x}\mathbf{x}}(\omega)$ by the formula of Eq. (1,1):

$$\sigma_{\mathbf{x}}^{2} = \int_{-\infty}^{\infty} \Phi_{\mathbf{x}\mathbf{x}}(\omega) d\omega ,$$

$$\sigma_{\dot{\mathbf{x}}}^{2} = \int_{-\infty}^{\infty} \omega^{2} \Phi_{\mathbf{x}\mathbf{x}}(\omega) d\omega . \qquad (4.3)$$

A second assumption is that large values of x(t) arrive independently of one another. (Ref. 31 shows that this assumption is quite conservative for narrow band processes.) This assumption leads to a Poisson probability function for the number of times, n, that a

large magnitude, U , is exceeded in time interval, t ,

$$P_{U}(n,t) = \frac{\lambda t}{n!} \exp(-\lambda t) \qquad (4.4)$$

The λt term is the expected number of times the load will be exceeded in time interval t. Figure $^{l_{\! +}}.1$ helps in explaining this and in bringing out a further point.

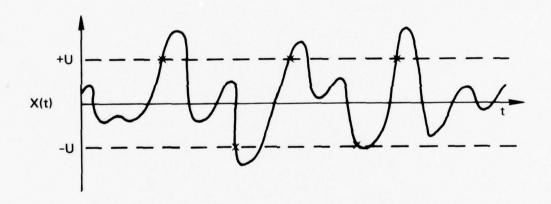


FIG. 4.1 -- Exceedances of U .

In the diagram, an exceedance occurs when x(t) crosses through U with a positive slope or through - U with a negative slope. Including the negative exceedances can be justified by the physical argument that the examples presented later deal with bending stresses in structures that are symmetric about their neutral axis. Therefore, a compressive stress of magnitude U is accompanied by a tension stress

of magnitude U on the opposite surface. Note that since the process has a zero mean, the number of negative exceedances can be assumed equal to the number of positive exceedances.

With this formulation, Eqs. (4.2) and (4.4) provide the basis for determining the expected time to the first arrival of value U. The λ term of Eq. (4.4) is twice the expected number of positive exceedances of U per unit time. After placing x(t) = U into Eq. (4.2), the expected number of exceedances can be determined by use of the formula for expected value:

$$\lambda = E(N_{U}) = 2 \int_{0}^{\infty} \frac{\dot{x}}{2\pi\sigma_{x}\sigma_{\dot{x}}} \exp(-U^{2}/2\sigma_{\dot{x}}^{2} - \dot{x}^{2}/2\sigma_{\dot{x}}^{2}) d\dot{x}$$

$$= \frac{1}{\pi} \frac{\sigma_{\dot{x}}}{\sigma_{x}} \exp(-U^{2}/2\sigma_{\dot{x}}^{2}) . \qquad (4.5)$$

With the use of Eq. (4.4), the probability of failure in time interval t is simply one minus the probability of no failure:

$$p_{F}(t) = 1 - e^{-\lambda t}$$
 (4.6)

The probability of failure at time t is found by differentiating Eq. (4.6) with respect to t . The expected time to failure is then found by multiplying this probability density function times t and

integrating it over times ranging from zero to infinity:

$$E(T) = \int_{0}^{\infty} t\lambda e^{-\lambda t} dt \qquad (4.7)$$

Integrating by parts yields

$$E(T) = 1/\lambda \qquad . \tag{4.8}$$

Equation (4.8) can now be coupled with Eq. (4.5) to provide the means for determining the constraint on the life of the structure due to first excursion failure. If it is specified that the stress in the structure cannot exceed some specified value \mathbf{U}_S in the time period \mathbf{L}_S , the constraint can be written in the form:

$$g_1 = 1 - L_S \pi \frac{\sigma_S^*}{\sigma_S} \exp(-v_S^2/2\sigma_S^2) \ge 0$$
 (4.9)

Here $\sigma_{\hat{S}}$ and $\sigma_{\hat{S}}$ are the root mean square values of the stress and the stress rate.

This constraint is applied independently to each element in the structure. It should be mentioned that the concept of fleet or lot size has been ignored here. Frequently, first excursion failure is defined as the time to failure of just one member of a larger sample. If the arrival times of the loads are independent from one sample member to another, the expected time to first failure of one structure in

a sample size of n is simply $1/n\lambda$. This would impose a more severe constraint on the individual structure, but, as was mentioned, this concept was arbitrarily disregarded.

2. Fatigue Failure

An evaluation of the fatigue life can be made using some of the results from the previous section, but it also requires further concepts. An assumption that makes the fatigue life calculation analytically straightforward is one that has come to be known as the Palmgren-Miner Theory (Ref. 45). This "theory" is based on the physically observable fact that a tension specimen that is loaded cyclically at a constant amplitude of stress, S , fails in fatigue after approximately $N_{\rm S}$ cycles. It is postulated that a structure that is loaded at this same stress level for $\eta_{\rm S}$ cycles $(\eta_{\rm S} < N_{\rm S})$ has been damaged to the extent that it is at the $\eta_{\rm S}/N_{\rm S}$ fraction of being failed. It is recognized that experimental results do not always support this theory, but it provides a simple general rule adaptable to analyses of the type presented here.

This theory is applied to a continuous random process by determining the rate at which peaks of a given magnitude occur. The rate of damage is then computed using the formula

$$DR = \int_{0}^{\infty} \frac{\eta(s) ds}{\eta(s)} , \qquad (4.10)$$

where

- $\eta\left(S\right)$ = number of stress peaks of magnitude $S \quad occurring \ per \ unit \ time \ ,$
- N(S) = number of cycles to failure at stress magnitude S .

For the purposes of this work, it is assumed that the damage done in a time interval $\,T\,$ is simply $\,DR\,\times\,T\,$.

The parameter N(S) in Eq. (4.10) can be obtained from curves that show the number of cycles to failure as a function of the stress amplitude, commonly referred to as S-N diagrams. A convenient analytical expression that is used in this work to represent this relationship, and one that is partially supported by data, is the familiar relation

$$N(S) S^b = c$$
 (4.11)

S is the stress amplitude and b and c are positive constants that must be determined empirically. This clearly gives $N(S) = c/S^b$.

The remaining factor needed for Eq. (4.10) is $\eta(S)$. Powell (Ref. $^1\!\!43$) presents an analysis that can be used to readily evaluate $\eta(S)$. This analysis starts by modifying Eq. $(^1\!\!4.5)$ to obtain the expected number of times a stress exceeds a specified positive value

S per unit time:

$$E[N^{+}(S)] = \frac{1}{2\pi} \frac{\sigma_{\dot{S}}}{\sigma_{S}} \exp(-s^{2}/2\sigma_{S}^{2}) \qquad (4.5a)$$

The derivative of this expression with respect to S can be considered a measure of the number of peaks occurring at the level S per unit time:

$$\eta(S) = -\frac{\partial E[N^{+}(S)]}{\partial S} = \frac{S}{2\pi} \frac{\sigma_{\dot{S}}^{*}}{\sigma_{\dot{S}}^{3}} \exp(-S^{2}/2\sigma_{\dot{S}}^{2}) . \qquad (4.12)$$

A point that must be considered here is that it is very difficult to specify what a cycle is for a random process. Equation (4.12) counts only the net number of peaks at level S with the "troughs" of magnitude S subtracted from the peaks. Figure 4.2 presents the reasoning behind this argument.

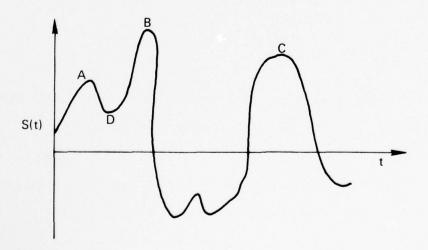


FIG. 4.2--Peaks in a Record of Random Noise.

There are three peaks in this diagram at points A, B, and C, plus one trough at D. Powell's method says that the damage done by this patch of noise is equivalent to the damage done by cycles with the magnitude of A, B, and C minus the damage resulting for a cycle of magnitude D. Without belaboring the point, on physical grounds this seems to be a better method of counting cycles than one that uses the gross number of peaks. Lin (Ref. 42) arrives at the same conclusion as that given below by assuming that the process is narrow band. For such a process, "troughs" with a positive magnitude are not likely to occur so that the problem of net versus gross number of peaks is of no importance. Finally, Yang (Ref. 46) derives an expression based on the magnitude of the excursion rather than the peak magnitude; this is clearly an improvement, but was discovered too late to be included in the present work.

The final step in the derivation is the substitution of the expressions for N(S) and $\eta(S)$ into Eq. (4.10):

DR =
$$\int_{0}^{\infty} \frac{s^{b+1}\sigma_{\dot{s}} \exp(-s^2/2\sigma_{\dot{s}}^2) ds}{2 c \pi \sigma_{\dot{s}}^3}$$
 (4.13)

The integral is evaluated by making the transformation $\left.S^2\right/2\sigma_S^2=\nu$, leading to

$$DR = \frac{\sigma_{\dot{S}}}{c\sigma_{S}\pi} \int_{0}^{\infty} (2\sigma_{S}^{2}v)^{b/2} e^{-v} dv$$

This integral can be evaluated by the use of Eq. (3.381.4) of Ref. 42

$$DR = \frac{\sigma_{\hat{S}}^{\bullet}}{2\pi e \sigma_{\hat{S}}} (2\sigma_{\hat{S}}^2)^{b/2} \Gamma \left(\frac{b+2}{2}\right) ,$$

where T is the gamma function.

To put this in constraint form, it is specified that the structure have a fatigue life greater than $\,L_{\hat{f}}\,$. The constraint is then written as

$$g_2 = 1 - DR \times L_f \ge 0$$
 (4.15)

This completes the description of the constraints used for the randomly loaded structure. It is seen that the structural response quantities that are required in order to evaluate the constraints are the root mean square values of the stress and the stress rate. The next section details how these can be obtained and also develops methods for obtaining the derivative quantities that are needed for the optimization process.

C. RESPONSE TO WHITE NOISE

A finite element representation of the response problem can be given by

$$[M]\{\vec{w}\} + [K]\{w\} = F\{E\}$$
 (4.16)

The right-hand side indicates that the equivalent forcing function is a scalar multiplying a vector that discretizes the uniform load. The scalar F has a white noise power spectrum:

$$\Phi_{\mathbf{FF}}(\omega) = N_{\mathbf{w}} - \infty \le \omega \le \infty$$
 (4.17)

Given this representation, the problem is to find the mean square values of the stresses, which are in turn a matrix function of the displacement for the examples dealt with here:

$$\{s\} = [T]\{w\}$$
 . (4.18)

The exact form of [T] depends on the structure being studied, but it is always independent of the excitation frequency and the design variables for the present study.

In order to make the problem meaningful, it is necessary to assume that the system has damping. Otherwise, the white noise excitation would result in unbounded resonances and an infinite mean square response. This was done by assuming that the structure has damping which is manifested by a complex shear modulus or Young's modulus. This, in turn, means that the stiffness matrix can be represented by:

$$[K] = (1 + i\alpha)[K_{0}] \qquad (4.19)$$

 $[{\rm K}_{\odot}]$ is a real matrix that is developed in the Appendix and $1+{\rm i}\alpha$ is a complex scalar with α representing the damping factor which is much less than unity. This same representation was used in Chapter III and, again, Ref. 36 contains a good discussion of it.

The response is determined by modal superposition. The modes used are the first mn modes of the system:

$$\{w\} = \sum_{i=1}^{mn} a_i \{p_i\} = [P]\{a\}$$
 , (4.20)

where the $\{p_i\}$'s are the mode shapes and the a_i 's are the modal participation factors. The mode shapes are independent of the excitation while the a_i 's are not, so the next step is to determine power spectra of the a_i 's .

At a given excitation frequency, ω_e , Eq. (4.16) becomes:

$$(-\omega_{P}^{2}[M] + [K])[P]{a} = F{E}$$
 . (4.21)

By premultiplying Eq. (4.21) by $[P]^T$, the equation for $\{a\}$ can be determined as a function of the generalized forces, masses and stiffnesses:

$$\left(-\omega_{\mathbf{e}}^{2}\left[\mathbb{M}\right]+\left[\mathbb{K}\right]\right)\left\{\mathbf{a}\right\} = \mathbf{F}\left[\mathbf{P}\right]^{\mathbf{T}}\left\{\mathbf{E}\right\}$$
 (4.22)

The eigenvectors are normalized so that the generalized masses are unity:

$$[\mathbb{M}] = [P]^{T}[M][P] = [I] ,$$

$$[\mathbb{K}] = [P]^{T}[K][P] = (1 + i\alpha) [\lambda] . \qquad (4.23)$$

[λ] is a diagonal matrix containing the eigenvalues of the system.

This is a system of mn uncoupled equations that can be solved independently for the modal participation factors:

$$[-\omega_{\mathbf{e}}^{2} + \omega_{\mathbf{i}}^{2}(1 + \mathbf{i}\alpha)] \ a_{\mathbf{i}} = F\{p_{\mathbf{i}}\}^{T}\{E\} \implies a_{\mathbf{i}}$$
$$= F\{p_{\mathbf{i}}\}^{T}\{E\}/[-\omega_{\mathbf{e}}^{2} + \omega_{\mathbf{i}}^{2}(1 + \mathbf{i}\alpha)] \qquad . \tag{4.24}$$

The term multiplying F is the transfer function $H_{a_iF}(j\omega)$ that relates a_i to F . This makes it possible to form the power spectra for the a's :

$$\Phi_{\mathbf{a}_{\mathbf{i}}\mathbf{a}_{\mathbf{j}}}(\omega) = H_{\mathbf{a}_{\mathbf{i}}F}(\mathbf{j}\omega) N_{\mathbf{w}} \overline{H_{\mathbf{a}_{\mathbf{j}}F}(\mathbf{j}\omega)} . \qquad (4.25)$$

The bar signifies the complex conjugate.

The most direct route to attaining the variances of the stress and stress rates is to express them in terms of the covariances of the

a 's . For computational purposes, this report distinguishes four separate covariance integrals:

$$I_{1} = \sigma_{\mathbf{a}_{1}\mathbf{a}_{1}}^{2} = \int_{-\infty}^{\infty} \Phi_{\mathbf{a}_{1}\mathbf{a}_{1}} d\omega ,$$

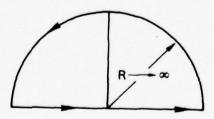
$$I_{2} = \Re \sigma_{\mathbf{a}_{1}\mathbf{a}_{1}}^{2} = \Re \int_{-\infty}^{\infty} \Phi_{\mathbf{a}_{1}\mathbf{a}_{1}} d\omega ,$$

$$I_{3} = \sigma_{\mathbf{a}_{1}\mathbf{a}_{1}}^{2} = \int_{-\infty}^{\infty} \omega^{2} \Phi_{\mathbf{a}_{1}\mathbf{a}_{1}}(\omega) d\omega ,$$

$$I_{l_{i}} = \Re \sigma_{\mathbf{a_{i}a_{j}}}^{2} = \Re \int_{-\infty}^{\infty} \omega^{2} \phi_{\mathbf{a_{i}a_{j}}}(\omega) d\omega$$
 , (4.26)

where $\Re e$ designates that only the real part is of interest.

The integrals can be evaluated by making a contour integration around the upper half plane. Combining terms from Eqs. (4.17), (4.24) and (4.25) into (4.26) gives:



$$\mathbf{1}_{1} = \mathbf{N}_{\mathbf{w}} (\{\mathbf{p}_{\mathbf{i}}\}^{\mathbf{T}} \{\mathbf{E}\})^{2} \oint_{\mathbf{C}} \frac{d\omega}{[\omega^{2} - \omega_{\mathbf{i}}^{2}(1 + \mathbf{i}\alpha)][\omega^{2} - \omega_{\mathbf{i}}^{2}(1 - \mathbf{i}\alpha)]} .$$
(4.27)

For convenience and clarity, set $\beta=\omega_{\mbox{\it i}}$. The integrand has no zeroes and four poles:

$$\mathbf{z}_{1} = \beta (1 + \mathbf{i}\alpha)^{\frac{1}{2}} ,$$

$$\mathbf{z}_{2} = -\mathbf{z}_{1} ,$$

$$\mathbf{z}_{3} = \beta (1 - \mathbf{i}\alpha)^{\frac{1}{2}} = \overline{\mathbf{z}}_{1} ,$$

$$\mathbf{z}_{4} = -\mathbf{z}_{3} = -\overline{\mathbf{z}}_{1} .$$

$$(4.28)$$

Only poles z_1 and z_4 are inside the contour. The relationships between the roots given by Eq. (4.28) and standard contour integration give

$$I_{1} = C_{1}^{2\pi i} \left[\frac{1}{(z_{1} - z_{2})(z_{1} - z_{3})(z_{1} - z_{4})} + \frac{1}{(z_{4} - z_{1})(z_{4} - z_{2})(z_{4} - z_{3})} \right],$$

where $c_1 \equiv N_w(\{p_i\}^T \{E\})^2$. Continuing:

$$I_{1} = 2\pi i C_{1} \left[\frac{1}{2z_{1}^{2} \Re e \ z_{1}^{2} i \Re z_{1}} + \frac{1}{2 \Re e \ z_{1}^{2} i \Re z_{1}^{2} z_{1}} \right]$$

$$= \frac{\pi C_{1}}{2 \Re z_{1}^{2} |z_{1}^{2}|^{2}} \cdot (4.29)$$

The magnitude of z_1 is calculated directly:

$$|z_1|^2 = \beta^2 (1 + \alpha^2)^{\frac{1}{2}}$$
 (4.30)

The $\operatorname{Am}(\mathbf{z}_1)$ calculation is a bit more difficult;

$$\mathbf{z}_{1} = \Re(\mathbf{z}_{1}) + i \Im(\mathbf{z}_{1}) = \beta(1 + i\alpha)^{\frac{1}{2}}$$

By equating the real and imaginary parts of z_1^2 , two equations that can be used to solve for $\Im (z_1)$ are formed:

$$2 \operatorname{Im}(\mathbf{z}_1) \operatorname{Re}(\mathbf{z}_1) = \beta^2 \alpha \Longrightarrow$$

$$\operatorname{Re}(\mathbf{z}_1) = \beta^2 \alpha / [2 \operatorname{Im}(\mathbf{z}_1)] \tag{4.31}$$

$$[\Re(z_1)]^2 - [\Im(z_1)]^2 = \beta^2 = \frac{\beta^4 \alpha^2}{4[\Im(z_1)]^2} - [\Im(z_1)]^2$$
 (4.32)

$$[\mathfrak{Im}(\mathbf{z}_1)]^2 = -\frac{\beta^2 \pm \sqrt{\beta^4 + \beta^4 \alpha^2}}{2} \qquad (4.33)$$

Since $\, {\rm Im}({\bf z}_1^{})\,\,$ is real, the minus sign can be rejected and

$$\mathfrak{Im}(\mathbf{z}_1) = \frac{\sqrt{2}}{2} \beta [(1 + \alpha^2)^{\frac{1}{2}} - 1)]^{\frac{1}{2}}$$
 (4.34)

By substitution of Eqs. (4.34) and (4.30) into the final result of Eq. (4.29)

$$I_{1} = \frac{c_{1}\pi}{\sqrt{2'\beta[(1+\alpha^{2})^{\frac{1}{2}}-1]^{\frac{1}{2}}\beta^{2}(1+\alpha^{2})^{\frac{1}{2}}}} . \qquad (4.35)$$

Since $\alpha < \text{O.1}$, it is appropriate to make the approximation that

$$\sqrt{1+\alpha^2} = 1 + \frac{\alpha^2}{2} + o(\alpha^4)$$
 (4.36)

The substitution of the first two terms of Eq. (4.36) into Eq. (4.35) gives:

$$I_{1} = \frac{c_{1}\pi}{\beta^{3}\alpha[1 + (\alpha^{2}/2)]}$$
 (4.35a)

It is now possible to neglect the $\alpha^2/2$ term compared with unity to get the final result:

$$\mathbf{I}_{1} = \mathbf{N}_{\mathbf{w}} \left(\left\{ \mathbf{p}_{i} \right\}^{\mathrm{T}} \left\{ \mathbf{E} \right\} \right)^{2} \pi / \omega_{i}^{3} \alpha \qquad (4.37)$$

The remaining integrals are evaluated in a similar fashion. Since the calculations are lengthy, but straightforward, only the final results are presented:

$$I_{2} = \frac{N_{\mathbf{w}} \{\mathbf{p_{i}}\}^{\mathbf{T}} \{\mathbf{E}\} \{\mathbf{E}\}^{\mathbf{T}} \{\mathbf{p_{j}}\} \pi \alpha (\omega_{i} + \omega_{j})}{2\omega_{i}\omega_{j} [(\omega_{i} - \omega_{j})^{2} + (\alpha^{2}/4)(\omega_{i} + \omega_{j})^{2}]}, \qquad (4.38)$$

$$\mathbf{I}_{3} = \mathbf{N}_{\mathbf{w}}(\{\mathbf{p}_{\mathbf{i}}\}^{\mathbf{T}}\{\mathbf{E}\})^{2} \pi/\omega_{\mathbf{i}}\alpha \qquad , \qquad (4.39)$$

$$I_{4} = \frac{N_{\mathbf{w}} \{\mathbf{p_{i}}\}^{\mathbf{T}} \{\mathbf{E}\} \{\mathbf{E}\}^{\mathbf{T}} \{\mathbf{p_{i}}\} \pi \alpha (\omega_{\mathbf{i}} + \omega_{\mathbf{j}})}{2[(\omega_{\mathbf{i}} - \omega_{\mathbf{j}})^{2} + (\omega_{\mathbf{i}} + \omega_{\mathbf{j}})^{2}(\alpha^{2}/4)]} \qquad (4.40)$$

The variances of the stresses are obtained by a linear combination of the covariances that have just been calculated. The examples in the sections to follow use the explicit relationships between the stress and the displacement. The general form of Eq. (4.18) is adequate for the present derivation:

$${S} = [T]{w} = [T][P]{a}$$
.

The power spectra of the stresses are, therefore, related to the power spectra of the modal participation factors by the simple relation:

$$[\Phi_{SS}(\omega)] = [T][P][\Phi_{aa}(\omega)][P]^{T}[\overline{T}]^{T}$$
 . (4.41)

The complex conjugate is included in the above equation because the [T] matrix contains a complex structural parameter. Since neither [T] nor [P] are functions of the excitation frequency, the stress variances are found by replacing $\Phi_{aa}(\omega)$ with the covariance matrix for the a's in Eq. (4.41),

$$[X_{SS}] = [T][P][X_{aa}][P]^{T}[\overline{T}]^{T}$$
 (4.42)

Similarly,

$$[\mathbf{X}_{\dot{\mathbf{S}}\dot{\mathbf{S}}}] = [\mathbf{T}][\mathbf{P}][\mathbf{X}_{\dot{\mathbf{a}}\dot{\mathbf{a}}}][\mathbf{P}]^{\mathbf{T}}[\overline{\mathbf{T}}]^{\mathbf{T}}$$

The square roots of the diagonal elements of $[X_{SS}]$ and $[X_{SS}^{\bullet}]$ are the rms values of the stresses and stress rates needed in order to evaluate Eqs. (4.9) and (4.15).

It is readily shown that these diagonal elements are real and that they involve only the real parts of the $[X_{aa}]$ matrix. To prove this, some preliminary notations must be defined.

Express [T] as $(1+i\alpha)[T_0]$, where $[T_0]$ is real. Define tp_{ij} as the i,jth element of $[T_0][P]$, and pt_{ij} as the i,jth element of $[P]^T[T_0]^T$.

Note that $tp_{ij} = pt_{ji}$ and that $X_{a_i a_j} = X_{a_j a_i}$.

The diagonal elements of the stress covariance matrix can therefore be explicitly expressed by:

$$X_{\mathbf{S_{i}S_{i}}} = (1 + \alpha^{2}) \sum_{j=1}^{mn} t_{\mathbf{P_{ij}}} \sum_{k=1}^{mn} X_{\mathbf{a_{j}a_{k}}} p_{\mathbf{k}i}$$

$$= (1 + \alpha^{2}) \sum_{j=1}^{mn} \left[(t_{\mathbf{P_{ij}}})^{2} X_{\mathbf{a_{j}a_{j}}} \right]$$

$$+ \sum_{\substack{k=1 \ k \neq j}}^{mn} t_{\mathbf{P_{ij}}} t_{\mathbf{P_{ik}}} X_{\mathbf{a_{j}a_{k}}} \right]$$

$$= (1 + \alpha^{2}) \left[\sum_{j=1}^{mn} (t_{\mathbf{P_{ij}}})^{2} X_{\mathbf{a_{j}a_{j}}} \right]$$

$$+ 2 \sum_{k=i+1}^{mn} t_{\mathbf{P_{ij}}} t_{\mathbf{P_{ik}}} \Re X_{\mathbf{a_{j}a_{k}}} \right] . \quad (4.43)$$

All the elements in the equation above are real and, as was to be proved, only the real parts of the $[X_{aa}]$ matrix are included. This explains why only the real parts of the integrals I_2 and I_4 of Eq. (4.26) were required.

This concludes the derivation of the terms needed for the constraint evaluation. A remaining task is the calculation of the derivatives needed for the gradient in the optimization algorithm.

1. Derivative Calculations

The design variables for these problems, the structural thicknesses, are manifested in the mass and stiffness matrices. The gradient technique of the optimization algorithm requires that the derivative of the constraints be calculated. This in turn requires that the derivatives be calculated for all the quantities used to compute the constraints and that are a function of the design variables.

The first step is the calculation of the derivatives of the eigenvalues and eigenvectors of the system. Fox and Kapoor (Ref. 15) presented a straightforward method for calculating these quantities, and this method is summarized below.

Consider the unforced system with a given eigenvalue and eigenvector:

$$(-\lambda_{i}[M] + [K])\{p_{i}\} = \{0\}$$
 . (4.44)

For ease of notation, set $[F_i] \equiv -\lambda_i[M] + [K]$.

The derivative of Eq. (4.44) with respect to the design variable t_j is

$$\left(-\lambda_{i} \frac{\partial [M]}{\partial t_{j}} + \frac{\partial [K]}{\partial t_{j}} - \frac{\partial \lambda_{i}}{\partial t_{j}} [M]\right) \{p_{i}\} + [F_{i}] \left\{\frac{\partial p_{i}}{\partial t_{j}}\right\} = 0 . \quad (4.45)$$

The system given by Eq. (4.44) is self-adjoint so that if Eq. (4.45) is premultiplied by $\{p_i\}^T$, the last term drops out, leaving

$$\frac{\partial^{\lambda}_{\mathbf{i}}}{\partial t_{\mathbf{j}}} \{ \mathbf{p_{i}} \}^{\mathbf{T}} [\mathbf{M}] \{ \mathbf{p_{i}} \} = \{ \mathbf{p_{i}} \}^{\mathbf{T}} \left[\frac{\partial [\mathbf{K}]}{\partial t_{\mathbf{j}}} - \lambda_{\mathbf{i}} \frac{\partial [\mathbf{M}]}{\partial t_{\mathbf{j}}} \right] \{ \mathbf{p_{i}} \} \qquad (4.46)$$

Since the eigenvectors have been normalized to make the generalized masses equal to unity, the eigenvalue derivative can be expressed as:

$$\frac{\partial^{\lambda}_{i}}{\partial t_{j}} = \{p_{i}\}^{T} \left[\frac{\partial [K]}{\partial t_{j}} - \lambda_{i} \frac{\partial [M]}{\partial t_{j}} \right] \{p_{i}\} \qquad (4.46a)$$

From Eq. (4.44), with the eigenvalue derivative calculated, the eigenvector derivative can be solved for:

$$[F_{\mathbf{i}}] \left\{ \frac{\partial P_{\mathbf{i}}}{\partial t_{\mathbf{j}}} \right\} = -\frac{\partial [F_{\mathbf{i}}]}{\partial t_{\mathbf{j}}} \{P_{\mathbf{i}}\} \qquad (4.47)$$

But since $\{F_i\}$ is singular, another equation is needed to specify the magnitude of $\{\partial p_i/\partial t_j\}$. This equation comes from differentiating the generalized mass:

$$\frac{\partial}{\partial t_{j}} \{p_{i}\}^{T}[M]\{p_{i}\} = 0 = 2\{p_{i}\}^{T}[M] \left\{\frac{\partial p_{i}}{\partial t_{j}}\right\} + \{p_{i}\}^{T} \frac{\partial[M]}{\partial t_{j}} \{p_{i}\} . \quad (4.48)$$

Equations (4.47) and (4.48) can be combined to give:

$$\begin{bmatrix} \begin{bmatrix} \mathbf{F_i} \end{bmatrix} \\ \mathbf{2} \begin{bmatrix} \mathbf{p_i} \end{bmatrix}^{\mathbf{T}} [\mathbf{M}] \end{bmatrix} \left\{ \frac{\partial \mathbf{P_i}}{\partial \mathbf{t_j}} \right\} = - \begin{bmatrix} \partial [\mathbf{F_i}] / \partial \mathbf{t_j} \\ {\mathbf{p_i}} \end{bmatrix}^{\mathbf{T}} (\partial [\mathbf{M}] / \partial \mathbf{t_j}) \end{bmatrix} \{ \mathbf{p_i} \} . \quad (4.49)$$

In order to obtain a square, non-singular matrix, both sides of Eq. (4.49) are premultiplied by $[F_i, 2[M]\{p_i\}]$ to obtain

$$\left[\left[\mathbf{F_{i}} \right]^{2} + 4 \left[\mathbf{M} \right] \left\{ \mathbf{p_{i}} \right\} \left\{ \mathbf{p_{i}} \right\}^{T} \left[\mathbf{M} \right] \right] \left\{ \frac{\partial \mathbf{p_{i}}}{\partial \mathbf{t_{j}}} \right\} = \left[- \left[\mathbf{F_{i}} \right] \frac{\partial \left[\mathbf{F_{i}} \right]}{\partial \mathbf{t_{j}}} \right] \\
- 2 \left[\mathbf{M} \right] \left\{ \mathbf{p_{i}} \right\} \left\{ \mathbf{p_{i}} \right\}^{T} \frac{\partial \left[\mathbf{M} \right]}{\partial \mathbf{t_{j}}} \right] \left\{ \mathbf{p_{i}} \right\} . \tag{4.50}$$

This is a matrix equation that can be used to solve for the eigenvector derivatives $\{\partial p_i/\partial t_j\}$. Note that since the matrix multiplying the eigenvector derivative is not a function of the design variable, it is necessary to decompose this matrix only once to solve for the n design variable derivatives. A further note is that experience with this method has indicated that it is frequently helpful to multiply Eq. (4.48) by λ_i as a scaling procedure.

The remaining steps in the derivative calculation are much less complicated. The derivatives of modal covariances I_1 and I_2 are given below as an example, but it seems of little purpose to show the

entire analysis here. A few terms must be derived first:

$$\omega_{\mathbf{i}}^{2} = \lambda_{\mathbf{i}} = \frac{\partial \omega_{\mathbf{i}}}{\partial t_{\mathbf{j}}} = \frac{1}{\partial \omega_{\mathbf{i}}} \frac{\partial \lambda_{\mathbf{i}}}{\partial t_{\mathbf{j}}},$$

$$\frac{\partial (\{p_{\mathbf{i}}\}^{T}\{E\})}{\partial t_{\mathbf{j}}} = \frac{\partial \{p_{\mathbf{i}}\}^{T}}{\partial t_{\mathbf{j}}} \{E\} \qquad (4.51)$$

Then:

$$\frac{\partial \mathbf{I_1}}{\partial \mathbf{t_j}} = \mathbf{I_1} \left[-\frac{3}{\omega_i} \frac{\partial \omega_i}{\partial \mathbf{t_j}} + \frac{2}{\{\mathbf{p_i}\}^T \{\mathbf{E}\}} \frac{\partial \{\mathbf{p_i}\} \{\mathbf{E}\}}{\partial \mathbf{t_j}} \right] \quad . \tag{4.52}$$

Designate:

$$\gamma \equiv \left[\left(\omega_{\mathbf{i}} - \omega_{\mathbf{k}} \right)^2 + \frac{\alpha^2}{4} \left(\omega_{\mathbf{i}} + \omega_{\mathbf{k}} \right)^2 \right] .$$

Then:

$$\frac{\partial I_{2}}{\partial \mathbf{t}_{j}} = I_{2} \left\{ \frac{1}{\{\mathbf{p_{i}}\}^{T}\{\mathbf{E}\}} \frac{\partial \{\mathbf{p_{i}}\}^{T}\{\mathbf{E}\}}{\partial \mathbf{t}_{j}} + \frac{1}{\{\mathbf{p_{k}}\}^{T}\{\mathbf{E}\}} \frac{\partial \{\mathbf{p_{k}}\}^{T}\{\mathbf{E}\}}{\partial \mathbf{t}_{j}} \right.$$

$$- \frac{\omega_{\mathbf{k}}}{\omega_{\mathbf{i}}(\omega_{\mathbf{i}} + \omega_{\mathbf{k}})} \frac{\partial \omega_{\mathbf{i}}}{\partial \mathbf{t}_{j}} - \frac{\omega_{\mathbf{i}}}{\omega_{\mathbf{k}}(\omega_{\mathbf{i}} + \omega_{\mathbf{k}})} \frac{\partial \omega_{\mathbf{k}}}{\partial \mathbf{t}_{j}} \right\}$$

$$- \frac{1}{\gamma} \left[\left(2(\omega_{\mathbf{i}} - \omega_{\mathbf{k}}) + \frac{\alpha^{2}}{2} (\omega_{\mathbf{i}} + \omega_{\mathbf{k}}) \right) \frac{\partial \omega_{\mathbf{i}}}{\partial \mathbf{t}_{i}} \right] (Cont'd)$$

$$+\left(-2(\omega_{\mathbf{i}}-\omega_{\mathbf{k}})+\frac{\alpha^{2}}{2}(\omega_{\mathbf{i}}+\omega_{\mathbf{k}})\right)\frac{\partial \omega_{\mathbf{k}}}{\partial t_{\mathbf{j}}}$$
 (4.53)

This should indicate that the remaining derivative calculations are tedious, but uncomplicated. It is mostly a matter of the continuous application of the chain rule until the final derivatives that are required are reached. These are the derivatives of the constraints, the first of which is given in Eq. (4.9);

$$g_1 = 1 - L_S \frac{\sigma_{\dot{S}}}{\sigma_S} e^{-U_S^2/2\sigma_S^2} \ge 0$$

The derivative is:

$$\frac{\partial \mathbf{g_1}}{\partial \mathbf{t_j}} = (\mathbf{g_1} - 1) \left[\frac{1}{\sigma_{\mathbf{S}}} \left(\frac{\mathbf{u_S^2}}{2\sigma_{\mathbf{S}}^2} - 1 \right) \frac{\partial \sigma_{\mathbf{S}}}{\partial \mathbf{t_j}} + \frac{1}{\sigma_{\mathbf{S}}} \frac{\partial \sigma_{\mathbf{S}}^*}{\partial \mathbf{t_j}} \right] \qquad (14.54)$$

Similarly for g_2 , from Eq. (4.15)

$$g_2 = 1 - L_F \frac{\sigma_S^{\bullet}}{2\pi c \sigma_S} (2\sigma_S^2)^{b/2} \Gamma\left(\frac{b+2}{2}\right)$$
.

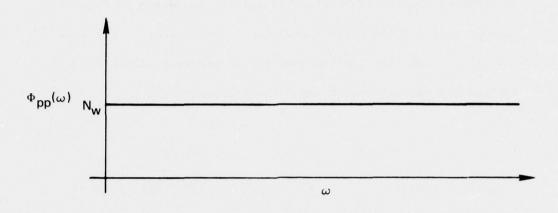
And the derivative is

$$\frac{\partial \mathbf{g}_{2}}{\partial \mathbf{t}_{j}} = (\mathbf{g}_{2} - 1) \left(\frac{1}{\sigma_{\dot{\mathbf{S}}}} \frac{\partial \sigma_{\dot{\mathbf{S}}}}{\partial \mathbf{t}_{j}} + \frac{(\mathbf{b} - 1)}{\sigma_{\mathbf{S}}} \frac{\partial \sigma_{\mathbf{S}}}{\partial \mathbf{t}_{j}} \right) . \tag{4.55}$$

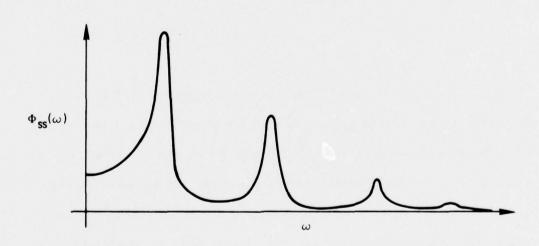
D. EXAMPLES

As in the previous chapter, cantilevered rods and beam examples were optimized. Figure 4.3(a) shows the power spectrum of the white noise excitation while Fig. 4.3(b) is a qualitative depiction of a response quantity. The peaks on the latter figure represent structural resonances which are the main contributors to the mean values of the response.

It is perhaps necessary to justify the use of a finite number of modes to represent the response of a structure excited by loads with a white noise spectrum. As mentioned in the introduction to this chapter, Bogdanoff and Goldberg (Ref. 40) show that the mean square values of the stress and displacement in an Euler-Bernoulli beam are finite when the beam is excited by the noise. They do this while taking into account an infinite number of modes and by assuming constant viscous damping. A further indication that a finite number of modes suffice is given by Eqs. (4.24) and (4.25) which show that the peaks of the spectra for the modal participation factors are inversely proportional to $\omega_{\mathbf{i}}^{4}$. This indicates that the contributions to the rms responses from the separate modes die off quickly as the mode number and, therefore the natural frequency increases. Finally an empirical justification for using a finite number of modes is given by the results below which show that solutions found using four modes differ only marginally from solutions using two modes.



(a) White Noise Excitation



(b) Representative Response

FIG. 4.3--Representative Power Spectral Density Shapes for a Structural System with a White Noise Input.

1. Torsion Rod

The thin walled rod of Section III.D.1 is used again in this section, except that a white noise excitation is now present. The following list of parameters repeats some of the previous values and adds new ones for the special requirements of this problem.

$$G = 3.75 \times 10^6 \text{ psi}$$
 $\rho_s = 0.1 \text{ lbm/in}^3$
 $R = 6 \text{ inches}$ $I_{\alpha 0} = 4.2 \text{ slugs}$
 $L = 120 \text{ inches}$ $\alpha = 0.05$
 $J_0 = 2\pi R^3 = 1352 \text{ in}^3$ $b = 8$
 $N_w = 1240 (1b)^2/\text{rad/sec}$ $c = 10^{41}$
 $U_S = 40,000 \text{ psi}$

The parameters b and c are from the equation $NS^b=c$ and were obtained by fitting an S-N curve for aluminum given in Crandall and Dahl (Ref. 46, Sec. 5-13). The value chosen for α is rather high and it is recognized that an important part of an actual design process using the methods described here would be to obtain more accurate and justifiable values for the α , b and c parameters.

The constraint placed on the fatigue life was that it be no less than one year, and the expected time to stress value $\,{\rm U}_{\rm S}\,$ was set to be no less than one-half year.

The results of the optimization algorithm are presented in Figs. 4.4 and 4.5. Figure 4.4 compares the optimal thickness distributions when two, three and eight elements are used to represent the structure. It is seen that as more elements are used, the total weight remains nearly constant while there is some qualitative difference in the distributions. For the eight element structure, more mass tends to be concentrated near the tip. More will be said about this later.

All the results presented in Fig. 4.4 used two structural modes in their solution. Figure 4.5 compares results of analyses using two modes and four modes. It is seen that there are some minor differences at the tip, but they have to be considered negligible. Table 4.1 gives numerical results for the two cases.

Element Number	Thickness		Fatigue Constraint		
	2 Modes	4 Modes	2 Modes	4 Modes	
1	1.694	1.698	9.5 · 10 ⁻³	5.93 · 10	
2	1.582	1.577	1.8 • 10-3	3.90 · 10	
3	1.382	1.392	4.0 • 10-3	1.04 • 10-3	
14	1.128	1.129	9.1 · 10 ⁻³	2.78 · 10 ⁻³	
5	0.8592	0.8754	4.8 • 10-3	9.37 · 10 ⁻³	
6	0.6111	0.6170	5.0 · 10 ⁻¹⁴	1.46 · 10 ⁻²	
7	0.5262	0.5230	0.925	0.874	
8	0.5618	0.5868	1.000	1.000	

TABLE 4.1--Comparison of Two and Four Mode Solutions.

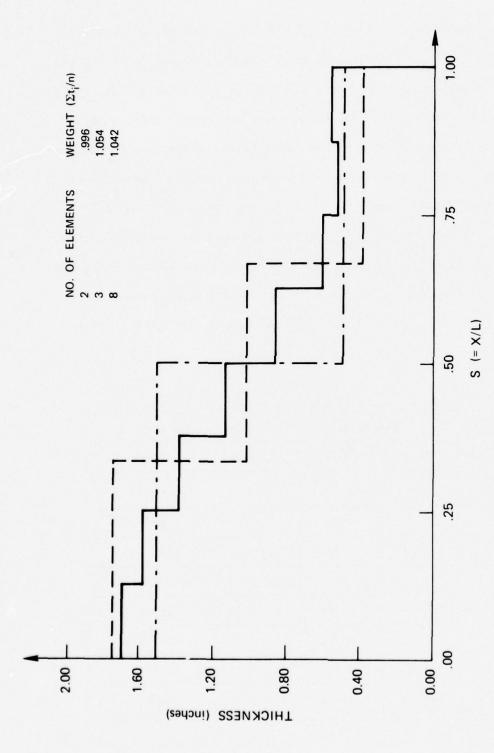


FIG. ...-Optimal Thickness Distributions for a Cantilevered Rod Excited by a Uniformly Distributed White Noise Torque.

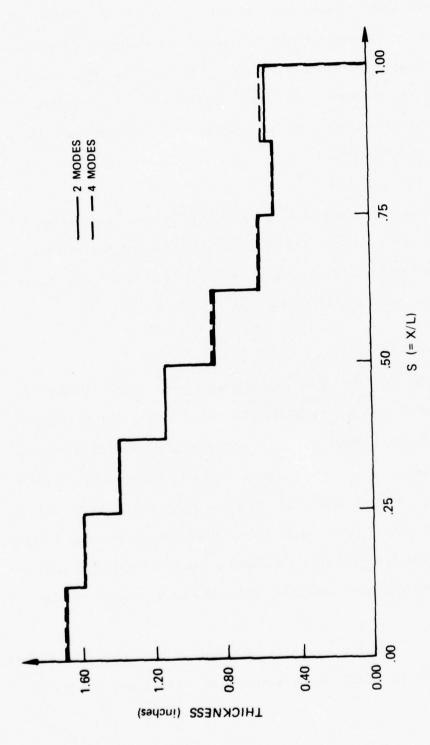


FIG. 4.5--Optimal Thickness Distribution for a Cantilevered Rod Excited by a Uniformly Distributed White Noise Torque - Comparison of Solutions Using Two and Four Natural Modes.

This shows that although the four mode solution took 50% more computer time to converge, it did not appreciably change the results. The fatigue constraint values are presented to show that the optimization proceeded to the same level in determining the active constraints. The values given are those computed using Eq. (4.15); therefore, the numbers near zero indicate that the constraint is almost exactly satisfied (i.e., it is active).

The optimization seems to have found that placing some weight at the tip provides an inertial load that relieves the inboard stress. Since this phenomenon is exhibited in the beam results as well, it is appropriate to consider this in somewhat more detail.

2. Effect of a Tip Mass

This section presents some findings of a brief study that was made to justify the optimal solutions that included a large finite thickness at the tip. In particular, the study sought to determine what effect a concentrated mass at the tip would have on the maximum stress in a cantilevered beam. The hypothesis was that the effect would be to reduce the stress. Obviously, this would not be the case for a static loading or for a low frequency harmonic excitation, but the results of the optimization indicated that something different was happening for the white noise excitation.

The model studied was a uniform cantilevered beam with a point mass at the tip. The excitation was assumed to be uniform across the span

and random in time with a white noise power spectral density. The mass of the beam was kept constant while the tip mass was varied as the only independent parameter.

The problem could be solved by a differential equation approach coupled with modal superposition as was done in Ref. 40. However, since a computer program that analyzed this type of problem using finite elements already existed, it was more expedient to use it. The next section presents the structural parameters and the excitation spectrum used for the analysis. The thickness distribution was held fixed for all elements at a value of one. A nonstructural point mass was added to the last element and was varied through a range of values.

Figures 4.6 and 4.7 present the results for the rms stress and stress rate, respectively, for four values of the concentrated mass, nondimensionalized by the mass of the beam. It is seen that the mass has the effect of reducing the maximum rms stress, which always occurs at the root. The effect on the rms stress rate is to increase its peak value, but since the stress is of far more importance in the evaluation of fatigue life than the stress rate, this increase is relatively unimportant. It is interesting to note that the higher modes are obviously present in the stress rate distribution but that the first two modes seem to dominate the stress distribution.

The main finding is that the addition of mass at the tip can improve the fatigue life. In hindsight it is clear what has happened:

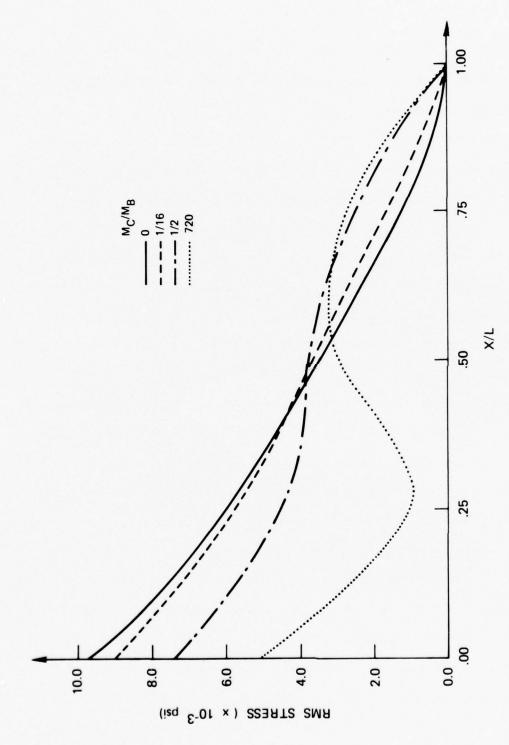


FIG. '..--Root Mean Square Stress in a Uniform Cantilevered Beam with a Concentrated Tip Mass Excited by Uniformly Distributed White Noise.

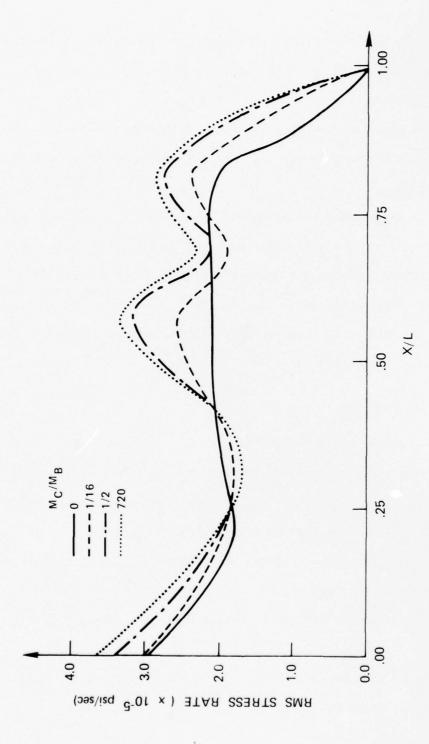


FIG. 4.7--Root Mean Square Stress Rate of the Beam of Fig. 1.0.

the added mass acts as an inertial force that resists the excitation and, in the limit as the mass becomes very large, acts as a simply supported boundary.

For the cantilevered rod, a similar effect takes place in that a mass would act to restrain the tip rotation and in the limit act as a fixed boundary.

This is an interesting and unanticipated result. A further study that could be done is a two design variable optimization study using the concentrated mass and the uniform thickness as the variables.

Constraints could be placed on the rms stress or on the fatigue life. The above analysis shows that the optimal concentrated mass would not be zero.

3. Cantilevered Beam

A beam example was optimized to see if it had any new, interesting characteristics. The methods of Section IV.B are directly applicable to the beam example so that the only changes necessary are the inclusion of the proper forms for the finite element representation of the beam structure. Since the Appendix and Chapter III are quite thorough in these aspects, they are not repeated here.

The properties chosen for the beam and the load are

Length = 240 inches $E = 10.5 \times 10^6 \text{ psi}$ Width = 30 inches $\rho_s = 0.1 \text{ lbm/in}^3$ Depth = 3.0 inches $\alpha = 0.05$

$$b = 8$$
 $c = 10^{1/4}$ $N_{W} = 0.01 (1b/in)^{2}/rad/sec$ $U_{S} = 140,000 psi$

The large width to depth ratio was chosen because of a future anticipated application of the model to aeroelastic problems where it would represent a wing.

The constraints were continued at one year for the fatigue life and one-half year for the expected time to failure.

A comparison of the results obtained using two elements and eight elements is presented in Fig. 4.8, while Fig. 4.9 compares results obtained from an analysis that used four modes with one that used two. The concentration of mass near the tip is more pronounced for the problem, but the qualitative effects are the same as for the rod example.

Table 4.2 compares the four mode and the two mode solutions.

Element	Thickness		Fatigue Constraint		First Excursion Failure Constraint	
	2 Modes	4 Modes	2 Modes	4 Modes	2 Modes	4 Modes
1	0.1750	0.1751	0.042	0.034	0.990	0.990
2	0.1335	0.1352	0.049	0.043	0.961	0.977
3	0.1016	0.1033	0.055	0.064	0.941	0.968
14	0.0801	0.0809	0.069	0.070	0.940	0.994
5	0.0596	0.0602	0.113	0.096	0.999	0.999
6	0.0381	0.0387	0.165	0.249	1.00	1.00
7	0.0554	0.0590	1.00	1.00	1.00	1.00
8	0.644	0.0647	1.00	1.00	1.00	1.00
Total	0.7078	0.7171				

TABLE 4.2--Cantilevered Beam: Comparison of Two and Four Mode Solutions

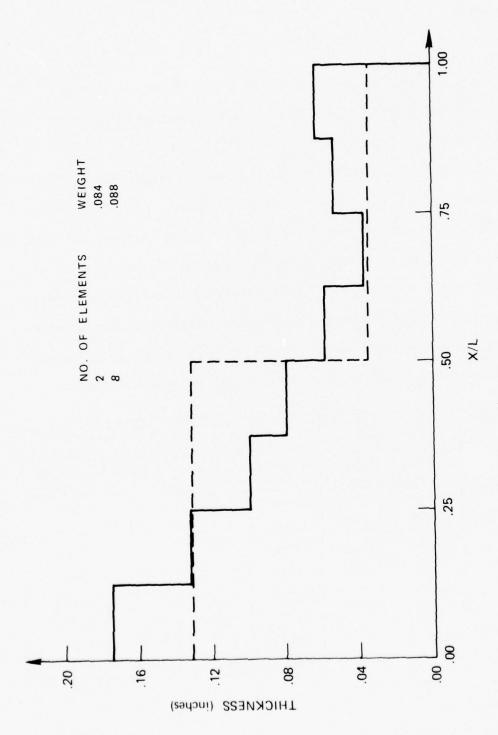


FIG. L.S--Optimal Thickness Distribution of a Cantilevered Beam Excited by a Uniformly Distributed White Noise Transverse Load.

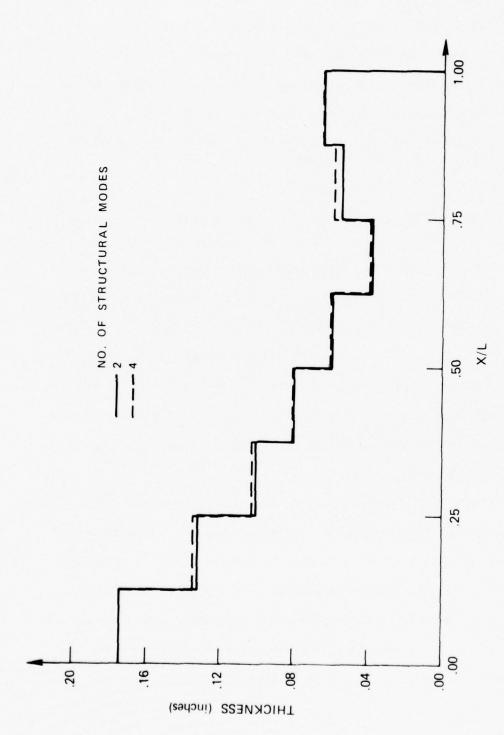


FIG. 4.9--Optimal Thickness Distribution for a Cantilevered Beam Excited by a Uniformly Distributed White Noise Transverse Load — Eff ct of the Number of Structural Modes.

The four mode solution is 1.3% heavier than the two mode solution; a disparity that is probably less than the percentage by which these solutions differ from the true optimum. It is possible that further iteration would make some of the constraints tighter, but it is felt that little information would be returned to justify the added computer time.

E. CONCLUDING COMMENTS

The results of the two examples tend to show that, as in some of the harmonically forced solutions of the previous chapter, there is a tendency for some of the mass to be concentrated near the tip. In fact, the solutions obtained for the white noise examples could perhaps be thought of as a superposition of the two solutions given for a single harmonic excitation, such as those of Fig. 3.6. It is not known whether this observation has any practical significance for the solution of this class of problems.

It is felt that a formulation of this type makes a useful contribution in that it presents new results and extends the methods of structural optimization into an almost unexplored field. Obviously, however, the examples studied in this chapter are mainly of theoretical interest. Methods of fracture mechanics combined with load spectra that are of great practical interest would aid greatly in the application of the techniques to more applied studies.

The next chapter does attempt to perform an optimization on a structure that is of more interest: an aircraft wing in the presence of atmospheric turbulence.

CHAPTER V

CONTINUOUS ATMOSPHERIC TURBULENCE

A. INTRODUCTION

Structural fatigue and failure resulting from stochastic loads are one of the most commonly occurring maintenance and safety problems for aircraft structures. The nature of these vehicles is such that there is a very high payoff in terms of performance and operating economy for savings made in the structural weight. These two facts combine to provide a powerful motivation for finding optimal structures under the condition of random aerodynamic excitation with fatigue life as one of their constraints. Specifically, this chapter deals with the minimization of the structural weight of an aircraft wing that is subjected to continuous atmospheric turbulence.

The formulation used in this study is, in keeping with the scope of the thesis, of a preliminary nature with a continual tradeoff made between physical realism and computational simplicity. The main objectives in the development of the mathematical models that are presented in the next section are to obtain a representation that is consistent in terms of level of sophistication and to retain the important elements of the problem. After the presentation of these models, it is necessary to develop the analytical tools needed for the constraint evaluation and then some results are presented.

B. COMPUTATIONAL MODELS

There are three distinct areas that have to be considered in the development of the mathematical representation of a wing excited by turbulence: (1) the structure of the wing, (2) the aerodynamic operators and (3) the disturbing gust forces. Before dealing with each of these separately, some general limitations on the analysis should be mentioned here.

The motion of the wing was constrained to consist of rigid body plunging motion plus transverse bending. A more general formulation would include at least rotational deformation and perhaps rigid body rotations as well. While it would not be impossible to include these, it is felt that the present formulation is the logical place to start.

A similar decision was made to limit the constraints to those dealing with the life of the structure. It is realized that an actual design has to meet a myriad of criteria so that the results presented here represent only the specific designs obtained for a specifically posed problem.

1. Structural Model

Many of the mathematical aspects of the present problem were provided by Ref. 32. In selecting a structural model to use in this study it seemed natural, therefore, to choose a wing that is used extensively in the examples of that text. In particular, Example 10.6 of that text presents an analysis that parallels much of what is presented below. Figure 5.1 shows a planform of that wing with its important dimensions.

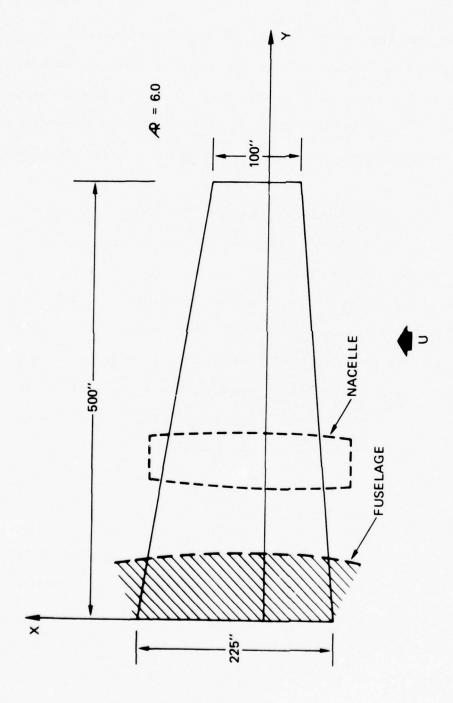


FIG. 5.1--Wing Planform.

As the figure shows, the structural model chosen includes a nacelle and fuselage. The masses of these two elements were held fixed during the optimization at the values of

$$m_{FUS} = 430.4 \text{ slugs}$$

$$m_{NAC} = 163.0 \text{ slugs}$$

The assumption regarding linearity between the design variables and the structural inertia and mass was retained in this chapter. By fitting data given in Ref. 32, the following factors of proportionality were obtained:

$$m(y) = mass/inch = 2.2 t(y) slugs/inch$$

EI = stiffness =
$$5.94 \cdot 10^{10} \text{ t(y) 1bs-in.}^2$$

The taper of the chord adds complexity to the numerical calculations that determine the mass and stiffness matrices. Section C of the Appendix details corrections that are made to the untapered results to account for this fact. In addition, the Appendix describes how the non-structural masses representing the nacelle and the fuse-lage are incorporated into the mass matrix.

Turbulence Model

The previous chapter dealt with the responses to a random excitation whose power spectrum was constant over all frequencies. Numerous studies have shown that this white noise assumption is inadequate as a model for atmospheric turbulence. Chapter 13 of Ref. 47 and Ref. 48 contain excellent discussions of the procedures used and the approximations made in the development of alternative models. From these references it was decided that the analytical expression for the turbulence spectrum that is best suited for the present study is the one designated the von Karman model. The power spectrum of the vertical component of the atmospheric turbulence given by this model is

$$\Phi_{\mathbf{w}_{\mathbf{g}}}(\Omega) = \frac{\sigma_{\mathbf{w}_{\mathbf{g}}}^{2}}{\pi} \frac{L_{\mathbf{T}}[1 + \frac{8}{3} (1.339 L_{\mathbf{T}}\Omega)^{2}]}{[1 + (1.339 L_{\mathbf{T}}\Omega)^{2}]^{11/6}}.$$
 (5.1)

The terms of this equation are defined in the list of symbols.

A number of crucial assumptions have to be made about the nature of the turbulence in order to arrive at this form (e.g., that the turbulence is homogeneous and that it has a Gaussian distribution). The adequacy of these assumptions are evaluated quite well in Ref. 48 and will not be discussed here.

Values for the turbulence scale and the mean square value of the turbulence had to be selected. From Ref. 48, values were chosen that

were typical for severe thunderstorm conditions. These were

$$L_{T} = 5000 \text{ ft.}$$
 , $\sigma_{w_{g}} = 1^{1/4} \text{ ft./sec.}$.

The scale length (which is a measure of the turbulence wavelength) is considerably greater than the 83 ft. span of the wing used for this study. This large difference in scale reinforces the approximation that the turbulence is one-dimensional with a uniform value across the span at any instant.

Figure 5.2 compares the von Karman spectrum used in the present study with the spectrum used in Example 10.6 of Ref. 32. It is necessary to present the comparison here because a later figure compares two bending moment spectra that were obtained using the two different excitation spectra. It is seen that the von Karman spectrum has a considerably higher proportion of its energy in the lower frequencies.

3. Aerodynamic Operators

The most important difference in the nature of the present problem compared to those of the previous chapters is in the manner in which the loading is exerted on the structure. In the previous chapter, the random disturbance was assumed to be transferred directly to the structure in some unspecified manner. In the present example, the aerodynamic loads that result from the unsteady gust differ in phase and magnitude from the gusts themselves. This is due to the fact that

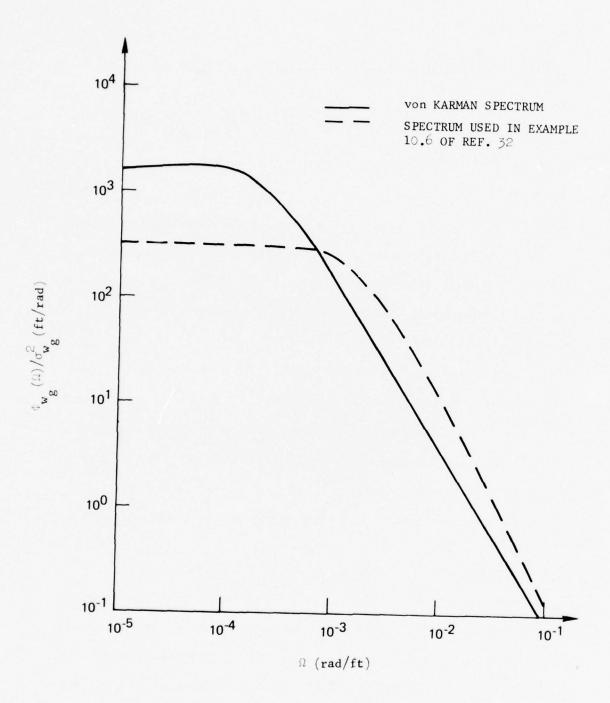


FIG. 7.2--Comparison of Excitation Spectra.

the loads on the structure, which are a function of the circulation, do not respond instantaneously to the gust. A further complication is the fact that the motion of the wing moving in response to the gust's excitation gives rise to additional forces.

This study is restricted to vertical motions only; therefore, the relevant load acting on the wing is the lift. As the previous paragraph indicates, this load can be separated into two components:

$$P = L_{m} + L_{g} (5.2)$$

 $L_{\rm g}$ is the direct lift associated with the impingement of the gust while $L_{\rm m}$ is the added lift resulting from the wing's motion. Values for these two components are developed in Chap. 5 of Ref. 32 for a two-dimensional airfoil in incompressible flow that is encountering a sinusoidal gust. These values are given by

$$\frac{L_g}{w_g} = 2\pi o_a U_b \left\{ C(k) \left[J_O(k) - iJ_1(k) \right] + iJ_1(k) \right\}, \qquad (5.3)$$

$$L_{m} = \pi \rho_{a} U^{2} \left[k^{2} - 2ik C(k)\right]h \qquad , \qquad (5.4)$$

where:

h = vertical displacement

C(k) = Theodorsen's function

 J_{\bigcirc} and J_{1} = Bessel functions of the first kind .

Theodorsen's function is a complex function of the reduced frequency and is an analytical representation of the change in amplitude and phase of the circulatory lift due to a vertical oscillation. It can be expressed explicitly in terms of Hankel functions, but for the low magnitudes of k of interest to this study, it was deemed adequate to use an approximation that is given by Fung in Section 6.9 of Ref. 49:

$$C(k) = 1.0 - \frac{0.165}{[1.0 - (0.0455i/k)]} - \frac{0.335}{[1.0 - (0.3i/k)]}$$
 (5.5)

Perhaps it is in order to point out here that the complex nature of the aerodynamics makes it unnecessary to include structural damping. This damping was required in the previous chapter in order to obtain finite response, but the out of phase component of the aerodynamics acts as a damping mechanism that limits the structural response to finite values regardless of the excitation frequency.

In order to apply these results to the problem at hand, a number of additional assumptions must be made. These are mainly the approximations that are used in aerodynamic strip theory:

- (1) The incompressible results are valid for the analysis. (The example considered has a free stream Mach number of 0.62 so that compressibility effects could be constructively considered.)
- (2) The reduced frequency is computed using a reference chord, as opposed to the local chord, resulting in a k that is constant

across the span. While this is not strictly necessary, it greatly simplifies the calculation. The range of actual reduced frequency values across the span is small enough so that the error introduced by this assumption is not large.

(3) The loads on the three-dimensional wing are the same as would occur at that wing station in a two-dimensional flow (except for the disparity in k values mentioned in the previous assumption).

It would be interesting, and not too difficult, to determine what effect these assumptions have on the final results. However, these were considered to be secondary matters that did not require evaluation for the present study.

Once these aerodynamic loads have been evaluated, it is necessary to put them into a form consistent with the finite element models developed for the mass and stiffness matrices. Again, the Appendix provides the details of how this is done.

Finally, values of the parameters necessary for calculating the aerodynamic loads are:

$$U = 696.8 \text{ ft/sec}$$
 , $\rho_{a} = 2.378 \times 10^{-3} \text{ slugs/ft}^{3}$, $\rho_{ref} = 6.771 \text{ ft}$.

C. RESPONSE QUANTITIES AND GRADIENT EVALUATION

The end result of the development of the models in the previous section is the construction of an equation of motion in the form:

$$(-\omega_e^2 [M] + [K] - [A]) \{w\} = \{G\}$$
 (5.6)

Some new terms have been added to the formulation used to study white noise. These are

- $\{{\tt G}\}$ = Vector representing the load due to a unit sinusoidal gust of frequency $\boldsymbol{\omega}_{\underline{e}}$.
- [A] = Matrix relating the loads on the aircraft due to the aircraft's oscillation at frequency $\omega_{\rm p}$.

The general method used in the previous chapter can be repeated here to find the root mean square response values for the stresses and the stress rates. However, the new elements of the problem necessitate going through a brief description of these methods. While it is not explicitly emphasized, it must be remembered that the analysis presented below is in terms of a unit gust excitation.

Modal superposition can again be used to obtain the response of the wing at a specified frequency:

$$\{w\} = \sum_{i=1}^{mn} \{p_i\} a_i = [P] \{a\}$$
 (5.7)

The $\{p_i^{}\}$ vectors are the eigenvectors of the system $(-\lambda_i^{}[M] + [K])\{p_i^{}\} = 0.0$ and the $a_i^{}$'s are the modal participation factors that are to be determined for the forced response. The next step is to premultiply Eq. (5.6) by $[P]^T$:

$$(-\omega_e^2 [I] + [\lambda] - [GA]) \{a\} = \{GG\}$$
 . (5.8)

The mode shapes have been normalized so that the generalized masses are unity. The new terms of Eq. (5.8) are clearly

$$[GA] = [P]^{T}[A][P] ,$$

$$\{GG\} = [P]^{T}\{G\} .$$

In the previous chapter, multiplying the equation of motion by the transposed eigenvector matrix uncoupled the equations in the a_i 's by diagonalizing the mass and stiffness matrices. The generalized aerodynamic matrix is not diagonal, however, so the system of equations for the $\{a\}$ vector have to be treated simultaneously.

Also, since [GA] and $\{GG\}$ vary in a complex fashion with the reduced frequency, it is necessary to evaluate Eq. (5.8) at a number of discrete reduced frequency values.

Once the modal participation factors have been found for a large enough number of reduced frequency values to represent the complete range of interest, it is possible to move on to the calculation of

the stresses. Once again, the methods of the previous chapter are inadequate for this problem. The difficulty now is that since the model permits rigid body motions, the bending moments cannot be calculated from a derivative of the displacement vector. Instead, external and inertial loads are summed and the bending moment is found from these forces and from the fact that the shear force and bending moment at the wing's tip are zero. The force acting is given by

$$F = L_g + L_m + m\omega_e^2 w$$

Or in matrix notation:

$$\{F\} = ([A] + \omega_{\rho}^{2} [M]) \{w\} + \{G\}$$
 (5.9)

The $\{F\}$ vector represents concentrated forces and moments acting at the node points. From this vector, it is possible to calculate the bending moment acting at any specified location on the wing. For the purposes of this analysis, the bending moments were computed at the center of each element plus an additional calculation at the wing's root.

Performing the moment summations at these points gives:

$$BM_{i} = \sum_{j=i}^{n} \left[F_{2j+1} + \frac{L}{2n} F_{2j} \left[2(j-1) + 1 \right] \right]$$
 (Cont'd)

and

$$BM_{Root} = \sum_{j=1}^{n} \left(F_{2j+1} + F_{2j} \frac{jL}{n} \right) \qquad (5.10)$$

This can be summarized by a matrix equation: $\{BM\} = [T]\{F\}$.

The vector of bending moments calculated in this way can be thought of as the admittance functions for the structure. The factor that is of prime interest is the mean square bending stress. Given the bending moment, the remainder of the calculation is quite straightforward. First, the admittance of the bending stress is calculated using the standard S = Mc/I formula. Proper account has to be made of the tapered property of the wing in this calculation as it enters into both the c and I terms in the stress equation. With the bending stress admittance calculated at a number of frequencies, the mean square response is calculated from:

$$\sigma_{SS}^2 = \int_0^\infty |s|^2 \Phi_{W_g}(\omega) d\omega \qquad (5.11)$$

The mean square stress rate is computed in a similar fashion:

$$\sigma_{SS}^{2} = \int_{0}^{\infty} \omega^{2} |s|^{2} \Phi_{\mathbf{w}_{\mathbf{g}}}(\omega) d\omega \qquad . \tag{5.12}$$

Simpson's rule was used in performing the numerical integrations.

Once these two parameters have been determined, the analysis of Section IV.B can be used to determine the fatigue life and time to first excursion failure at the wing stations of interest. This analysis will not be repeated here.

The changes in formulation described above also create some differences in the way the gradients are calculated. Again, only the new details are described in this section, since the previous chapter is available to provide added detail.

The eigenvalue and eigenvector derivatives are found in the same manner as previously except that the rigid body mode allows certain simplifications. Specifically, since the rigid body frequency is zero, the derivatives of this frequency are trivally zero:

$$\frac{\partial^{\lambda} \mathbf{1}}{\partial \mathbf{t_{j}}} = 0 \qquad \mathbf{j} \approx 1, 2, \dots, \mathbf{n} \qquad . \tag{5.13}$$

The rigid body mode shape is a vector given by relation:

$$\{p_1\}^T = \eta\{1,1,0,1,...,1,0\} \equiv \eta\{u\}^T$$
 , (5.14)

where η is the normalizing factor used to obtain $\{p_1\}^T[M]\{p_1\}=1.0=\eta^2\{U\}^T[M]\{U\}$.

Since the mass matrix varies with the design variables, the rigid body mode does have a derivative with respect to the design

variables that can be evaluated by the use of the relationship just obtained:

$$2\eta\{\mathbf{U}\}^{\mathbf{T}}[\mathbf{M}]\{\mathbf{U}\} \quad \frac{\partial \eta}{\partial \mathbf{t_{j}}} = -\eta^{2}\{\mathbf{U}\}^{\mathbf{T}} \quad \frac{\partial[\mathbf{M}]}{\partial \mathbf{t_{j}}} \quad \{\mathbf{U}\} \qquad ,$$

$$\therefore \quad \frac{\partial \eta}{\partial \mathbf{t_{j}}} = -\eta^{3}\{\mathbf{U}\}^{\mathbf{T}} \quad \frac{\partial[\mathbf{M}]}{\partial \mathbf{t_{j}}} \quad \{\mathbf{U}\}/2 \qquad . \tag{5.15}$$

The matrix triple product $\{U\}^T$ $(\partial_j[M]/\partial_j)$ $\{U\}$ can be shown to be equal to the structural mass of the jth element, m_j , divided by the design variable t_j . The derivative expression for the mode shape then becomes:

$$\frac{\partial \{p_1\}}{\partial t_j} = \frac{\partial \eta}{\partial t_j} \{u\} = -\frac{\eta^3}{2} \frac{m_j}{t_j} \{u\} .$$

The next step is the determination of the derivative of the modal participation factors. Recall Eq. (5.8):

$$(-\omega_e^2 [I] + [\lambda] - [GA]) \{a\} = \{GG\}$$
.

Taking the derivative with respect to the thickness of the $\,\mathrm{j}^{\,\mathrm{th}}$ element gives:

$$\left(-\omega_{\mathbf{e}}^{2} \left[\mathbf{I}\right] + \left[\lambda\right] - \left[\mathbf{GA}\right]\right) \left\{\frac{\partial \mathbf{a}}{\partial t_{\mathbf{j}}}\right\} = \frac{\partial \left[\mathbf{P}\right]^{T}}{\partial t_{\mathbf{j}}} \left\{\mathbf{G}\right\} - \left(\mathbf{Cont'd}\right)$$

$$\left(\frac{\partial}{\partial t_{j}} \left[\lambda\right] - 2[P]^{T}[A] \frac{\partial [P]}{\partial t_{j}}\right) \{a\} \qquad (5.16)$$

As in previous cases of this type, the matrices on the left-hand sides of Eqs. (5.8) and (5.16) are the same, regardless of which design vector is of interest. Therefore, the matrix decomposition of $(-\omega_e^2 \ [\ I\] + [\ \lambda\] - [GA])$ needs to be evaluated only once for the n + 1 systems of 2n + 1 simultaneous equations.

Another note is that the derivative of the generalized aerodynamics matrix involves only the mode shapes since the aerodynamics matrix, [A], is not a function of the design variable. This is different from flutter optimization problems, where the aerodynamics are indirectly a function of the design variable because the flutter frequency is contained in the matrix (Ref. 50).

Finally, note that even though matrix [GA] is symmetric, the derivative $\partial [GA]/\partial t_1$ is not.

The remaining derivative calculations can now be evaluated:

$$\left\{ \frac{\partial \mathbf{w}}{\partial \mathbf{t}_{j}} \right\} = \frac{\partial [P]}{\partial \mathbf{t}_{j}} \left\{ \mathbf{a} \right\} + [P] \left\{ \frac{\partial \mathbf{a}}{\partial \mathbf{t}_{j}} \right\} ,$$

$$\left\{ \frac{\partial F}{\partial \mathbf{t}_{j}} \right\} = \omega_{\mathbf{e}}^{2} \frac{\partial [M]}{\partial \mathbf{t}_{j}} \left\{ \mathbf{w} \right\} + (\omega_{\mathbf{e}}^{2} [M] + [A]) \left\{ \frac{\partial \mathbf{w}}{\partial \mathbf{t}_{j}} \right\} ,$$

$$\left\{ \frac{\partial BM}{\partial \mathbf{t}_{j}} \right\} = [T] \left\{ \frac{\partial F}{\partial \mathbf{t}_{j}} \right\} .$$
(5.17)

Another new derivative that must be evaluated is:

$$\frac{\partial |\mathbf{s_i}|^2}{\partial \mathbf{t_j}} = 2\overline{\mathbf{s}} \frac{\partial \mathbf{s_i}}{\partial \mathbf{t_j}} , \qquad (5.18)$$

where the bar indicates the complex conjugate.

Since the bending stress is proportional to the bending moment and inversely proportional to the element thickness, $(S_i = cp_i BM_i/t_i)$, where cp_i is the constant of proportionality), the bending stress derivative is given by

$$\frac{\partial \mathbf{S_i}}{\partial \mathbf{t_i}} = \mathbf{cp_i} \frac{\partial \mathbf{BM_i}}{\partial \mathbf{t_i}} - \frac{\mathbf{cp_i}}{\mathbf{t_i^2}} \quad \mathbf{BM_i} \quad \mathbf{\delta_{ij}} \quad , \quad (5.19)$$

where δ_{ij} is the Kronecker delta.

Finally,

$$\frac{\partial}{\partial t_{i}} \sigma_{\mathbf{S}_{i}\mathbf{S}_{i}}^{2} = \int_{0}^{\infty} \Phi_{\mathbf{w}_{g}} \frac{\partial}{\partial t_{i}} |\mathbf{S}|^{2} d\omega , \qquad (5.20)$$

and similarly for the stress rate. The remaining derivatives for the constraints and the objective function are identical in form to those of the previous chapter and are not repeated here.

D. RESULTS

As the above descriptions have perhaps indicated, the function evaluation and gradient calculation require a considerable amount of computation. Consider an example that has N elements and a mesh of

NF discrete frequencies used in the response calculations. Further specify that MN natural modes are used for modal superposition. Then each function evaluation requires the solution of a 2N+1 eigenvalue problem. In addition, the MN linear simultaneous equations given by Eq. (5.8) must be solved NF separate times. If gradient information is desired, the MN simultaneous equations given by Eq. (5.15) must be solved NF \times N times. An additional factor is that unless one is very clever or sacrifices programming speed and clarity, the arrays needed for the computation quickly fill the computer's available core. E.g., a reasonable way to dimension $\partial S/\partial t_j$ of Eq. (5.19) is $\partial S(N+1,NF,N)$ signifying that each of the N+1 stress values for each of the NF frequencies has derivatives with respect to N different design variables.

For these reasons, the examples done for the thesis were kept as simple as possible while retaining the capability of obtaining meaningful results.

The first example used three structural elements and retained the rigid body mode plus one bending mode. Twenty-nine reduced frequency values ranging, at equal intervals, from 0.0 to 0.28 were used. Although this first example was worked mainly as a check on the algorithm, the results are of sufficient interest to be presented here. The constraints were identical with those of the previous chapter in that the fatigue life was specified to be greater than one year while the time to first excursion failure was specified to be greater than one-half year.

The initial and optimal thickness distributions for this example are

$$\{t\}_{i} = \begin{cases} 1.00 \\ 0.90 \\ 0.50 \end{cases}$$
 $\{t\}_{o} = \begin{cases} 0.04965 \\ 0.02539 \\ 0.01146 \end{cases}$

A plot of the final thickness distribution is given in Fig. 5.3. The active constraints designated on the figure are all first excursion failure type constraints.

The marked reduction in weight is partially due to the fact that the initial configuration is extremely overdesigned with respect to the constraints considered here. The rms stress at the root for the initial design is approximately 600 psi; a value so far below the specified ultimate strength level of 40000 psi as to be insignificant. This should not be too surprising, since the textbook example from which the model was obtained was not intended to be near a critical value with respect to this particular constraint. It is surprising that the weight is reduced by a factor greater than twenty. This fact is discussed following the presentation of the second and last example.

The final example used five elements to represent the structure and retained two bending modes plus the rigid body mode. The same

The cost function used for the wing examples was the sum of the design variables. Due to the taper of the wing, this is not exactly proportional to the structural weight; therefore, the final thickness distribution is not the minimum weight solution. This oversight was detected after the two examples were completed, and it did not seem a large enough error to require re-optimizations with their attendant computer costs.

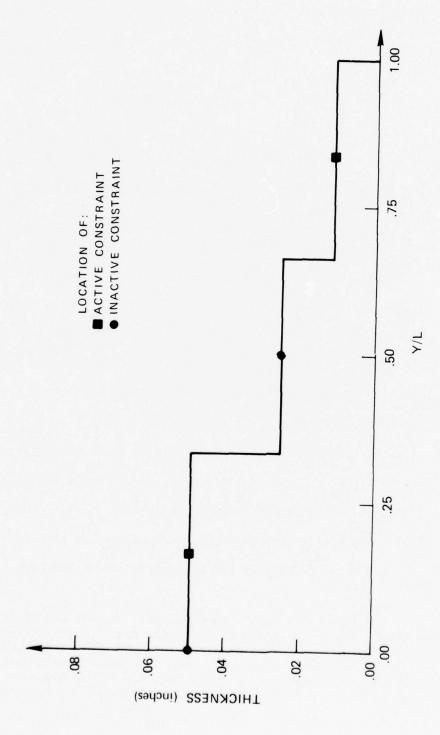


FIG. 5.5--Optimal Thickness Distribution for a Wing Excited by Continuous Atmospheric Turbulence Three Finite Elements .

number of reduced frequencies were used. Since the previous example had permitted an optimal design that was unrealistically light, the constraint lives were multiplied by a factor of ten. The fatigue life was therefore constrained to be greater than ten years and the time to first excursion failure was required to be greater than five years. The remaining parameters were left unchanged.

Figure 5.4 compares the power spectral density of the root bending moment obtained from Example 10.6 of Ref. 32 with that obtained using the initial design and the models developed for the present study. The different turbulence spectra used for the two cases account for the majority of the discrepancy, while some differences in the modelling of the structure account for the shift in the location of the second peak. In the figure, the first peak is almost entirely due to the rigid body response while the second peak occurs very close to the natural frequency of the first bending mode. The second bending mode occurs at such a high frequency that it does not have an effect on the root bending moment. Of interest here is the fact that the two solutions are qualitatively the same, indicating that the computer analysis has been done correctly.

The initial and optimal thickness values, as well as the rms values of the stress and stress rate for the final design are given in Table 5.1.

Figure 5.5 plots the final thickness distribution and indicates where the constraints are active. In this example, all the active constraints were of the fatigue type.

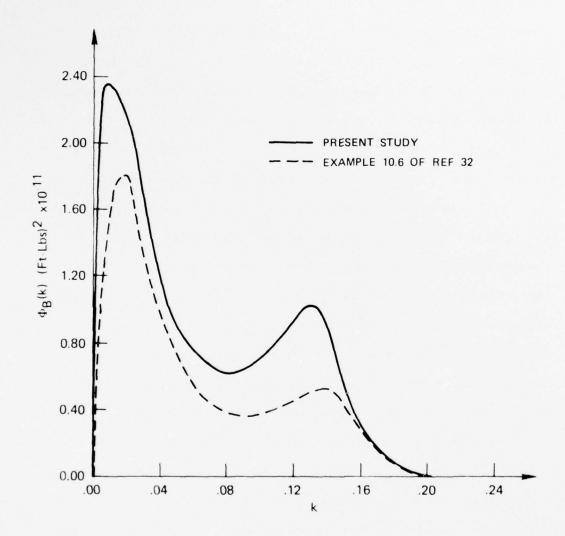


FIG. 5.---Root Bending Moment Power Spectra of Initial Design.

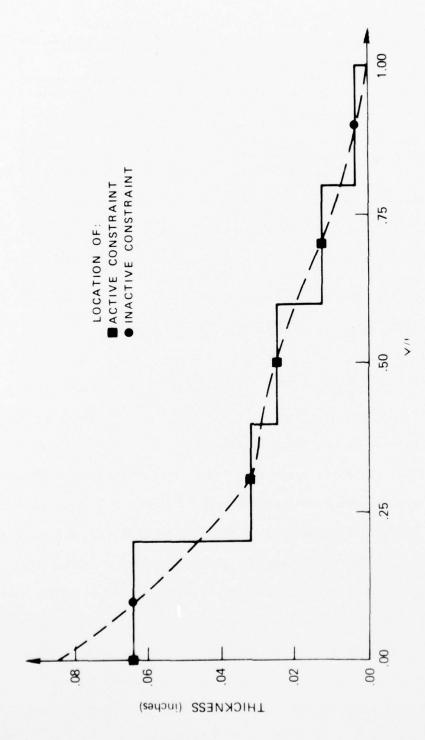


FIG. 5.5--Optimal Thickness Distribution for a Wing Excited by Continuous Atmospheric Turbulence.

Element	Thickness		Final Design	
	Initial	Optimal	RMS Stress	RMS Stress Rate
Root			4338 psi	25,706 psi/sec
1	1.00"	0.0628"	5965	18,562
2	0.955	0.0312	5521	31,506
3	0.915	0.0245	5733	24,971
24	0.810	0.0125	5394	34,877
5	0.380	0.0035	51 57	32,590

TABLE 5.1--Wing in a Turbulent Atmosphere

with the constraint lives multiplied by ten from the previous example, there is a very large weight decrease from the initial to the final design. Part of the explanation for this behavior is indicated by Fig. 5.6. This figure shows the power spectral density of the root bending moment for the final design. A comparison of this figure with Fig. 5.4 points out two things: (1) The area under the power spectrum, and hence the rms bending moment, for the final design is substantially less than the area under the comparable curve for the original design and (2) the response to the first bending mode has disappeared in the optimal design. These two results are related to the fact that, as the weight is reduced, the inertial loads become increasingly less important compared to the aerodynamic loads.

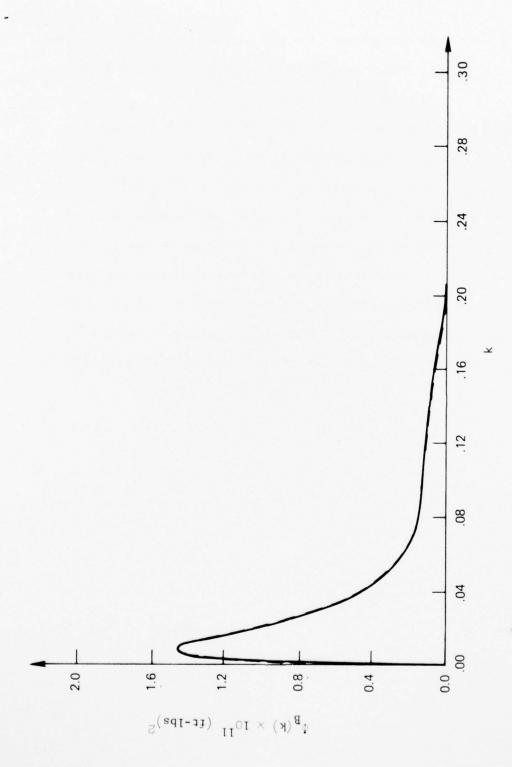


FIG. 5.c -- Root Bending Moment Power Spectrum of the Optimal Design.

Of course the rms stresses are considerably greater for the final design since the stresses are inversely proportional to the design variables.

This example dramatically illustrates a tenet of structural optimization that is frequently ignored; viz., for the final result to be useful, all the design conditions that the structure will be required to meet must be considered simultaneously. Because this work was primarily interested in studying the effect of stochastic loads in the optimization process, other constraints that would have made the final design more meaningful were left out of the analysis. The following, concluding chapter offers some suggestions as to how the optimal design of a wing could include more complete design conditions.

CHAPTER VI

CONCLUSIONS AND RECOMMENDATIONS

A number of comments about the behavior and significance of the solutions have already been made. Sections II.D, III.E and IV.E are devoted to discussions of the material presented in their respective chapters. This final chapter reiterates and expands on these comments and lists areas that would benefit from further study.

A general conclusion is that despite the complications introduced by dynamic loadings, methods of mathematical programming can be applied to studies of this type. This is not a surprising, or even new, conclusion. Accordingly, the main contributions of this thesis must reside in the formulation of the analyses and in some of the interesting results obtained.

In particular, the discovery of disjoint feasible regions in Chapter III is of theoretical and perhaps practical interest. The two design variable example of Section III.A demonstrates the concepts of disjointness with a simplicity that makes it valuable as an instructive tool. The ease of the formulation, coupled with the large amount of information garnered, also reinforces the maxim that simple cases should be examined first. It is felt that some of the studies of optimization with dynamic loading have ignored this rule and have thereby suffered from a lack of understanding of the basic principles involved.

It is realized that the optimal structures shown in Chapter III with a first natural frequency that is less than the excitation frequency are impractical because of their inability to sustain even moderate static loads. However, when a design is influenced by a harmonic loading, it may be possible to obtain a more suitable structure by "loosening" it so that one or more natural frequencies are less than the forcing frequency rather than by stiffening it so that all natural frequencies are higher.

A design procedure that is related to this concept is that of "detuning". In this procedure, masses are added or moved on the structure in a manner that minimizes resonant responses. Another example is the "soft mounting" of nacelles. In the latter technique, the mounts minimize nacelle motion by giving the nacelle-mount combination a first natural frequency that is less than the predominant excitation frequency. Methods developed in this thesis can aid these design practices by performing them in a more systematic fashion.

The results of Chapter IV indicate that the optimal structure can differ markedly from intuitive designs that are based on static strength alone. Another conclusion is that the response to white noise can be adequately estimated by a very small number of modes. For the problems studied, the first two modes were of primary importance and further modes added little to the final results while increasing the computer time for solution significantly.

The results of the preceding chapter, dealing with a wing in atmospheric turbulence, make it clear that care must be taken to adequately formulate problems of this nature. The example chosen had an initial design that was much too stiff to make a comparison between the initial and final designs meaningful. Also a number of features should be added to the model studied. Among these are additional loading and constraint conditions to insure that the optimal structure has adequate strength to withstand normal flight loads and landing impacts. The torsional modes are probably also of importance and should be included in further investigations. When other factors, such as fracture toughness, flaw growth, realistic aircraft structures and improved aerodynamics are added to this list, the analysis is clearly one that is beyond the scope of this developmental work. Hopefully, it has provided some of the techniques that a more ambitious research group could build upon.

One aspect of most papers on structural optimization which is absent from the present study is the presentation of the amount of computer time necessary for a problem's solution. Since the time to solution was not considered to be an important factor in the problems worked here, no attempt was made to minimize it. An indication of the magnitude of the computation time required is given by the fact that each design iteration for the problem of Chapter V required approximately a minute of CPU time on Stanford's IBM 360/67 in the "Quick" partition. By using a more efficient compiler and by using approximate techniques for the analysis, it seems quite conceivable that this figure could be reduced by roughly a factor of ten. For problems with a larger number of design

variables, these efficiencies are clearly needed in order to make the optimizations manageable from a computer resources standpoint.

Aside from the above comments on problem formulation and computational efficiency, further investigations could be conducted in a number of areas. Some of these that the author finds intriguing and of importance to gaining an understanding of the principles of structural optimization with dynamic loading include the following:

- (1) Further work on the function space solutions of Chapter III.

 The most desirable goal would be analytical solutions for a range of constraint and loading conditions. Unfortunately, analytical results to date have been minimal despite considerable efforts made in a search for such results.
- (2) Solving the two point boundary value problems of Section III.C by numerical methods could also be a worthwhile activity. Pierson (Ref. 10) describes an excellent algorithm that can be used to iteratively solve these types of problems.
- (3) Design of optimal two-dimensional structures, such as plates and shells, with a harmonic or other dynamic excitation. To the author's knowledge, this is uncharted territory and should provide a wealth of problems and new results. It is anticipated that the disjoint feasible regions will continue to be a complicating factor in the search for optimal solutions for the harmonically loaded structures.
- (4) For problems with stochastic excitation, this work uses relatively simple failure criteria. The discipline of fracture mechanics

has recently developed more sophisticated methods for predicting a structure's damage due to random loads. These methods should have application to the optimization problems.

(5) The problems of Chapter IV should be solved for a range of such parameters as structural damping, load magnitude, and constraints. This would show the qualitative effects that these parameters have on the solutions and might even point out some new properties of stochastic optimization problems.

These are suggestions that relate directly to the investigations of this thesis. There are, of course, many other problems involving optimization of structures under dynamic excitation that are of interest and importance. It is the author's view that the most critical current task for the optimizer is that of acquainting the designer with the techniques of optimization so that they can jointly determine where the methods are of most value. It is felt that this work has broadened the application of optimization methods and has therefore enhanced their attractiveness and usefulness. Hopefully, this promise will be furthered and fulfilled.

REFERENCES

- Sheu, C. Y., and Prager, W., "Recent Developments in Optimal Structural Design," <u>Applied Mechanics Reviews</u>, Vol. 21, No. 10, Oct. 1968, pp. 985-992.
- 2. Fox, R. L., Optimization Methods for Engineering Design, Addison Wesley, Reading, Massachusetts, 1971.
- Gellatly, R. A., Editor, <u>Structural Optimization</u>, AGARD Lecture Series No. 70, Hampton, Virginia, October 1974.
- 4. Schmit, L. A., Jr., Editor, <u>Structural Optimization Symposium</u>,
 American Society of Mechanical Engineers, New York, Nov. 1974.
- 5. Pierson, B. L., "A Survey of Optimal Structural Design Under Dynamic Constraints," <u>International Journal for Numerical Methods</u> in Engineering, Vol. 4, No. 4, July-Aug. 1972, pp. 491-499.
- 6. Ashley, H., and McIntosh, S. C., Jr., "Application of Aeroelastic Constraints in Structural Optimization," Proceedings of the Twelfth International Congress of Applied Mechanics, Springer, Berlin, 1969.
- 7. Weisshaar, T. A., "An Application of Control Theory Methods to the Optimization of Structures Having Dynamic or Aeroelastic Constraints," SUDAAR 412, Stanford University, Department of Aeronautics and Astronautics, October 1970.

- 8. Armand, J., and Vitte, W. J., "Foundations of Aeroelastic Optimization and Some Applications to Continuous Systems," SUDAAR No. 390, Stanford University, Department of Aeronautics and Astronautics, January 1970.
- 9. Turner, M. J., "Design of Minimum Mass Structures with Specified Natural Frequencies," <u>AIAA Journal</u>, Vol. 5, No. 3, March 1967, pp. 406-412.
- 10. Pierson, B. L., "Application of a Gradient Projection Optimal Control Method to a Class of Panel Flutter Optimization Problems," ISU-ERI-AMES 73186, Iowa State University, Ames, Iowa, 1973.
- 11. Icerman, L. J., "Optimal Structural Design for Given Dynamic Deflection," <u>International Journal of Solids and Structures</u>, Vol. 5, No. 5, May 1969, pp. 473-490.
- 12. Brach, R. M., "Optimum Design of Beams for Sudden Loadings,"

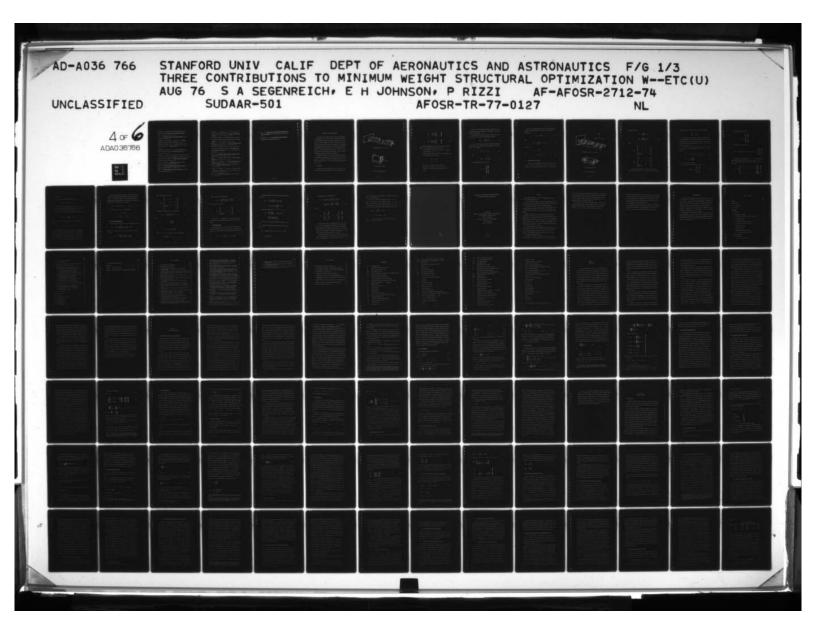
 Proceedings of the ASCE Journal of the Eng. Mechanics Division,

 Vol. 94, No. EM6, Dec. 1968, pp. 1395-1407.
- 13. Brach, R. M., "Minimum Dynamic Response for a Class of Simply Supported Beam Shapes," <u>International Journal of Mechanical Sciences</u>, Vol. 10, No. 5, May 1968, pp. 429-439.
- 14. Fox, R. J., and Kapoor, M. P., "Structural Optimization in the Dynamic Response Regime: A Computational Approach," <u>AIAA Structural Dynamics and Aeroelasticity Specialist Conference</u>, New Orleans, Louisiana, April 1969, pp. 15-22.

- 15. Fox, R. J., and Kapoor, M. P., "Rates of Change of Eigenvalues and Eigenvectors," <u>AIAA Journal</u>, Vol. 6, No. 12, Dec. 1968, pp. 2426-2429.
- Levy, H. J., <u>Minimum Weight Design Under Dynamic Loading</u>, Ph.D.
 Thesis, New York University, 1972.
- 17. Levy, H. J., and Wolf, B. M., "Fully Stressed Dynamically Loaded Structures," ASME Publication 74-WA/DE-19, ASME Winter Annual Meeting, Nov. 1974.
- 18. Venkayya, V. B., Khot, N. S., and Berke, L., "Application of Optimality Criteria Approaches to Automated Design of Large Practical Structures," Second Symposium on Structural Optimization, AGARD Conference Proceedings No. 123, Milan, Italy, April 1973.
- 19. Venkayya, V. B., and Khot, N. S., "Design of Optimum Structures to Impulse Type Loading," <u>AIAA/ASME/SAE 15th Structures</u>, <u>Structures</u>, <u>Structures, <u>Structures</u>, <u>Structures</u>, <u>Structures, <u>Structures</u>, <u>Structures</u>, <u>Structures, <u>Structures</u>, <u>Structures, <u>Structures, <u>Structures</u>, <u>Structures, <u>Structures</u>, <u>Structures, <u></u></u></u></u></u></u></u></u>
- 20. Solnes, J., and Holst, O. L., "Optimization of Framed Structures
 Under Earthquake Loads," 5th World Conference on Earthquake
 Engineering, Rome, June 1973, (Preprint Paper 376).
- 21. Nigam, N. C., and Narayanan, S., "Structural Optimization in Aseismic Design," 5th World Conference on Earthquake Engineering, Rome, June 1973, (Preprint Paper 374).

- 22. Nigam, N. C., "Structural Optimization in Random Vibration Environment," AIAA Journal, Vol. 10, No. 4, April 1972, pp. 551-553.
- 23. Kato, B., Nakamura, V., and Anraku, H., "Optimum Earthquake Design of Shear Buildings," ASCE Proceedings, Journal of the Engineering Mechanics Division, Vol. 98, No. EM4, Aug. 1972, pp. 891-910.
- 24. Cassis, J. H., "Optimum Design of Structures Subjected to Dynamic Loads," UCLA-ENG-7451, UCIA, School of Engineering and Applied Science, June 1974.
- 25. Plaut, R. H., "Optimal Structural Design for Given Deflection
 Under Periodic Loading," Quarterly of Applied Mathematics, Vol.
 29, No. 2, July 1971, pp. 315-318.
- 26. Mroz, Z., "Optimal Design of Elastic Structures Subjected to Dynamic, Harmonically Varying Loads, Zeitschrift fur Angewandte Mathematik und Mechanik, Vol 50, No. 5, May 1970, pp. 303-309.
- 27. Hilton, H. H., and Feigen, M., "Minimum Weight Analysis of Structures Based on Structural Reliability," <u>Journal of the Aerospace</u>

 Sciences, Vol. 27, No. 9, Sept. 1960, pp. 641-652.
- 28. Kalaba, R., "Design of Minimal Weight Structures for Given Reliability and Cost," <u>Journal of the Aerospace Sciences</u>, Vol. 29, No. 3, March 1962, pp. 355-356.
- 29. Moses, F., and Kinser, D. E., "Optimum Structural Design With Failure Probability Constraints," AIAA Journal, Vol. 5, No. 6, June 1967, pp. 1152-1158.



- 30. Araslanov, A. M., "Calculation of Minimum Weight Beams Under Random Loading," The Journal of the Astronautical Sciences, Vol. XIX, No. 2, Sept.-Oct. 1971, pp. 150-158.
- 31. Lin, Y. K., <u>Probabilistic Theory of Structural Dynamics</u>, McGraw-Hill Book Co., New York, 1967.
- 32. Bisplinghoff, R. L., Ashley, H., and Halfman, R. L., Aeroelasticity, Addison-Wesley, Reading, Massachusetts, 1955.
- 53. Fletcher, R., and Powell, M. J. D., "A Rapidly Convergent Descent Method for Minimization," <u>Computer Journal</u>, Vol. 6, No. 2, 1963, pp. 163-168.
- 34. Vanderplaats, G. N., and Moses, F., "Structural Optimization by Methods of Feasible Directions," <u>Computers and Structures</u>, Vol. 3, No. 4, July 1973, pp. 739-755.
- 35. Segenreich, S., and Rizzi, P., "Some Properties of Axial or Free Vibration Frequencies of Rods," AIAA Journal, Vol. 13, Aug. 1975, pp. 1111-1112.
- 36. Scanlan, R. H., and Rosenbaum, R., <u>Aircraft Vibration and Flutter</u>,
 Dover Publications, Inc., New York, 1968.
- 37. Bryson, A. E., and Ho, Y., <u>Applied Optimal Control</u>, Blaisdell Publishing Company, Waltham, Massachusetts, 1969.
- 38. Murphy, G. M., Ordinary Differential Equations and Their Solutions, Van Nostrand Reinhold Co., New York, 1960.
- 39. Weaver, W., Computer Programs for Structural Analysis, Van Nostrand Reinhold Company, New York, 1967.

- 40. Bogdanoff, J. L., and Goldberg, J. E., "On the Euler Bernoulli Beam Theory With Random Excitation," <u>Journal of the Aero/Space</u>
 Sciences, Vol. 27, No. 5, May 1960, pp. 371-376.
- 41. Yang, J-N, and Trapp, W. J., "Reliability Analysis of Aircraft Structures Under Random Loading and Periodic Inspection," AIAA Journal, Vol. 12, No. 12, Dec. 1974, pp. 1623-1630.
- 42. Gradshteyn, I. S., and Ryzhik, I. M., <u>Table of Integrals, Series</u>, and Products, Academic Press, New York and London, 1965.
- 43. Powell, A., "On the Fatigue Failure of Structures Due to Vibrations Excited by Random Pressure Fields," The Journal of the Acoustical Society of America, Vol. 30, No. 12, December 1958, pp. 1130-1135.
- 144. Papoulis, A., <u>Probability</u>, <u>Random Variables and Stochastic Processes</u>, McGraw-Hill Book Company, New York, 1965.
- 45. Miner, M. A., "Cumulative Damage in Fatigue," <u>Journal of Applied Mechanics</u>, Vol. 12, Sept. 1945, pp. 159-164.
- 46. Crandall, S. H., and Dahl, N. C., Editors, An Introduction to the Mechanics of Solids, McGraw-Hill Book Company, New York, 1959.
- 47. Etkin, B., <u>Dynamics of Atmospheric Flight</u>, John Wiley & Sons, Inc., New York, 1972.
- 48. Houbolt, J. C., Steiner, R., and Pratt, K. G., "Dynamics Response of Airplanes to Atmospheric Turbulence Including Flight Data on Input and Response," NASA TR-R-199, 1964.
- 149. Fung, V. C., <u>The Theory of Aeroelasticity</u>, Dover Publications, Inc., New York, 1969.

- 50. Gwin, L. B., Optimal Sizing of Complex Structural Systems for Flutter Requirements, Ph.D. Thesis, Stanford University, May 1973.
- 51. Przemieniecki, J. S., <u>Theory of Matrix Structural Analysis</u>, McGraw-Hill Book Company, New York, 1968.

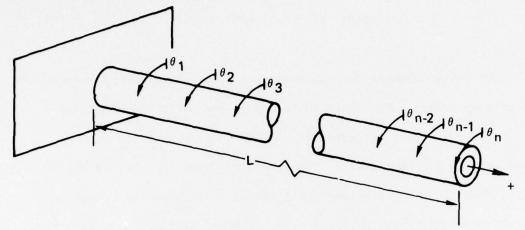
APPENDIX: FINITE ELEMENT MODELS

The finite element formulations used in the thesis are presented in this appendix. The first two sections deal with the representation of rod and beam elements with constant cross sections. A standard text on finite elements (e.g., Ref. 51) contains most of the results shown in these sections; they are included here for completeness and to demonstrate the notation used. A third section deals with the representation of the tapered wing used in the fifth chapter of the thesis. It is necessary to go into added detail in order to indicate the adjustments that the tapered elements require. Lastly, the aerodynamic matrices needed in Chapter V are formulated.

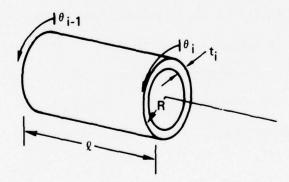
Throughout the Appendix, a distinction is made between matrices that represent a single element and those that represent an assembled structure. The former are denoted by a subscript that defines the element being considered (e.g., $\left[K\right]_{i}$) while the latter have no subscript (e.g., $\left[K\right]$).

A. TORSION ROD

Figure A.1 shows the rod and the degrees of freedom used. For a single element, the mass and stiffness matrices are represented by:



a Representation Using n Elements



(b) Individual Rod Element

FIG. A.1--Cantilevered Rod.

$$[K]_{i} = \begin{pmatrix} \frac{GJ}{\ell} \end{pmatrix}_{i} \begin{bmatrix} 1 & -1 \\ & & \\ -1 & & 1 \end{bmatrix}$$

$$[M]_{i} = \left(\frac{\mathbf{I}_{\alpha}\ell}{6}\right)_{i} \begin{bmatrix} 2 & 1 \\ & & \\ 1 & 2 \end{bmatrix} \qquad (A.1)$$

From these elements matrices, the final matrices are readily assembled. Some assumptions made when this is done are:

- (1) The one-dimensional structure is divided into n elements of equal length: $\ell = L/n$.
- (2) The rod is a thin walled tube with structural properties that are proportional to the thickness:

$$(GJ)_{i} = GJ_{0}t_{i}$$
,
 $(I_{\alpha})_{i} = I_{\alpha 0}t_{i}$. (A.2)

 GJ_{\bigcirc} and $\mathrm{I}_{\bigcirc\bigcirc}$ are constants for the structure.

(3) The cantilevered boundary condition is accounted for by deleting the degree of freedom associated with the root station. The matrix is then assembled by adding the contributions of the individual elements at the node points. The assembled [M] and [K] matrices have dimensions $n\times n$.

The equivalent force vectors are needed to represent a uniform load across the rod. They are found by using the formula

$$\{P_{eq}\}_{i} = p_{x}l \int_{0}^{1} \{a\} ds$$
 (A.3)

Here $\{a\}$ gives the relation between the discrete displacement representation and the continuous actual displacement. For rod elements, $\{a\}^T$ is given by

$$\{a\}^{T} = \{1.0 - s, s\}$$
 . $(A.4)$

Then

$$\left\{ \mathbf{P}_{\mathbf{eq}} \right\}_{\mathbf{i}} = \mathbf{p}_{\mathbf{x}} \ell \left\{ \frac{\frac{1}{2}}{\frac{1}{2}} \right\}$$
 (A.5)

The assembled equivalent force vector is

$$\{P\} = p_{\mathbf{x}} \ell \begin{cases} 1\\1\\1\\1\\\vdots\\1\\\frac{1}{2} \end{cases}$$
 (A.6)

Another finite element matrix needed is one for determining the stresses. The relation between the stress and the displacement is found using:

$$S_i = G\{b\}^T\{\theta\}$$
 , (A.7)

where

$$\{b\}^{T} = \frac{R}{\ell} \frac{d\{a\}^{T}}{ds} = \frac{R}{\ell} \{-1, 1\}$$
 (A.8)

Therefore,

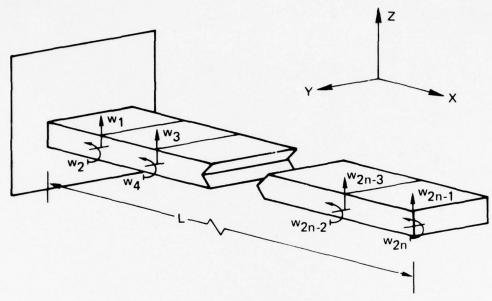
$$s_1 = \frac{GR}{\rho} \theta_1$$

and

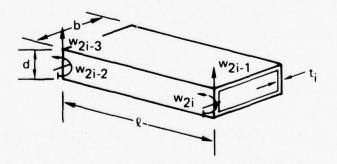
$$\mathbf{S}_{\mathbf{i}} = \frac{\mathbf{GR}}{\ell} (\theta_{\mathbf{i}} - \theta_{\mathbf{i-1}}) \qquad (A.9)$$

B. CANTILEVERED BEAM IN BENDING

Figure A.2 shows the beam and the degrees of freedom used in this thesis. Note that a slope as well as a vertical deflection are used at each node. The mass and stiffness matrices for a single element



(a) Representation Using n Elements



(b) Individual Beam Element

FIG. A.2--Cantilevered Beam.

are given by (Ref. 51)

$$[K]_{i} = \left(\frac{EI}{\ell^{3}}\right)_{i} [KO]$$
,

$$[M]_{i} = \left(\frac{\rho_{s}^{A\ell}}{\mu_{20}}\right)_{i} [MO] \qquad , \qquad (A.10)$$

where

[KO] =
$$\begin{bmatrix} 12 & 6\ell & -12 & 6\ell \\ & 4\ell^2 & -6\ell & 2\ell^2 \\ & & 12 & -6\ell \\ & & & 4\ell^2 \end{bmatrix}$$

$$[MO] = \begin{bmatrix} 156 & 22\ell & 54 & -13\ell \\ & 4\ell^2 & 13\ell & -3\ell^3 \\ & & & & \\ & & 156 & -22\ell \\ & & & & \\ & & & & \\ & & & & \\ & & & & \\ & & & & \\ & & & & \\ & & & & \\ & & & & \\ & & & & \\ & & & & \\ & & & & \\ & & & & \\ & & & & \\ & & & & \\ & & & & \\ & & & & \\ & & & & \\ & & & & \\ & & & & \\ & & & \\ & & & \\ & & & \\ & & & \\ & & & \\ & & & \\ & & & \\ & & & \\ & & & \\ & & & \\ & & & \\ & & & \\ & & & \\ & & & \\ & & \\ & & & \\ &$$

As in the previous section, the structure is divided into $\,$ n equal elements of length $\,\ell\,=\,L/N\,$. The inertia and cross sectional

areas are expressed as linear functions of the element thickness:

$$(EI)_{i} = EI_{O}t_{i} ,$$

$$(\rho A)_{i} = \rho A_{O}t_{i} .$$
(A.12)

The cantilevered boundary condition requires that the degrees of freedom corresponding to the root displacement and slope be eliminated. The assembled mass and stiffness matrices can again be formed by adding contributions from the individual elements at the nodes. The assembled matrices have dimensions $2n \times 2n$.

The equivalent force vector and the stress vector are found in the same way as in the previous section with the $\left\{a\right\}^T$ and $\left\{b\right\}^T$ vectors replaced by

$$\{a\}^{T} = \{1 - 3s^{2} + 2s^{3}, (s - 2s^{2} + s^{3})\ell,$$

 $3s^{2} - 2s^{3}, (-s^{2} + s^{3})\ell\}^{T},$ (A.13)

$$\{b\}^{T} = \frac{d}{2\ell^{2}} \left\{\frac{d^{2}a}{ds^{2}}\right\}^{T} , \qquad (A.14)$$

where d is the depth of the beam.

Using Eq. (A.3), the equivalent force vector is

$$\{p_{eq}\}_{i} = p_{x}\ell \begin{cases} 1\\ \ell/12\\ 1\\ -\ell/12 \end{cases} . \tag{A.15}$$

The assembled vector has the form:

$$\{P\} = p_{\mathbf{x}} \ell \begin{pmatrix} 1 \\ 0 \\ 1 \\ 0 \\ \vdots \\ 0 \\ 1 \\ -\ell/12 \end{pmatrix} \qquad (A.16)$$

The stress vector is found using:

$$S_{i} = E\{b\}^{T}\{w\} = \frac{Ed}{2\ell^{2}} \{-6+12s, (-4+6s)\ell, 6-12s, (-12+6s)\ell\}^{T} \begin{cases} w_{2i-3} \\ w_{2i-2} \\ w_{2i-1} \\ w_{2i} \end{cases}$$
(A.17)

If the stresses are calculated at $s=\frac{1}{2}$, the above relation is greatly simplified in that the first and third elements of $\left\{b\right\}^T$ are zero. This was done for this thesis giving an assembled stress vector of the form

$$\{S\} = \frac{Ed}{2\ell} \begin{bmatrix} 0 & 1 & 0 & 0 & 0 & - & - & - & - & 0 & 0 \\ 0 & -1 & 0 & 1 & 0 & 0 & - & - & - & 0 & 0 \\ 0 & 0 & 0 & -1 & 0 & 1 & - & - & - & 0 & 0 \\ - & - & - & - & & & & & & \\ 0 & 0 & 0 & - & - & - & -1 & 0 & 1 & 0 & 0 \\ 0 & 0 & 0 & - & - & - & -1 & 0 & 1 & 0 & 0 \\ 0 & 0 & 0 & - & - & - & 0 & 0 & -1 & 0 & 1 \end{bmatrix} \begin{pmatrix} w_1 \\ w_2 \\ w_3 \\ - \\ - \\ w_{2n-1} \\ w_{2n} \end{pmatrix}$$
(A.18)

C. TAPERED WING

This section develops the matrices needed for Eq. (5.6):

$$(-\omega_{e}^{2} [M] + [K] - [A]) \{w\} = \{G\}$$
 . (5.6)

The wing used for this analysis is shown in Fig. 5.1. The linear taper of the chord adds complexity to the analyses of the previous sections and these complications are outlined in this section.

The first step is to represent the nondimensional semi-chord length

$$a(y) = b/b_{ref} = \frac{b_{root}}{b_{ref}} (1.0 - y/t_f) \qquad (A.19)$$

For the wing used, the numerical values of the parameters are given by

$$b_{root} = 112.5$$
", $t_f = 900$ ", $b_{ref} = 81.24$ ".

It is assumed that the thickness to chord ratio remains constant across the span so that the aerodynamic thickness is also linearly tapered. In order to avoid further complications of doubtful utility, the structural thickness is held constant across the length of an element. The consequences of these two assumptions are that the mass varies as $(1.0 - y/t_f)^3$.

As in the previous section, submatrices that deal with a single element are the building blocks that make up the final assembled matrices. It is therefore necessary to have structural properties expressed in terms of each element. As an example, the dimensional chord length for the ith element can be expressed as:

$$C_{i}(s) = C_{root} \alpha_{i}(1 - s/\delta_{i}) \qquad 0 \le s \le 1$$
 . (A.20)

By the use of Eq. (A.19), it can be shown that

$$\alpha_{\mathbf{i}} = 1 - L(\mathbf{i} - 1)/nt_{\mathbf{f}},$$

$$\delta_{\mathbf{i}} = \frac{nt_{\mathbf{f}}}{L} + 1 - \mathbf{i} = \frac{nt_{\mathbf{f}}}{L} \alpha_{\mathbf{i}}.$$
(A.21)

1. Mass and Stiffness Matrices

The mass matrix for an element is found by evaluating the integral:

$$[M]_{i} = t_{i} \rho_{s} A_{root} \frac{L}{n} \int_{\Omega}^{1} \alpha_{i} \left(1 - \frac{s}{\delta_{i}}\right) \{\eta\} \{\eta\}^{T} ds \qquad , \qquad (A.22)$$

where $\left\{\eta\right\}^{T}$ is identical to $\left\{a\right\}^{T}$ given in Eq. (A.13). The integration gives

$$[M]_{i} = \frac{t_{i} \rho_{s} A_{root} L \alpha_{i}}{n} \left([MO] - \frac{[M1]}{2\delta_{i}} \right) . \quad (A.23)$$

[MO] is given in Eq. (A.11) and

$$[M1] = \begin{bmatrix} 72 & 14\ell & 54 & -12\ell \\ & 3\ell^2 & 14\ell & -3\ell^2 \\ & & & & \\ & & & & \\ & & & & \\ & & & & \\ & & & & \\ & & & & \\ & & & & \\ & & & & \\ & & & & \\ & & & & \\ & & & & \\ & & & & \\ & & & & \\ & & & & \\ & & & & \\ & & & & \\ & & & & \\ & & & & \\ & & & & \\ & & & \\ & & & & \\ & & & \\ & & & \\ & & & \\ & & & \\ & & & \\ & & & \\ & & & \\ & & & \\ & & & \\ & & & \\ & & & \\ & & & \\ & & & \\ & & & \\ & & \\ & & & \\$$

Similarly, the stiffness matrix is evaluated using

$$[K]_{i} = E \left(\frac{n}{L}\right)^{3} \int_{0}^{1} I_{i} \{\beta\} \{\beta\}^{T} ds \qquad , \qquad (A.25)$$

where

$$\{\beta\}^{T} = \left\{\frac{\partial^{2} \eta}{\partial^{2} s}\right\}^{T}$$

and

$$I_{i} = \frac{1}{2} I_{0} t_{i} \alpha_{i}^{3} \left(1 - \frac{s}{s_{i}}\right)^{3} .$$

Since $s/\delta_{\mathbf{i}} << 1$, it is reasonable to make the approximation

$$\left(1 - \frac{s}{\delta_i}\right)^3 \simeq 1 - \frac{3s}{\delta_i}$$
.

Then, Eq. (A.25) is evaluated to give

$$[K] = EI_{O} \left(\frac{\alpha_{i}^{n}}{L}\right)^{3} \left([KO] - \frac{3[KI]}{\delta_{i}}\right) \qquad (A.26)$$

[KO] is given in Eq. (A.11) and

Note that as t_f , and therefore δ_i , become large, the mass and stiffness matrices approach the untapered results of the previous section.

2. Aerodynamic Matrices

The aerodynamic matrix [A] results from the motion and can be formulated in a manner very similar to that used for the mass matrix. From Eq. (5.4), the distributed lift resulting from the motion is given by:

$$L_{\mathbf{m}}(\mathbf{y}) = \pi \rho_{\mathbf{a}} \mathbf{U}^{2} \left[[\mathbf{a}(\mathbf{y})\mathbf{k}]^{2} - 2i\mathbf{a}(\mathbf{y})\mathbf{C}(\mathbf{k}) \right] \mathbf{h}$$
 (5.4a)

The equivalent matrix for the finite element representation is found using

$$[A]_{i} = \pi \rho_{\mathbf{a}} \mathbf{U}^{2} \ell \int_{0}^{1} \left[(\alpha_{i} \mathbf{k})^{2} \left(1 - \frac{\mathbf{s}}{\delta_{i}} \right)^{2} \right]$$

$$- 2ikC(\mathbf{k}) \alpha_{i} \left(1 - \frac{\mathbf{s}}{\delta_{i}} \right) \left[\{\eta\} \{\eta\}^{T} d\mathbf{s} \right]. \qquad (A.28)$$

Using the approximation that $(1.0 - s/\delta_i)^2 \approx 1.0 - 2s/\delta_i$:

$$[A]_{i} = \frac{\pi \rho_{a} U^{2} \ell}{420} \left[\left(\alpha_{i}^{2} k^{2} - 2i\alpha_{i} kC(k) \right) \right]$$

$$- \frac{2(\alpha_{i}^{2} k^{2} - ikC(k)) [M1]}{2\delta_{i}}$$

$$(A.29)$$

The [MO] and [M1] matrices are defined in Eqs. (A.11) and (A.24).

The distributed load resulting directly from the gust is given by Eq. (5.3):

$$\frac{L_g}{w_g} = 2\pi \rho_a Ub_{ref} a(y) \left\{ C(k) \left[J_O(k) - iJ_1(k) \right] + iJ_1(k) \right\}$$

$$\equiv 2\pi \rho_a Ub_{ref} a(y) K(k)$$
.

The equivalent force is determined from

$$\{G\}_{i} = 2\pi \rho_{\mathbf{a}} U b_{\mathbf{ref}} \ell K(\mathbf{k}) \int_{0}^{1} \alpha_{i} \left(1 - \frac{\mathbf{s}}{\delta_{i}}\right) \{\eta\} d\mathbf{s}$$

$$= 2\pi \rho_{\mathbf{a}} U b_{\mathbf{ref}} \ell K(\mathbf{k}) \alpha_{i} \left[\{G0\} - \frac{\{G1\}}{\delta_{i}}\right] , \qquad (A.30)$$

where:

$$\{GO\} = \begin{cases} 1/2 \\ \ell/12 \\ 1/2 \\ -\ell/12 \end{cases} \qquad \{G1\} = \frac{1}{60} \begin{cases} 9 \\ 2\ell \\ 21 \\ -3\ell \end{cases}$$

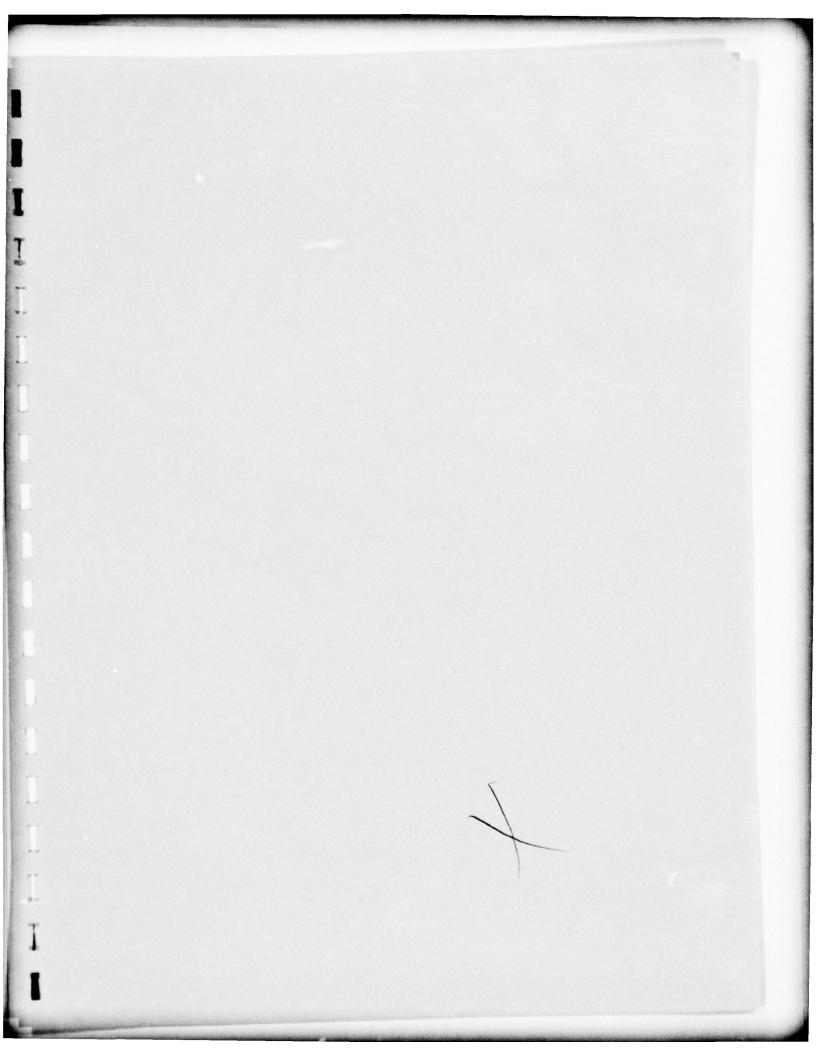
Assembling the matrices is straightforward and is not performed here. The one boundary condition that enters in the assemblage procedure comes from the assumption that the deflections are symmetric about the fuselage. This requires that the slope of the displacement be zero at the root, which in turn requires that the degree of freedom associated with this boundary condition be eliminated.

A remaining task is the inclusion of the nonstructural masses of the fuselage and nacelle into the mass matrix. The fuselage is handled readily by approximating it as a point mass stationed at the root. This mass is simply added to the single element in the mass matrix that deals with the root displacement.

The nacelle is slightly more complicated in that it is not positioned at a node point of the finite element structure. The procedure used is to determine which element contains the nacelle and to then add to the mass matrix of that element terms corresponding to the equivalent mass of the nacelle obtained using a formula similar to that of Eq. (A.00):

$$[M]_{NAC} = M_{NAC} \int_{0}^{1} S(s - s_{NAC}) \{\eta\} \{\eta\}^{T} ds$$

$$= M_{NAC} \{\eta(s_{NAC})\} \{\eta(s_{NAC})\}^{T} , \qquad (A.51)$$



THE OPTIMIZATION OF STRUCTURES WITH COMPLEX CONSTRAINTS VIA A GENERAL OPTIMALITY CRITERIA METHOD

A DISSERTATION

SUBMITTED TO THE DEPARTMENT OF AERONAUTICS AND ASTRONAUTICS

AND THE COMMITTEE ON GRADUATE STUDIES

OF STANFORD UNIVERSITY

IN PARTIAL FULFILLMENT OF THE REQUIREMENTS

FOR THE DEGREE OF

DOCTOR OF PHILOSOPHY

by

Paulo Rizzi

July 1976

ABSTRACT

This study investigates two separate, interdependent topics in the field of structural optimization:

(1) An algorithm is developed for the minimum weight design of structures subject to several non-linear inequality constraints. The structural weight is considered to depend linearly on the design variables.

The algorithm is based on a simple recursion formula derived from the Kuhn-Tucker necessary conditions for optimality. The Gauss-Seidel iterative method for linear systems is used to determine the set of active constraints.

Examples studied include truss structures and box beams subject to static loads with constraints imposed on stresses and displacements, as well as member sizes. For the latter structures, constraints on the fundamental natural frequency and flutter speed are also imposed. The results obtained show that the method is fast, efficient and general, when compared to competing techniques. Extension of the method to include equality constraints and nonlinear merit functions is discussed.

(2) Minimum-weight design of one-dimensional, elastic structures under dynamic loading is studied. Methods of optimal control theory are applied to a cantilever bar driven sinusoidally by an axial force at the tip.

Constraints include maximum allowable stress amplitude at any point along the bar, and minimum cross-sectional area.

In the absence of damping, the design space is disjoint, and many local optima exist. Solutions are worked out in detail for continuous bars,

with the excitation frequency less than, then greater than, the fundamental free-vibration frequency. The latter results overcome a limitation inherent in previous analyses. Above a certain excitation frequency, two or more arcs with different constraints characterize the optimal design; a concentrated tip mass is also needed in some cases.

Free vibrations of the optimal designs are analyzed. A study of the forced-response mode shapes, along with parallel solutions to the same problem made with finite elements, furnish background for a critique of the difficulties in going to higher frequencies than those treated here.

with the excitation frequency less than, then greater than, the fundamental free-vibration frequency. The latter results overcome a limitation inherent in previous analyses. Above a certain excitation frequency, two or more arcs with different constraints characterize the optimal design; a concentrated tip mass is also needed in some cases.

Free vibrations of the optimal designs are analyzed. A study of the forced-response mode shapes, along with parallel solutions to the same problem made with finite elements, furnish background for a critique of the difficulties in going to higher frequencies than those treated here.

ACKNOWLEDGEMENTS

The author wishes to express his appreciation to Dr. Samuel C. McIntosh, Jr. who aided in the original definition of the thesis. Professor Holt Ashley assumed the adviser duties, and his enthusiasm and orientation were invaluable to bring this work to completion. Constructive comments and suggestions were obtained from fellows Erwin H. Johnson and Solly A. Segenreich; professors Arthur E. Bryson and John V. Breakwell of Stanford; Dr. Garret N. Vanderplaats of the Nasa Ames Research Center; and professors Hirokazu Miura and Lucien A. Schmit, Jr. of UCLA.

The Coordenação de Aperfeiçoamento de Pessoal de Nivel Superior (CAPES-MEC) provided generous financial support through a scholarship. Additional funds for computer expenses were partially supplied by NASA (Contracts NGL-05-020-498 and NGL-05-020-243) and by the Air Force Office of Scientific Research (Contract AFOSR 74-2712)

TABLE OF CONTENTS

								Pa	ige
ABSTR	ACT .				•			. :	iii
ACKNO	WLEDG	EMENTS							v
LIST	OF II	LUSTRATIONS							ix
LIST	OF TA	BLES					٠	. 2	kii
NOMEN	ICLATU	RE						.x:	iii
ı.	INTRO	DUCTION		٠					1
II.	AN OF	TIMIZATION ALGORITHM							7
	2.1	Introduction and Summary of Previous Research							7
	2.2	Problem Formulation							12
	2.3	Redesign Equation							14
	2.4	Active-Passive Element Identities							17
	2.5	Determination of Active Constraints	•						18
	2.6	Constraint Reduction							21
	2.7	Relaxation Parameter				•			22
	2.8	Cutoff Criteria							24
	2.9	Basic Weight-Reduction Algorithm							25
	2.10	Possible Extensions and Discussion							26
III.	NUME	RICAL EXAMPLES							30
	3.1	Introduction							30
	3.2	Flutter Equation and Solution							31

		<u>p</u>	age
	3.3	The Flutter Constrained Problem	34
	3.4	Generalized Coordinates	37
	3.5	Gradients of the Generalized Mass and Stiffness Matrices	40
	3.6	Computer Program for Analysis and Design	42
	3.7	Sample Applications and Comparison with other Work	43
		3.7.1 Planar, Ten-Bar Cantilever Truss (Problems 1 - 4)	45
		3.7.2 Twenty-Five Bar Space Truss (Problem 5)	46
		3.7.3 Eighteen-Element Wing Box Beam (Problem 6)	47
		3.7.4 150 (130) Element Swept Wing (Problems 7A and 7B)	49
	3.8	Rectangular Wing with Static and Dynamic Constraints	51
		3.8.1 Static Constraints Only (Problem 8A)	53
		3.8.2 Frequency Conctraint Only (Problem 8B)	54
		3.8.3 Frequency and Static Constraints (Problem 8C)	54
		3.8.4 Flutter Constraint Only (Problem 8D)	55
		3.8.5 Flutter and Static Constraints (Problem 8E)	55
	3.9	Swept Wing with Static and Flutter constraints (Problem 9) .	56
	3.10	Discussion and Additional Data on Examples	58
		3.10.1 Fixed and Updated Modes. Numerical Results	58
		3.10.2 Convergence Difficulties in Wing-Examples	60
		3.10.3 Additional Data on Examples	62
	3.11	Concluding Comments	63
IV.		ONIC EXCITATION	65
	4.1	Introduction	65
	4.2	Continuous Bar	70
	4.3	Two-Design Variable Example	73
	4.4	First-Mode Solutions	74
	4.5	Second-Mode Solutions	84
	4.6	Natural Frequencies	90
	4.7	Finite-Element Solutions	94
	4.8	Concluding Comments	99

																Ī	page
V. CONCLUSIONS AND RECOMENDATIONS					٠	٠	•			•		•		٠			101
REFERENCES																	104
APPENDIX A OPTIMALITY CONDITIONS .																	111
ADDENDIY B DELATIONS RETWEEN EXCIT	יAיד	ON	1 7	NI) N	ΓAL	ווי	7AT	, F	RI	TOE	IEN	1C.	TE.	5		114

LIST OF ILLUSTRATIONS

	page
1.	Flow Diagram for Redesign Operation
2.	Flow Diagram for $\frac{\lambda}{2}$ Calculation
3.	Planar Ten Bar Cantilever Truss
4.	Iteration Histories for Problems 1 and 2 Planar Ten Bar Cantilever Truss
5.	Iteration Histories for Problem 3 Planar Ten Bar Cantilever Truss 123
6.	Iteration Histories for Problem 4 Planar Ten Bar Cantilever Truss 124
7.	Twenty Five Bar Space Truss
8.	Iteration Histories for Problem 5 Twenty Five Bar Space Truss 126
9.	Eighteen Element Wing Box Beam
10.	Iteration Histories for Problem 6 Eighteen Element Wing Box Beam. 128
11.	150 (130) Element Swept Wing
12.	Iteration Histories for Problems 7A and 7B 150(130) Element Swept Wing
13.	Thirty Three Design Variable Rectangular Wing. Dimensions 132
14.	Thirty Three Design Variable Rectangular Wing. Structural Box 133
15.	Iteration Histories for Problems 8 (A, B, C and E) Rectangular Wing
16.	Iteration History for Problem 8D Rectangular Wing with Flutter Constraints
17.	33-Design Variable Rectangular Wing. Final Material Distribution 136
18.	Rectangular Wing. Problem 8A. Critical Constraints 138
19.	Rectangular Wing. Problem 8C. Critical Constraints 139
20.	Rectangular Wing. Problem 8E. Critical Constraints 140
21.	V-g Diagram for Final Design of Rectangular Wing under a Flutter Constraint only. Problem 8D
22.	V-g Diagrams for Initial and Final Designs of the Rectangular Wing under Static and Flutter Constraints. Problem 8E 142
23.	Swept Wing. Dimensions of the Aerodynamic Planform 143
24.	V-g Diagram for the Final Static Design of the Swept Wing (Prob- lem 7B) with a 400 lbs. Mass Distributed evenly among the Eight Nodes of the Tip (Upper Wing Half only)

	<u> </u>	age
25.	V-g Diagrams for Initial and Final Designs of the Swept Wing with a 5000 lbs. Mass evenly Distributed on the Structural Boxes' trailing Edge (Upper Wing Half only). Problem 9	145
26.	Iteration History for Problem 9 Swept Wing with Static and Flutter Constraints	146
27.	Critical V-g Curves Obtained for the Final Design of the Rectan- gular Wing under Static and Flutter Constraints. Comparison of Three Distinct Dynamic Models	147
28.	Two idealizations of a cantilever, elastic bar of length l , excited in axial vibration by a sinusoidal varying force at the free end. A concentrated Mass $M_{\rm T}$ may be attached at the tip. For finite-element modeling, the bar is divided into $$ n uniform segments of equal length	148
29.	Illustrating the feasible design spaces (unshaded) for a simple, two-design-variable bar forced from its tip at the dimensionless frequency $\lambda_{\rm e}$; a and a _T are, respectively, the constant cross-sectional area and a parameter to represent the tip mass.	149
30.	Total dimensionless volume for the uniform cross-sectional area bar, as a function of the dimensionless excitation frequency $\lambda_{\bf e}$	150
31.	Matching point s = γ between the unconstrained and stressed arc, plotted vs. frequency parameter α for first-mode designs.	151
32.	Dimensional total weight (or volume) of the first-mode optimal design as a function of α . Above α = 1.0908, the fully-stressed design is shown for comparison	152
33.	Dimensionless cross-sectional area distributions of the first-mode optimal designs, plotted as a function of the distance along the bar for three values of the frequency parameter $\alpha.$ The corresponding finite-element solutions are also shown	153
34.	Matching point $s = \gamma$ between the stressed and minimum-area arcs, plotted vs. α for second-mode designs at eight values of parameter δ	154
35.	Dimensionless cross-sectional area distributions of the second-mode optimal design, plotted vs. distance along the bar when $\alpha=1.0$ and $\delta=10$. Continuous and two finite-element solutions	155
36.	Dimensionless total weight (or volume) of the second-mode optimal designs as a function of α and δ . The first-mode curve from Fig. 32 is shown dotted. To the right of the dash-dot line, the two-arc solutions of Section 4.5 are no longer optimal	156
37.	Dimensionless tip-weight (or volume) of the second-mode optimal designs plotted as a function of α and δ	157
38.	Comparison of optimal dimensionless weights (or volumes), obtained with variable and constant cross-sectional area, for $\delta=5$.	158

		page
39.	Fundamental natural frequency of the first-mode optimal designs, plotted vs. α	159
40.	First two dimensionless natural frequencies of the second-mode optimal designs, plotted vs. α	160
41.	Finite-element optimal solution for $n=20$, $\alpha=2.0$, and $\delta=10$.	161
42.	Mode shape of forced response for the Fig. 41 design	162

LIST OF TABLES

	<u>pa</u>	ge
1.	Final Designs for the ten bar planar truss	63
2.	Final Designs for Problem 5. Twenty Five Bar Space Truss 1	64
3.	Final Designs for Problem 6. Eighteen Element Wing Box Beam 1	64
4.	Final Designs for the Swept Wing	65
5.	Load Data for 33-Design Variable Rectangular Wing	66
6.	Final Designs for the 33-Design Variable Rectangular Wing 1	67
7.	Final Design for Problem 9. Swept Wing under Static and Flutter Constraints	68
8.	Designs Obtained after 15 and 50 Iterations, for Problems 8A and 8E	69
9.	Iteration Histories for Examples Studied in Chapter III 1	70
10.	Summary of Results of Chapter III	71

NOMENCLATURE

Ā	Aerodynamic matrix
A	Generalized aerodynamic force matrix
Ą	Vector of cross-sectional areas
A(x)	Bar cross-sectional area
A a	Matrix of coefficients of polynomials for aerodynamic forces
A _i	Cross-sectional area of element i
ą	Objective function gradient (constant)
<u>a</u>	Vector of dimensionless cross-sectional areas
a(s)	Dimensionless bar cross-sectional area (= A() σ_{max}/P)
a T	Dimensionless bar tip mass $(= M_T \sigma_{max}/Pl)$
b	Reference length
ç	Vector of resizing factors
Ď	Diagonal matrix
D	Diagonal matrix
Е	Young's modulus
F	Matrix of constraint gradients
ţ(x)	Vector of normalized inequality constraint functions
<u>Ģ</u>	Structural damping matrix
G	Generalized structural damping matrix
g(x)	inequality constraint function
g	damping parameter
H()	Hamiltonian function

```
Vector of normalized equality constraint functions
h(x)
         z-displacements per unit amplitude of the i<sup>th</sup> mode
         Identity matrix
         Vector with all components equal to unity
         complex (=\sqrt{-1})
j
ĸ
         Stiffness matrix
         Generalized stiffness matrix
Κ
K<sub>i</sub>
         Elemental stiffness matrix
         Unit elemental stiffness matrix
k
         Reduced frequency (= wb/V)
k,
         Distinct values of the reduced frequency
         Bar length
         Mass matrix
M
         Generalized mass matrix
         Matrix of force systems
         Amplitude of tip-force
         Adjoint eigenvector
P
         Vector of force amplitudes
P
         Generalized aerodynamic force matrix (modified)
Q
         Coefficients of polynomials for generalized aerodynamic force
Qi
         Vector of complex amplitudes
q
         free-stream dynamic pressure (= 1/2 \rho_m V^2)
q_{\infty}
Re()
         Real part of complex quantity
         Nondimensional spatial coordinate
```

Time

Vector of interpolation functions t(x,y)Vector of displacement amplitudes u(x)Mode of forced response Free-vibration modes $u_{i}(x)$ V airstream speed; total volume Flutter speed of the aeroelastic system V_{Fo} Given and constrained value of the flutter speed r Pseudo harmonic oscillation frequency vector of dimensionless displacement amplitudes Dimensionless mode of forced response v(s) W(x)Structural weight Nonstructural weight Vector of tranverse displacements X Design variable vector â Optimum design variable vector Cartesian coordinates x,y,z Matrix of generalized coordinates \mathbf{Z} Relaxation parameter Dimensionless excitation frequency (= $\omega_{\rm e}$ 2 $\sqrt{
ho/2E}$) a Dimensionless natural frequencies $\alpha_{\mathbf{i}}$ Initial value for the relaxation parameter Relaxation parameter multiplication factor Dimensionless stress limit (= σ_{max}/E) A() Incremental value Matching point of two different arcs Tolerance for design process

Tolerance for Gauss-Seidel iterations

```
Constraint tolerance
ε<sub>f</sub>
          Minimum-area parameter (= P/o A )
8
          Initial constraint thickness
          Multiplier for the constraint thickness
          Vector of Lagrangian multipliers (inequality constraints)
          Vector of adjoined functions
\lambda()
          Excitation frequency parameter (= \omega_{\rm e} 1 \sqrt{\rho/E} )
          Dimensionless modal frequencies
          Vector of Lagrangian multipliers (equality constraints)
\mu_{i} ( )
          Multiplier functions
          Poisson's ratio or iteration number
          Lagrangian multipliers
          Material density
         Air density
          Stress amplitude
          Circular frequency
          Excitation frequency
          Natural frequencies
         Complex frequency; = (1 + jg)/\omega^2
∇()
         Gradient operation
( )<sup>T</sup>
         Transpose
()
         Differentiation
( )
          Differentiation
```

Note: Additional nomenclature is explicitly defined in the text.

CHAPTER I

INTRODUCTION

The primary function of any structure is to support externally applied loads and to transfer them to the reaction points while, at the same time, satisfying other specified requirements. Structural analysis is the field that studies known structural configurations which are subjected to known distributions of static or dynamic loads and displacements, determining whether the design requirements are satisfied. The structural designer, then, is interested in finding (among a large number of alternates) the most efficient design for the specified load environment.

As cheaper computational facilities became available, efforts have been directed to the automatation of structural design. In general, structural synthesis applied to aerospace structures requires the selection of configuration, member sizes, and materials. At present it is not feasible to consider all these parameters except in cases where the loading environment and design criteria are very simple. For this reason, in developing synthesis methods, attention has been focused on the variation of one parameter (say member sizes) to achieve minimum weight, with the other two parameters fixed. An aerospace structure is normally subjected to a large number of requirements (e.g., stresses, displacements, stability, natural frequency, flutter speed, fatigue life, creep, etc.). Although all design conditions must be considered in structural

synthesis, it is economically feasible to consider only some of them automatically at one time. However, the significant progress that has already been made in the development of structural-synthesis methods indicate that, in the near future, large optimal structural configurations that satisfy all design criteria are going to be generated automatically.

Since the beginning of the last decade, two important trends have developed in structural optimization which represent two complementary methods of solution. One involves research into the basic principles governing optimum structures. The approach is that of the classical calculus of variations and it is applicable to simple, continuous structures. It has been used by Keller (Ref. 1) for the problem of the tallest column, by Niordson (Ref. 2) for the optimization of a beam with fixed natural frequency, by Turner (Ref. 3) for his now classical bar. Variational principles were also used by Prager (Ref. 4), Prager and Taylor (Ref. 5) and Taylor (Ref. 6) to develop optimality criteria for continuous systems.

The other approach makes use of numerical methods and algorithms for optimizing complex structures. The structure to be optimized is either one with discrete characteristics such as an airplane wing, or continuous one which is first discretized. The structural synthesis concept developed along two main lines in applications and in methods of optimization:

(a) with respect to applications: (1) special purpose applications to fundamental problems involving a broad range of complex requirements

and loading environments (Refs. 7-15), and (2) general purpose applications based on the finite-element analysis of general structures, considering multi-behavioral constraints under a multiplicity of distinct loading conditions (Refs. 16-20).

(b) with respect to methods of optimization: (1) application of relatively standard concepts of nonlinear programming techniques for the purpose of redesign (Refs. 9-19), and (2) methods based on fully-stressed design and optimality critera (Refs. 21-34). A fine account of the origins of the terms "mathematical programming" and "optimality criteria", as they are used today in structural optimization, is given by Segenreich (Ref. 34).

For an excellent introduction to the concepts of mathematical optimization, the reader is referred to a text by Wilde and Beightler (Ref. 35). The computational aspects of mathematical programming are presented in a book by Jacoby, et al., (Ref. 36). A more general view of the field of structural optimization can be obtained from a series of survey papers (Refs. 37-39). In 1968, Sheu and Prager (Ref. 37) cited 146 publications, including prior surveys, with more than the usual amount of attention paid to continuous (as contrasted with discrete) structural representations. Pierson's (Ref. 38) is the only known review paper that emphasizes dynamic conditions. He cites 61 papers divided between those investigations that place constraints on structural natural frequencies and those (fewer in number) where some property of the forced dynamic response is considered. Since 1972, a few papers that could be added to this list are cited in Ref. 13, Ch. 1. A review and assessment

of the state-of-the-art for optimization under aeroelastic constraints, as of mid-1974, can be found in a paper by Stroud (Ref. 39). Chapter 1 of the work by Schmit and Miura (Ref. 20) is an excellent and up-to-date survey on methods of structural synthesis. Two recent symposium proceedings, edited by Gellatly (Ref. 40) and Schmit (Ref. 41), provide state-of-the-art descriptions of various portions of the field.

The research that led to this dissertation is centered on two methods of solution in structural optimization. First attention is directed to the most problematic aspect of structural synthesis: the development of a fast and efficient redesign algorithm to be used in general purpose programs. Efforts were made to keep the restrictions on the application of the method to as few as possible. The goal was to build an "optimizer" general enough to replace the existing inefficient ones. The algorithm, therefore, should not be problem-dependent. Generality is also kept in the sense that it can incorporate advances in other aspects of structural synthesis, such as efficient analysis and sensitivity analysis.

The potential of the redesign method is shown by means of several applications. Its efficiency is determined by comparing with results obtained by other methods. Its generality is confirmed by the application to multi-behavioral constrained problems. I. e., wings under several static loading conditions are subjected to constraints on stresses, displacements, frequency, flutter speed and member sizes. Although these applications were meant to be pure exercises, the generation of the structural synthesis program took most of the time spent in the research. This was so because available analysis programs deal with either only static constraints or with a single complex requirement such as flutter,

stability or forced dynamic response. Programs that consider various failure modes typically provide only for constraint evaluations, with no information on the constraint derivatives which are needed for efficient redesign. The synthesis program used in this research was obtained by suitably modifying the SAD (Structural Analysis and Design) program (Ref. 43), which considers static and frequency constraints, to allow:

- (a) for the addition of a flutter constraint in the analysis, and
- (b) for redesign by means of a routine based on the optimization algorithm developed here. Because of its simplicity and efficiency, the method developed by Segenreich (Ref. 34) for flutter optimization was chosen.

A second area of research is the optimization of a continuous, one-dimensional structure under harmonic excitation. Optimal control techniques are used to find the analytical solution for the optimum shape of a cantilever bar excited harmonically at its free end, with constraints placed on the stress amplitude and cross-sectional area along the span. Investigation of this problem was started by Johnson (Ref. 13), who obtained solutions for a finite-element representation of the bar. As will be seen, this problem involves a design space with multiple feasible regions and multiple optima. Solutions are obtained for two of these optima and a procedure to obtain others is suggested. Due to the paucity of studies dealing with the optimization of dynamically loaded structures, it is felt that this work makes significant contribuitions to the basic understanding of this type of problem. For the first time an analytical solution for more than one of the many local optima is found.

Since a global minimum is ultimately sought in every optimization problem, the understanding of the local optima may prove invaluable when complex structures are considered. The success achieved here in finding solutions that analytically detail the effects of the various parameters points out the difficulties that will be encountered when dealing with more complex problems in this area, as well as alternatives in handling these difficulties.

The core of the dissertation is contained in three chapters. The optimization algorithm is developed in Chapter II. Chapter III contains information about the structural design program used to test the algorithm, as well as a description of the examples considered and the results obtained. The structural optimization of the harmonically excited bar is treated in Chapter IV. Chapters II and III can be considered independent of Chapter IV. A summary of previous research for each subject is given in the introductory sections of the respective chapters.

Finally, the last chapter briefly summarizes the results obtained and indicates areas that merit further study. A more detailed discussion of the results is presented at the end of Chapters II, III and IV.

CHAPTER II

AN OPTIMIZATION ALGORITHM

2.1 INTRODUCTION AND SUMMARY OF PREVIOUS RESEARCH

The optimal design of structures can be considered as an iterative process, each iteration consisting of two steps: 1) an analysis of the structure at the current design, and 2) a redistribution of material. In the analysis cycle the behavioral constraints are checked and changes in the behavior caused by material redistribution are predicted (sensitivity analysis). In the redesign cycle, material is added or subtracted in order to minimize the merit function (weight) and satisfy the constraints.

In 1960 it was first suggested by Schmit (Ref. 15) that finite-element analysis methods (analysis step) and nonlinear programming methods (for redesign) could be coupled to generate structural design capabilities. The first major effort to apply mathematical programming techniques to the optimization of complex structures was reported in Refs. 16 and 17. These general purpose programs consider static stress and displacement limits under multiple load conditions, and minimum member sizes; and involve structures of fixed geometry that can be modeled by bars, shear panels and plane stress membrane (triangular or quadrilateral) elements. Another work that merits attention is that reported in Refs. 18 and 19. This work

introduces the capability of considering stressed-skin structures with holes and cut-outs and the finite-element library is augmented by two "beam-like" elements. These two major efforts showed that techniques borrowed from operations research could be used together with finite-element programs for structural synthesis purposes. This success was, however, hindered by an efficiency barrier encountered when large examples were considered. Analyses required large computation times and too many analyses were required by the mathematical programming algorithms for convergence to an optimal design.

In an effort to reduce computational effort and acomodate large problems, many investigators (Refs. 21-27) focused research on the implementation of simple recursion formulas derived from the properties of the final optimal solution, turning away from the sophisticated numerical search procedures typical of mathematical programming. Optimality criteria methos started from the fully-stressed design concept. The first general purpose programs based on this concept were reported in Refs. 21-25. In Ref. 26 the displacement constraints were handled by a numerical search procedure and examples with up to 1200 degrees-of-freedom were considered. In Ref. 27 the displacement constraints were handled by an optimality criterion procedure and the method was applied to several examples. In most cases satisfactory results were obtained in 10 resizing cycles or less.

The success of these early investigations led to a new "school" in the field of structural optimization. Namely, that of the use of optimality criteria methods for redesign purposes. Taig and Kerr (Ref. 28) presented a procedure based on generalized energy criteria. Multiple

constraints are dealt with by a formula involving element energies and their "target energies". A similar concept is used here for the same purpose. In Ref. 28, several test examples were treated and results for two practical problems were presented. In Ref. 29, optimality criteria and redesign formulas were presented for stress, displacement, frequency and buckling constraints. The full advantages of the method are brought out by presenting results for several large examples. The work by Berke and Khot (Ref. 30) provides a state-of-the-art view of the field as of late-

Kiusalaas (Refs. 31-32) advanced the original concept of resizing by means of optimality criteria by introducing a parameter in the redesign relation, with the aim of improving convergence of the algorithm. The method was presented in reference 31 and results for stability problems were given in reference 32. Segenreich (Ref. 34) used a parameter-dependent redesign formula such that monotonic weight decrease would result. The procedure handled only one equality constraint. Results presented include those for examples involving a constraint on the static compliance, natural frequency and flutter speed. In a later work, Segenreich and McIntosh (Ref. 33) extended the method for multiple equality constraints.

Other investigators (Refs. 42-52) concentrated efforts on design oriented structural analysis. Here the idea is to improve the efficiency of the analysis step and thus reduce the computational time. Improved efficiency can be achieved by:

(a) Reducing the number of design variables by appropriate linking;

that is, control the size of several elements by a lingle design variable (e.g., members of a symmetric truss under symmetric loading).

- (b) Reducing the number of constraints by the "throw away" (Ref. 42) and "regionalization" concepts coupled with a selective sensitivity analysis (Ref. 20). The essential idea of the "regionalization" concept is to divide the structure into regions and, at each stage of the design process, consider only the most critical stress constraint within each region, for each loading condition. The "throw away" concept is based on temporarily ignoring, at a particular stage of the design, the constraints that are redundant or very inactive. Selective sensitivity analysis is achieved by organizing the finite-element program in such a way as to compute the gradients of only the constraints of interest (those remaining after regionalization and throw away).
- (c) Using iterative methods (Ref. 43), basis reduction (Refs. 34, 44, 45 and 46), and reorganizing the structure of finite-element methods (Refs. 51 and 52) for efficient reanalysis. Iterative methods may be efficient if one considers that after the first design cycle, a good approximation for the response of the next design is available (design steps are usually small). Basis reduction has been widely used in dynamic analysis by the introduction of modal coordinates instead of nodal coordinates, thus reducing the size of the problem. Classical finite-element methods were developed for the purpose of performing a single analysis at a time. By reorganization of the analysis process to take advantage of the need for multiple analyses, considerable efficiency can be achieved.
 - (d) Using effective sensitivity analysis methods (Refs. 47-48); e.g.,

the calculation of first order Taylor series expansions (Refs. 49-50) to set up approximate analyses and therefore reduce the required number of complete analyses.

One last improvement in the performance of the analysis step can be achieved if one recognizes that a given design condition can be redefined in an alternative, simpler way. Segenreich (Ref. 34) has shown that efficiency can be improved by imposing a constraint on the imaginary part of the aeroelastic eigenvalue for a fixed free stream velocity, rather than on the flutter speed directly.

In choosing the algorithm for the redesign cycle, several features are desirable; the method should be:

- (a) efficient , i.e., the number of analyses should be kept as low as possible,
- (b) general , in the sense that no restrictions should be imposed on the type of the behavioral constraints that can be handled,
- (c) computationally fast , i.e., the time spent in each redesign should be kept to a minimum, and
 - (d) proven to converge to an optimum, or very near optimum, design.

Structural design algorithms using mathematical programming techniques usually satisfy only (b) and (d). Conversely, optimality criteria methods normally have only characteristics (a) and (c).

The scope of the work presented in this chapter entails the development of an algorithm for the weight-minimization of multi-constrained,

^{*} This is useful mainly when mathematical-programming methods are employed for redesign. Normally these methods involve a direction finding problem and a one-dimensional search in this direction. This search requires a certain number of function evaluations (analyses) which need not be precise. Therefore a complete analysis need be performed only prior to the direction finding problem.

general structures of fixed geometry, having the qualities described above. Briefly, the algorithm is derived from the rigorous optimality conditions (Kuhn-Tucker) and is parameter-dependent in order to achieve improved convergence characteristics. The redesign formula used is that of Kiusalaas (Ref. 31). Linear constraints (size limits) are handled much in the same way as by Kiusalaas (Refs. 31 and 32). The number of constraints is reduced by a simple "throw away" technique used previously by Vanderplaats (Ref. 54). To deal with the remaining multiple constraints, a method inspired by the work by Taig and Kerr (Ref. 28) is developed. "Inconsequent" constraints are deleted by a procedure based on the Gauss-Seidel iterative method for linear systems (Ref. 53). This development of the redesign procedure is detailed in the following sections.

2.2 PROBLEM FORMULATION

An optimization problem can be formulated as:

Find
$$\underset{X}{\text{Min }} W(\underset{z}{x})$$
 (2.2.1)

subject to constraints

$$f_{\dot{j}}(x) \le 0$$
 $\dot{j} = 1, 2, ... K$ (2.2.2)

$$h_{\dot{j}}(x) = 0$$
 $\dot{j} = 1, 2, ... M$ (2.2.3)

where x is a (N x 1) design vector.

The necessary conditions for local minimum are the well known Kuhn-Tucker conditions (Ref. 36) and are given by:

$$\nabla W(\hat{\mathbf{x}}) + \sum_{j=1}^{M} \mu_{j} \nabla h_{j}(\hat{\mathbf{x}}) + \sum_{j=1}^{K} \lambda_{j} \nabla f_{j}(\hat{\mathbf{x}}) = 0$$
 (2.2.4)

$$\lambda_{i} \ge 0$$
 (j=1,2,... K) (2.2.5)

$$\sum_{j=1}^{K} \lambda_j f_j(\hat{x}) = 0$$
 (2.2.6)

$$f_{j}(\hat{x}) \le 0$$
 $(j=1,2,...K)$ (2.2.7)

$$h_{j}(\hat{x}) = 0$$
 (j=1,2,... M) (2.2.8)

where $\mu_{\dot{j}}$ and $\lambda_{\dot{j}}$ represent Lagrange multipliers and $\, \hat{x} \,$ represents the minimum point.

The problem as stated by equations (2.2.1) through (2.2.3) is very general in its form. The structural optimization problems considered in this dissertation are, in fact, sub-problems of this general furmulation. For example, consider the structural optimization problem where the objective function is the structural weight. When the design variables are selected to size structural elements rather that define their major dimensions, the weight can be expressed as a linear function

$$W(x) = W_0 + \sum_{i=1}^{N} a_i x_i = W_0 + a^T x$$
 (2.2.9)

with $W_{\rm O}$ the weight of the structure not associated with the design variables (e.g., non-structural weight). If member size limits are specified, it is convenient to separate them from constraints (2.2.2)

$$(x_i)_{\min} \le x_i \le (x_i)_{\max}$$
 (i=1,2,... N) (2.2.10)

For the sake of simplicity, consider only inequality constraints (2.2.2). By applying conditions (2.2.4) through (2.2.7) to this particular case, one derives the optimality criterion:

$$a_{i} + \sum_{j=1}^{K} \lambda_{j} \frac{\partial f_{j}}{\partial x_{i}} \begin{cases} = 0 & \text{if } (x_{i})_{\min} < x_{i} < (x_{i})_{\max} \\ \ge 0 & \text{if } x_{i} = (x_{i})_{\min} \\ \le 0 & \text{if } x_{i} = (x_{i})_{\max} \end{cases}, (i=1,2,..N) (2.2.11)$$

where

$$\lambda_{j} \begin{cases} = 0 & \text{if } f_{j} < 0 \\ \geq 0 & \text{if } f_{j} = 0 \end{cases}$$
 (j=1,2,... K) (2.2.12)

All functions are evaluated at $\hat{\mathbf{x}}$. Equation (2.2.12) requires additional explanation. If there are K behavioral constraints, only some of them are active (\mathbf{f}_j = 0) at the optimal design and thus enter the optimality criterion. The inactive constraints (\mathbf{f}_j < 0) are eliminated by setting λ_j = 0 for the appropriate values of j.

2.3 REDESIGN EQUATION

As shown by Kiusalaas (Ref. 31), the basic function of the optimization algorithm is to solve Eqs. (2.2.11) and (2.2.12) by successive, linearized iterations starting from some initial design. The design variables at iteration $\nu + 1$ are related to those of the previous iteration by

$$\mathbf{x}_{i}^{v+1} = \begin{cases} c_{i}^{v} \mathbf{x}_{i}^{v} & \text{if } (\mathbf{x}_{i})_{\min} < c_{i}^{v} \mathbf{x}_{i}^{v} < (\mathbf{x}_{i})_{\max} \\ (\mathbf{x}_{i})_{\min} & \text{if } c_{i}^{v} \mathbf{x}_{i}^{v} \le (\mathbf{x}_{i})_{\min} \\ (\mathbf{x}_{i})_{\max} & \text{if } c_{i}^{v} \mathbf{x}_{i}^{v} \ge (\mathbf{x}_{i})_{\max} \end{cases}, (i = 1, 2, ... N) \quad (2.3.1)$$

with the redesign factor c_{i}^{V} given by

$$c_{i}^{\vee} = \alpha - \frac{(1-\alpha)}{a_{i}} \sum_{j=1}^{K} \lambda_{j} \left(\frac{\partial f_{j}}{\partial x_{i}} \right)^{\vee} \qquad (i = 1, 2, \dots N)$$
 (2.3.2)

Here α is a scalar relaxation parameter that ranges in value from zero

to unity, and is adjusted so as to improve convergence. Before c_{i}^{ν} can be evaluated, the vector of Lagrangian multipliers λ_{j}^{ν} must be evaluated. The λ_{j}^{ν} are chosen in such a way that the design $(\nu+1)$ is "critical" with respect to the constraints j, i.e., satisfies $f_{j}^{\nu+1}=0$ to a first order approximation. At this stage it is convenient to define as active any element for which $(x_{i})_{\min} < c_{i}^{\nu} x_{i}^{\nu} < (x_{i})_{\max}$, and as passive the elements $c_{i}^{\nu} x_{i}^{\nu} \le (x_{i})_{\min}$ and $c_{i}^{\nu} x_{i}^{\nu} \ge (x_{i})_{\max}$. Assume, for the time being, that the identities of the active and passive elements are known a priori. Also assume that the identities of the behavioral constraints that are active at the optimum is known, i.e., R, the set of constraints for which strict equality is observed at the optimum is determined. To first order:

$$\Delta f_{r} = \sum_{i}^{N} \frac{\partial f_{r}}{\partial x_{i}} \Delta x_{i} \qquad r \in \mathbb{R}$$
 (2.3.3)

where

$$\Delta f_{r} = -f_{r} \qquad r \in R \qquad (2.3.4)$$

$$\Delta \mathbf{x}_{i} = \begin{cases} (c_{i} - 1) & \mathbf{x}_{i} & \text{if active} \\ \mathbf{x}_{i}^{*} - \mathbf{x}_{i} & \text{if passive} \end{cases}$$
 (i =1,2,... N) (2.3.5)

with x_i^* the proper value, depending on whether the element i is passive with respect to its lower or upper bound. Using Eqs. (2.3.2), (2.3.4) and (2.3.5) in Eq. (2.3.3):

[†] Note that active elements are those whose side constraints are "loose" (or inactive). The word "active" was chosen in this case because if the side constraint is "loose" the element is "working" to its full extent.

$$f_{r} = (1 - \alpha) \sum_{j \in \mathbb{R}} \lambda_{j} \sum_{i}^{\text{act}} \frac{\partial f_{r}}{\partial x_{i}} \frac{x_{i}}{a_{i}} \frac{\partial f_{j}}{\partial x_{i}} + (1 - \alpha) \sum_{i}^{\text{act}} \frac{\partial f_{r}}{\partial x_{i}} x_{i}$$

$$- \sum_{i}^{\text{pas}} \frac{\partial f_{r}}{\partial x_{i}} (x_{i}^{\star} - x_{i}) \qquad r \in \mathbb{R}$$
(2.3.6)

With the definitions:

$$\theta_{a} = \{ \theta_{r}^{a} \} ; \quad \theta_{r}^{a} = \sum_{i}^{act} \frac{\partial f_{r}}{\partial x_{i}} x_{i}$$

$$\theta_{p} = \{ \theta_{r}^{p} \} ; \quad \theta_{r}^{p} = \sum_{i}^{pas} \frac{\partial f_{r}}{\partial x_{i}} (x_{i}^{*} - x_{i})$$

$$\xi = \left[F_{jr} \right] ; \quad F_{jr} = \left(\frac{\partial f_{r}}{\partial x_{j}} \right)_{act}$$

$$\xi = \left[D_{ij} \right] ; \quad D_{ij} = \delta_{ij} \frac{x_{i}}{a_{j}}$$

$$\xi = \left[D_{ij} \right] ; \quad D_{ij} = \delta_{ij} \frac{x_{i}}{a_{j}}$$

$$\xi = \left[D_{ij} \right] ; \quad D_{ij} = \delta_{ij} \frac{x_{i}}{a_{j}}$$

$$\xi = \left[D_{ij} \right] ; \quad D_{ij} = \delta_{ij} \frac{x_{i}}{a_{j}}$$

where δ is the Kronecker delta, one can write Eqs. (2.3.6) and (2.3.2) in vector form:

$$(1 - \alpha) \left(\mathbf{F}^{\mathrm{T}} \stackrel{\mathbb{D}}{=} \mathbf{F} \right) \stackrel{\lambda}{=} \mathbf{f} + \stackrel{\theta}{=} - (1 - \alpha) \stackrel{\theta}{=} a$$
 (2.3.8)

$$c = i - (1 - \alpha) \bar{p} + \lambda \qquad (2.3.9)$$

with i a vector with all components equal to unity.

Equations (2.3.8) and (2.3.9), together with (2.3.1) are the design equations. As one can see, (2.3.8) can be solved for λ only if the

identities of active and passive members are known beforehand. Also, R was assumed to be known. Finally, the question of how to determine the proper value of the relaxation parameter α must be answered.

2.4 ACTIVE-PASSIVE ELEMENT IDENTITIES

One has, basically, two ways of dealing with the active-passive character of the design variables. Segenreich (Ref. 34) chose to fix the identities of passive elements. That is, once a design variable reaches its extreme allowable value, it is equated to this value for the remainder of the optimization process. This strategy eliminates the need for calculating the derivatives of the constraints with respect to the passive design variables. Since one cannot assure that this strategy will lead to the true optimum, the optimality conditions must be checked at the end of the optimization process. In case these are not met, a perturbation of the final design must be performed and the optimization restarted. A second approach is used by Kiusalaas (Refs. 31 and 32) and others (Refs. 25 and 25). Since one does not know a priori the identities of the active and passive members, the minimization cycle is carried out by a trialand-error procedure. At the start of an iteration, one assumes an activepassive list. One proceeds to calculate the new design vector, updating the active-passive list if necessary. If the list is changed, one recalculates the design vector using the updated active-passive list. This process is continued until no updating is necessary, and then a new optimization cycle is started. This strategy requires the derivatives of the constraints with respect to all design variables. Furthermore, one

cannot assure convergence of the trial-and-error procedure, although the method has shown to be very effective (Refs. 25, 27 and 32).

Although the latter approach was chosen here, one must not disregard the merits of the former, especially for problems where it is expected that a large number of design variables will be at their extreme values.

2.5 DETERMINATION OF ACTIVE CONSTRAINTS

It should be clear that in some cases the determination of the set of critical constraints R should not present any difficulty. This is the case for optimization problems involving: 1) a single equality or inequality constraint (Ref. 34), or 2) multiple equality constraints (Ref. 33). R is then simply the set of all constraints considered. Furthermore, if only equality constraints are considered, no sign restrictions are imposed on the Lagrangian multipliers (recall the Kuhn-Tucker conditions 2.2.4 through 2.2.8). The linear system (2.3.8) can be solved directly once the value of α has been specified.

Suppose, however, that multiple inequality constraints have been specified, and consider a near optimal design. It is apparent that, in this case, the determination of R is difficult. Kiusalaas (Refs. 31 and 32) suggests a trial-and-error method for the determination of the active constraints. The general idea is to assume initially that all constraints are active and to solve the system of equations (2.3.8) for the Lagrangian multipliers. The constraints associated with negative components of λ are then considered to be non-active, since the multipliers must be positive (see Eq. 2.2.12). The corresponding rows and

columns are eliminated from equation (2.3.8). This process is continued untill all the remaining components of λ are positive. This method has been successfully applied to an example where two primary constraints were specified (Ref. 32). It has been suggested (Ref. 31) that the proposed method is practical and efficient if only a few constraints are imposed, and that it is exceedingly expensive for most practical problems. Another point must not be overlooked: it may happen that constraints that were deleted because of their association with negative components of λ are, in fact, active and should not have been dropped. Suppose that at the beginning there are m constraints, and that the first solution of (2.3.8) gives r negative components. It may well be that the deletion of only some of the constraints associated with these components results in a reduced system having all components of the new solution positive. This phenomenon occuring at a near optimal design suggests that the deletion of all constraints associated with the r negative components may turn out to be a poor strategy. One could, therefore, think of deleting only the constraint associated, say, with the most negative Lagrangian multiplier. If the original strategy was considered to be exceedingly expensive for most practical problems, the modified one would be prohibitive, since for every constraint deleted a solution to a new linear system must be obtained.

If, instead of solving the resultant systems by matrix inversion or decomposition, one is able to use some iterative scheme, constraints could be deleted as soon as a component of λ reaches a negative value. Since one would like this scheme to be fast and convergent, a reasonable choice is the Gauss-Seidel iterative method (Ref. 53).

Consider the linear system

$$\mathbf{B} \hat{\lambda} = \mathbf{d} \tag{2.5.1}$$

Let

$$C = -\begin{bmatrix} 0 & b_{12}/b_{11} & \dots & b_{1n}/b_{11} \\ b_{21}/b_{22} & 0 & \dots & b_{2n}/b_{22} \\ \vdots & \vdots & & \vdots \\ b_{n1}/b_{nn} & b_{n2}/b_{nn} & 0 \end{bmatrix}; b = \begin{pmatrix} d_1/b_{11} \\ d_2/b_{22} \\ \vdots \\ d_n/b_{nn} \end{pmatrix}$$
(2.5.2)

Define

$$\lambda_{i}^{V} = \sum_{j=1}^{i-1} c_{ij} \lambda_{j}^{V} + \sum_{j=i+1}^{n} c_{ij} \lambda_{j}^{V-1} + b_{i} \qquad (i = 1, 2, ... n)$$
 (2.5.3)

and consider $\sum_{j=1}^{0}... = \sum_{j=n+1}^{n}... = 0$.

quation (2.5.3) is the iteration formula. As one can see, one value is computed at a time, thus enabling the elimination of a constraint as soon as its respective multiplier becomes negative.

A sufficient condition for convergence of the method is that B be symmetric and positive definite (Ref. 53). Here

$$B = F^{T} D F (2.5.4)$$

is clearly symmetric. Since, for the class of problems dealt with in this dissertation, D is diagonal with all elements positive, B is positive definite when non-singular. Hence, the method should converge.

B is non-singular if the constraint gradients are linearly independent. This is clearly not the case when there are more constraints than design variables, which is usually the rule. In this case constraints should be eliminated by some other means first (e.g., "throw away").

2.6 CONSTRAINT REDUCTION

At each stage of the design process, the method outlined in Section 2.5 eliminates all non-critical constraints, as well as some critical and near critical constraints. Since most structural design optimization problems carry a large number of inequality constraints, it would be a formidable task to deal with all constraints. All constraint gradients would be needed at each stage, causing convergence difficulties (see ¶ on page 20). It is, therefore, convenient to reduce the number of constraints by some other means and to perform the deletion process on the reduced number of constraints. One efficient way of reducing the number of constraints is the regionalization approach, coupled with the throw-away concept (Ref. 20).

Another way, which is simple in nature and proven to be efficient, is the use of the "constraint thickness" concept (Ref. 54). For constraint reduction purposes only, define as active, the constraint that satisfies

$$-\delta \le f_{j}(x) \le \delta \tag{2.6.1}$$

Further, define violated constraints as those for which

$$f_{j}(x) > \delta \tag{2.6.2}$$

It is then very easy to delete the constraints that are neither active or violated, i.e.,

$$f_{\frac{1}{2}}(x) < -\delta \tag{2.6.3}$$

In order to ensure that the same "constraint thickness" 2δ may be applied to all design constraints, it is necessary to normalize the constraint functions. For example, if some behavioral quantity g(x) is not to exceed

a specified value g_{max} , the corresponding constraint function would be

$$f_{j}(x) = \frac{g(x)}{g_{max}} - 1 \le 0$$
 (2.6.4)

This approach was chosen for its simplicity. It should be noted that the "constraint thickness" can be changed during optimization. It might be reasonable to start with a rather large initial value, such as $2\delta_0=0.4$, and to systematically decrease 2δ at successive stages of the optimization. Usually it is convenient to define a lower bound, $2\delta_{\min}$, which would characterize the maximum acceptable constraint thickness at the final design. Thus a design would not be usable even if just one constraint satisfies inequality (2.6.2) with $\delta=\delta_{\min}$. For the sake of simplicity:

$$\delta^{\vee} = \delta^{\vee -1} \delta_{\mathbf{x}} \; ; \quad 0 \le \delta^{\vee}_{\mathbf{x}} \le 1 \; ; \quad 0 < \delta^{\vee = 0} < 0.2$$
 (2.6.5)

where the superscript ν refers to design iteration ν , $\delta_{\mathbf{x}}$ is a multiplier, and $\delta^{\nu=0}=\delta_{\mathbf{0}}$ is an initial value.

2.7 RELAXATION PARAMETER

Perhaps the most difficult question to deal with concerns the proper value of the relaxation parameter α . If it is assumed that the elastic stiffness matrix $\left[\textbf{K}_i \right]$ of a typical (ith) element has the form

$$\begin{bmatrix} \kappa_{i} \end{bmatrix} = \begin{bmatrix} k_{i} \end{bmatrix} x_{i}^{m} \tag{2.7.1}$$

(where the unit stiffness matrix $\begin{bmatrix} k_i \end{bmatrix}$ is independent of the design variable x_i), one can show that, for a certain class of problems, a proper value of α is

$$\alpha = m/(m+1) \tag{2.7.2}$$

Under certain assumptions, Kiusalaas (Ref. 32) demonstrated the correctness of (2.7.2), for the design of structures with buckling constraints. It appears that his proof can also be adapted to designs with stress and displacement constraints. If a problem involves elements with several different m, one could take an average value. Alternatively one could, with minor modifications of design equations (2.3.8) and (2.3.9), assign different α 's for different elements.

For problems with just one constraint, Segenreich (ref. 34) chose α so as to cause a certain percentage reduction in the objective function, specifying limits on the allowable percentage change in the design variables. An extension of the same concept to problems with multiple equality constraints is available in reference 33. Since an extension of this approach to the present case would be extremely costly, due mainly to the constraint deletion process (which is α -dependent), it cannot be efficiently used.

Experience has shown that α is related to step size in the following way: the smaller α , the larger the step. The step size is not absolute and depends also on the constraint and objective function gradients. It decreases as the angle between the gradient of the intersection of the active constraint hyper-surfaces and the gradient of the ojective hyper-plane decreases. Since the redesign formulas are strictly applicable to small design changes, at the start of the optimization one chooses α so as to produce a relatively small step size. At the end of the optimization, when the angle mentioned above is very small, α is chosen so as to produce a relatively large step. Then the change in the design is going to be small

in any event. Analogous to the "constraint thickness", 2δ , choose

$$\alpha^{\nu} = \alpha^{\nu-1} \alpha_{\mathbf{x}} ; \quad 0 < \alpha^{\nu=0} < 1 ; \quad 0 < \alpha_{\mathbf{x}}^{\nu} < 1$$
 (2.7.3)

Note the similarity to equation (2.6.5).

2.8 CUTOFF CRITERIA

It is common practice to define a termination criterion for every iterative process. As it has been shown, three different iterative operations are used in the method: one related to the determination of the active-passive character of the design variables; a second related to the determination of the active-passive nature of the constraints (through the evaluation of λ); and, a third related to the resizing operation itself.

With respect to the active-passive character of the design variables, it is convenient to define a maximum permissible number of iterations, $k_{\text{max}} \text{ , since in some cases convergence might not be achieved.}$

The procedure that calculates $\hat{\lambda}$ is terminated whenever one of the following conditions is satisfied: (i) the number of iterations exceeds a prescribed value j_{max} ; or (ii)

$$\lambda_{\mathbf{r}} > 0 \qquad \qquad \mathbf{r} \in \mathbb{R} \tag{2.8.1}$$

and

$$|\lambda_r - \lambda_r^{\vee -1}| \le \varepsilon_{\lambda}$$
 $r \in \mathbb{R}$ (2.8.2)

The design process is terminated whenever one of the following cutoff criteria is met: (i) the number of redesign cycles exceeds a prescribed

number i_{max} ; or (ii)

and

$$a_{i} + \sum_{j=1}^{R} \lambda_{j} \frac{\partial f_{j}}{\partial x_{i}} \begin{cases} \geq -\varepsilon_{o} \\ \leq \varepsilon_{o} \end{cases} \quad \text{if } x_{i} \quad \text{is active} \\ \geq 0 \quad \text{if } x_{i} = (x_{i})_{\min} \\ \leq 0 \quad \text{if } x_{i} = (x_{i})_{\max} \end{cases}$$
 (2.8.4)

Inequality (2.8.3) is concerned with feasibility, and inequalities (2.8.4) correspond to the optimality criterion (see Eqs. 2.2.11 and 2.2.12). It is important to note that the use of the last convergence criterion leads to a mathematical optimum. If, in an engineering problem, the feasible region is "flat" near the optimum, convergence might be slow. One would get a series of sub-optimal designs, which could look very different although each would have nearly the same objective value. Since, from an engineering standpoint, one is normally concerned with designs that have a minimum or near-minimum cost value, it might be adequate to consider the optimization process converged if the change in the objective function during a fixed number of iterations is less than a specified value (Refs. 22 and 54). Although it has not been specifically used, this criterion will be referred to when discussing the examples.

2.9 BASIC WEIGHT-REDUCTION ALGORITHM

Figure 1 shows the flow diagram of the redesign algorithm based on the

concepts developed in this chapter. It is assumed that an initial design is available along with the necessary optimization parameters. Essentially no restrictions are imposed on the feasibility of the initial design. Experience has shown, however, that numerical difficulties may develop if the initial design satisfies all constraints or violates some by a large margin, say 30%. If that is the case, the initial design vector should be scaled proportionately up or down in order to correct this deficiency.

The method for the calculation of $\tilde{\chi}$, based on the previous discussion, is outlined in the flow diagram of Fig. 2. Here NAC is the number of active and violated constraints (see section 2.6). Also, by comparison of Eqs. (2.5.1) and (2.3.8), and taking (2.5.4) into account:

$$d = \frac{1}{1-\alpha} \left(f + \theta_{p} \right) - \theta_{a}$$
 (2.9.1)

The vector $\hat{\chi}$ is continually updated so that the converged values obtained in one design iteration may be used as the starting values in the next cycle. The reasoning is that during later cycles of the optimization process when, hopefully, the active constraints at the optimum are set, one does not expect major changes in the components of $\hat{\chi}$ from one iteration to the next. $\hat{\chi}=0$ is used as a starting point.

2.10 POSSIBLE EXTENSIONS AND DISCUSSION

There are classes of structural optimization problems that cannot be solved by the method as outlined. For example, there are problems where equality constraints are also among those specified. Automated design of structures for optimum geometry (Ref. 55), which involves an optimization

problem with nonlinear objective function, provides another example.

The algorithm can be extended to deal with equality constraints with a minor modification. Once there are no sign restrictions on the Lagrangian multipliers associated to equality constraints, the $\lambda_{\hat{1}}$'s corresponding to these constraints are allowed to take negative values.

To solve an optimization problem involving nonlinear objective function, one would have to compute

$$a_{i} = \frac{\partial W}{\partial x_{i}} \qquad (i = 1, 2, \dots N)$$

at every design point and proceed as before. Since the reciprocal of a_1 is used to evaluate λ , no component of the objective function gradient may vanish along the path followed by the optimization process.** Unconstrained minima, therefore cannot be obtained. Also, if the components of the objective function gradient are not all of the same sign, convergence of the Gauss-Seidel method is no longer assured. Nevertheless, it is felt that this method could be applicable to problems with constrained optima if the merit function is not highly nonlinear.

It should be noted that the convergence of the Gauss-Seidel iterative method is not uniform; as a result, a constraint may be deleted too soon, that is, a temporarily negative value may be calculated for a multiplier that is actually positive. Chances are, however, that such a phenomenon occurs, if at all, at the early stages of the optimization process. Then it would not be critical since it would only result in a design that is

^{**} A way to avoid this difficulty is to temporarily ignore the design variable associated to a vanishing gradient component (to first order a change in this variable does not influence the objective value).

more infeasible with respect to the deleted constraint than it would normally be. At the final stages of the design, however, the set of active constraints is practically determined and a good estimate of the λ -components is available. The Gauss-Seidel iterations should therefore be smooth even if a previously-unaccounted-for active constraint $(\lambda_{j}^{v-1} = 0)$ is introduced. The non-uniformity of convergence should be observed only locally and the chance of deleting an active constraint is minimal. It should also be noted that a particular design is driven toward a linear approximation of the active-constraint-surface intersection. As a consequence the stability of the optimization process might be endangered if a a design point is "far" from a critical constraint ($\lambda_i > 0$), in case this constraint is not "quasi-linear". This situation arises (even if the constraints are only moderately nonlinear) at the first redesign step if the initial design is "excessively" feasible. In this dissertation, when this is the case, the initial step is performed with $\alpha=1$ and only the "closest" constraint is considered, while its associated λ_i is permitted to take on a negative value. In order to prevent divergence at this point, it may sometimes be necessary to devise a substitute scheme to drive the design closer to the most critical constraint. In the middle stages of the design, the step size should be smaller when higly nonlinear constraints are considered in order to prevent the obtaining of a design "far" from the critical constraints. It is believed that in some cases the step size to prevent divergence could be so small as to be inconsequent. It would then perhaps be better to use normal ($\alpha \approx 0.5$) step sizes and drive the design close to the constraint by using scaling procedures (see Ref. 32).

Finally, it is also useful to observe that, while the strategy used to delete the constraints may be very efficient at the final stages of the optimization process, alternative strategies may be more suitable for intermediate stages. The components of λ are not Lagrangian multipliers during the intermediate stages and, therefore, it is not necessary to restrict them to the non-negative region. In this dissertation alternative strategies have not been tried except, as pointed out above, for the first step if the design is excessively feasible.

CHAPTER III

NUMERICAL EXAMPLES

3.1 INTRODUCTION

The redesign algorithm developed in Chapter II requires the constraint and constraint gradient values at every design iteration. It is therefore necessary to use a finite-element analysis program that is capable of providing the required information.

Since developing new structural analysis capabilities is outside the scope of this work, available analysis schemes were used in order to test the redesign algorithm. For the static analysis with constraints on the displacements and stresses under multiple loading conditions and dynamic analysis with natural frequency constraints, the appropriate module of a program under development by Vanderplaats (Ref. 43) was chosen. In order to deal with a flutter speed constraint, the method of Refs. 8 and 34 was modified as explained in the next four sections. The resulting program is capable of dealing with a large class of structures subject to a few or all the following constraints: displacement, stress, Euler colum buckling, frequency, flutter speed and element size.

The method of references 8 and 34 was developed from the notion that there is no reason to use the flutter speed directly as a constraint. The same design problem is properly posed by regarding the positiveness of g (the damping factor in a standard V-g analysis - Ref. 57, pg. 565) as the

constraint, with aerodynamic forces calculated at an airstream velocity equal to the specified flutter speed limit.

The primary advantage of this approach is that it is not necessary to evaluate the flutter speed at each design iteration. Only the current value of g is calculated, which is an easy task since g is nothing but the ratio of the imaginary to real parts of the complex eigenvalue of the flutter eigensystem (Ref. 57, pg. 565). Another advantage of this method is apparent when compressible aerodynamics must be used. When $g \le 0$ is employed as a primary constraint, the dependence of the aerodynamic matrix on airstream Mach number is completely eliminated, and the evaluation of g and g-derivatives is fast and precise. Conversely, if the flutter speed is used directly as a constraint, derivatives as well as the evaluation of the current flutter speed must reflect the dependence of the aerodynamic matrix on the Mach number. It is apparent that this requires a larger computational effort and introduces a source of potential impreciseness.

The main objective of this chapter is to present results for a variety of examples that test the quality of the algorithm developed in Chapter II. For this reason, no systematic effort was made to develop highly efficient analyses. It is believed that the current program could be improved considerably by method oulined, e.g. in reference 20.

3.2 FLUTTER EQUATION AND SOLUTION

The matrix form of the flutter equation for a finite-element model of a structure is

^{*} Air density and Mach number are fixed.

$$\{\vec{K} (\vec{I} + j\vec{G}) - \omega^2 \vec{M} + \vec{A}\} w = 0$$
 (3.2.1)

(see Eq. (35) of Ref. 56) where $\bar{\mathbf{k}}$, $\bar{\mathbf{g}}$, $\bar{\mathbf{M}}$ and $\bar{\mathbf{A}}$ are the stiffness, structural damping, mass and aerodynamic matrices, respectively; and $\bar{\mathbf{w}}$ is a vector of displacements at the nodes of the finite-element model. To reduce the order of the problem, a limited number of normal vibration mode vectors z^1 , z^1 , ... z^n are used as generalized coordinates, that is

$$\mathbf{w} = \mathbf{Z} \mathbf{q} \tag{3.2.2}$$

q being the complex amplitudes of the modes. If Eq. (3.2.2) is used, Eq. (3.2.1) may be transformed into

$$\left\{ \underbrace{K}_{x} \left(\underbrace{\mathbf{i}}_{x} + \mathbf{j} \underbrace{\mathbf{g}}_{x} \right) - \omega^{2} \underbrace{M}_{x} - \mathbf{q}_{\infty} \underbrace{A}_{x} \right\} \underbrace{q}_{x} = 0$$
 (3.2.3)

where

$$\begin{array}{l}
\overset{\mathbf{K}}{\mathbf{z}} = \overset{\mathbf{Z}^{T}}{\mathbf{x}} \overset{\mathbf{K}}{\mathbf{z}} \overset{\mathbf{Z}}{\mathbf{z}} \\
\overset{\mathbf{G}}{\mathbf{z}} = \overset{\mathbf{K}^{-1}}{\mathbf{z}} \overset{\mathbf{Z}^{T}}{\mathbf{x}} \overset{\mathbf{K}}{\mathbf{z}} \overset{\mathbf{G}}{\mathbf{z}} & \overset{\mathbf{Z}}{\mathbf{z}} \\
\overset{\mathbf{M}}{\mathbf{z}} = \overset{\mathbf{Z}^{T}}{\mathbf{x}} \overset{\mathbf{M}}{\mathbf{z}} \overset{\mathbf{Z}}{\mathbf{z}} \\
\overset{\mathbf{A}}{\mathbf{z}} = -(1/\mathbf{q}_{\infty}) \overset{\mathbf{Z}^{T}}{\mathbf{z}} \overset{\mathbf{A}}{\mathbf{z}} \overset{\mathbf{Z}}{\mathbf{z}}
\end{array}$$
(3.2.4)

and $q_{\infty} = 1/2 \rho_{\infty} V^2$ is the free-stream dynamic pressure.

For a given aerodynamic configuration, the aerodynamic matrix \tilde{A} is a function of the air density ρ_{∞} , Mach number M , and reduced frequency $k=b\omega/V$, where b is a reference length, and V is the free-stream velocity. The dependence of \tilde{A} on ρ_{∞} is linear so that \tilde{A} is a function of k and M only.

For problems with many degrees-of-freedom, is is usually costly to calculate and store the aerodynamic matrix $\frac{1}{4}$. Hence, instead of calculating $\frac{1}{4}$ from Eq. (3.2.4), it is more convenient to evaluate it directly as a matrix of generalized aerodynamic forces (see Ref. 56):

$$A_{ij}(k,M) = -\iint_{S} \frac{\Delta p^{j}(x,y) h^{i}(x,y)}{q_{\infty}} dx dy$$
 (3.2.5)

where Δp^j is the pressure difference between the upper and lower surfaces per unit amplitude of the j^{th} mode, and h^i are the z-displacements per unit amplitude of the i^{th} mode. If $\underline{t}(x,y)$ is a suitable interpolation formula, $h^i(x,y)$ can be obtained from \underline{z}^i (displacement vector at the structural grid of the i^{th} mode)

$$h^{i}(x,y) = t^{T}(x,y) z^{i}$$
 (3.2.6)

$$G = g I \tag{3.2.7}$$

with I the identity matrix. Equation (3.2.3) then takes the form

$$\left(\underbrace{\mathbf{y}}_{\mathbf{y}} + \frac{\mathbf{q}_{\infty}}{\omega^2} \mathbf{A} - \Omega \mathbf{K}\right) \mathbf{q} = 0 \tag{3.2.8}$$

where $\Omega = (1 + jg)/\omega^2$.

This equation represents a complex, nonlinear eigenvalue problem in the three real parameters ρ_{∞} , M, and k. Usually either the Mach number or air-density is fixed, and the eigenproblem is solved for the other two parameters. A very well known method for solving the nonlinear eigenvalue

problem (3.2.8) is the V-g method (Ref. 57, pg. 565). Suppose that the air density is fixed. The V-g method then requires the solution of a series of linear eigenproblems for assumed values of k, determining a set of curves in the V-g plane. The curve that crosses the V-axis at the lowest value of V is the critical one and this value represents the flutter speed if it is consistent with the Mach number and air density.

Normally, in order to match the velocity obtained, it is necessary to perform this process for a few prescribed values of the Mach number.

3.3 THE FLUTTER CONSTRAINED PROBLEM

In order to include flutter constraints in the design procedure, because of its simplicity and efficiency, the approach of Refs. 8 and 34 is used.

Let V_{FO} be specified and consistent with a given Mach number and altitude. It is required that the flutter speed be greater than V_{FO} . This constraint can be defined as (Refs. 8 and 34)

$$g \le 0 \tag{3.3.1}$$

for the critical V-g curve at $V = V_{PO}$. With the definition

$$Q = \frac{q_{\infty}}{\omega^2} \mathbf{A} = \frac{1}{2} \rho_{\infty} \left(\frac{\mathbf{b}}{\mathbf{k}}\right)^2 \mathbf{A} \tag{3.3.2}$$

the eigenproblem (3.2.8) can be written as

$$(M + Q - \Omega K) q = 0$$
(3.3.3)

^{*} For zero structural damping. Defining flutter to occur at g=0 is a conservative criterion - a small amount of damping will always be present.

⁺ See section 3.2.

For fixed Mach number and air density, Q depends only on k. Since Q must be evaluated at several values of k in order to determine the V-g crossover, it is convenient and usually accurate to calculate A at a relatively small number of k-values and then interpolate for the additional points. In this dissertation, the interpolating functions used were p^{th} -order polynomials:

$$Q = \sum_{i=1}^{p+1} k^{(i-3)} Q_i$$
 (3.3.4)

where

$$Q_{i} = \frac{1}{2} \rho_{\infty} b^{2} A_{i}$$
 (3.3.5)

Here A are the coefficient matrices obtained by fitting polynomials to the aerodynamic force matrices calculated at p+l values of k , that is, by solving the linear system

$$\sum_{i=1}^{p+1} k_{j}^{(i-1)} \underset{\approx}{A}_{i} = \underset{\approx}{A}(k_{j}) \qquad (j = 1, 2, ... p+1)$$
(3.3.6)

where k_{i} are distinct values of the reduced frequncy.

The analysis step, if only the flutter constraint is considered, can be summarized as follows:

(a) Assumptions - The Mach number and air density (altitude) are given, along with the lower limit on the flutter speed. A set of generalized coordinates z^i is available at the beginning of the design process and the z-components of these coordinates are fixed throughout the optimization.

[¶] For a given set of generalized coordinates.

^{*} See section 3.4 for discussion.

Since the z^{i} -dependence of A is influenced only by the z-components of z^{i} (see section 3.2), A is a function of k only. No restrictions are placed on the type of the unsteady aerodynamic theory to be used in the computation of A (subsonic, piston theory, doublet lattice, etc.). An estimate of the reduced frequency at which $V = V_{FO}$ (for the critical V-g curve), at the initial design is available, and the V-g curve that is critical at the start of the design process is assumed to remain critical.

(b) Constraint evaluation - Since the speed V is fixed during optimization, the reduced frequency will change as the redesign proceeds. If r is a frequency estimated in order to calculate $k=rb/V_{FO}$ and ω is viewed as the frequency obtained by solving the complex eigenproblem - $\omega = \sqrt{1/Re\left(\Omega\right)} \text{ - the current value of g (considering the critical mode)}$ has to be calculated for $\omega=r$. This is done by an iterative scheme. A series of solutions for the eigenproblem is necessary until $|r-\omega|<\epsilon$. A new frequency is estimated by means of the recursion formula

$$\mathbf{r}^{\vee+1} = \frac{\omega^{\vee} - \mathbf{r}^{\vee} \left(\frac{\mathbf{d}_{\omega}}{\mathbf{d}\mathbf{r}}\right)^{\vee}}{1 - \left(\frac{\mathbf{d}_{\omega}}{\mathbf{d}\mathbf{r}}\right)^{\vee}}$$
(3.3.7)

where

$$\frac{d\omega}{dr} = -\frac{\omega^3 b}{2 v_{FO}} Re \left[\frac{\underline{p}^T (\partial Q/\partial k) \underline{q}}{\underline{p}^T \underline{k} \underline{q}} \right]$$
(3.3.8)

[†] The constraint need not be active (g=0) at this point, that is, the initial structure may have a flutter speed that is either larger or smaller than V_{FO} .

The design space may be disjoint (Refs. 8, 12). The flutter speed may vary discontinuously with the design parameters, and this method fails. Alternative flutter constraints which are based on continuous parameters of the flutter phenomenon have been proposed (Refs. 12 and 58).

and with ν representing the iteration number for the calculation of g . The derivatives $\partial Q/\partial k$ are calculated directly from Eq. (3.3.4). When a new design is considered, a new frequency is estimated by

$$r^{V+1} = \sum_{i=1}^{N} \left(\frac{\partial \omega}{\partial \mathbf{x}_{i}} \right)^{V} \Delta \mathbf{x}_{i} + \omega^{V}$$
 (3.3.9)

Here ν represents the cycle of the design process and Δx_i represents change in design variables $(x_i^{\nu} - x_i^{\nu-1})$ at iteration ν . The sensitivity analysis requires the adjoint eigenvectors (Ref. 31). Therefore the scheme above is also used to solve the adjoint eigenproblem. The analysis includes a method for tracking the proper mode (critical V-g curve) and has the capability of calculating a complete V-g diagram after a specified number of redesigns (for complete details of the analysis see Ref. 34).

(c) Sensitivity analysis - The redesign operation requires the gradient of the constraint $(\partial g/\partial x_i)$ and the constraint evaluation. The gradient of the frequency $(\partial \omega/\partial x_i)$ is also needed as one can see from Eq. (3.3.9). The expressions for the gradients depend explicitly on p (the adjoint eigenvector), g, $\partial M/\partial x_i$, $\partial K/\partial x_i$, $\partial Q/\partial x_i$, M, and K, as well as on the flutter parameters and are given in Ref. 8. The complex eigenvectors p and p are calculated during constraint evaluation, p and p are determined for a given set of generalized coordinates and $\partial Q/\partial K$ from Eq. (3.3.4). The evaluation of the remaining needed quantities, $\partial M/\partial x_i$ and $\partial K/\partial x_i$ is discussed next.

3.4 GENERALIZED COORDINATES

When only a single flutter analysis is required, it is common practice

to use the natural vibration modes as generalized coordinates in order to reduce the flutter problem (Ref. 57). For the design process, wherein the analysis has to be repeated many times, there is an advantage to using a fixed set of modes, even though the structure is being changed during the process (Refs. 11 and 34). This approach is motivated primarily because it avoids the recomputation of modes (free-vibration analysis) and the aerodynamic forces associated with these modes. For accurate results, a large number of these "artificial" modes seems to be necessary if a structure considerably different from the initial design is encountered. The use of many such degrees-of-freedom increases the size of the problem and entails complicated mode shapes. Corresponding difficulties may be encountered in finding accurate interpolation functions that are needed for the determination of the aerodynamic forces (see section 3.2). An alternative approach is to use continuously updated modes as generalized coordinates (Ref. 52). This has the advantage of requiring a reduced number of structural modes for accurate analyses, but it requires the computation of natural modes and aerodynamic forces at every design step. One could also think of an approach that periodically updates the modes, after several design iterations. With respect to gradient calculations, the same remarks apply. For convergence of the flutter parameter derivatives, even more modes are required (Ref. 59).

In the present research, preliminary optimization results were obtained by using fixed modes. When, however, the final structure was reanalyzed with its natural modes as generalized coordinates, it was observed that the resulting flutter speed was violating the constraint by as much as 15%.

Admittedly, no convergence studies were performed for the two examples

carried out, and the number of modes used was small (6 for the rectangular wing described in section 3.8). The fact that the results obtained with fixed modes in all preliminary cases were unconservative (i.e., the speed $V_{_{\rm I\!P}}$ was overestimated) forced the search for an alternative approach.

It is believed that the explanation for the unconservative flutter predictions is the excessive "stiffening" of the structure introduced by the model (fixed modes). If one considers the stiffness matrix partitioned into implane and transverse directions, one can write the equation of static equilibrium:

$$\begin{bmatrix} K_{21} & K_{22} \\ K_{21} & K_{22} \end{bmatrix} \begin{bmatrix} Z_{21} \\ Z_{2} \end{bmatrix} = \begin{bmatrix} P_{21} \\ P_{22} \end{bmatrix}$$

$$\begin{bmatrix} Z_{21} & K_{22} \\ P_{22} \end{bmatrix} = \begin{bmatrix} P_{21} \\ P_{22} \end{bmatrix}$$

$$(3.4.1)$$

where \underline{z} are the displacements resulting from the application of the force systems \underline{p} , and 1, 2 represent, respectively, the transverse and inplane directions. It is common practice, for slender wing structures, to assume that the static and dynamic forces in the inplane directions are neglegible by comparison with those in the transverse direction, that is, $\underline{p}_2 \simeq \underline{0}$ (Ref. 10). If \underline{z} is taken to be composed by the natural modes of the initial design, and inserted in Eq. (3.4.1), \underline{p}_2 will, in fact, be neglegible. Now, if \underline{z} is fixed and \underline{p}_2 is calculated for a considerably different design, the results show that \underline{p}_2 may not be so small, thus violating the reasonable hypothesis $\underline{p}_2 = \underline{Q}$. Apparently an unrealistically high value for the potential energy of the structure is estimated.

In this work, the z-components (transverse) of the natural modes of the initial structure are retained in order to avoid repetitive evaluations

of the aerodynamic force matrices. The x and y-components (inplane) are calculated from the condition $P_{x_2} = 0$, that is

$$Z = \begin{bmatrix} I \\ Z \\ -K_{*22} & K_{*21} \end{bmatrix} Z_{*1}$$

$$(3.4.2)$$

This approach is used because preliminary results showed that: 1) greater accuracy is achieved, and 2) the calculated flutter speed for the final design is smaller than the value obtained if modes of the final structure are used, i.e., the approach appears to be conservative.

3.5 GRADIENTS OF THE GENERALIZED MASS AND STIFFNESS MATRICES

The gradients of the flutter parameters ($\partial g/\partial x_i$ and $\partial \omega/\partial x_i$) depend on the gradients of the generalized mass and stiffness matrices ($\partial M/\partial x_i$ and $\partial K/\partial x_i$). Differentiating the generalized stiffness matrix (Eq. 3.4.4) with respect to design variable x_i one obtains:

$$\frac{\partial \mathbf{K}}{\partial \mathbf{x}_{i}} = \frac{\partial \mathbf{Z}^{\mathbf{T}}}{\partial \mathbf{x}_{i}} \tilde{\mathbf{K}} \mathbf{Z} + \mathbf{Z}^{\mathbf{T}} \tilde{\mathbf{K}} \frac{\partial \mathbf{Z}}{\partial \mathbf{x}_{i}} + \mathbf{Z}^{\mathbf{T}} \frac{\partial \tilde{\mathbf{K}}}{\partial \mathbf{x}_{i}} \mathbf{Z}$$
(3.5.1)

Because K is symmetric,

$$\frac{\partial \mathbf{z}^{\mathrm{T}}}{\partial \mathbf{x}_{i}} \tilde{\mathbf{x}} \mathbf{z} = \mathbf{z}^{\mathrm{T}} \tilde{\mathbf{x}} \frac{\partial \mathbf{z}}{\partial \mathbf{x}_{i}}$$
 (3.5.2)

and Eq. (3.5.1) can be written as

Once again, the results are compared by using the same number of modes. The "true" flutter speed is taken to be the result given when modes of the final structure are used. In reality convergence of this solution should be checked.

$$\frac{\partial \mathbf{K}}{\partial \mathbf{x_i}} = 2 \mathbf{Z}^{\mathbf{T}} \mathbf{\bar{K}} \frac{\partial \mathbf{Z}}{\partial \mathbf{x_i}} + \mathbf{Z}^{\mathbf{T}} \frac{\partial \mathbf{\bar{K}}}{\partial \mathbf{x_i}} \mathbf{Z}$$
(3.5.3)

From definition (3.4.2) of $\frac{z}{z}$, $\frac{\partial z}{\partial x}$ can be evaluated

$$\frac{\partial \mathbf{Z}}{\partial \mathbf{x}_{i}} = \begin{bmatrix} \mathbf{Q} & \mathbf{Q} \\ \mathbf{K}_{22}^{-1} & \begin{pmatrix} \partial_{\mathbf{x}_{22}}^{\mathbf{K}} & \mathbf{K}_{21}^{-1} & \mathbf{K}_{21}^{\mathbf{K}} - \frac{\partial_{\mathbf{x}_{21}}^{\mathbf{K}}}{\partial \mathbf{x}_{i}} \end{pmatrix} \end{bmatrix}_{=1}^{Z}$$

$$(3.5.4)$$

or

$$\frac{\partial Z_{1}}{\partial \mathbf{x}_{1}} = Q$$

$$\frac{\partial Z_{2}}{\partial \mathbf{x}_{1}} = -\kappa_{22}^{-1} \left(\frac{\partial K_{22}}{\partial \mathbf{x}_{1}} Z_{2} - \frac{\partial K_{21}}{\partial \mathbf{x}_{1}} Z_{1} \right)$$
(3.5.5)

With a mathematical constraint definition, the Kuhn-Tucker conditions for optimality require exact expressions for the constraint gradients. For redesign purposes, however, approximate expressions for the gradients may be used. Gwin (Ref. 11), for example, makes the suposition that the aerodynamic matrix does not depend on a design change. Kiusalaas (Ref. 32), when studying problems with buckling constraints, assumes that the prebuckling state is statically determinate. When displacement gradients are calculated by the dwmy load method, it is usually assumed that the changes in the internal forces are neglegible during redesign (Ref. 31). Here, the use of changing modes for the analysis does not imply, therefore, a need to calculate derivatives based on changing modes. Although it would not be difficult to include operations based on Eqs. (3.5.3) and (3.5.4) in a computer code, this was not done because of limited core

disponibility. A simplifying assumption is made that, for redesign purposes, the changes in the generalized coordinates are neglegible, that is, $\frac{\partial Z}{\partial x_i} \approx 0$. With this assumption, the expressions for the gradients of the generalized mass and stiffness matrices can be written, respectively:

$$\frac{\partial \mathbf{M}}{\partial \mathbf{x}_{i}} = \mathbf{z}^{\mathbf{T}} \frac{\partial \mathbf{M}}{\partial \mathbf{x}_{i}} \mathbf{z}$$

 $\frac{\partial \mathbf{K}}{\partial \mathbf{x_i}} = \mathbf{z}^{\mathrm{T}} \frac{\partial \mathbf{\bar{K}}}{\partial \mathbf{x_i}} \mathbf{z}$

i

(3.5.6)

3.6 COMPUTER PROGRAM FOR ANALYSIS AND DESIGN

A computer program for analysis and design (SAD) is under development by Vanderplaats (Ref. 43). The SAD program currently deals with static stress, Euler buckling, displacement, frequency and member size constraints. The finite-element library contains the following elements: TRUSS, constant strain triangles (CST), rectangular membranes, and symmetric shear panels (SSP). The optimization module is based on a modification of Zoutendijk's method of feasible directions (Ref. 60). The CDC 7600 version of the SAD program can accommodate approximately: (a) a total of 400 elements, (b) 300 displacements degrees-of-freedom, (c) 50 design variables, and (d) 5 loading conditions. Because of core limitation, and because disk storage is not used, the elemental stiffness, mass and transformation matrices are recalculated during each iteration. The static analysis is

performed by the displacement method, using matrix decomposition and solution. The dynamic analysis is performed by the "subspace iteration method" (Ref. 61). Only gradients of active and violated constraints are evaluated. The program is organized in a way to allow design variable linking.

The analysis module (constraint evaluation and sensitivity) of SAD program has been modified for the present research to allow for a constraint on the flutter speed. The computer code for flutter is based on the developments presented in the last four sections. The optimization module of the SAD program has been replaced by a computer code based on the developments of Chapter II. The computer program thus obtained has been tested extensively and some of the results obtained are presented in the next sections. All computations were performed in a CDC 7600 machine.

3.7 SAMPLE APPLICATIONS AND COMPARISONS WITH OTHER WORK

In this section the efficiency of the redesign algorithm is demonstrated through comparison with known solutions from the literature.

Results for four examples, chosen from an extensive collection available in Ref. 20, are presented. Results obtained here are compared only with those of Ref. 20 - the latter compare favorably with other solutions found in the literature. All examples involve static loading conditions, with constraints placed on stresses, displacements and member sizes.

The first example involves a planar, ten-bar cantilever truss. A set of seven sub-problems is considered. In Ref. 20 these examples are numbered, respectively, 1A, 1B, 1C, 1D, 2, 3 and 4. The second example is a

twenty-five bar space truss subject to two loading conditions. It is numbered 5 in Ref. 20. These first two examples were originally stated in Ref. 24, and solutions are also available in Refs. 25, 27 and 42. The third example involves an eighteen-element wing box beam, subject to two distinct loading conditions. This example has been previously studied in references 17 and 27. In Ref. 20 it is referred to as problem 8A. The last example is an idealized representation of a swept wing subject also to two distinct loading conditions. The swept wing is treated with and without the use of TRUSS elements to represents leading and trailind edge spar caps. The numbers used in Ref. 20 are, respectively, problems 9A and 9C.

Parameters needed for the optimization runs are not the same for all examples. It is therefore convenient to adopt an optimization parameter vector

$$OPV = \{i_{max}, \epsilon_{o}, \alpha_{o}, \alpha_{x}, \delta_{o}, \delta_{x}, j_{max}, \epsilon_{\lambda}, k_{max}, \epsilon_{f}\}$$
(3.7.1)

the components of which are defined in Chapter II (Sections 2.6 - 2.8). It is observed that the present optimization procedure yields a sequence on infeasible designs (some $f_i(x) > 0$). A design is referred to as usable if all constraints are satisfied within 2×10^{-3} , i.e., satisfying inequality (2.8.3) with $\epsilon_f = 0.002$. One must note, however, that final designs satisfy (2.8.3) with much smaller values of ϵ_f . The infeasibility of the final designs is indicated in the presentation of the numerical results.

3.7.1 Planar, Ten-Bar Cantilever Truss (Problems 1 - 4)

The first series of examples relate to the planar, ten-bar truss shown in Fig. 3. The displacements at nodes 5 and 6 are set to zero, and it is then apparent that this set of examples involves eight independent degrees-of-freedom. No design valriable linking is performed, therefore the number of design variables is ten. Seven distinct sub-problems are considered. Unless otherwise noted, the material properties are $\sigma_{\text{max}} = \pm 25 \text{ ksi}$, $\rho = 0.1 \text{ lb/in}^3$, and $E = 10 \times 10^6 \text{ psi}$. Lower bounds of 0.10 in2 are placed on all bar areas, and the initial design is obtained by setting all areas to 10 in². The first four sub-problems involve a single loading condition, constituting of 100-kip downward loads applied at nodes 4 and 2. Problem 1A is completely defined above. Problems IB, 1C, and 1D have the allowable stress in element 9 modified to ± 30 ksi, ±50 ksi, and ±70 ksi, respectively. Problem 2 is the same as Problem 1A, except that the loading condition consists of 50-kip upward loads applied at nodes 1 and 3, and 150-kip downward loads appied at nodes 2 and 4. The last two cases involving the ten-bar truss have vertical displacement limits equal to \$\pm 2.0\$ in. specified at all nodes in addition to the stress and minimum size constraints. Problem 3 has the loading condition of Problem 1A, and Problem 4 that of Problem 2. For all examples in this subsection $OPV = \{16; 0.01; 0.9; 0.85; 0.1; 0.95; 50; 0.00001; 4; 0.002\}$

The final design for all examples are listed in Table 1. Iteration

When only stress constraints are specified (Problems 1 and 2), it is trivial to see ahead-of-time that the optimal truss is a statically determinate one. From an engineering point of view, therefore, this may look as a rather "silly" example. Nevertheless, the design procedure is able to successfully "pick" the best statically determinate truss (members 2, 5, 6 and 10 deleted instead of 4, 5 and 9) for Problems 1.

histories for Problems 1 and 2 are given in Fig. 4, whereas those for Problems 3 and 4 appear, respectively, in Figs. 5 and 6. The final designs in all examples are the same as those reported in Ref. 20. The number of iterations needed for convergence can also be considered to be the same. Note that Problems 3 and 4 were started from a different initial design (which is infeasible) than that used in Ref. 20 for the correspending problems. There, the initial areas were set to 30.0 in². It is believed that this change should not influence the number of iterations required. The critical constraints are those reported in Ref. 20, and the Kuhn-Tucker conditions for optimality are satisfied in all cases. The constraints at the final design are satisfied to within 1.5 x 10⁻⁵, which is regarded as neglegible. For Problems 1, a sequence of usable designs is started after 9 iterations; for Problems 2 and 3, after 6; and for Problem 4 only after 11 iterations.

3.7.2 Twenty-Five Bar Space Truss (Problem 5)

Attention is now directed to the space truss shown in Fig. 7. After linking (see Table 2) this example has eight independent design variables. An initial cross-sectional area of 2.0 in² and a minimum member size of 0.01 in² is specified for all elements. The truss (with material properties $E = 10 \times 10^6$ psi, $\rho = 0.1$ lb/in³, $\sigma_{max} = 40$ ksi in tension and allowable stress in compretion given in Ref. 20, Table 32) is subjected to two loading conditions (ibid, Table 31). Displacement limits of 0.35 in. on nodes 1 through 6 in the x, y and z directions are imposed.

The OPV was the same as used for the ten-bar truss. Final designs are shown in Table 2. It is seen that the results obtained by this method are practically the same as those obtained in Ref. 20. Iteration histories

are depicted in Fig. 8. The number of iterations needed to satisfy the optimality conditions (Kuhn-Tucker) is 10, one more than in Ref. 20, and constraints are satisfied within 8×10^{-7} at the final design. Critical constraints are also the same as reported in Ref. 20. A sequence of usable designs began after 8 iterations. It is interesting to note that because of the structural symmetry, the nature of load conditions and the design variable definitions, some redundancies occur in the constraints. Under load condition 1 (see Ref. 20, Table 31), the displacements of the nodes 1 and 2 in the y-direction are identical, independent of the values of the design variables. Under load condition 2, equal displacements and stresses (some oposite in sign) occur in pairs. The constraint gradients, therefore, are parallel in pairs, introducing singularities which could possibly generate difficulties for the calculation of λ (see section 2.5). In the present calculation, however, the iterative method for finding the λ , efficiently eliminated one constraint of each pair without any convergence difficulties. If problems of this kind do occur, one should leave the redundant constraints out of the problem definition when possible (for instance, by imposing less stringent limits for these constraints). Another possibility would be to provide the optimization algorithm with a capability of eliminating linearly dependent gradients.

3.7.3 Eighteen-Element Wing Box Beam (Problem 6)

Consider the idealized wing box beam shown in Fig. 9. Since the structure is symmetric with respect to the x-y plane, only the upper half is modeled, using five TRUSS elements, five CST elements and eight SSP elements.

The material properties are: $E = 10 \times 10^6 \text{ psi}$, $\rho = 0.1 \text{ lb/in}^3$, $\mu = 0.3$ and $\sigma_{\text{max}} = \pm 10 \text{ ksi}$. The wing is subjected to two distinct loading conditions consisting of a 5-kip upward load at node 1 (condition 1) and a 10-kip upward load at node 2 (condition 2). The TRUSS elements have an initial cross-sectional area of 0.98 in² and a lower size limit of 0.1 in². The CST and SSP elements have an initial thickness of 0.196 in. and lower size limit of 0.02 in. After linking (see Table 3) this example has 16 design variables. Displacement constraints are imposed that require the z-deflection of unsupported nodes to fall between -2 in. and +2 in.

The OPV was again the same as for the truss examples. The final designs obtained are shown in Table 3. It is observed that, although the final weight is practically the same as in Ref. 20, some difference in the material distribution results. This behavior suggests a "flat" design space, i.e., the gradients of the weight and that of the intersection of the critical constraint surfaces are nearly parallel in a fairly large region near the optimum. The critical constraints are those reported in Ref. 20, with the addition of the minimum size constraint for TRUSS element 4. Since the constraints at the final design are satisfied within 4.5×10^{-6} , and the optimality conditions satisfied, it is perhaps safe to assume that this solution is closer to the mathematical minimum than that of Ref. 20. The iteration histories are shown in Fig. 10. A usable design sequence is generated after 9 design steps, and convergence is achieved after 15 iterations.

CST = Constant Strain Triangle

SSP = Symmetric Shear Panel

See Ref. 43 for the derivation of stiffness and mass matrices.

3.7.4 150 (130) Element Swept Wing (Problems 7A and 7B)

Consider the idealized swep-wing structure shown in Fig. 11. The upper half of the wing is modeled by sixty CST elements to represent the skin, seventy SSP elements for the vertical webs and twenty TRUSS elements to represent the spar caps. The wing without spar caps is referred to as Problem 7A; and with the TRUSS elements as Problem 7B. Extensive variable linking is employed (see Table 4). When the TRUSS elements are present (Problem 7B), the initial area is set to 0.02 in for all elements. The lower and upper bounds on this area are, respectively, 0.01 and 1.50 in². The CST elements have lower size limit of 0.02 in. The initial thickness is set to 0.2 in. for elements 1 through 24 and to 0.1 in. for elements 25 through 60. The lower size limit and initial thickness for all SSP elemets are, respectively, 0.02 and 0.20 inches. The material, with properties: $E = 10.6 \times 10^6 \text{ psi}$, $\mu = 0.3$, $\rho = 0.096 \text{ lb/in}^3$, and $\sigma_{\text{max}} = \pm 25 \text{ ksi, is the same for all elements.}$ Loads data can be found in Ref. 20, Table 57. Displacement constraints, imposed at nodes 41 and 44 only, require that the z-deflections fall between -60 and +60 inches.

The optimization runs were performed with the following parameters: $OPV = \{16; 0.01; 0.75; 0.9; 0.1; 0.95; 50; 0.00001; 4; 0.002\}.$ The iteration histories are depicted in Fig. 12.

Comparing the results for problem 7A (no spar caps) with those obtained in Ref. 20, one notes that the designs are similar, although some variables differ by more than 10%. The critical constraints for the final design are: minimum member size for CST elements 49 through 60; stress in CST elements 8, 14 and 20 under load condition 1; stress in SSP elements 3 and 42 under load condition 1, and in SSP elements 3 and 42 under load

condition 2. In Ref. 20, the same set of critical constraints was found, with the exception of the stress in SSP element 3 under load condition 2. There the stress was reported to be critical in SSP element 5. After only 7 iterations (firts usable design) the weight is less than that reported in Ref. 20 for the final design. The differences in final weights is only about 0.2%. One notes the slow convergence. The additional weight reduction after iteration 7 is only about 0.1%. If the optimization is discontinued when the weight does not change more than 0.1% for, say, 3 iterations, a final weight of 2463.18 lbs. is obtained after 9 iterations. The optimality conditions are not satisfied and the design process is terminated after 16 steps, the maximum number allowed. At the final design, constraints are satisfied within 3.5 x 10⁻⁵.

When spar caps are added to the wing (Problem 7B) a quite different material distribution than that of Ref. 20 results. The most significant differences are in the final sizes of the TRUSS and SSP elements. It is observed that all forward spar cap members are at their minimum size, and that the aft spar cap members are near their minimum with the exception of the member at the root, which assumes its maximum allowable area. In Ref. 20, all truss elements present much larger areas. The web material distribution differences are more pronounced in the outboard portion of the wing. The final weight of 2445.76 lbs., which is obtained here, represents an improvement of approximately 0.7% on the result of Ref. 20. The set of critical constraints is the same as for Problem 7A, with the

It must be noted that all results were compared with those that appeared in a "draft" of the report (Ref. 20). ACCESS 1 (the program of Ref. 20) had a programming error which influenced the results for this example. The error has since been corrected, and the final report presents results for this example that are signifficantly better.

following additions: minimum area for TRUSS elements 1 through 10 and maximum area for TRUSS member 11. It is seen that a usable design is found at iteration 7, with a weight of 2464.84 lbs., within 0.7% of the minimum achieved. It is also seen that at cuttoff (16 iterations) the weight is decreasing at a rate of about 0.1% per iteration, which might make it possible to obtain solutions that might be lighter by as much as 1% if the process is allowed to continue. It is interesting to note that the weight reduction from iterations 8 through 11 (\approx 4 lbs.) is significantly less than the gain from iterations 12 through 16 (\approx 13 lbs.). If the design operation is stopped when the change in weight is less than 0.1% through 3 iterations, a design of 2462.80 lbs. would be obtained after 9 cycles, which is approximately the final weight obtained in Ref. 20. The most critical constraint is satisfied within 2×10^{-5} .

3.8 RECTANGULAR WING WITH STATIC AND DYNAMIC CONSTRAINTS

This section is presented to show that the method is general in the sense that multi-behavioral constrained problems can be solved, as long as the finite-element analysis program provides the constraint and constraint gradient information for a particular design. Results for five examples involving static stress, displacement, frequency, flutter speed and size constraints are presented. All examples involve the rectangular wing which has been considered by others (Refs. 8 and 9). The geometry of the wing is shown in Fig. 13. The structural box is depicted in Fig. 14. The structure is taken to be symmetric with respect to the x-y plane, which corresponds to the wing middle surface. The upper half of the wing

See note + on page 50.

is modeled using 12 TRUSS elements to represent the spar caps, 12 CST elements for the skin and 15 SSP elements for the vertical webs. After linking there are 33 design variables (see Table 6). The material properties are the same for all elements. They include the allowable stresses (± 25 ksi), the specific weight (0.1 lb/in³), the modulus of elasticity (10.5 x $\pm 10^6$) and the Poisson's ratio (0.3). For all examples, minimum size constraints of 0.1 in² for TRUSS elements and 0.01 in. for CST and SSP elements are imposed. The initial cross-sectional areas of bar elements are set at 2.0 in². The thicknesses of the CST, and SSP elements 13 through 15 are 0.040 in. The remaining SSP elements of the initial design (1 through 12) are taken to be 0.08 in. thick.

The first example (Problem 8A) considers static constraints only.

The wing structure is subjected to two distinct loading conditions and constraints are placed on stresses and displacements. The detailed list of nodal loads for both loading conditions is given in Table 5. The transverse deflection at the tip (nodes 13 and 14) is constrained to be less than 11 inches for both loading conditions.

A second example (Problem 8B) considers the same wing structure with a constraint placed on the fundamental natural frequency only. This is constrained to be not lower than 3.83 hz.

The third example combines the constraints of Problems 8A and 8B, that is, the wing has static and frequency constraints. This example is numbered Problem 8C.

Problem 8D is the wing with a restriction placed on the flutter speed. The wing is free of static loads but the flutter speed is constrained to be larger than 797 ft/sec at $\rho_{\rm air}=1.0~{\rm x}~10^{-7}~{\rm lbs.sec}^2/{\rm in}^4$ (approximately

5000 ft altitude). The doublet-lattice method (Ref. 62) was used to calculate three dimensional generalized aerodynamic forces for five different values of the reduced frequency. The flow was assumed incompressible (Mach number zero) and the coefficient matrices $\frac{A}{2}$ (see Section 3.3) were calculated by fitting the aerodynamic data with a fourth order polynomial in k (reduced frequency). The flutter speed for the initial design is found to be 797 ft/sec, and the flutter frequency, 8.78 hz.

The last example (Problem 8E) combines the flutter constraint of Problem 8D with the static constraints of Problem 8A.

The final designs obtained are shown in Table 6. Iteration histories for all examples except Problem 8D (flutter constraint only) are depicted in Fig. 15. Figure 16 shows the iteration history for Problem 8D. Figure 17 shows, schematically, the final material distributions for Problems 8A, 8B, 8C and 8D. The critical constraints for Problems 8A, 8C and 8D are depicted schematically in Figs. 18, 19 and 20, respectively. A summary of the results follows:

3.8.1 Static Constraints Only (Problem 8A)

OPV = {15; 0.01; 0.9; 0.85; 0.1; 0.95; 50; 0.00001; 4; 0.002} is the optimization parameter vector used to run Problem 8A. A sequence of usable designs begins after 7 iterations. At this point the weight (100.666 lbs.) is only about 0.1% larger than the final obtained. The optimality conditions are not satisfied and the optimization was terminated after reaching the maximum number of iterations allowed (15). The critical constraints at the final design (see Fig. 18) are the following: minimum size of TRUSS members 11 and 12, CST elements 9 through 12, and SSP elements 11, 13, 14

and 15; displacements at nodes 13 and 14 under load condition 2; and stresses on SSP elements 1, 2 and 3, also under load condition 2. Constraints at the final design are satisfied within 3×10^{-6} .

3.8.2 Frequency Constraint Only (Problem 8B)

Here, OPV = $\{15; 0.01; 0.9; 0.85; 0.1; 0.95; 50; 0.00001; 4; 0.002\}$ was selected. A sequence of usable designs starts after 4 iterations, when the weight is 106.891 (within 0.1% of the final weight obtained). he maximum number of iterations was reached and the frequency constraint is satisfied within 4×10^{-5} at the final design.

3.8.3 Frequency and Static Constraints (Problem 8C)

Since the results for the last two examples indicated the existence of a "flat" design space (close to the optimum considerable different designs have the same weight), the maximum number of iterations was reduced to 10 for this example. All other optimization parameters were kept the same as those for Problem 8A. After only 5 cycles, usable designs are obtained. The total weight at this point (107.472) is practically the same as that for the final design, when the constraints are satisfied to 6 x 10⁻⁵. The final material distribution is similar to that obtained in Problem 8B with the exception of the SSP elements near the root (see Table 6 and Fig. 17). The critical constraints (see Fig. 19) are found to be: minimum size of TRUSS members 12 and 14, CST elements 9 through 12 and SSP elements 13, 14 and 15; stress on SSP elements 1 through 4 under load condition 2; and the frequency.

3.8.4 Flutter Constraint Only (Problem 8D)

OPV = {16; 0.01; 0.75; 0.9; 0.1; 0.95; 50; 0.00001; 4; 0.002} are the optimization parameters for the computer run of Problem 8D. The designs obtained during optimization are usable after the second iteration. After 6 cycles the total weight (40.971 lbs) represents 102.5% of the final weight obtained. At the final design, more than half the elements are at their minimum size. These include all the TRUSS elements, CST elements 9 and 10, and SSP elements 3, 4, 5, 8, 10, 12 and 13 (see Table 6). This finding appears to be typical for flutter optimization problems, when no additional constraints are imposed (Refs. 8 and 9). At the final design, the damping factor is $g < 6 \times 10^{-5}$, and the flutter frequency is 6.34 hz. The V-g diagram for the final design is shown in Fig. 21.

3.8.5 Flutter and Static Constraints (Problem 8E)

This last example in this section was run with the same optimization parameters as Problem 8B. After the sixth iteration all subsequent designs are usable, and the constraints at the termination of the optimazation process (15 cycles) are satisfied, i.e., less than 2 x 10⁻⁶. The optimality conditions are not satisfied at cutoff. For all examples involving the rectangular wing, including this one, almost no weight reduction is achieved after a few cycles. Here the weight after 6 iterations (100.535 lbs) is approximately 0.2% larger than the final obtained. One must note that the final design for flutter and static constraints is lighter then when only static constraints are imposed (Problem 8A). This apparent inconsistency is eliminated if the design process is permitted

to run longer in both cases (see section 3.10). The critical constraints are identified to be the same as for Problem 8A, with the exception of the minimum size of CST elements 9 and 10, and with the addition of the flutter speed (see Fig. 20). The final design flutter frequency is 7.95 hz. The V-g diagrams for both, the initial and final, designs are shown in Fig. 22. Note that no "drift" in the constrained flutter speed is observed.

3.9 SWEPT WING WITH STATIC AND FLUTTER CONSTRAINTS (PROBLEM 9)

A second example involving a constraint on the flutter speed is considered in this section. This example involves the swept wing with the same loads, constraints and initial design as in Problem 7B (see Fig. 11 for structural box) with an additional constraint on the flutter speed. The aerodynamic planform is shown in Fig. 23.

Initially, the flutter speed of the final static design (see Table 4 - Problem 7B) of the wing with a mass of 400 lbs evenly distributed among the last 8 nodes of the tip (upper-wing half) was calculated. Six modes were used for the dynamical modeling and the doublet-lattice method was employed to obtain the unsteady aerodynamic forces. A matched flutter speed of 900 ft/sec at Mach = 0.92 (approx. 34000 ft.) was obtained. The corresponding V-g diagram is depicted in Fig. 24. A requirement to increase the flutter speed to 966 ft/sec (approx. 17000 ft. at M = 0.92) with the least possible weight penalty was imposed. By examining Fig. 24, it is clear that the method used for the flutter optimization must fail. The critical V-g curve has negative slope at g = 0. Furthermore, for a certain range of V, the function g(V) is multivalued. At V = 966 ft/sec,

therefore, the design is feasible or not, depending on where the V-g curve is being considered. One other difficulty that may be expected is due to the fact that in the neighborhood of the g = 0 crossing, the slope of the V-g curve jumps from very large negative to very large positive values. The iterative scheme for the constraint evaluation (see section 3.3) should therefore also fail.

A second attempt was made by considering the initial static design of the swept wing with a mass of 5000 lbs. evenly distributed on the 10 nodes corresponding to the structure's trailing edge. Admittedly, this corresponds to an unrealistic situation, but it serves the purpose of testing the algorithm. The V-g diagram is shown in Fig. 25. Here, again, the critical V-g curve cannot be followed for optimization purposes, as explained above. Although the curve corresponding to the second g=0 crossing (curve 3 in Fig. 25) is also multivalued at certain values of V, it is suitable for optimization because it has a positive slope near g=0 (V = 1020 ft/sec). If the design changes are small enough such that g=0 at every design step, only the neighborhood of g=0 will be of interest. The flutter constraint is specified as $g\le 0$ at V=1020 ft/sec, with V=1020 ft/sec, which is the flutter speed of the initial design). The optimization was run with the following parameter vector:

 $OPV = \{16; 0.01; 0.75; 0.9; 0.1; 0.95; 50; 0.00001; 4; 0.001\}$

The final design is shown in Table 7 and the iteration history is depicted in Fig. 26. After 8 iterations a usable design of 2695.30 lbs. is obtained. The next 8 cycles account for less than 0.2% weight reduction.

A final design of 2692.10 lbs. is reached. The most critical constraint

at the final design is the damping factor g (1.5 x 10⁻⁴). The V-g diagram for the final design is also shown in Fig. 25. It is interesting to notice that for this unrealistic example, even though the second V-g curve was tracked through the optimization process, very little drift is noticed in the critical V-g crossing. The flutter speeds of the final (900 ft/sec and initial designs differ by only 2%.

To conclude this section it must be reported that an error was made when defining the aerodynamic planform. The leading edge angle is inconsistent with the given dimensions (see Fig. 23). When the aerodynamic forces were calculated, instead of the correct value (24.2°), 25.78° was used. As a result, the area of the tip is reduced in comparison to that of Fig. 23. This should have an effect on the value of the flutter speed, although it is not believed to be the cause of the behavior of the critical V-g curves (Figs. 24, 25). This behavior is interpreted as a violent onset of flutter, similar to that previously reported in Refs. 38 and 77, when considering swept wings.

3.10 DISCUSSION AND ADDITIONAL DATA ON EXAMPLES

Numerical results obtained by using fixed and updated modes as generalized coordinates, and additional data on all examples considered are presented in this section. Also, convergence difficulties encountered when dealing with wing structures (Problems 7, 8 and 9) are briefly discussed.

3.10.1 Fixed and Updated Modes. Numerical Results.

In order to compare the two alternative ways of defining the generalized coordinates (see section 3.4), results for two numerical examples are presented in this sub-section. The natural modes of an original design are used to evaluate the flutter speed or natural frequencies of a modified design and compared with the exact results that are obtained when natural modes of the modified design are employed. The two different approaches will be referred to as updated modes if the transformation presented in section 3.4 is employed and as fixed modes otherwise.

Consider first the rectangular wing of section 3.8. The original design is taken to be the initial design for optimization. The modified design corresponds to the final material distribution obtained for the example where flutter and static constraints were imposed (Table 6, Problem 8E). The actual calculated flutter speed is 803 ft/sec. When using fixed modes, the flutter speed is 843 ft/sec, which is about 5% larger. By using updated modes the error is less than 0.7% (V_F = 797 ft/sec). Figure 27 depicts the critical V-g curves. The results tend to indicate that the use of updated modes may be adequate. One must, however, note that no final conclusions may be drawn since only 6 modes were used to obtain the results, and no convergence study was made. By using a sufficiently large number of modes, a single value for the flutter speed should be obtained. The number of modes needed for convergence to this value should then be a parameter for comparison.

Consider now the swept wing of sub-section 3.7.4. A weight of 400 lbs. (double, if upper and lower halfs are considered) is uniformely distributed in the 8 nodes nearest to the tip (nodes 37-44, Fig. 11). The original design is the final structure when only static constraints are considered (Table 4, Problem 7B). The first four natural frequencies of the modified structure (initial design for optimization run - Problem 7B-)

Within the framework of finite-element theory.

are shown below:

natural frequencies (hz)

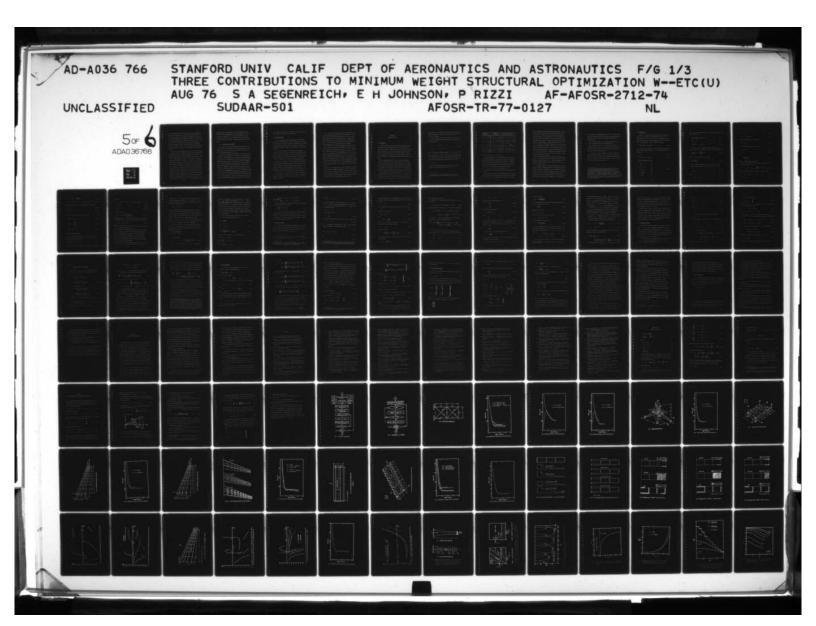
frequency number	actual	fixed modes	(error)	updated modes	(error)
1	2.031	2.101	(3.4%)	2.055	(1.2%)
2	9.239	9.865	(6.8%)	9.362	(1.3%)
3	16.78	20.00	(19.2%)	18.42	(9.8%)
4	22.49	25.98	(15.5%)	23.84	(6.0%)

The actual frequency values are, in fact, exact within the framework of the finite-element approach. By using 6 modes for the modal analysis, it is seen that the results obtained by updating modes are considerably more accurate than those obtained when modes are fixed. If only the first two natural frequencies are of interest, the error is only about 1%. This is considerably lower than the error (3.4%) resulting from the use of fixed modes for calculating just the first natural frequency.

These preliminary results indicate the feasibility of the use of updated modes as generalized coordinates for the dynamical modeling of aircraft wings. A definite conclusion about the effectiveness of this method, as opposed to the use of fixed modes for the same purposes, may only be reached when the computational requirements (time, core space, etc) for both methods are fully determined. Further research should be aimed in this direction.

3.10.2 Convergence Difficulties in Wing-Examples

The optimization processes for all examples involving the swept and rectangular wings were terminated "abnormally", that is, cutoff sources



when the maximum number of iterations was reached. All these examples present a "flat" design space, and the final material distributions found may differ considerably from the optimal ones although the final weight corresponds approximately to the minimum. The statement "the final design does not satisfy the optimality condition" means that Eq. (2.2.4) (or 2.2.11) is not satisfied. Although cutoff criterion (2.8.4) is desirable if a mathematical minimum is seeked, it may be inefficient when engineering problems are considered. In the latter case, adequate termination criteria should be specified in conformity with the requirements of the problem in question.

An attempt to find the mathematical optima for two of the rectangular wing examples was made. The optimization processes for Problems 8A and 8E were allowed to run longer. The designs obtained after 50 iterations are compared to those previously presented, obtained after 15 cycles, in Table 8. It is seen that, after 50 iterations, the final weights for Problems 8A and 8E are, respectively, 99.614 lbs. and 100.048 lbs. The inconsistency observed in section 3.8.5 (after 15 iterations the final design for static and flutter constraints is lighter than when only static constraints are specified) is thus eliminated. In both cases the material distributions, when compared to those obtained after 15 iterations, are substantially different. The vertical web material distributions are seen to be practically the same, but the skin and spar cap sizings are completely different. The same is essentially true if the final designs for Problems 8A and 8E are compared. Apparently a change in the spar cap material distributions can be compensated for by an appropriate modification of the skin. The results also indicate that it is possible to obtain two different sub-optimal designs of equal weight satisfying approximately the same stiffness and strength requirements that have considerably different flutter speeds. It is believed that if a wing structure presents a "flat" design space with respect to static constraints, a material redistribution which raises the flutter speed is possible without appreciable weight penalty.

3.10.3 Additional Data on Examples

The iteration histories for all examples considered are given numerically in Table 9. For completeness, the weights corresponding to usable designs $(g_i(x) \le 0.002)$ and the value of the most critical constraint at the final design $(\max g_i(x))$ are also shown.

A summary of the results obtained, including CPU run times, is given in Table 10. The CPU times spent in the major parts of the design process are indicated. The INPUT/OUTPUT block includes an unecessary analysis that was performed due to a programming error, as well as a complete V-g diagram calculation made when a flutter constraint was considered. The ANALYSIS block includes the calculation of V-g diagrams every 5 design iterations (25 reduced frequencies for the rectangular wing and 35 points for the swept wing). Examinations of Table 10 shows that the total run times are modest when considering the problem size. It is also observed that the time for redesign (OPTIMIZATION block) is minimal. The growth with problem size is modest in absolute terms and negligible when compared to the total CPU time. The ratio, total/redesign (CPU time), varies from 41 (for Problem 9) to 2.82 (for problem 1A). It is seen that relatively large CPU times are spent in the SENSITIVITY ANALYSIS block. When flutter is considered,

the time spent for analysis is also considerable. No efforts were made in order to maximize the efficiency of these two blocks.

3.11 CONCLUDING COMMENTS

It has been demonstrated that a simple recursion formula derived from the Kuhn-Tucker conditions for optimality, together with a procedure to delete non-active constraints based on the Gauss-Seidel iterative method for linear systems, can be used to develop an efficient weight-reduction algorithm for structural optimization. The algorithm has three desirable qualities:

- (a) it is computationally fast when compared with mathematical programming algorithms. The steps in the redesign cycle are minimal, since only the construction of a coefficient matrix and solution by an iterative scheme is required. At early stages of the design, the solution need not be precise, so that only a few Gauss-Seidel iterations are performed.
- (b) it is efficient, in the sense that a small number of steps (analyses) is required for convergence of the design process. The efficiency of the method is demonstrated by comparing the results obtained for four different problems to those reported by Schmit and Miura (Ref. 20). The number of analyses required is approximately the same as in Ref. 20 for most examples. When more iterations are needed, a better design results. The optimality conditions are satisfied by most of the final designs.
- (c) it is general, in the sense that no restrictions are imposed on the type of behavioral constraints. The results for the rectangular wing demonstrate that efficiency is maintained for a large class of structural optimization problems.

In Ref. 20 efficiency is obtained mainly by using approximation concepts, which may also be incorporated in the present algorithm. Also, the constraints are represented by truncated Taylor series of the reciprocal design variables, which uses up core space and time. Furthermore, for complex constraints (e.g., flutter speed, stability) no approximation concepts are currently available. The generality of the present method may be very important when such complex constraints are considered.

In all examples it is seen that the optimization path passes through the infeasible region, which must be considered as a handicap. Furthermore, no formal proof of convergence is available. This may be unacceptable if one regards optimal design as a purely mathematical exercise. What mitigates the seriousness of the former disadvantage is the fact that the amount of infeasibility is very slight ($\sim 10^{-3}$) after only a few iterations; designs thereafter can be considered as usable. At the final design the infeasibility is neglegible ($g_i \leq 10^{-5}$), a finding which compares favorably with results obtained by other methods. From an engineering point of view, the lack of proof of convergence is felt to be outweighed by effectiveness of the algorithm in handling a very large number of structural optimization problems.

Extensions in the generality of the method are possible. When strict equality constraints are among those imposed, the method can be applied with minor change. Extension to problems with nonlinear objective function appears feasible and straightforward. With these extensions, it is hoped that the method proposed herein may provide a possible optimization module for practical and efficient large-scale structural syntheses.

CHAPTER IV

HARMONIC EXCITATION

4.1 INTRODUCTION

Finding the optimal design of general structures excited by arbitrary dynamic loads involves difficulties that are not encountered when only static loads are present. The dynamic excitation introduces inertia forces into the calculation of the total loads acting on the structure, and these forces can have an important effect on the optimal solutions. Johnson (Ref. 13) shows that the varying loads introduce a further complexity, in that it is possible to have disconnected feasible regions and numerous local optima.

Among the simplest problems to solve are those of one-dimensional structures of minimum weight and excited by harmonically varying loads, with the interest focused only on the steady state response. By assuming that the structure responds at the excitation frequency, the time parameter can be eliminated from the equations of motion and an analytical approach to the problem can be attempted for simple structures. To date, even for these simple problems, no global solutions are available in the literature.

The main conclusion from the investigation of Ref. 13 is that the natural frequencies of the structure play a central role in creating the many feasible regions. Structures respond vigorously when excited near a natural frequency; accordingly, the optimal designs try to stay away from these

resonant conditions. The number of distinct feasible regions depends on the number of degrees-of-freedom that are considered and on the value of the excitation frequency.

Segenreich and Rizzi (Ref. 63) have shown that the eigenvalues for a cantilever rod represented by equal length finite-elements (see Fig. 28) have prescribed limits:

$$0 \le \omega_{i} \le \nu \qquad (i = 1, 2, \dots, r)$$

$$(4.1.1)$$

$$\nu \le \omega_{j} \le 2\nu \qquad (j = s, s + 1, \dots, r)$$

where r, s depend on the number of elements, n. If n is even, r=n/2 and s=(n+2)/2. For n odd, r=s=(n+1)/2. The value of ν is fully determined once n is set and the material properties specified. It is interesting to note that for an odd number of finite elements, the middle frequency is independent from the area distribution, that is

$$\omega$$
 (n + 1)/2 = ν

As a function of the excitation frequency, therefore, the distinct feasible regions for possible optimal designs are given by:

^{*} According to Ref. 63, $\nu = (n/l)(3E/\rho)^{1/2}$, where ρ , E, l are the material density, Young's modulus and rod length, respectively.

Excitation Frequency	n	Number of Regions	Eigenvalue Relationships	
$\omega_{\mathbf{e}} = 0$	odd/even	1	$\omega_{e} < \omega_{i}$ (i = 1,2, n)	
0 < ω _e < ν	even	n/2 + 1	$u^{\omega}i^{\omega}e^{\omega}i+1$ (i = 0,1, n/2)	
	odd		$\omega_{i}^{<\omega} e^{<\omega}_{i+1}$ (i = 0,1, (n-1)/2)	
$\omega_{e} = v$	even	1	$\omega_{\rm n/2} < \omega_{\rm e} < \omega_{\rm (n/2+1)}$	
	odd	0	$\omega_{\rm e} = \omega_{\rm (n+1)/2}$ (Resonance)	
ν < ω _e < 2ν	even	n/2 + 1	$\omega_{i}^{<\omega}e^{<\omega}$ i+1 (i = n/2, n)	
	odd	(n + 1)/2	$\omega_{i}^{<\omega} e^{<\omega}_{i+1}$ (i = (n+1)/2 n)	
$\omega_{\rm e} > 2v$	odd/even	1	$\omega_{e} > \omega_{i}$ (i = 1,2, n)	

It should be clear that, unless an algorithm can be devised to seek the global optimum directly, it is necessary to search for the numerous minima and pick the design that represents the lowest one. Furthermore, if the rod is represented in its continuous form, by the use of the differential equations of equilibrium, an infinite number of local optima (corresponding to the infinite number of distinct regions where $\omega_{\bf i} < \omega_{\bf i+1} \ ; \ {\bf i} = 0, \ 1, \ 2, \ \ldots$) would result.

The motivation for this chapter comes primarily from the following two points:

(a) First, very few analytical solutions for harmonically excited structures are available in the literature, none of which dealt with constraints on stresses. By the use of energy methods, Icerman (Ref. 64) was able to

develop an optimality criterion for one-dimensional structures excited by a point load with an equality constraint on the displacement directly under the load. In order to derive his criterion, which was based on Rayleigh's inequality, it was necessary that the excitation frequency be less than the first natural frequency. Plaut (Ref. 66) generalized this investigation with respect to the loading; While optimality criteria are obtained for several examples, no explicit solutions were shown. Mroz (Ref. 65) replaced the displacement constraint by one on the dynamic compliance. Johnson (Ref. 13) was able to reproduce some results of Ref. 64 by using methods of optimal control. He also showed that physically unrealistic solutions may result if a single displacement constraint is imposed. To avoid this difficulty, he suggests that additional constraints (e.g., inequality constraints on the stresses and/or minimum size limits on the design variables) be specified.

(b) Second, all analytical solutions presented to date are such that $\omega_{\rm e} < \omega_{\rm l}$, i.e., the excitation frequency is smaller than the first natural frequency. Solutions for which $\omega_{\rm e} > \omega_{\rm l}$ were first presented in Ref. 13, but the results were obtained numerically, with the structure being represented by finite elements.

The "technology transfer" of methods from optimal control theory and trajectory analysis to minimum-weight design of continuous structures was pioneered by Ashley and McIntosh (Ref. 67). They introduced constraints on natural frequencies, as well as aeroelastic eigenvalues like divergence or flutter speed. Weisshaar (Ref. 68) and Armand and Vitte (Ref. 69) systematized the approach, examining constraints on minimum thickness and the addition of nonstructural mass. Armand (Ref. 70) adapted optimal

control theory for distributed-parameter systems (i.e., systems described by partial differential equations) to calculate minimum-weight shear plates and sandwich plates with prescribed fundamental natural frequency and minimum thickness.

The results obtained in these investigations encouraged the application of the control techniques to the following problem:

The cantilever bar of Fig. 28 (a) is subjected to a harmonically oscillating axial load at the tip, with constraints imposed on the steady-state peak stress and the minimum cross-sectional area. The optimal (minimum volume) area distribution is desired.

In this chapter, the bar is modeled in its continuous form and two distinct solutions are obtained. Then, finite elements are employed and solutions are calculated by using the optimization algorithm described in Chapter II. The use of these two methods provides a check on the correctness of the results by either method alone.

One can show that two other structural configurations occur whose design for minimum weight is mathematically analogous to the bar:

⁽a) Cantilever rod undergoing torsional excitation at its tip - the outer cross-sectional shape and size of the rod are fixed, but its wall is sufficiently thin so that the torsional rigidity GJ and polar moment of inertia I are both directly proportional to the (variable) skin thickness t(x). $^{\rm p}$ Constraints are placed on the minimum value of t and shear-stress amplitude. A concentrated tip inertia I may be carried.

⁽b) Stubby cantilever beam whose lateral displacements are controled mainly by its shear rigidity. The beam is forced transversally at the tip, possibly carrying a tip mass.

4.2 CONTINUOUS BAR

Figure 28 (a) shows a bar with continuously varying cross section, fixed at x=0 and subject to a harmonically varying load $P e^{j\omega_e t}$ applied at the end x=l. At this end (x=l) a concentrated mass, M_T , may be attached. Writing the axial displacement $u(x) e^{j\omega_e t}$ and eliminating the time dependence , one gets the well known equation:

$$E[A(x) u'(x)]' + \omega_e^2 \rho A(x) u(x) = 0$$
 (4.2.1)

Here E is the Young's modulus, ρ is the material density and the prime denotes differentiation with respect to \mathbf{x} . The associated boundary conditions are

$$u(0) = 0$$
 (4.2.2)

$$E A(l) u'(l) = P + M_T \omega_e^2 u(l)$$
 (4.2.3)

Introducing nondimensional variables

$$s = x/l$$

$$v = u/l$$

$$\lambda_e^2 = \omega_e^2 l^2 \rho/E$$

$$a = A \sigma_{max}/P$$

$$a_T = \frac{M_T}{l} \frac{\sigma_{max}}{P}$$

$$\beta = \sigma_{max}/E$$

$$(4.2.4)$$

with σ_{max} the maximum allowable stress, the above equations can be transformed respectively to

$$\frac{d}{ds}\left|a(s)\frac{dv}{ds}(s)\right| + \lambda_e^2 a(s) v(s) = 0$$
 (4.2.5)

$$v(0) = 0$$
 (4.2.6)

$$a(1) \frac{dv}{ds}(1) = \beta + \lambda_e^2 a_T v(1)$$
 (4.2.7)

The task is to find a variable-area design of minimum volume (or weight), such that the peak-stress does not excees the specified value σ_{max} :

Minimize
$$J = a_T + \int_0^1 a(s) ds$$
 (4.2.8)

subject to Eqs. (4.2.5), (4.2.6), 4.2.7) and

$$\left|\frac{\sigma}{E}\right| = \left|\frac{dv}{ds}\right| \le \beta \tag{4.2.9}$$

It is convenient to express Eq. (4.2.5) in terms of first order equations, as generally used in control theory (see Ref. 71). Let

$$\mathbf{x}_1 = \mathbf{v} \tag{4.2.10}$$

$$x_2 = a \frac{dv}{ds} \tag{4.2.11}$$

then

$$\dot{\mathbf{x}}_1 = \frac{\mathbf{x}_2}{a}$$
 , $\mathbf{x}_1(0) = 0$ (4.2.12)

$$\dot{\mathbf{x}}_2 = -\lambda_{\mathbf{e}}^2 \ \mathbf{a} \ \mathbf{x}_1 \tag{4.2.13}$$

$$\mathbf{x}_{2}(1) - \beta - \lambda_{e}^{2} \mathbf{a}_{T} \mathbf{x}_{1}(1) = 0$$
 (4.2.14)

The stress constraint, Eq. (4.2.9) transforms to

$$\frac{|\mathbf{x}_2|}{a} - \beta \le 0 \tag{4.2.15}$$

and if minimum-area constraints are enforced, then

$$-a(s) + \frac{1}{\delta} \le 0$$
 (4.2.16)

$$-a_{T} \leq 0$$
 (4.2.17)

with

$$\delta = \frac{P}{\sigma_{\text{max}} A_{\text{min}}}$$
 (4.2.18)

Here A_{\min} is the allowable minimum area.

The optimality conditions for this problem can now be written (see Appendix A). The Hamiltonian is

$$H = a + \lambda_1 \frac{x_2}{a} - \lambda_e^2 \lambda_2 a x_1 + \mu_1 \left(\frac{|x_2|}{a} - \beta \right) + \mu_2 \left(\frac{1}{\delta} - a \right)$$
 (4.2.19)

It follows from the various necessary conditions in Appendix A that,

$$1 - \lambda_1 \frac{\mathbf{x}_2}{a^2} - \lambda_2^2 \lambda_2 \mathbf{a} \mathbf{x}_1 - \mu_1 \frac{|\mathbf{x}_2|}{a^2} - \mu_2 = 0$$
 (4.2.20)

$$\dot{\lambda}_1 = \lambda_2^2 \text{ a } \lambda_2 \tag{4.2.21}$$

$$\dot{\lambda}_2 = -\frac{\lambda_1}{a} - \mu_1 \frac{\text{sign}(\mathbf{x}_1)}{a} \tag{4.2.22}$$

1 -
$$v_1 \lambda_e^2 x_1(1) - v_2 = 0$$
 if $a_T \neq constant$ (4.2.23)

The boundary conditions on λ are given by Eqs. (A.15) and (A.16),

$$\lambda_1(0) = 0 ag{4.2.24}$$

$$\lambda_1(1) = -v_1 \lambda_e^2 a_T$$
 (4.2.25)

$$\lambda_2(1) = \nu_1$$
 (4.2.26)

and the non-negativity conditions on the multipliers:

$$v_{2} \begin{cases} = 0 & \text{if } a_{T} > 0 \\ \geq 0 & \text{if } a_{T} = 0 \end{cases}$$

$$(4.2.27)$$

$$\mu_1 \begin{cases} = 0 & \text{if } \frac{|\mathbf{x}_2|}{a} < \beta \\ \geq 0 & \text{if } \frac{|\mathbf{x}_2|}{a} = \beta \end{cases}$$
 (4.2.28)

$$\mu_{2} \begin{cases} = 0 & \text{if } a > 1/\delta \\ \geq 0 & \text{if } a = 1/\delta \end{cases}$$
 (4.2.29)

4.3 TWO-DESIGN VARIABLE EXAMPLE

This section seeks the minimum-weight design for the cantilever bar of constant area with axial harmonic load. Equations of Section 4.2 can be specialized for this case to give:

Minimize
$$J = a + a_T$$

$$a, a_T$$
(4.3.1)

If $a_{\overline{T}}$ is specified to be a constant, this equation should be dropped.

subject to

$$\ddot{\mathbf{x}}_1 = -\lambda_e^2 \mathbf{x}_1$$
; $\mathbf{x}_1(0) = 0$, $\mathbf{a} \dot{\mathbf{x}}_1(1) - \lambda_e^2 \mathbf{a}_T \mathbf{x}_1(1) = \beta$ (4.3.2)

$$\beta \geq |\dot{\mathbf{x}}_1| \tag{4.3.3}$$

$$a \geq 1/\delta \tag{4.3.4}$$

$$a_{rr} \geq 0 \tag{4.3.5}$$

The solution of (4.3.2) is

$$\mathbf{x}_{1}(s) = \frac{\beta \sin \lambda_{e} s}{\lambda_{e} (a \cos \lambda_{e} - a_{T} \lambda_{e} \sin \lambda_{e})}$$
(4.3.6)

Differentiating (4.3.6), using the result in inequality (4.3.3) and noting that the maximum of $|\dot{\mathbf{x}}|$ is given for $\cos \lambda_e s = 1$ ($\lambda_e s = n\pi$, n=0,1,..):

$$\begin{vmatrix} a \cos \lambda_e - a_T \lambda_e \sin \lambda_e \end{vmatrix} \ge 1$$
 (4.3.7)

Equations (4.3.1), (4.3.4), (4.3.5), and (4.3.7) form a linear programming problem in two design variables a, and a_m .

The motivation for representing the structure by two design variables is that it is possible to depict the design space graphically, thereby obtaining a qualitative description of what will be encountered when a variable-area distribution is considered. In this particular case, it is easy to calculate the optimal design for the whole range of excitation frequencies. The optimal weights (volumes) will then provide upper bounds for the solutions of the original problem.

The design spaces for the two-variable case are depicted in Fig. 29. Feasible portions of these spaces are left unshaded; the total weight

(proportional to a + a_T) is constant along the 45° sloping lines used to shade the infeasible regions. When $n\pi < \lambda_e < (2n+1)\pi/2$, $n=0,1,\ldots$ (case A), the design space is disjoint. This behavior can be explained by considering the resonance condition

$$a \cos \lambda_{e} = a_{T} \lambda_{e} \sin \lambda_{e}$$
 (4.3.8)

In Fig. 29, caseA, equation (4.3.8) is represented by the dashed line. This line (infinite stresses) divides the design space into two regions. Designs that satisfy the stress constraint can be found at some distance from the resonance line in both of these regions. Since the resonance line extends to infinity, two distinct feasible regions exist. When $(2n+1)\pi/2 < \lambda_e < (n+1)\pi, \ n=0,1, \ldots \ (case B), \ only \ one feasible region results. This is so because, in this case, no resonance situation is possible <math display="block"> (\cos \lambda_e / \sin \lambda_e < 0 \ , \ and \ Eq. \ (4.3.8) \ cannot be satisfied).$

The solution of a linear program (optimum) is practically allways at an intersection of constraints, which are straight lines (see Ref. 78).

Here, in either case (A or B), the minimum occurs at one of the vertices

(1 or 2) shown in Fig. 29:

Possible minimum
$$1$$
 is
$$a = |\sec \lambda_e|, a_T = 0$$
(4.3.8)

Possible minimum (2) is

$$a = 1/\delta$$
 , $a_T = \frac{1 + (1/\delta) \cos \lambda_e \operatorname{sign}(\sin \lambda_e)}{\lambda_e |\sin \lambda_e|}$ (4.3.9)

When $\lambda_{\rm e}$ is in the vicinity of nm, n = 0, 1, ... then the global

minimum is given by (1) (Eq. 4.3.8). Conversely, when $\lambda_e \approx (2n+1)\pi/2$, then the global minimum is given by (2) (Eq. 4.3.9). As λ_e increases, therefore, (1) and (2) alternate as the global minimum. This behavior is depicted in Fig. 30 for δ = 5. Because a_T is inversely proportional to λ_e when the global minimum is given by Eq. (4.3.9), the total weight decreases as the excitation frequency is increased, * as can be seen in Fig. 30 from the dash-dotted envelope curve. For high excitation frequencies the optimal design is dominated by (2), i.e., (1) is a global optimum only in a small range of λ_e .

The natural frequencies of the optimal designs can be determined (Ref. 57, Chapter 3) as characteristic roots of

$$\frac{a_{\mathrm{T}}}{a} = \frac{1}{\lambda_{\mathrm{i}}} \frac{\cos \lambda_{\mathrm{i}}}{\sin \lambda_{\mathrm{i}}} \tag{4.3.10}$$

For $a_{T} = 0$,

$$\lambda_{i} = \pi/2, 3\pi/2, \dots$$
 (4.3.11)

For $a_T \neq 0$,

$$\frac{\delta + \cos \lambda_{e} \operatorname{sign}(\sin \lambda_{e})}{\lambda_{e} |\sin \lambda_{e}|} = \frac{\cos \lambda_{i}}{\lambda_{i} \sin \lambda_{i}}$$
(4.3.12)

By using Eqs. (4.3.11) and (4.3.12) it is easy to show that:

given
$$n\pi < \lambda_e < (n+1)\pi$$

for design (2)
$$\lambda_{n+1} < \lambda_{e} < \lambda_{n+2}$$

For a fixed ratio $\sin \lambda_e / \cos \lambda_e$.

for design (1)
$$\begin{cases} \lambda_{n} < \lambda_{e} < \lambda_{n+1}^{\dagger} & \text{if } \lambda_{e} < (2n+1)\pi/2 \\ \lambda_{n+1} < \lambda_{e} < \lambda_{n+2} & \text{if } \lambda_{e} > (2n+1)\pi/2 \end{cases}$$

Concluding this section, it should be noted that the force transmitted to the wall (fixed end), F, is given by

$$\frac{|\mathbf{F}|}{\mathbf{P}} = \begin{cases} \left| \sec \lambda_{\mathbf{e}} \right| & \text{for } \mathbf{a_{\mathbf{T}}} = 0 \\ 1/\delta & \text{for } \mathbf{a_{\mathbf{T}}} \neq 0 \end{cases}$$
 (4.3.13)

It is clear that, if the bar is to be used as a vibration isolator, independently of the total weight, only solutions for which $a_T \neq 0$ are of interest. This is because only then is the force transmitted less than the applied one. In realistic vibration isolation problems, a constraint on |F| would naturally have to be imposed.

4.4 FIRST MODE SOLUTIONS

In this section, the optimal variable-area distribution of a bar whose fundamental frequency of free-vibration is greater than the excitation frequency is seeked. From the results of Appendix B, this can only occur if the bar is vibrating in phase with the applied load, i.e.,

$$x_1 \ge 0$$
 , $0 \le s \le 1$ (4.4.1)

It is assumed that no tip mass is present (a $_{\rm T}$ = 0), and no minimum-area constraints are imposed. * Let there be a point s = γ , 0 $\leq \gamma$ < 1 such that

^{· \ \}lambda_0 \ \Delta_0

^{*} No minimum-area constraints are needed because, as will be seen, the minimum area occurs at s=1 and a(1)=1 (A=P/ σ_{max}), which is considered to be larger than any reasonable value for the minimum area.

$$\frac{\mathbf{x}_2}{\mathbf{a}} \begin{cases} < \beta & 0 \le \mathbf{s} < \gamma \\ = \beta & \gamma \le \mathbf{s} \le 1 \end{cases}$$
 (4.4.2)

i.e., the stress constraint is inactive on the arc $0 \le s < \gamma$ and active otherwise.* The latter condition is described as "fully stressed" when $\gamma = 0$. Consider now these arcs separately and find γ in order to satisfy the optimality conditions;

(a) Arc
$$\gamma \leq s \leq 1$$

Here, from Eq. (4.4.2),

$$\frac{x_2}{a} = \frac{dx_1}{ds} = \beta \tag{4.4.3}$$

whose integral yields a response mode shape that is just a straight line:

$$x_1 = \beta (s - \gamma + \theta) \tag{4.4.4}$$

with θ , a constant to be determined $\left[\theta=x\ (\gamma)/\beta\right]$. It is now convenient to make a transformation in the independent variable. Let

$$\bar{s} = s - \gamma + \theta \tag{4.4.5}$$

Then Eq. (4.4.4) can be written

$$\mathbf{x}_1 = \beta \bar{s}$$
 , $\theta \leq \bar{s} \leq \psi$ (4.4.6)

with

$$\psi = 1 - \gamma + \theta \tag{4.4.7}$$

Segenreich and Rizzi (Ref. 72) proved that "fully-stressed" solutions are optimal for low excitation frequencies and observed that, for higher frequency values, stress constraints are "loose" near the fixed end.

By differentiating Eq. (4.4.3) and substituting the result in Eq. (4.2.13), a differential equation in the transformed variable of (4.4.6) is obtained for $a(\bar{s})$:

$$\dot{a} = -\lambda_e^2 \bar{s} a \tag{4.4.9}$$

with the bouldary condition given by Eq. (4.2.14) if $a_{_{\rm T\!\!\!\!T}}$ is set to zero

$$a(\psi) = 1$$
 (4.4.10)

The solution of Eq. (4.3.9) is

$$a(\bar{s}) = e^{\alpha^2(\psi^2 - \bar{s}^2)}$$
 (4.4.11)

where

$$\alpha = \frac{\lambda_{\mathbf{e}}}{\sqrt{2}} = \omega_{\mathbf{e}} \ \mathcal{I} \sqrt{\frac{\rho}{2E}}$$
 (4.4.12)

From Eq. (4.2.22), using Eq. (4.2.20) with μ_2 = 0 and taking Eqs.

(4.4.3) and (4.4.6) into account, one gets

$$\dot{\lambda}_2 = -\frac{1}{\beta} + \lambda_e^2 \bar{s} \lambda_2 \tag{4.4.13}$$

which has the solution

$$\lambda_2 = \frac{e^{-(\alpha \bar{s})^2}}{\alpha \beta} \left\{ c_2 e^{-(\alpha \theta)^2} - \int_{\alpha \theta}^{\alpha \bar{s}} e^{-t^2} dt \right\}$$
 (4.4.14)

Equation (4.4.14) involves an integral that can be evaluated in terms of the error function

$$\operatorname{erf}(\mathbf{x}) = \frac{2}{\sqrt{\pi}} \int_{0}^{\mathbf{x}} e^{-t^{2}} dt$$
 (4.4.15)

which is tabulated (e.g., Ref. 73).

Using Eqs. (4.4.11), and (4.4.14) in terms of (4.4.15) in Eq. (4.2.21) one can derive

$$\dot{\lambda}_1 = \frac{2\alpha}{\beta} e^{(\alpha\psi)^2} C_2 e^{-(\alpha\theta)^2} - \frac{\sqrt{\pi}}{2} \left[erf(\alpha\bar{s}) - erf(\alpha\theta) \right]$$
 (4.4.16)

With boundary condition (4.2.25) and $a_{_{\rm T\!P}}$ = 0, (4.4.16) can be integrated:

$$\lambda_{1} = \frac{\alpha}{\beta} \sqrt{\pi} e^{(\alpha \psi)^{2}} \left\{ \frac{2}{\sqrt{\pi}} C_{2} e^{-(\alpha \theta)^{2}} (\bar{s} - \psi) - \bar{s} \left[\operatorname{erf}(\alpha \bar{s}) - \operatorname{erf}(\alpha \theta) \right] \right\} + \psi \left[\operatorname{erf}(\alpha \psi) - \operatorname{erf}(\alpha \theta) \right] \right\} + \frac{1 - e^{\alpha^{2}} (\psi^{2} - \bar{s}^{2})}{\beta} (4.4.17)$$

The quantity μ_1 can now be found by substituting the appropriate expressions in Eq. (4.2.20), and remembering that μ_2 = 0

$$\frac{\mu_{1\beta}}{a} = -\alpha\sqrt{\pi} e^{(\alpha \bar{s})^{2}} \left\{ \frac{2}{\sqrt{\pi}} c_{2} e^{-(\alpha \theta)^{2}} (2\bar{s} - \psi) + \psi \left[erf(\alpha \psi) - erf(\alpha \theta) \right] - 2\bar{s} \left[erf(\alpha \bar{s}) - erf(\alpha \theta) \right] \right\} + 2 - e^{-\alpha^{2}} (\psi^{2} - \bar{s}^{2})$$
(4.4.18)

(b) Arc $0 \le s < \gamma$

In this region the stress constraint is, by hypothesis, inactive. From inequality (4.2.28) μ_1 = 0 , and the optimality conditions reduce to:

$$1 - \frac{x_2}{a^2} \lambda_1 - \lambda_e^2 x_1 \lambda_2 = 0 (4.4.19)$$

$$\dot{x}_1 = \frac{x_2}{a}$$
 , $x_1(0) = 0$ (4.4.20)

$$\dot{\mathbf{x}}_2 = -\lambda_{\mathbf{e}}^2 \ \mathbf{a} \ \mathbf{x}_1$$
 (4.4.21)

$$\dot{\lambda}_1 = \lambda_0^2 \ a \ \lambda_2 \tag{4.4.22}$$

$$\dot{\lambda}_2 = -\frac{\lambda_1}{a}$$
 , $\lambda_2(0) = 0$ (4.4.23)

The general solution involves (see Ref. 3)

$$\lambda_2 = -\frac{C_4}{C_3} \mathbf{x}_1 \tag{4.4.24}$$

$$\lambda_1 = \frac{C_4}{C_3} x_2 \tag{4.4.25}$$

These relations lead eventually to

$$x_1 = \frac{B}{\lambda_e} \sinh(C \pm \lambda_e s)$$
 (4.4.26)

with

$$B^2 = \frac{C_3}{C_4} \tag{4.4.27}$$

Also C_3 , C_4 are the values of \mathbf{x}_2 and λ_1 at $s=\gamma$. B and C can be determined from the condition on \mathbf{x}_1 at s=0 and from the fact that, by hypothesis, the stress constraints becomes active at $s=\gamma$. $\dot{\mathbf{x}}$ (γ) = β gives C=0 and

$$B = \frac{\beta}{\cosh \lambda_{\beta} \gamma} \tag{4.4.28}$$

Equation (4.4.26) can, therefore, be rewritten as

$$x = \frac{\sinh \lambda_{e} s}{\lambda_{e} \cos \lambda_{e} \gamma} \tag{4.4.29}$$

A first order differential equation in a(s), with the appropriate boundary condition, can now be written

$$\dot{a} \cosh \lambda_e s + 2\lambda_e a \sinh \lambda_e s = 0$$
 , $a(\gamma) = \frac{C_3}{\beta}$ (4.4.30)

This has the solution

$$a(s) = \frac{C_3}{\beta} \left(\frac{\cosh \lambda_e \gamma}{\cosh \lambda_e s} \right)^2 \tag{4.4.31}$$

Undetermined constants can now be calculated by imposing continuity at $s=\gamma$. Continuity of \mathbf{x}_1 gives

$$\theta = \frac{\tanh \lambda_{\mathbf{e}}}{\lambda_{\mathbf{e}}} \tag{4.4.32}$$

and continuity of a gives

$$c_3 = \beta e^{\alpha^2 (\psi^2 - \theta^2)}$$
 (4.4.33)

By use of Eqs. (4.4.27) and (4.4.28), one finds

$$C_4 = \cosh^2 \lambda_{e} \gamma e^{\alpha^2 (\psi^2 - \theta^2)}$$
 (4.4.34)

 C_2 is given from the continuity of λ_2 :

$$C_2 = -\frac{\cosh \lambda_e \gamma \sinh \lambda_e \gamma}{\sqrt{2}}$$
 (4.4.35)

From the continuity of $\partial H/\partial a$ (Eq. 4.2.20), and since $\tilde{\mathbf{x}}$, a and $\tilde{\lambda}$ are continuous it follows that μ_1 is also continuous; therefore, γ can now be determined from the condition $\mu_1=0$ at $s=\gamma$ ($\tilde{s}=\theta$). This gives

$$0 = 2 - \alpha \sqrt{\pi} e^{(\alpha \theta)^2} \psi \left[erf(\alpha \psi) - erf(\alpha \theta) \right]$$
$$- e^{-\alpha^2 (\psi^2 - \theta^2)} - 2\alpha C_2 (2\theta - \psi)$$
(4.4.36)

For a given excitation frequency, γ can be calculated by solving

If the optimal solution is fully-stressed $(\gamma = 0)$, μ_1 does not, necessarily, vanish.

the transcedental equation (4.4.36). When $\alpha \le 1.0908$, this calculation shows that there is no junction point within length $0 \le \gamma \le 1$ of the bar. For larger α , the single meaningful root thus obtained is plotted in Fig. 31. It starts from $\gamma = 0$ with infinite slope $d\gamma/d\alpha$ and tends asymptotically to $\gamma = 1$. The sign of $\frac{\mu_1 \beta}{a}$ (from Eq. 4.4.18) turns out to be positive for all s, $\gamma < s \le 1$, given a consistent pair (α, γ) .

In the range $0 \le \alpha \le 1.0908$, the consistent pair is considered to be $(\alpha, 0)$. One identifies this situation with the so called "fully-tressed" solution, and realizes that it is optimal for quite a wide range of excitation frequencies. As a matter of fact, for aluminum bars $(E \cong 10 \times 10^6 \text{ psi}; \ \rho \cong 0.26 \times 10^{-3} \text{ lb.sec}^2/\text{in}^4)$ the fully-stressed solution is optimal for $0 \le \lambda_e \le \frac{3 \times 10^5}{l}$ rad/sec, where l is in inches. This is a rather high upper limit unless the bar is extremely long.

The area distribution of these designs may be summarized as

$$a(s) = e^{\alpha^2 (\psi^2 - \theta^2)} \left(\frac{\cosh \lambda_e \gamma}{\cosh \lambda_e s} \right)^2 , \qquad 0 \le s < \gamma$$
 (4.4.37)

$$a(\bar{s}) = e^{\alpha^2(\psi^2 - \bar{s}^2)}$$
, $\theta \le \bar{s} \le \psi$ (4.4.38)

When the area distribution is integrated over the length, the following dimensionless weight (or volume) results:

$$\frac{V\sigma_{\text{max}}}{P} = \int_{0}^{1} a(s) ds \qquad (4.4.39)$$

$$= \frac{e^{(\alpha\psi)^{2}}}{\sqrt{2}\alpha} \left\{ \frac{\cosh(\sqrt{2}\alpha\gamma) \sinh(\sqrt{2}\alpha\gamma)}{e^{(\alpha\theta)^{2}}} + \sqrt{\frac{\pi}{2}} \left[\text{erf}(\alpha\psi) - \text{erf}(\alpha\theta) \right] \right\}$$

This range can be much smaller for shear beams and rods in torsion.

Equation (4.4.39) is plotted vs. α in Fig. 32 and compared, in the higher range, with the corresponding fully stressed designs. Although the separation between the two is not signifficant until α exceeds about 1.5, nevertheless the rapidly rising weight of both leads one to suspect that better designs might be discovered than these, requiring as they do large amounts of material to force ω_1 to exceed ω_2 .

Because of manner in which P and σ_{max} enter the problem statement, a single parameter family of solutions emerges. Three typical dimensionless area distributions a = $A\sigma_{max}/P$ are plotted in Fig. 33 (continuous dotted curves), for α = 0 to α = 1.3. Note that over the entire length the dynamic solutions display areas larger than what would withstand the same force applied statically (α = 0). This explains why no minimum-area constraint seemed necessary for the first-mode analysis.

4.5 SECOND-MODE SOLUTIONS

As discussed in Appendix B, the response of the bar in the frequency range $\omega_1 < \omega_2$ must be in antiphase with the applied load, i.e., $\mathbf{x}_1(\mathbf{s}) \leq 0$ except possibly in a small region near the tip. It can then be reasoned that a tip mass may be required $(\mathbf{a}_T \neq 0)$ to satisfy boundary condition (4.2.14). It definitely proves necessary to enforce the minimum-gauge constraint (4.2.16) to avoid a tendency toward vanishing area at the point of zero slope in the response mode $\mathbf{x}_1(\mathbf{s})$.

In solving the problem, it is assumed that there is a point $s=\gamma$, $0<\gamma\le 1$, for which only the stress constraint is active in $0\le s<\gamma$ and only the minimum-area constraint is active in $\gamma< s\le 1$, i.e.,

for $0 \le s < \gamma$

$$\frac{\mathbf{x}_1}{\mathbf{a}} = -\beta \tag{4.5.1}$$

$$\mu_2 = 0$$
 (4.5.2)

and for $\gamma < s \le 1$

$$a = 1/\delta$$
 (4.5.3)

$$\mu_1 = 0 \tag{4.5.4}$$

As in Section 4.4, both arcs are considered separately:

(a) Arc $0 \le s < \gamma$

In a way similar to Section 4.4 (a) , it is not difficult to find:

$$\mathbf{x}_1 = -\beta s \tag{4.5.5}$$

$$\mathbf{x}_2 = -\beta \mathbf{a} \tag{4.5.6}$$

$$a = \frac{1}{\delta} e^{\alpha^2 (\gamma^2 - s^2)}$$
 (4.5.7)

$$\lambda_2 = \frac{1}{\alpha \beta} e^{(\alpha s)^2 \sqrt{\pi}} \operatorname{erf}(\alpha s) \tag{4.5.8}$$

$$\lambda_1 = \frac{\alpha}{\delta \beta} \sqrt{\pi} e^{(\alpha \gamma)^2} \left[\operatorname{serf}(\alpha s) - \operatorname{yerf}(\alpha \gamma) \right] + \frac{1}{\delta \beta} \left[e^{\alpha^2 (\gamma^2 - s^2)} - 1 \right] + C_1 \quad (4.5.9)$$

$$\frac{\mu_{1\beta}}{\alpha} = 2 + \alpha \sqrt{\pi} e^{(\alpha s)^{2}} \left[2s \operatorname{erf}(\alpha s) - \gamma \operatorname{erf}(\alpha \gamma) \right]$$

$$+ e^{-\alpha^{2} (\gamma^{2} - s^{2})} (C_{1} \delta \beta - 1)$$
(4.5.10)

with C_1 the value of λ_1 at $s = \gamma$.

(b) Arc γ < s \leq 1

It is now convenient to define

For this arc $a(\bar{s}) = 1/\delta = \text{constant}$, and $\mu_1 = 0$. Eqs. (4.2.12) and (4.2.13) therefore have solutions

$$\mathbf{x}_1 = \mathbf{C}_2 \sin \lambda_{\mathbf{e}}^{\mathbf{S}} + \mathbf{C}_3 \cos \lambda_{\mathbf{e}}^{\mathbf{S}} \tag{4.5.12}$$

$$\mathbf{x}_2 = \frac{1}{\delta} \lambda_e \left(C_2 \cos \lambda_e \bar{s} - C_3 \sin \lambda_e \bar{s} \right) \tag{4.5.13}$$

The coefficients C_2 and C_3 are determined from the continuity of \mathbf{x}_1 and \mathbf{x}_2 at $\bar{\mathbf{s}}=0$ (s = γ), so that the last two equations can be rewritten as

$$x_1(\bar{s}) = -\frac{\beta}{\lambda_e} (\sin \lambda_e \bar{s} + \gamma \lambda_e \cos \lambda_e \bar{s})$$
 (4.5.14)

$$\mathbf{x}_{2}(\bar{s}) = -\frac{\beta}{\delta} (\cos \lambda_{e} \bar{s} - \gamma \lambda_{e} \sin \lambda_{e} \bar{s})$$
 (4.5.15)

In a similar way, the solutions for λ_1 , λ_2 are found to be

$$\lambda_1 = B_1 \sin \lambda_e \ddot{s} + B_2 \cos \lambda_e \ddot{s} \tag{4.5.16}$$

$$\lambda_2 = -\frac{\lambda e}{\delta} \left(B_1 \cos \lambda_e \bar{s} - B_2 \sin \lambda_e \bar{s} \right) \tag{4.5.17}$$

With a finite tip mass, Eq. (4.2.27) gives $v_2 = 0$ and

$$v_1 = \frac{1}{\lambda_0^2 \mathbf{x}_1(\psi)} \tag{4.5.18}$$

From Eq. (4.2.14), using Eqs. (4.5.14) and (4.5.15) evaluated at $\tilde{s} = \psi$,

one gets

$$a_{T} = \frac{1}{\delta \lambda_{e}} \left[\frac{\delta + \cos \lambda_{e} \psi - \gamma \lambda_{e} \sin \lambda_{e} \psi}{\sin \lambda_{e} \psi + \gamma \lambda_{e} \cos \lambda_{e} \psi} \right]$$
(4.5.19)

The coefficients B_1 and B_2 may now be determined by using Eqs. (4.2.25) and (4.2.26), which represent the boundary conditions for λ_1 and λ_2 at $\bar{s}=\psi$;

$$B_{2} = \frac{\delta \sin \lambda_{e} \psi - \gamma \lambda_{e}}{\beta \lambda_{e} \left[\sin \lambda_{e} \psi + \gamma \lambda_{e} \cos \lambda_{e} \psi \right]^{2}}$$
(4.5.20)

$$B_{1} = -\frac{\delta \cos \lambda_{e} \psi + 1}{\beta \lambda_{e} \left[\sin \lambda_{e} \psi + \gamma \lambda_{e} \cos \lambda_{e} \psi \right]^{2}}$$
(4.5.21)

 λ_1 and λ_2 can therefore be written as

$$\lambda_{1} = \frac{1}{\delta \beta} \frac{\delta \cos \lambda_{e} (\psi - s) - \gamma \lambda_{e} \sin \lambda_{e} s + \cos \lambda_{e} s}{\left| \sin \lambda_{e} \psi + \gamma \lambda_{e} \cos \lambda_{e} \psi \right|^{2}}$$
(4.5.22)

$$\lambda_{2} = \frac{\delta}{\beta \lambda_{e}} \frac{\sin \lambda_{e} (\psi - s) - \gamma \lambda_{e} \cos \lambda_{e} s - \sin \lambda_{e} s}{\left| \sin \lambda_{e} \psi + \gamma \lambda_{e} \cos \lambda_{e} \psi \right|^{2}}$$
(4.5.23)

The constant C_1 is determined by enforcing continuity on λ_1 at $s=\gamma$.

$$C_1 = \frac{1}{\delta \beta} \frac{\delta \cos \lambda_e \psi + 1}{\left| \sin \lambda_e \psi + \gamma \lambda_e \cos \lambda_e \psi \right|^2}$$
(4.5.24)

From (4.2.20), with $\mu_1 = 0$, $\mu_2(\bar{s})$ can be calculated:

$$\mu_{2} = 1 + \delta \left[\cos \lambda_{e} (\psi - \bar{s}) + \gamma \lambda_{e} \sin \lambda_{e} (\psi - \bar{s}) \right]$$

$$+ 1 - \gamma^{2} \lambda_{e}^{2} \cos 2\lambda_{e} \bar{s} - 2\gamma \lambda_{e} \sin 2\lambda_{e} \bar{s}$$

$$(4.5.25)$$

The junction point, $s = \gamma$, is determined from the continuity condition on λ_2 . Equations (4.5.23) and (4.5.8) are now combined to give

$$\sqrt{\frac{\pi}{2}} = \frac{\delta \sin\sqrt{2\alpha\psi} - \gamma\sqrt{2\alpha}}{e^{(\alpha\gamma)^2} \operatorname{erf}(\alpha\gamma) \left| \sin\sqrt{2\alpha\psi} + \gamma\sqrt{2\alpha} \cos\sqrt{2\alpha\psi} \right|^2}$$
(4.5.26)

By using (4.5.24), Eq. (4.5.10) can be written as

$$\frac{\mu_1 \beta}{a} = 2 + e^{-\alpha^2 (\gamma^2 - s^2)} \left\{ \frac{\delta \cos \sqrt{2} \alpha \psi + 1}{\left[\sin \sqrt{2} \alpha \psi + \gamma \sqrt{2} \alpha \cos \sqrt{2} \alpha \psi \right]^2} - 1 \right\}$$

$$+ \sqrt{\pi} \alpha e^{(\alpha s)^2} \left[2s \operatorname{erf}(\alpha s) - \gamma \operatorname{erf}(\alpha \gamma) \right] , 0 \le s < \gamma$$
 (4.5.27)

Given an excitation frequency parameter α and minimum-area constraint δ , the transcedental relation (4.4.26) can be solved by trial for the corresponding γ . Figure 34 displays the resulting values of γ plotted vs. α for a wide selection of minimum-gauge parameters $\delta = P/A_{min\ max}$. To ensure optimality, the signs of μ_1 and μ_2 must be checked. It is found that, for a given δ and sufficiently large α , $\mu_2(\mathbf{x})$ is not positive for all s between γ and 1, so that the proposed solutions are not optimal. In Fig. 34 this limitation is represented by the broken line. Its onset indicates that more than two arcs are needed in the optimal design (to the right of the line, solutions have an arc that is unconstrained near the tip - see Section 4.8).

The critical point turns out to be at $s=\psi$ (s = 1). For a consistent pair (α, γ) , $1+(1-\gamma^2\lambda_e^2)\cos 2\lambda_e\psi-2\gamma\lambda_e\sin 2\lambda_e\psi=0$ determines the critical λ_e .

For values of α to the left of the broken line, μ_1 can be shown to be positive for all s, $0 \le s < \gamma$. A typical area distribution, for $\alpha = 1$ and $\delta = 10$, is depicted in Fig 35. Total dimensionless volumes are plotted vs. α , in Fig. 36. These were obtained by adding the tip volumes (Eq. 4.5.19) to the distributed area integrations:

$$\frac{V\sigma_{\text{max}}}{PT} = \int_{0}^{1} a(s) ds + a_{\text{T}} = \frac{1}{\delta} \left\{ \frac{\sqrt{\pi}}{2\alpha} e^{(\alpha\gamma)^{2}} \operatorname{erf}(\alpha\gamma) + \frac{\delta + (1-2\gamma)\sqrt{2\alpha}\sin\sqrt{2\alpha\psi} + (1+2\alpha^{2}\gamma - 2\alpha^{2}\gamma^{2})\cos\sqrt{2\alpha\psi}}{\sqrt{2\alpha}(\sin\sqrt{2\alpha\psi} + \gamma\sqrt{2\alpha}\cos\sqrt{2\alpha\psi})} \right\} (4.5.28)$$

In Fig. 36, the dimensionless volumes of the first-mode solutions are also shown. It is seen that, when $\alpha \lesssim 0.63$, the latter proves superior to any possible second-mode solution. At higher forcing frequencies, on the other hand, a selection of designs with $\omega_1 < \omega_e$ is available which can save substantial weight. For completeness, the behavior of the dimensionless tip mass $a_T = V_{T \text{ max}}/Pl$ is shown in Fig. 37.

Finally, the variable-area optimal volumes are compared to those obtained with constant-area bars in Fig. 38. One notes the excellent agreement, specially when $\lambda_1 < \lambda_e$. Note also that the constant-area results, as expected, provide an upper bound for the optimal variable-area design.

A surprising mathematical feature of the second-mode solutions is the discontinuous behavior of Lagrange multipliers μ_1 and μ_2 at the matching point s=\gamma. An error was first suspected when it was discovered that μ_1 drops from a finite positive value to zero when passing outboard across s=\gamma, whereas μ_2 jumps from zero to just the size needed to make H and $\partial H/\partial a$ (Eqs. 4.2.19 and 4.2.23) properly continuous. It was subsequently therefore that the last two terms in Eq. (4.2.19) might as well have been written $\mu_1\{|\mathbf{x}_2|/\beta-a\}+\mu_2\{1/\delta-a\}$, and might have been interpreted as a single constraint of the general form $\mu\{f(\mathbf{x}_2)-a\}$. The discontinuity in μ itself is then found to disappear. At s= γ , there are slope discontinuities in $\mu(s)$, a(s) and the function f(s), but such phenomena are acceptable and often encountered in control-theory applications.

4.6 NATURAL FREQUENCIES

In this section, the natural frequencies of the optimal bar are studied. The unforced equilibrium equation is:

$$\frac{d}{ds}\left[a(s)\frac{dv}{ds}\right] + \lambda_i a(s) v = 0$$
 (4.6.1)

with the boundary conditions

$$v(0) = 0$$
; $a \frac{dv}{ds}\Big|_{s=1} = a_T \lambda_i v(1)$ (4.6.2)

Let $t = \alpha s$ and denote $\frac{d}{dt}()$ by (), then Eq. (4.6.1) transforms

$$\dot{v} + \frac{\dot{a}}{a}\dot{v} + 2 \eta v = 0$$
 , $0 \le t \le \alpha$ (4.6.3)

and

to

$$\mathbf{v}(0) = 0$$
 ; $\dot{\mathbf{v}}(\alpha) = 2 \, \eta \, \alpha \frac{\mathbf{a}_{\mathbf{T}}}{\mathbf{a}(\alpha)} \, \mathbf{v}(\alpha)$ (4.6.4)

with $\eta = \lambda_i^2/2\alpha^2$.

Consider, for the moment, the fully-stressed solution (first-mode). Substituting the expression for the area distribution (see Eq. 4.4.38 with γ = 0) and taking into account the change in variables (eq. 4.6.3), one gets

$$\ddot{v} - 2 t \dot{v} + 2 \eta v = 0$$
 (4.6.5)

This is the Hermite equation, and its general solution, according to Murphy (Ref. 74, page 322) reads

$$v(t) = v_{o} \left\{ 1 + \sum_{\nu=1}^{\infty} \frac{2^{\nu} \left[(-n) (2-\eta) \dots (2\nu-2-\eta) \right]}{(2\nu)!} t^{(2\nu)} \right\}$$

$$+ v_{1} \left\{ t + \sum_{\nu=1}^{\infty} \frac{2^{\nu} \left[(1-\eta) (3-\eta) \dots (2\nu-1-\eta) \right]}{(2\nu+1)!} t^{(2\nu+1)} \right\}$$

$$(4.6.6)$$

From the boundary condition at t=0 it follows that $v_0=0$, and v(t), $\dot{v}(t)$ can be written:

$$v(t) = v_1 \left\{ t + \sum_{\nu=1}^{\infty} \frac{2^{\nu} \left[(1-\eta) (3-\eta) \dots (2\nu-1-\eta) \right]}{(2\nu+1)!} t^{(2\nu+1)} \right\}$$
 (4.6.7)

$$\dot{\mathbf{v}}(\mathsf{t}) = \mathbf{v}_1 \left\{ 1 + \sum_{\nu=1}^{\infty} \frac{2^{\nu} \left[(1-\eta) (3-\eta) \dots (2\nu-1-\eta) \right]}{(2\nu)!} \, \mathbf{t}^{(2\nu)} \right\}$$
 (4.6.8)

For the first-mode solution, $a_T=0$. To satisfy the boundary condition at $t=\alpha$, with non-zero v ($v_1\neq 0$), it is necessary that

$$1 + \sum_{\nu=1}^{\infty} 2^{\nu} \left\{ \frac{(\alpha^2 - \alpha_1^2) (3\alpha^2 - \alpha_1^2) \dots [(2\nu - 1)\alpha^2 - \alpha_1^2]}{(2\nu)!} \right\} = 0$$
 (4.6.9)

For this convergent series, it is evident that Eq. (4.6.8) can only be satisfied if $\alpha_i > \alpha$, i.e., the natural frequencies of the fully-stressed bar are larger than the excitation frequency. The fundamental natural frequency is given as a function of the excitation α in Fig. 39. Note that, as α increases, α_l tends asymptotically to α , i.e., the fully-stressed bar is excited near resonance; this fact explains the

^{*} Applying the ration test: Ratio = $a_n/a_{n+1} = \frac{\alpha^2 - \alpha_1^2/(2\nu+1)}{(2\nu+1)}$. It is clear that there exists N, for which: R < 1, for any ν larger than N.

behavior of the volume curve given in Fig. 32.

For $\alpha \geq 1.0908$ the optimal solution is not fully stressed, but the transition from fully-stressed to partially-stressed and subsequent variations in the area distribution (as α is increased) are also continuous. It follows that $\alpha_i > \alpha$, since $\alpha_i < \alpha$ would require that for a certain α the bar be in resonance, which is absurd once the solutions have been shown to be optimal. Therefore, for the whole range of excitation frequencies, the optimal bar that is vibrating in phase with the load has natural frequencies that are larger than the excitation frequency. A formal proof that the last statement is correct is given in Appendix B.

Consider now the second-mode solutions. In the range $0 \le t \le \alpha \gamma$ (o $\le s \le \gamma$), equations (4.6.7) and (4.6.8) hold. In the interval $\alpha \gamma \le t \le \alpha$, $\alpha(t) = 1/\delta$ and $\dot{\alpha}/\alpha = 0$. Equation (4.6.5) can, therefore, be written as

$$\dot{\mathbf{v}} + 2 \eta \mathbf{v} = 0 \tag{4.6.10}$$

with the general solution

$$v(t) = B_1 \sin \sqrt{2\eta} t + B_2 \cos \sqrt{2\eta} t$$
 (4.6.11)

Enforcing continuity at $t = \alpha \gamma$ gives:

$$A_1 \quad v_1 = B_1 \sin\theta\gamma + B_2 \cos\theta\gamma$$

$$\frac{A_2}{\sqrt{2n}} \quad v_1 = B_1 \cos\theta\gamma - B_2 \sin\theta\gamma$$

$$(4.6.12)$$

where

$$\theta = \sqrt{2\eta} \alpha \tag{4.6.13}$$

 $[\]dot{a}/a$ is the same for fully-stressed first-mode and second-mode solutions. Compare (4.4.38) with $\gamma=0$ and (4.4.7).

$$A_{1} = (\alpha \gamma) + \sum_{\nu=1}^{\infty} 2^{\nu} \frac{\left[(1-\eta) (3-\eta) \dots (2\nu-1-\eta) \right]}{(2\nu+1)!} (\alpha \gamma)^{(2\nu+1)}$$

$$A_{2} = 1 + \sum_{\nu=1}^{\infty} 2^{\nu} \frac{\left[(1-\eta) (3-\eta) \dots (2\nu-1-\eta) \right]}{(2\nu)!} (\alpha \gamma)^{(2\nu)}$$

Solving for B_1 , B_2 :

$$B_{1} = v_{1} \left\{ \frac{A_{2}}{\sqrt{2\eta}} \cos\theta \gamma + A_{1} \sin\theta \gamma \right\}$$

$$B_{2} = v_{1} \left\{ A_{1} \cos\theta \gamma - \frac{A_{2}}{\sqrt{2\eta}} \sin\theta \gamma \right\}$$

$$(4.6.15)$$

The boundary condition at $t = \alpha$ gives

$$\sqrt{2\eta}$$
 (B₁ cos θ - B₂ sin θ) = $2\eta\alpha a_{T}^{-}\delta$ (B₁ sin θ + B₂cos θ) (4.6.16)

Using (4.6.15) in (4.6.16) an simplifying,

$$A_2\cos\theta\psi - A_1\sqrt{2\eta}\sin\theta\psi = Z\sqrt{\eta} (A_2\sin\theta\psi + A_1\sqrt{2\eta}\cos\theta\psi) \qquad (4.6.17)$$

with ψ = 1- γ , and Z = $a_{T}\delta\alpha\sqrt{2}$. Using (4.5.19), one derives

$$Z = \frac{\delta + \cos \lambda_{e} \psi - \gamma \lambda_{e} \sin \lambda_{e} \psi}{\sin \lambda_{e} \psi + \gamma \lambda_{e} \cos \lambda_{e} \psi}$$
(4.6.18)

Here, as defined in Section 4.2, $\delta = P/(\sigma_{max}^{A} A_{min})$ is the minimum-area parameter.

The natural frequencies are obtained by solving Eq. (4.6.17) numerically. In Fig. 40 the first and second natural frequencies are shown as functions of α , when δ = 10. In Appendix B it is formally proven that

for the second mode solutions, $\alpha_1 < \alpha < \alpha_2$. This is confirmed by the plots in Fig. 40.

4.7 FINITE-ELEMENT SOLUTIONS

When a structure is modeled by finite elements, the steady-state equation of motion (Ref. 75) is

Here, $\frac{K}{z}$ and $\frac{M}{z}$ are the assembled stiffness and inertia matrices, u, the vector of displacement amplitudes and p, the vector of load amplitudes.

In the case of the bar (Fig. 28-b), the element stiffness and inertia matrices can be written, respectively, as (Ref. 75)

$$\begin{vmatrix}
K_{i} \\
 \end{vmatrix} = \frac{E}{I_{i}} \begin{bmatrix}
A_{i} & -A_{i} \\
 -A_{i} & A_{i}
\end{bmatrix}$$

$$\begin{vmatrix}
M_{i} \\
 \end{vmatrix} = \frac{\rho I_{i}}{6} \begin{bmatrix}
2A_{i} & A_{i} \\
 -A_{i} & 2A_{i}
\end{bmatrix}$$
(4.7.2)

where ${\bf A_i}$ and ${\bf I_i}$ are, respectively, the cross-sectional area and the length of the i-th element. The load vector in this case is

$$\mathbf{p} = \begin{cases}
0 \\
0 \\
\vdots \\
\vdots
\end{cases}$$
(4.7.3)

Let the bar be divided into n elements of equal length l/n, and let

$$\underline{\mathbf{a}} = \frac{\sigma_{\text{max}}}{P} \underbrace{A}_{\underline{v}} \tag{4.7.4}$$

denote the design variables. If the displacements are transformed to

$$\underline{\mathbf{v}} = \frac{\mathbf{n}}{l} \frac{\mathbf{E}}{\mathbf{max}} \underline{\mathbf{u}} \tag{4.7.5}$$

with degrees-of-freedom numbered sequentially as in Fig. 28(b), and the left end assumed fixed, Eq. (4.7.1) becomes

$$\bar{\mathbf{g}} \quad \mathbf{y} = \bar{\mathbf{p}} \tag{4.7.6}$$

or

$$\begin{bmatrix} (a_1+a_2)\Gamma_1 & -a_2\Gamma_2 & 0 & 0 & \dots \\ -a_2\Gamma_2 & (a_2+a_3)\Gamma_1 & -a_3\Gamma_2 & 0 & \dots \\ 0 & -a_3\Gamma_2 & (a_3+a_4)\Gamma_1 & -a_4\Gamma_2 & \dots \\ 0 & 0 & -a_4\Gamma_2 & \dots \\ \vdots & \vdots & \ddots & \vdots & \vdots \\ -a_n\Gamma_2 & a_n\Gamma_1 \end{bmatrix} \begin{bmatrix} 0 \\ 0 \\ 0 \\ 0 \end{bmatrix}$$

Here, a_i is a component of vector a_i , and

$$\Gamma_{1} = 1 - \frac{\omega_{e}^{2} \rho \ell^{2}}{3En^{2}} = 1 - \frac{2\alpha^{2}}{3n^{2}}$$

$$\Gamma_{2} = 1 + \frac{\omega_{e}^{2} \rho \ell^{2}}{6En^{2}} = 1 + \frac{\alpha^{2}}{3n^{2}}$$

$$(4.7.8)$$

The stress constraints can be written as

$$g_{i} = \left(\frac{\sigma_{i}}{\sigma_{max}}\right)^{2} - 1 \leq 0 \tag{4.7.9}$$

and σ_{i} , the stress on element i , is given (Ref. 13) by:

$$\sigma_{i} = \left(\frac{n}{\ell}\right) E \left(u_{i} - u_{i-1}\right) \tag{4.7.10}$$

with u_0 = 0. Using Eq. (4.7.4) and designating s_i = σ_i/σ_{max} , the last two equations can be rewritten as

$$g_{i} = s_{i} - 1 \le 0$$
 (4.7.11)

$$s_i = v_i - v_{i-1}$$
 (4.7.12)

By differentiating (4.7.6) with respect to a_j , an expression for the $\partial v/\partial a_j$ vector is obtained:

$$\frac{\bar{K}}{\bar{x}} = \frac{\partial \bar{Y}}{\partial a_{j}} = -\frac{\partial \bar{K}}{\partial a_{j}} \bar{y}$$
 (4.7.13)

With $\partial v/\partial a_j$ determined, the constraint derivative is found directly

$$\frac{\partial g_{i}}{\partial a_{j}} = 2 s_{i} \left\{ \frac{\partial v_{i}}{\partial a_{j}} - \frac{\partial v_{i-1}}{\partial a_{j}} \right\}$$
 (4.7.14)

Here, once again, by definition: $\partial \mathbf{v} / \partial \mathbf{a}_{i} = 0$.

All necessary quantities for a solution using the technique of Chapter II are now determined. A computer program was written to perform the structural analysis that required α , n, a (the minimum area = $1/\delta$) and a_0 (initial design vector) to be read in along with the optimization parameters.

Figure 33 shows the area distributions obtained for three different values of α , with n=10 and $a_{\min}=0$. The elements that are not critical with respect to the stress constraint are shaded. Note the excellent agreement with the results obtained with the continuous model.

Figure 35 depicts the area distributions when $\alpha=1.0$, $a_{\min}=0.1$ ($\delta=10$), for two values of n. Note the importance of the model in this case. The last element attempts to model the concentrated mass found in the continuous solution and, unless l/n is very small, the true physical situation is not well represented. If accurate results are sought with a small number of elements, the concentrated mass should be considered as a design variable and lumped appropriately into the mass matrix.

When seeking to isolate first- or second-mode solutions in the finite-element calculations, one must carefully select the initial design vector. The method of Chapter II proceeds through the infeasible region and is therefore unaware of the design space's multiple connectivity. The local optima that are found depend on the initial design. It is believed that higher response modes could be treated by imposing the additional constraint $\alpha_{\bf i} < \alpha < \alpha_{\bf i+1}$. Unfortunately these higher frequencies seem to be very sensitive to design-vector changes, and the method of Chapter II might fail. Perhaps an unconstrained search procedure, with large penalties associated to the frequency constraints, has a greater chance of success (see, e.g., Refs. 13 or 20).

A second-mode a-distribution computed by finite elements, with $n=20,\;\alpha=2.0\;\;\text{and}\;\;a_{\min}=0.1\;\;(\delta=10)\;\text{is plotted in Fig. 4l.}\;\;\text{As shown}$ in Fig. 36, this case falls well outside the parameter range where the two-arc continuum solutions of Section 4.5 are optimal. The dimensionless

volume of 0.342 does, however, appear to lie roughly on an extrapolation of the curve in Fig. 36. There are still outboard mass values, but the indication is that an actual concentrated mass at the tip is no longer necessary for optimality.

The plot in Fig. 42 is the response mode u(x) corresponding to the design of Fig. 41, with each of the 20 element displacements approximated by a straight line. As well as it can be determined from the discretized solution, this is a case of three matched arcs. Over the segment marked A, u(x) is a perfectly straight line since the stress constraint is active. The elements between (x/l) = 0.45 and 0.75 are at a_{\min} , so that in the arc approximately defined by C the minimum-gauge constraint applies. Here u(x) has the expected sinusoidal shape and goes through a "loop". Neither constraint is active on arc D, but the length is too short to ascertain how u(x) is behaving. Finally, the single elements B', C' and A' are designated as two matching zones plus a zone for adjustment to the tip boundary condition. It is expected that these latter segments shrink to points as $n \to \infty$.

If it were attempted to solve for the continuous bar corresponding to Figs. 41 and 42, it is clear how the three arcs would have to be specified. The matching points $s=\gamma_1$ and γ_2 would be among the 10 or more unknowns to be found from a set of transcedental matching relations. When considering the three distinct arcs, then

(a)
$$0 \le s \le \gamma_1 : \mu_2 = 0$$
 , $x_2/a = -\beta$

(b)
$$\gamma_1 \leq s \leq \gamma_2 : \mu_1 = 0$$
 , $a = 1/\delta$

(c)
$$\gamma_2 \le s \le 1 : \mu_1 = 0 , \mu_2 = 0$$

At $s = \gamma_1$, both, $\mathbf{x}_2 = -\beta$ a and $a = 1/\delta$ apply. At s = 1, $\mathbf{x}_2 = \beta$ a if $a_m = 0$.

The main practical difficulty arises in the unconstrained arc (c). Its system of governing ddifferential equations resembles that encountered in Section 4.4 (Eqs. 4.4.19 through 4.4.23). Because simple, homogeneous boundary conditions no longer apply, convenient relations like (4.4.24) and (4.4.25) cannot be assumed. An analytical solution to this nonlinear system of differential equations has not been found.

4.8 CONCLUDING COMMENTS

In this chapter only two of the infinite number of possible minimum-weight designs were obtained analitically. Furthermore, the second result $(\omega_1 < \omega_2 < \omega_2) \text{ was calculated only for a limited range of the parameter } \alpha.$ The finding of higher mode solutions hinges on the ability to solve the following system of equations:

$$1 - \frac{\mathbf{x}_2}{a^2} \lambda_1 - \lambda_e^2 \mathbf{x}_1 \lambda_2 = 0$$

$$\dot{\mathbf{x}}_1 = \mathbf{x}_2/\mathbf{a}$$

$$\dot{\mathbf{x}}_2 = -\lambda_{\mathbf{e}}^2 \mathbf{a} \mathbf{x}_1$$

$$\dot{\lambda}_1 = \lambda_e^2 \ a \ \lambda_2$$

$$\dot{\lambda}_2 = -\lambda_1/a$$

in the interval $\gamma_i < s \le \gamma_{i+1}$, with general non-homogeneous boundary conditions. Then, the only remaining difficulty would be in finding the proper sequence of arcs and devising an efficient method for performing the very tedious calculations to determine the junction points γ_i .

Some direct conclusions from what has been done are:

- (a) Variational calculus techniques, as adapted from automatic control literature, provide a valuable tool in the design of one-dimensional structures under certain classes of dynamic loading. Although not as effective as energy methods in providing sufficient conditions for global optimality, they enable one to penetrate the barrier of $\omega_{\alpha} > \omega_{1}$.
- (b) As pointed out by Johnson (Ref. 13), the natural frequencies of the structure play a central role in creating many local optima and multiple feasible regions. Since there are no a priori ways to identify the global best design, solution methods must be capable of finding more than one optimum.
- (c) Specification of minimum-size constraints is often necessary to ensure meaningful optima.
- (d) A concentrated mass must sometimes be included in the design to satisfy a boundary condition, although it is not felt that they will be required at interior points.
- (e) The amplitude of the applied load and the maximum allowable stress do not influence the behavior of the solution for a given $\,\alpha$, other than to fix the response amplitudes.
- optimal solution, the continuum approach may be impractical. Finite-element approximations then offer a viable alternative. Special care must be taken both, in modeling and in the optimal search: frequency-range constraints may be needed to isolate various local optima associated with higher forcing frequencies.

^{*} This is, of course, not true when minimum size constraints are involved. Then the solution will remain unchanged only if $P/\sigma_{max}A_{min}$ is invariant.

Finally, the question of practical applications needs to be addressed. In seeking them, one turns to structures intended for dynamic force transmission, vibration isolation and shock mounting. To be rigorous, the present designs are limited to cases where:

- (a) The applied tip force or torque is transmitted from its source through an essentially massless medium, like a soft spring.
 - (b) Steady-state sinusoidal loads predominate over transient ones.
- (c) Stresses due to static loads are neglegible compared to dynamic stresses.

It is difficult to think of a practical situation where these conditions occur simultaneously. An application that comes to mind is the "soft mounting" of an engine by using a shear-beam as support. It appears then that (b) and (c) may be satisfied. The method of this chapter could then be applied with the addition of a prescribed tip mass $^{\rm M}_{\rm Tp}$. No particular difficulties should be encountered when searching for the solution.

CHAPTER V

CONCLUSIONS AND RECOMENDATIONS

A number of comments about the methods and solutions have already been made. Sections 2.10, 3.11 and 4.8 are devoted to discussing the material presented in their respective chapters. This final chapter reiterates on these comments and lists areas for further study.

Two distinct results were obtained in this dissertation. First, it has been shown that the performance of the theoretical optimality criteria algorithm, as proposed by Kiusalaas (Ref. 31) and augmented here by a modified Gauss-Seidel procedure for the determination of the active constraints, is equivalent to that of the most efficient mathematical programming algorithm for a large class of structural optimization problems. Then it has been shown that variational calculus techniques, as adapted from the automatic control literature, provide a insightful tool in the design of one-dimensional structures under certain classes of dynamic loading.

The examples of Chapter III serve to measure the performance of the redesign algorithm. Results were obtained for optimization problems involving structures under static and dynamic loadings. Realistic constraints on stress, displacement and member size limits, as well, lower bounds on natural frequencies and flutter speed were considered. In view

of the successful solution of these different examples, it is believed that the redesign algorithm can safely be considered to be quite general. Throughout these examples the same level of high efficiency was maintained.

The idea of using $g \le 0$ as the constraint rather than using $V_F \ge V_{FO}$ directly, as proposed in Ref. 34, has proven to be a sound way to efficiently formulate flutter optimization problems. The concept of updated generalized coordinates as presented in Section 3.4 appears to be promising. When compared to fixed modes, updated generalized coordinates have shown to lead to more accurate flutter reanalyses.

Further investigations in a number of areas related to Chapters III and IV could be conducted. Some of these that the author finds particularly important include the following:

- (1) Demonstrating that the theoretical basis of this optimality criteria and mathematical programming algorithms are not so far apart. These two categories have always been considered to be completely different both from the theoretical and the numerical point of view. Since this work demonstrates that the efficiency of both categories are equivalent, it remains to be shown that they are also close theoretically in order to modify this belief. It appears that the present algorithm is very close to the "gradient projection" algorithm of mathematical programming (Ref. 36). It is important to uncover this correlation in order to determine under which conditions the algorithm can be proven to converge to an optimum.
- (2) Implement the extensions suggested in Section 2.10 and determine under which practical circumstances the changed algorithm would maintain its efficiency. The extension to problems with a nonlinear objective

function is important if one wishes to optimize structures for geometry.

- (3) Study problems with highly non-linear constraints and determine which modifications have to be done in order to avoid divergence.
- (4) An extensive analysis to determine the tradeoff between the computer requirements and accuracy for the three different dynamic models for flutter optimization: Fixed modes, partially updated modes (as in Section 3.4), and completely changing modes (as in Ref. 59). When large examples are considered, it is important to choose the model that is appropriate to the specific case being studied.

The results obtained in Chapter IV for the design of a bar under harmonic excitation serve to confirm some conclusions and hypothesis by Johnson (Ref. 13):

- (a) The natural frequencies of the structure do play a central role in creating the many local optima and, in the absence of damping, multiple feasible regions.
- (b) It is often necessary to specify minimum-gauge constraints to ensure meaningful optimal designs.
- (c) A concentrated mass must sometimes be included in a design to satisfy a boundary condition. At interior points, however, it is felt that this should not be required although large distributed mass concentrations may result.

Concluding, it is felt that this work has broadened the application of optimization methods both, for the basic understanding of complex problems and for the construction of practical solutions. Further, it is hoped that these contributions will be taken up and extended by others so then they can play a role in the growing practical application of optimization methods.

REFERENCES

- 1. Keller, J. B., "The Shape of the Strongest Column," Archive for Rational Mechanics and Analysis, Vol. 5, 1960, pp. 275-285.
- Niordson, F. I., "On the Optimal Design of a Vibrating Beam," Quarterly of Applied Mathematics, Vol. 23, No. 1, April 1965, pp 47-53.
- Turner, M. J., "Design of Minimum Mass Structures with Specified Natural Frequencies," AIAA Journal, Vol. 5, No. 3, March 1967, pp. 406-412.
- 4. Prager, W., "Optimality Criteria in Structural Design," *Proc. Natl. Acad. Sci.*, 61, 1968, pp. 794-796.
- 5. Prager, W. and Taylor, F. E., "Problems of Optimal Structural Design,"

 Journal of Applied Mechanics, Vol. 35, No. 1, March 1968, pp. 102-106.
- Taylor, J. E., "Optimum Design of a Vibrating Bar with Specified Minimum Cross Section," AIAA Journal, Vol. 6, No. 7, July 1968, pp. 1379-1381.
- Turner, M. J., "Optimization of Structures to Satisfy Flutter Requirements," AIAA Journal, Vol. 7, No. 5, May 1969, pp. 945-951.
- 8. Segenreich, S. A. and McIntosh, S. C., "Weight Minimization of Structures for Fixed Flutter Speed Via an Optimality Criterion," AIAA/
 ASME/SAE 16th Structures, Structural Dynamics and Materials conference, Denver, Colorado, May 1975.
- Rudisill, C. S., and Bathia, K. G., "Optimization of Complex Structures to Satisfy Flutter Requirements," AIAA Journal, Vol. 8, No. 8, 1971, pp. 1487-1491.
- 10. Rao, S. S., "Automated Optimum Design of Aircraft Wings to Satisfy Strength, Stability, Frequency and Flutter Requirements," Ph.D. Dissertation, CWRU, Cleveland, Ohio, 1971.

- 11. Gwin, L. B. and Taylor, R. F., "A General Method for Flutter Optimization," AIAA Journal, Vol. 12, No. 12, December 1973, pp. 1613-1617.
- 12. Haftka, R. T., "Parametric Constraints with Application to Optimization for Flutter Using a Continuous Flutter Constraint," AIAA Journal, Vol. 13, No. 4, April 1975, pp. 471-475.
- 13. Johnson, E. H., "Optimization of Structures Undergoing Harmonic or Stochastic Excitation," Ph.D. Dissertation, Department of Aeronautics and Astronautics, Stanford University, June 1975 (also NASA CR-142,936)
- 14. Rubin, C. P., "Minimum-Weight Design of Complex Structures Subject to a Frequency Constraint," *AIAA Journal*, Vol. 8, No. 5, May 1970, pp. 923-927.
- 15. Schmit, L. A., "Structural Design by Systematic Synthesis," *Proc. 2nd Conf. on Electronic Computation*, ASCE, 1960, pp. 105-132.
- 16. Gellatly, R. A., Gallagher, R. H. and Luberacki, W. A., "Development of a Procedure for Automated Synthesis of Minimum Weight Structures," AFFDL-TDR-64-141, October 1964.
- 17. Gellatly, R. A., "Development of Procedures for Large Scale Automated Minimum Weight Structural Design," AFFDL-TR-66-180, 1966.
- 18. Karnes, R. N. and Tocher, J. L., "Automatic Design of Optimum Hole Reinforcement," Boeing Report D6-23359, 1968.
- 19. Tocher, J. L. and Karnes, R. N., "The Impact of Automated Structural Optimization on Actual Design," AIAA Paper No. 73-361, April 1971.
- Schmit, L. A. and Miura, H., "Approximation Concepts for Efficient Structural Synthesis," NASA CR-2552, (in preparation), 1975.
- 21. Venkayya, V. B., Khot, N. S. and Reddy, V. S., "Optimization of Structures Based on the Study of Strain Energy Distribution," *Proc. 2nd Conf. on Matrix Methods in Structural Mechanics WPAFB*, AFFDL-tr-68-150, 1968, pp. 111-153.

- 22. Dwyer, W., Rosenbaum, J., Shulman, M. and Pardo, H., "Fully-stressed Design of Airframe Structures," *Proc. 2nd Conf. on Matrix Methods in Structural Mechanics*, WPAFB, AFFDL-TR-68-150, 1968, pp. 155-181.
- 23. Lansing, W., Dwyer, W., Emerton, R. and Ranalli, E., "Application of Fully-Stressed Design Procedures to Wing and Empennage Structures,"

 Journal of Aircraft, Vol. 8, No. 9, 1971, pp. 683-688.
- 24. Venkayya, V. B., "Design of Optimum Structures, " Computers and Structures, Vol. 1, No. 1/2, August 1971, pp. 265-309.
- 25. Gellatly, R. A., Berke, L. and Gibson, W., "The Use of Optimality Criteria in Automated Structural Design," *Proc. 3rd Conf. on Matrix Methods in Structural Mechanics*, AFFDL-TR-71-160, 1971, pp. 557-590.
- 26. Dwyer, W. J., Emerton, R. K. and Ojalvo, I. U., "An Automated Procedure for the Optimization of Practical Aerospace Structures," AFFDL-TR-70-118, 1971.
- 27. Gellatly, R. A. and Berke, L., "Optimal Structural Design," AFFDL-TR-70-165, February 1971.
- 28. Taig, I. C. and Kerr, R. I., "Optimization of Aircraft Structures with Multiple Stiffness Requirements," 3rd Symposium on Structural Optimization, AGARD-CP-123, Milan, Italy, April 1973.
- 29. Venkayya, V. B., Khot, N. S. and Berke, L., "Application of Optimality Criteria Approaches to Automated Design of Large Practical Structures," 2nd Symposium on Structural Optimization, AGARD-CP-123, Milan, Italy, April 1973.
- 30. Berke, L. and Khot, N. S., "Use of Optimality Criteria Methods for Large Scale Systems," *Lectures on Structural Optimization*, AGARD-LS-70, Hampton, Virginia, October 1974.
- 31. Kiusalaas, J., "Minimum Weight Design of Structures Via Optimality Criteria," NASA TN D-7115, 1972.
- 32. Kiusalaas, J., "Optimum Design of Structures with Buckling Constraint," Int. Journal of Solids and Structures, Vol. 9, No. 7, July 1973, pp. 863-878.

- 33. Segenreich, S. A. and McIntosh, S. C., "Weight Optimization under Multiple Equality Constraints using Optimality Criterion," AIAA Preprint, AIAA/ASME/SAE 17th Structures, Structural Dynamics and Materials Conference, King of Prussia, Pa., May 1976.
- 34. Segenreich, S. A., "Weight Optimization under Flutter Constraint," Ph.D. Dissertation, Department of Aeronautics and Astronautics, Stanford University, Stanford, California, 1975.
- 35. Wilde, D. J. and Beightler, C. S., Foundations of Optimization, Prentice Hall Inc., Englewood Cliffs, 1967.
- 36. Jacoby, S. L., Kowalik, J. S. and Pizzo, J. T., Iterative Methods for Nonlinear Optimization Problems, Prentice-Hall, 1972
- 37. Sheu, C. Y. and Prager, W., "Recent Developments in Optimal Structural Design," *Applied Mechanics Reviews*, Vol. 21, No. 10, October 1968, pp. 985-992.
- 38. Pierson, B. L., "A survey of Optimal Structural Design Under Dynamic Constraints," Int. Journal for Numerical Methods in Engineering, Vol. 4, No. 4, July-August 1972, pp. 491-499.
- 39. Stroud, J. W., "Automated Structural Design with Aeroelastic Constraints: A Review and Assessment of the State of the Art," Proc. ASME Winter Annual Meeting, New York, November 1974.
- 40. Gellatly, R. A., Editor, Structural Optimisation, AGARD-LS-70, Hampton, Virginia, Oct. 1974.
- 41. Schmit, L. A., Editor, Structural Optimization Symposium, American Society of Mechanical Engineers, New York, N. Y., November 1974.
- 42. Schmit, L. A. and Farshi, B., "Some Approximation Concepts for Structural Synthesis," AIAA Journal, Vol. 12, No. 5, 1974, pp. 692-699.
- 43. Vanderplaats, G. N., "Structural Analysis and Design Program, Users Manual," NASA-TMX (in preparation), Nasa Research Center, Moffet Field, California.

- 44. Melosh, R.J. and Luik, R., "Approximate Multiple Configuration Analysis and Allocation for Least Weight Structural Design," AFFDL-TR-67-29, 1967.
- 45. Fox, R. L. and Miura, H., "An Approximate Analysis Technique for Design Calculations," AIAA Journal, Vol. 1, No. 1, 1971, pp. 177-179.
- 46. Noor, A. K. and Lowder, H. E., "Approximate Techniques of Structural Reanalysis," *Computers and Structures*, Vol. 4, No. 4, 1974, pp. 801-812.
- 47. Fox, R. L., "Constraint Surface Normals for Structural Synthesis Techniques," AIAA Journal, Vol. 3, No. 8, 1965, pp.1516-1517.
- 48. Fox, R. L. and Kapoor, M. P., "Rates of Change of Eigenvalues and Eigenvectors," AIAA Journal, Vol. 6, No. 12, 1968, pp. 2426-2429.
- 49. Storaasli, O. O. and Sobieszczanski, J., "On the Accuracy of the Taylor Approximation for Structural Resizing," AIAA Journal, Vol. 12, No. 2, 1974, pp. 231-233.
- 50. Schmit, L. A. and Fox, R. L., Structural Synthesis, AIAA Educational Programs, New York, 1970.
- 51. Bathia, K. G., "Rapid Iterative Reanalysis for Automated Design," NASA TN D-6534, 1971.
- 52. Haftka, R., "Automated Procedure for Design of Wing Structures to Satisfy Strength and Flutter Requirements," NASA TN D-7264, 1973.
- 53. Carnahan, B., Luther, H. D., and Wilkes, J. O., Applied Numerical Methods, Willey, New York, N. Y., 1969.
- 54. Vanderplaats, G. N. and Moses, F., "Structural Optimization by Methods of Feasible Directions," Computer and Structures, Vol. 3, No. 4, 1973, pp. 739-755.
- 55. Vanderplaats, G. N. and Moses, F. "Automated Design of Trusses for Optimum Geometry," *Proc. of the ASCE*, Journal of the Structural Division, Vol. 98, No. ST6, March 1972, pp. 671-690.

- 56. Yates, E. C., "Flutter and Unsteady-Lift Theory," in Performance and Dynamics of Aerospace Vehicles, NASA SP-258, pp. 289-373.
- 57. Bisplinghoff, R. L., Ashley, H. and Halfman, R. L., Aeroelasticity, Addison-Wesley, Cambridge, Mass., 1955.
- 58. McCullers, L. A. and Lynch, R. W., "Composite Wing Design for Aeroelastic Requirements," *Proc. of Symposium on Fibrous Composites in Flight Vehicle Design*, Ohio, September, 1972, AFFDL-TR-72-130.
- 59. Haftka, R. T. and Yates, E. C., "On Repetitive Flutter Calculations in Structural Design," presented at the AIAA 12th Aerospace Sciences Meeting, Washington, D. C., 1974.
- 60. Vanderplaats, G. N., "CONMIN A Fortran Program for Constrained Function Minimization User's Manual," NASA TMX-62-282, Aug. 1973
- 61. Bathe, K. J. and Wilson, E. L., "Large Eigenvalue Problems in Dynamic Analysis," *Proc. ASCE*, *Journal of the Engineering Mechanics Division*, Vol. 98, No. EM6, Dec. 1972, pp. 1471-1485.
- 62. Albano, E. and Rodden, W. P., "A Doublet-Lattice Method for Calculating Lift Distributions on Oscillating Surfaces in Subsonic Flow,"

 AIAA Journal, Vol. 7, No. 2, February 1969, pp. 279-285.
- 63. Segenreich, S. A. and Rizzi, P., "Properties of Axial or Torsional Free-Vibrational Frequencies of Rods," AIAA Journal, Vol. 13, No. 8, August 1975, pp. 1111-1112.
- 64. Icerman, L. J., "Optimal Structural Design for Given Dynamic Deflection," Solids and Structures, Vol. 5, No. 5, May 1969, pp. 473-490.
- 65. Mroz, Z., "Optimal Design of Elastic Structures Subjected to Dynamic, Harmonically Varying Loads," Zeitschrift für Angewandte Mathematik und Mechanik, Vol. 50, No. 5, May 1970, pp. 303-309.
- 66. Plaut, R. H., "Optimal Structural Design for Given Deflection Under Periodic Loading," *Quarterly of Applied Mathematics*, Vol. 29, No. 2, July 1971, pp. 315-318.

- 67. Ashley, H. and McIntosh, S. C., "Application of Aeroelastic Constraints in Structural Optimization," Proc. 12th International Congress of Applied Mechanics, Springer-Verlag, Berlin, 1969.
- 68. Weisshaar, T. A., "An Application of Control Theory Methods to the Optimization of Structures Having Dynamic or Aeroelastic Constraints," SUDAAR 412, Department of Aeronautics and Astronautics, Stanford University, Stanford, California, October 1970.
- 69. Armand, J. P. and Vitte, W. J., "Foundations of Aeroelastic Optimization and Some Applications to Continuous Systems," SUDAAR 390, Dept. Aeronautics and Astronautics, Stanford University, January 1970.
- 70. Armand, J. P., "Applications of the Theory of Optimal Control of Distributed Parameter Systems to Structural Optimization," NASA CR-2044, June, 1972.
- 71. Bryson, A. E. and Ho, Y. C., Applied Optimal Control, Revised Printing, Hemisphere Pub. Corp., Washington, D. C., 1975.
- 72. Segenreich, S. A. and Rizzi, P. "Optimal Fully-Stressed Solutions for the Harmonically Excited Vibrating Rod," COPPE No. 25.75, Universidade Federal do Rio de Janeiro, R. J., Brazil, 1975.
- 73. Abramowitz, M. and Stegun, I. A., Handbook of Mathematical Functions, Dover Publications, Inc., New York, N. Y., 1970.
- 74. Murphy, G. M., Ordinary Differential Equations and Their Solution, Van Nostrand Reinhold Co., New York, N. Y., 1960.
- 75. Przemieniecki, J. S., Theory of Matrix Structural Analysis, McGraw Hill Book Co., Inc., New York, N. Y., 1968.
- 76. Morse, P. M. and Feshbach, H., Methods of Theoretical Physiscs, McGraw Hill Book Co., Inc., N. Y., 1953, pp. 719-724.
- 77. Bisplinghoff, R. L. and Ashley, H., Principles of Aeroelasticity, Wiley & Sons, Inc., New York, 1962.
- 78. Dantzig, G., Linear Programming and Extensions, Princeton Univ. Press, Princeton, N. J., 1963.

APPENDIX A

OPTIMALITY CONDITIONS

Consider the problem:

Minimize
$$J = \int_0^1 a(s) ds$$
 (A.1)

subject to

$$\dot{x} = f(x, a, s) \tag{A.2}$$

$$C_1(\mathbf{x}, \mathbf{a}, \mathbf{s}) \leq 0 \tag{A.3}$$

$$C_2(a, s) \leq 0 \tag{A.4}$$

$$C_3(a_{\mathbf{T}}) \leq 0 \tag{A.5}$$

$$\psi\left[\mathbf{x}\left(1\right), \ \mathbf{a}_{\mathbf{T}}\right] = 0 \tag{A.6}$$

with some boundary conditions on x specified at s=0, and some at s=1. The necessary conditions for optimality can be derived using the calculus of variations. As in reference 71, adjoin the constraints to y with multiplier functions:

$$\bar{\mathbf{J}} = \mathbf{a}_{\mathbf{T}} + \mathbf{v}_{1} \psi \left[\mathbf{x} (1), \mathbf{a}_{\mathbf{T}} \right] + \mathbf{v}_{2} \mathbf{c}_{3} (\mathbf{a}_{\mathbf{T}}) + \int_{0}^{1} \{\mathbf{H} - \lambda^{\mathbf{T}} \dot{\mathbf{x}} \} d\mathbf{s}$$
 (A.7)

with the Hamiltonian

$$H = a(s) + \lambda^{T} f + \mu_{1} C_{1} + \mu_{2} C_{2}$$
 (A.8)

and conditions on the multiplier functions associated to inequalities (A.3), A(4), and A(5) (Ref. 71)

$$v_{2} \begin{cases} \leq 0 & \text{if} \quad C_{3}(a_{T}) = 0 \\ = 0 & \text{if} \quad C_{3}(a_{T}) \leq 0 \end{cases}$$

$$(A.9)$$

$$\mu_1 \begin{cases} \leq 0 & \text{if } C_1(\mathbf{x}, a, s) = 0 \\ = 0 & \text{if } C_1(\mathbf{x}, a, s) < 0 \end{cases}$$
 (A.10)

$$\mu_{2} \begin{cases} \leq 0 & \text{if } C_{2}(a, s) = 0 \\ = 0 & \text{if } C_{2}(a, s) < 0 \end{cases}$$
 (A.11)

Integrating last term of Eq. (A.7) by parts, one obtains

$$\bar{J} = a_{T} + v_{1}\psi + \mu_{2}C_{3} + \lambda^{T}_{x}|_{s=0} - \lambda^{T}_{x}|_{s=1} + \int_{0}^{1} \{H + \lambda^{T}_{x}\} ds \quad (A.12)$$

and taking the first variation

$$\delta \bar{\mathbf{J}} = \left[1 + v_1 \frac{\partial \psi}{\partial \mathbf{a_T}} + v_2 \frac{\partial C_3}{\partial \mathbf{a_T}} \right] \delta \mathbf{a_T} + \left[v_1 \frac{\partial \psi}{\partial \mathbf{x}} - \tilde{\lambda}^T \right] \delta \tilde{\mathbf{x}} \Big|_{\mathbf{s}=1} + \left[\tilde{\lambda}^T \delta \tilde{\mathbf{x}} \right]_{\mathbf{s}=0}$$

$$+ \int_0^1 \left\{ \frac{\partial \mathbf{H}}{\partial \mathbf{a}} \delta \mathbf{a} + \left[\frac{\partial \mathbf{H}}{\partial \tilde{\mathbf{x}}} + \tilde{\lambda}^T \right] \delta \tilde{\mathbf{x}} \right\} d\mathbf{s}$$
(A.13)

It would be tedious to determine the variations $\delta_{\mathbf{x}}(s)$ produced by given $\delta_{\mathbf{a}}(s)$ for arbitrary $\lambda(s)$, so that the multiplier functions $\lambda(s)$ are chosen to cause the coefficients of $\delta_{\mathbf{x}}$ in Eq. (A.13) to vanish

$$\dot{\lambda}^{\mathrm{T}} + \frac{\partial H}{\partial \mathbf{x}} = 0 \tag{A.14}$$

with the boundary conditions

$$\left[v_1 \frac{\partial \psi}{\partial \mathbf{x_i}} - \lambda_i\right]_{s=1} = 0 \quad \text{if} \quad \delta \mathbf{x_i}(1) \neq 0 \quad (A.15)$$

and

$$\lambda_{i}(0) = 0 \quad \text{if} \quad \delta \mathbf{x}_{i}(0) \neq 0$$
 (A.16)

For an extremum, $\delta \vec{J}$ must be zero for arbitrary $\delta a(s)$; this can only happen if

$$\frac{\partial \mathbf{H}}{\partial a} = 0 \quad , \quad 0 \le \mathbf{s} \le 1 \tag{A.17}$$

and

$$\left[1 + \nu_1 \frac{\partial \psi}{\partial \mathbf{a_T}} + \nu_2 \frac{\partial C_3}{\partial \mathbf{a_T}}\right] = 0 \tag{A.18}$$

if $a_{\underline{T}}$ is not specified to be a constant.

It is necessary to note that in solving the problem, constrained and unconstrained arcs must be pieced together to satisfy all the necessary conditions. If the control, a(s), is continuous across the junction points of unconstrained and constrained arcs, it follows (Ref. 71) that λ , $\partial H/\partial a$ and H are continuous. The same is true if the junction points of differently constrained arcs are considered.

If the boundary condition of a certain state x_i is specified at \bar{s} , with \bar{s} either zero or one, than $\delta x_i(\bar{s}) = 0$ and $n\bar{o}$ boundary condition on $\lambda_i(\bar{s})$ is obtained.

Although the derivation of the necessary conditions for optimality is made with $a_{_{\rm T}}$ variable, the results are valid for $a_{_{\rm T}}$ = constant.

APPENDIX B

RELATIONS BETWEEN EXCITATION AND NATURAL FREQUENCIES

In this appendix some relations between the response and the freevibration mode shapes of a class of dynamic problems are determined.

Consider the class of forced vibration problems that can be represented by the differential equation

$$\{a(x) \ u'(x)\}' + \lambda_e^2 m(x) u(x) = 0, 0 \le x \le 1$$
 (B.1)

with the boundary conditions

$$u(0) = 0$$
 , $a(1) u'(1) = p^2 + q^2 \lambda_e^2 u(1)$ (B.2)

It is assumed that a(x) and m(x) are positive definite. It is further assumed that p^2 , q^2 and λ_e^2 are positive, that is

$$a(x) > 0$$
 , $m(x) > 0$
 $\lambda_e^2 \ge 0$, $p^2 \ge 0$, $q^2 \ge 0$ (B.3)

The associated eigenvalue problem is

$$\{a(x) \ u_{i}(x)\}' + \lambda_{i}^{2} m(x) u_{i}(x) = 0, 0 \le x \le 1$$
 (B.4)

$$u_{i}(0) = 0$$
, $a(1) u'_{i}(1) = q^{2} \lambda_{i}^{2} u_{i}(1)$ (B.5)

Here λ_i^2 are the eigenvalues and u_i the associated eigenfunctions. It can easily be shown that λ_i are real, strictly positive and $\lambda_i \neq \lambda_j$ if $i \neq j$, i.e., eigenvalues do not repeat. It also can be shown that the

eigenfunctions are orthogonal with respect to m(x), that is $\int_0^1 u_i(x) \ m(x) \ u_j(x) \ dx = 0 \ \text{if} \ i \neq j.$

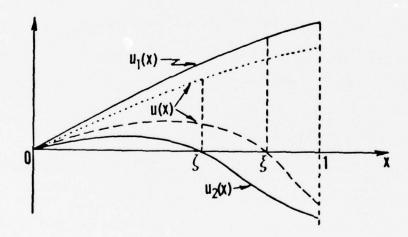
For comparison, a relation between the response and natural modes is necessary. Multiplying (B.1) by $u_i(x)$ and (B.2) by u(x), and subtracting, one obtains:

$$a\{(u u'_{i} - u_{i} u')\} \approx (\lambda_{e}^{2} - \lambda_{i}^{2}) u_{i} m u$$
 (B.6)

Now integrate from $\mathbf{x}=0$ to any $\mathbf{x}\leq 1$, taking into account the homogeneous boundary conditions at $\mathbf{x}=0$, to get

$$a\{u \ u_i' - u_i \ u'\} = (\lambda_e^2 - \lambda_i^2) \int_0^x u_i(x) \ m(x) \ u(x) \ dx$$
 (B.7)

Consider the sketch below;



It is assumed, without proof, that $u_1(\mathbf{x})$ has no zeroes in the interval $0 \le \mathbf{x} \le 1$. If this is true, than $u_2(\mathbf{x})$, which is associated with $\lambda_2(\lambda_1 \le \lambda_2 \le \lambda_3 \ldots \le \lambda_1 \ldots)$, has exactly one node (see Ref. 76, pg. 719). Only the relation between the response mode and the first two natural

modes is of interest here. Three distinct cases may develop:

- (1) u(x) has no nodes.
- (2) u(x) has one zero which lies between ζ and 1.
- (3) u(x) has one or more zeroes, the first of which (closest to the origin) lies between 0 and ζ .

The first situation is represented in the sketch above by the dotted curve, the second by the dashed line, and the third can be visualized by interchanging the illustrated u(x) and $u_2(x)$.

Consider first the situation when u(x) has one node. Evaluating (B.6) at $x = \zeta$, with i = 2 and dividing through by $u(\zeta)$ $u'(\zeta)$ one obtains:

$$a(\zeta) = (\lambda_e^2 - \lambda_2^2) \int_0^{\zeta} \left[\frac{u_2(\mathbf{x})}{u_2'(\zeta)} \right] m(\mathbf{x}) \left[\frac{u(\mathbf{x})}{u(\zeta)} \right] d\mathbf{x}$$
 (B.8)

It is clear that, in order to satisfy this equation, $\lambda_e < \lambda_2$. Moreover, if the first node of u(x) is to the left of the node of $u_2(x)$, one obtains $\lambda_e > \lambda_2$ by interchanging u and u_2 . By the same reasoning, in either case, as long as u(x) has at least one node, $\lambda_0 > \lambda_1$.

Summarizing the results obtained so far:

- (a) If the response mode has one node which is located beyond the node of the second natural mode, then $\lambda_1 < \lambda_e < \lambda_2$.
- (b) If the response has at least one node that is located inside to the node of u (x), then $\lambda_1 < \lambda_2 < \lambda$.

Note that the sign of the terms in brackets is independent of the sign of the numerators.

Compare u and u_1 at $x=\xi$ to obtain this result. Note that the existence of ξ does not play any role in deriving the result $\lambda_e < \lambda_2$.

Now consider the situation when u(x) has no nodes. With relation to u, nothing is changed: Eq. (B.8) can be used the same way and the the result, $\lambda_e < \lambda_2$, holds. To compare with u_1 , evaluate (B.6) at x=1, with i=1, to obtain

$$-p^{2} = (\lambda_{e}^{2} - \lambda_{1}^{2}) \left\{ q^{2} u(1) + \int_{0}^{1} \left[\frac{u_{1}(x)}{u_{1}(1)} \right] m(x) u(x) dx \right\}$$
 (B.9)

Here an interesting situation develops. The relation between $\lambda_{\rm e}$ and $\lambda_{\rm l}$ depends on the sign of $u({\bf x})$, since the expression to the right of $(\lambda_{\rm e}^2 - \lambda_{\rm l}^2)$ takes the sign of $u({\bf x})$. Equation (B.9) is satisfied when

$$\lambda_{e} < \lambda_{1}$$
 and $u(x) > 0$, $0 < x < 1$ (B.10)

$$\lambda_{e} > \lambda_{1}$$
 and $u(x) < 0$, $0 < x < 1$ (B.11)

This behavior can be explained if one realizes that the response "changes phase" by 180° each time λ_e passes through a λ_n of the system. This is so because, near resonance, the response is dominated by a term proportional to $u_n(\mathbf{x})/(\lambda_n^2 - \lambda_e^2)$. Obviously, this changes sign as λ_e passes through λ_n . If one looks at a vicinity of $\mathbf{x}=0$, say $\mathbf{x}=\epsilon$ (ϵ small),

$$u(\varepsilon) > 0 \quad \text{if} \quad \lambda_{e} < \lambda_{1}$$

$$u(\varepsilon) < 0 \quad \text{if} \quad \lambda_{1} < \lambda_{e} < \lambda_{2}$$

$$\vdots \quad \vdots \quad \vdots \quad \vdots \quad \lambda_{i} < \lambda_{e} < \lambda_{i+1}$$

$$(B.12)$$

Completing the results obtained:

- (c) 0 < λ_e < λ_l if and only if the response is positive, i.e., $u(x) \leq 0, \ 0 \leq x \leq 1.$
 - (d) $\lambda_1 < \lambda_e < \lambda_2$ if the response is negative.
- (e) Because of (B.12) and (c), no response that is positive in the vicinity of \mathbf{x} = 0 exists if $\lambda_1 < \lambda_2 < \lambda_2$.

One may ask why the results obtained by analyzing Eq. (B.8) are independent of the sign of u(e) (see ¶ on page 116). The reason is that these results are independent of the boundary condition on the response at $\mathbf{x}=1$. In other words, although it was assumed that the boundary condition was satisfied, no question was raised as to the existence of such a solution. In this case, the boundary condition is such that $u(\epsilon) < 0$. For a problem with a different boundary condition, $u(\epsilon)$ may be conceivably positive, but the result $\lambda_{\alpha} < \lambda_{2}$ must hold.

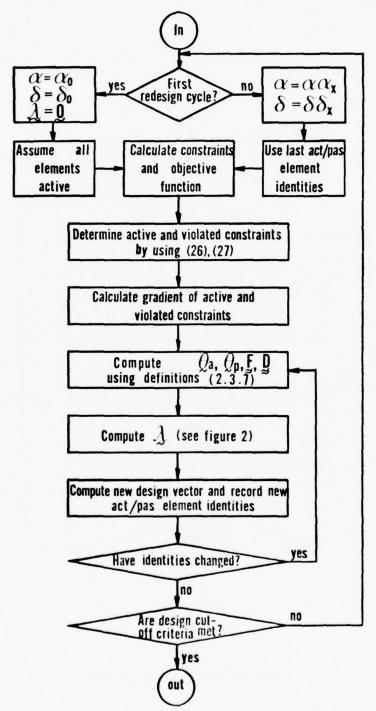


Fig. 1 Flow Diagram for Redesign Operation.

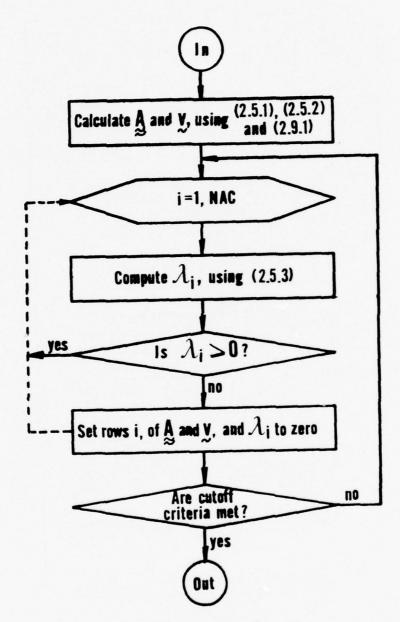


Fig. 2 Flow Diagram for $\stackrel{\textstyle .}{{\cal L}}$ calculation.

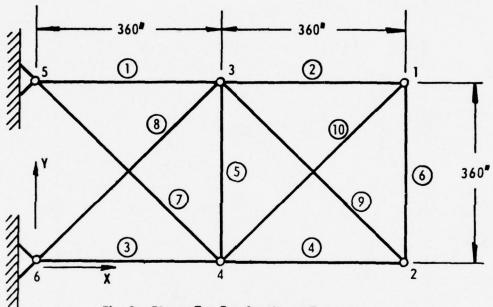


Fig. 3 Planar Ten Bar Cantilever Truss

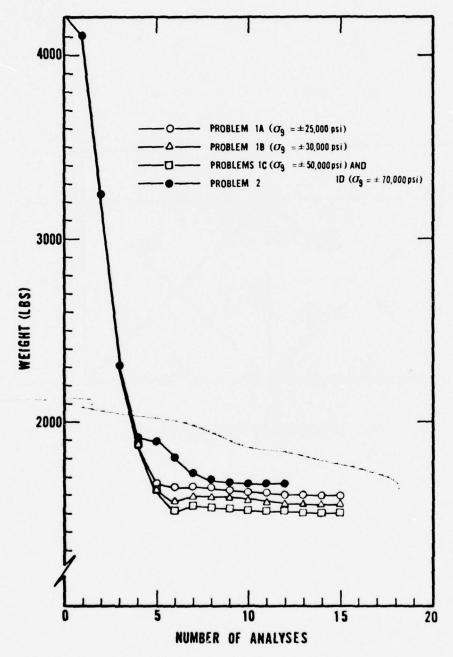


Fig. 4 Iteration Histories for Problems 1 and 2 Planar Ten Bar Cantilever Truss.

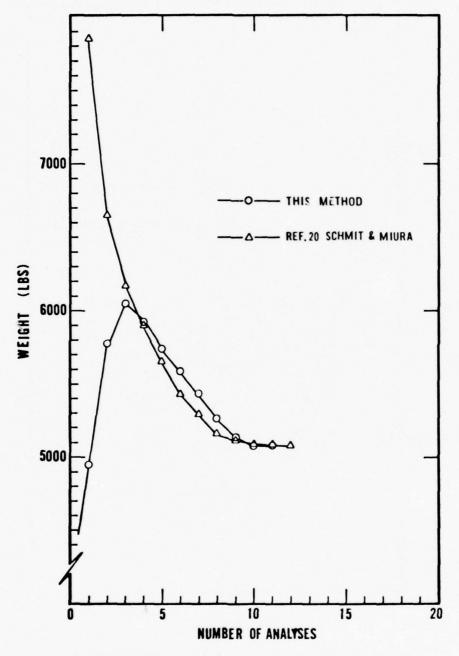


Fig. 5 Iteration Histories for Problem 3 Planar Ten Bar Cantilever Truss.

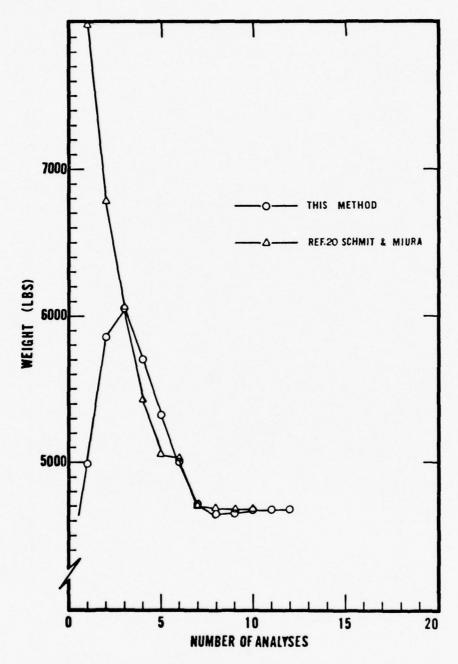


Fig. 6 Iteration Histories for Problem 4 Planar Ten Bar Cantilever Truss.

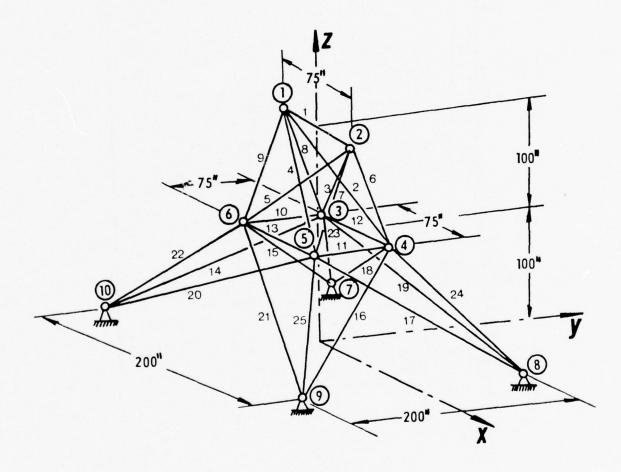


Fig. 7 Twenty Five Bar Space Truss.

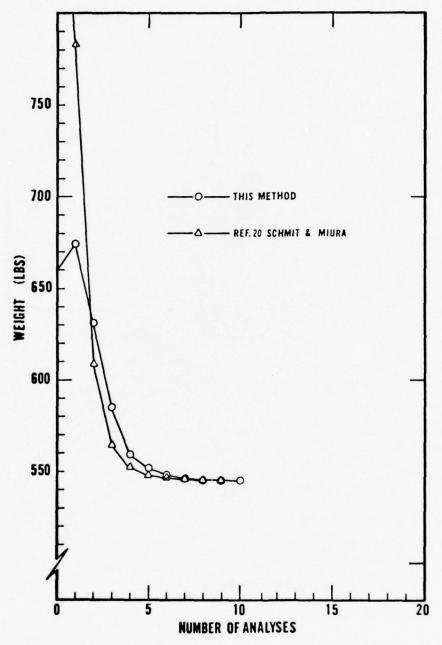


Fig. 8 Iteration Histories for Problem 5 Twenty Five Bar Space Truss.

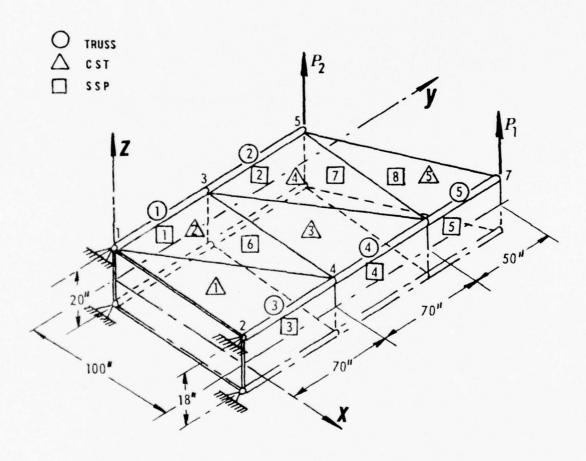


Fig. 9 Eighteen Element Wing Box Beam.

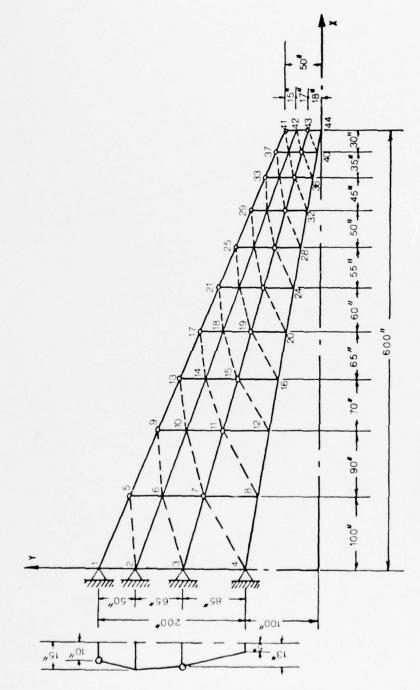


Fig. 11 (a) 150 (130) Element Swept Wing. Structural Box.

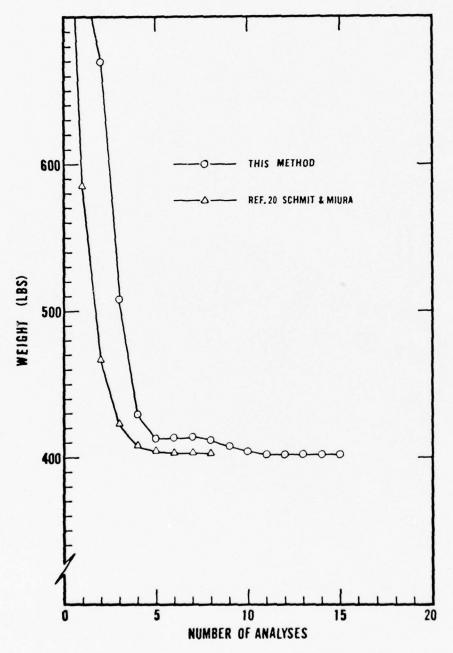


Fig. 10 Iteration Histories for Problem 6 Eighteen Element Wing Box Beam.

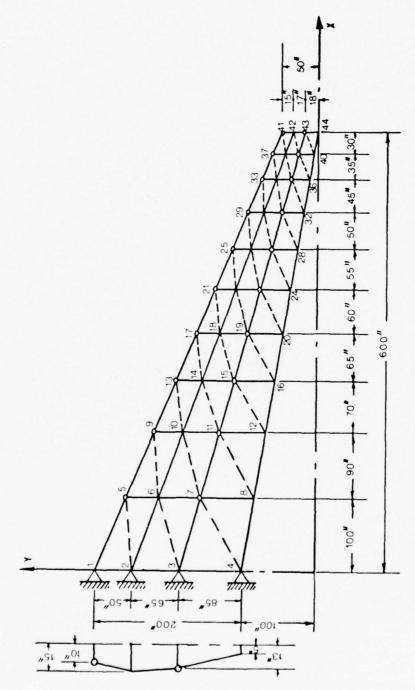


Fig. 11 (a) 150 (130) Element Swept Wing. Structural Box.

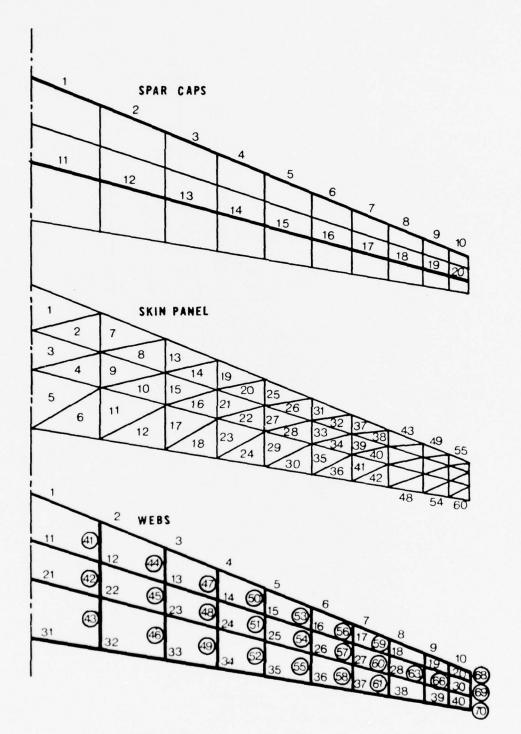


Fig.11 (b) 150 (130) Element Swept Wing. Element Numbering.

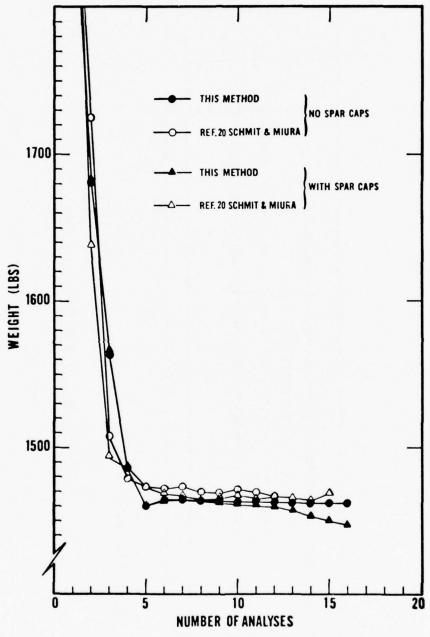


Fig. 12 Iteration Histories for Problems 7A & 7B 150 (130) Element Swep Wing.

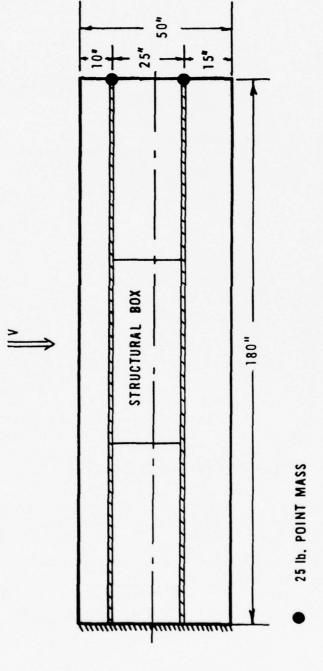


Fig. 13 Thirty Three Design Variable Rectangular Wing. Dimensions.

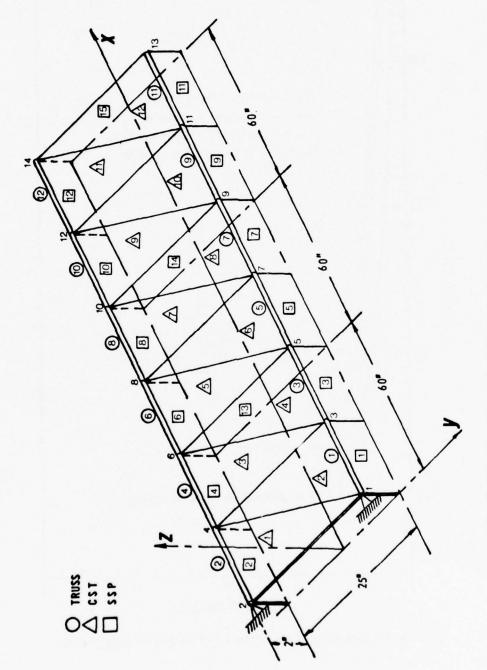


Fig.14 Thirty Three Design Variable Rectangular Wing. Structural Box.

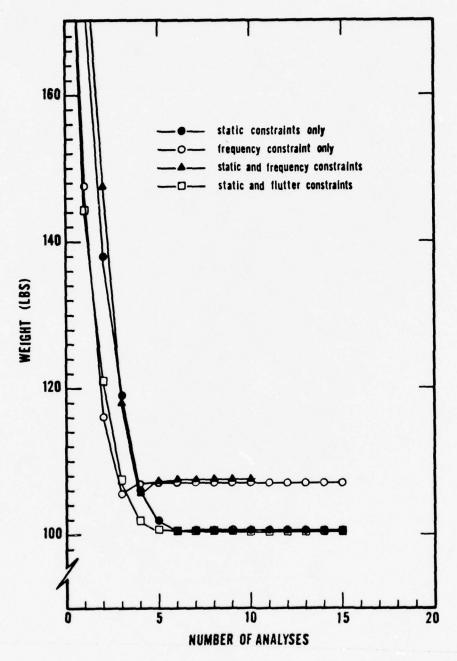


Fig. 15 Iteration Histories for Problems 8 (A.B.C&E) Rectangular Wing.

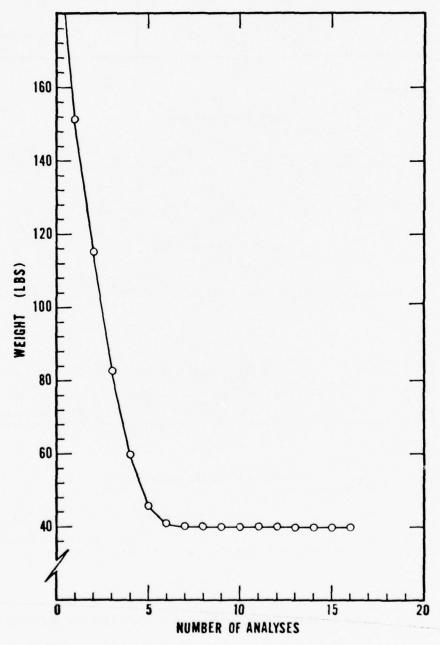


Fig.16 Iteration History for Problem 8D Rectangular Wing with Flutter Constraint.

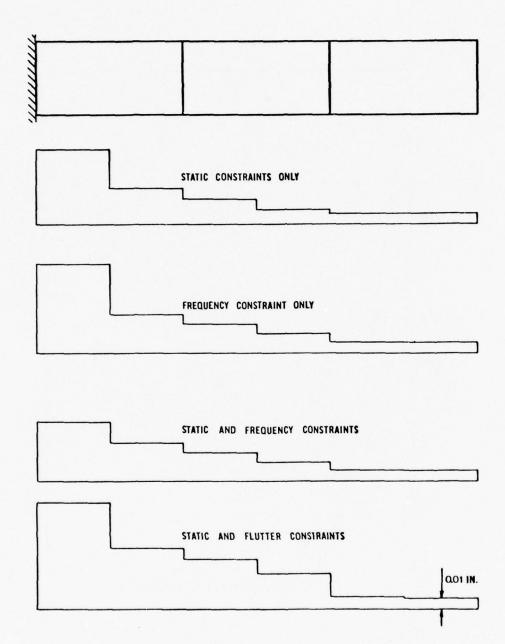


Fig. 17 (a) 33-Design Variable Rectangular Wing. Final Skin Thickness Distribution.

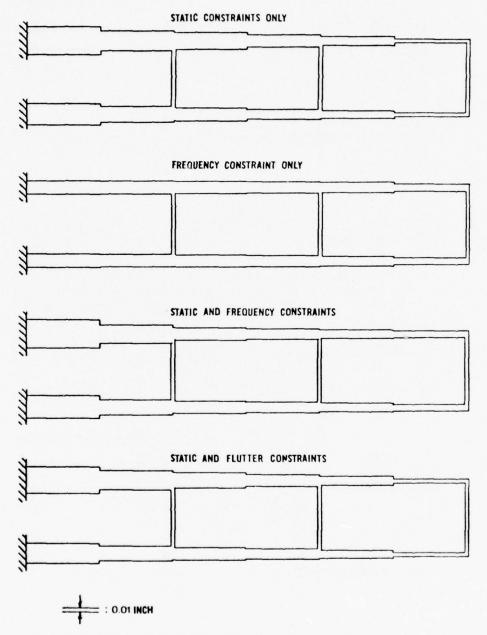


Fig. 17 (b) 33-Design Variable Rectangular Wing. Final Web Thickness Distribution .

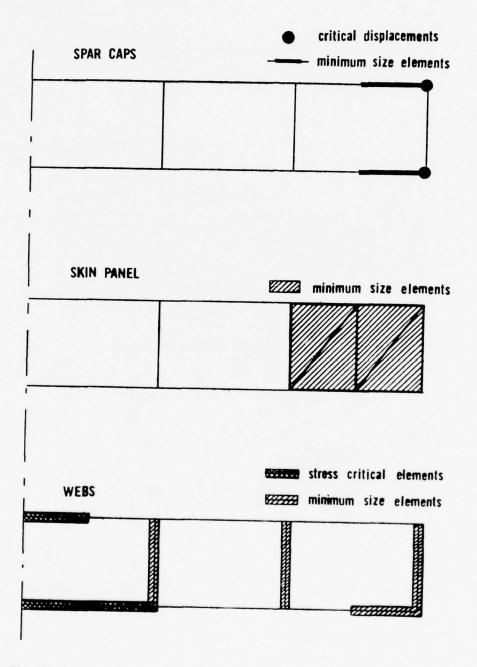


Fig. 18 Rectangular Wing. Problem 8A. Critical Constraints.

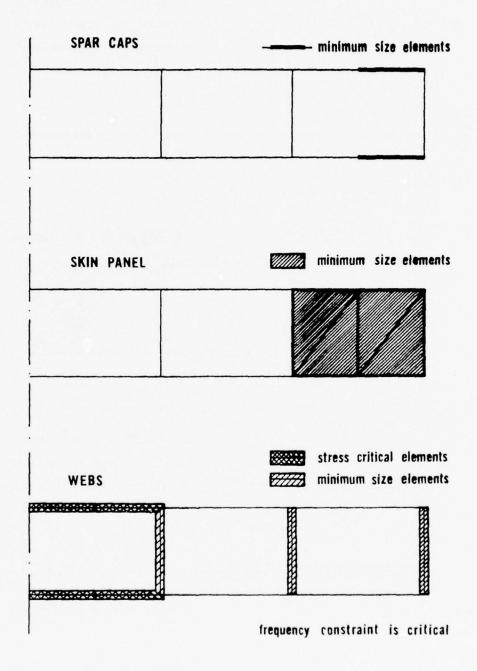


Fig. 19 Rectangular Wing. Problem 8C. Critical Constraints.

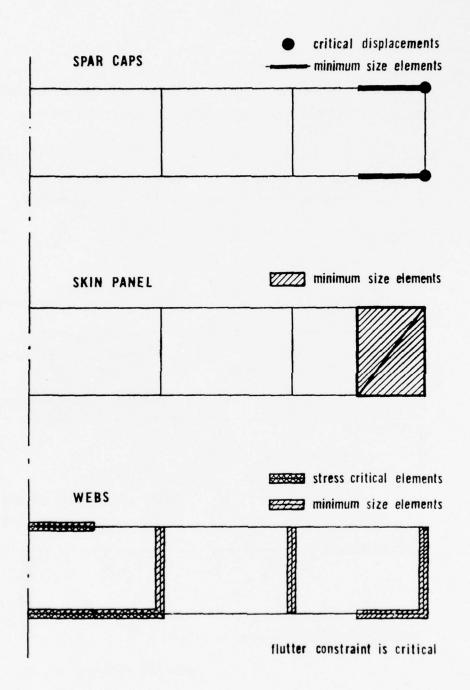


Fig. 20 Rectangular Wing. Problem 8E. Critical Constraints.

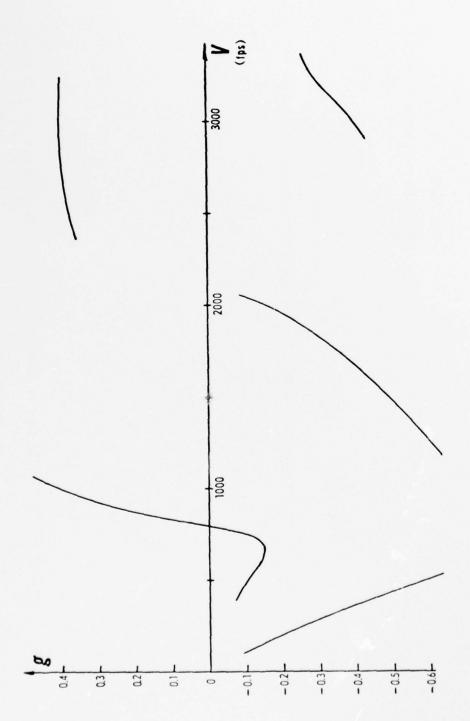


Fig. 21 V-g Diagram for Final Design of the Rectangular Wing under a Flutter Constraint only. Problem 8D.

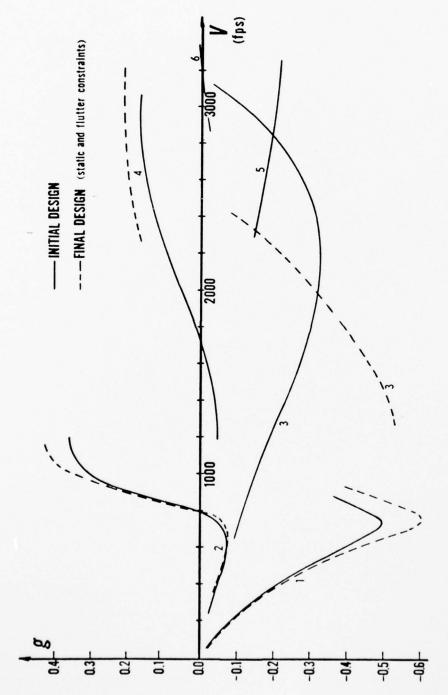
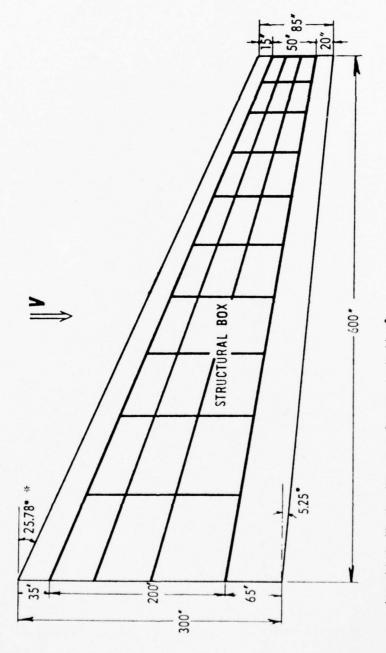


Fig.22 V-g Diagram for Initial and Final Designs of the Rectangular Wing under Static and Flutter Constraints. Problem 8E.



4. Inconsistent with other dimensions. Correct value is 24.23°.

Fig. 23 Swept Wing. Dimensions of the Aerodynamic Planform.

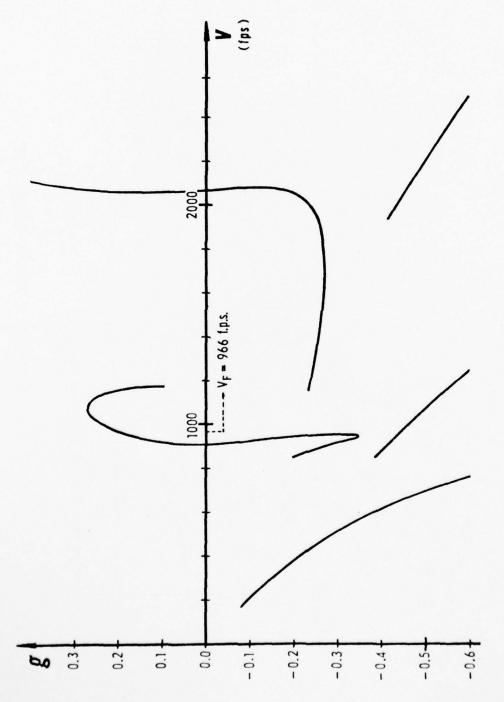


Fig. 24 V-g Diagram for the Final Static Design of the Swept Wing (Problem 7B) with a 400 lbs Mass Distributed evenly among the Eight Nodes of the Tip (Upper Wing Half only).

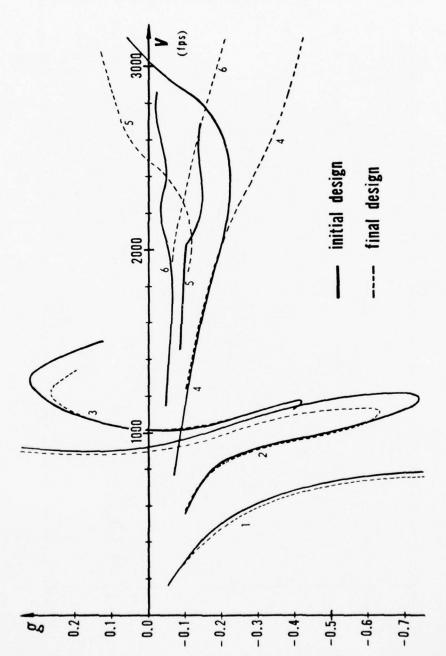


Fig. 25 V-g Diagrams of Initia and Final Designs of the Swept Wing with a 5000 lbs. Mass evenly Problem 9. Distributed on the Structural Boxes' Trailing Edge (Upper Wing-Half only).

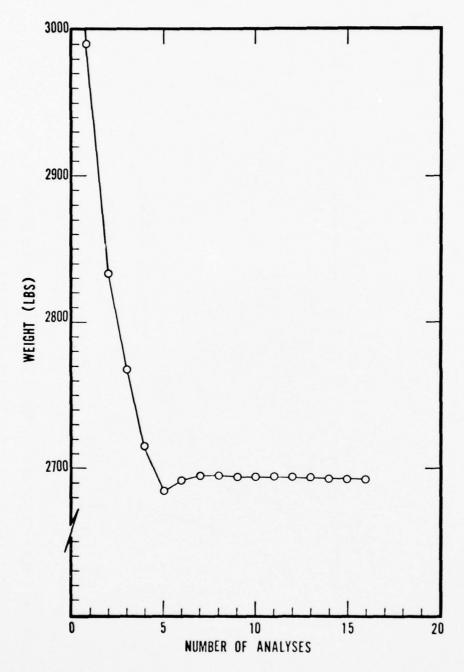


Fig. 26 Iteration History for Problem 9 Swept Wing with Static & Flutter Constraints

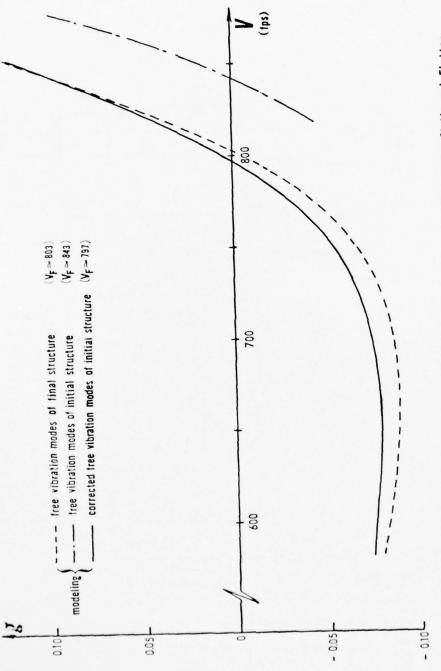
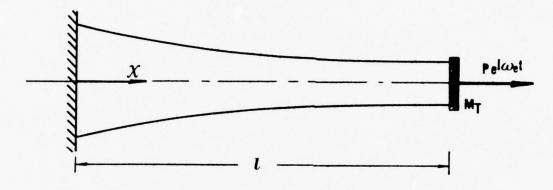
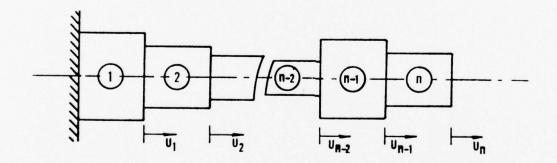


Fig. 27 Critical V-g Curves Obtained for the Final Design of the Rectangular Wing under Static and Flutter Constraints. Comparison of three Distinct Dynamic Models.

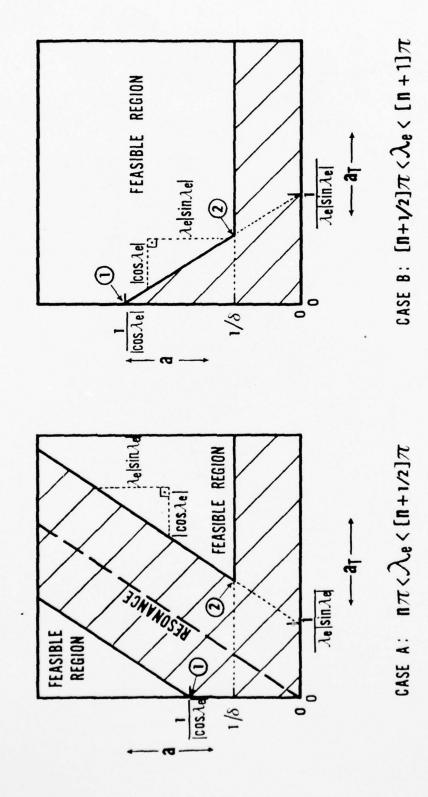


(a) CONTINUOUS AREA DISTRIBUTION

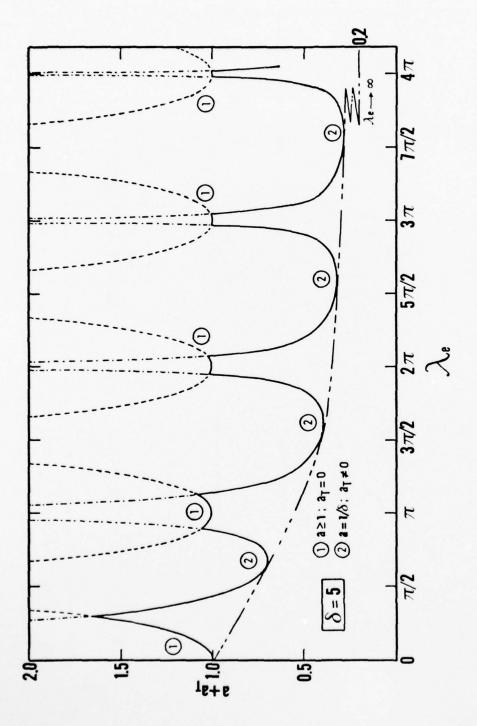


(b) FINITE ELEMENT REPRESENTATION

Fig. 28 Two idealizations of a cantilever, elastic bar of length $\,l$, excited in axial vibration by a sinusoidal varying force at the free end. A concentrated mass ${\rm M}_{\rm T}$ may be attached at the tip. For finite-element modeling, the bar is divided into n uniform segments of equal length.



Illustrating the feasible design spaces (unshaded) for a simple, two-design-variable bar forced from its tip at the dimensionless frequency $\lambda_{\rm e}$; a and ${\rm a_T}$ are, respectively, the constant cross-sectional area and a parameter to represent the tip mass. Fig. 29



Total dimensionless volume for the uniform cross-sectional area bar, as a function of the dimensionless excitation frequency $^{\lambda}_{\rm e}$. Fig. 30

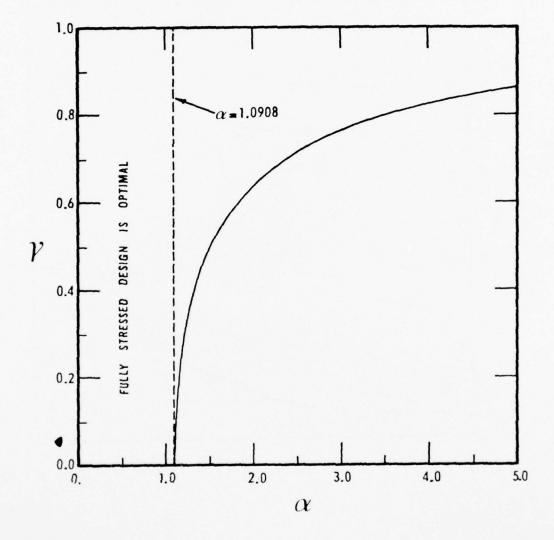


Fig. 31 Matching point $s=\gamma$ between the unconstrained and stressed arcs, plotted vs. frequency parameter α for first-mode designs.

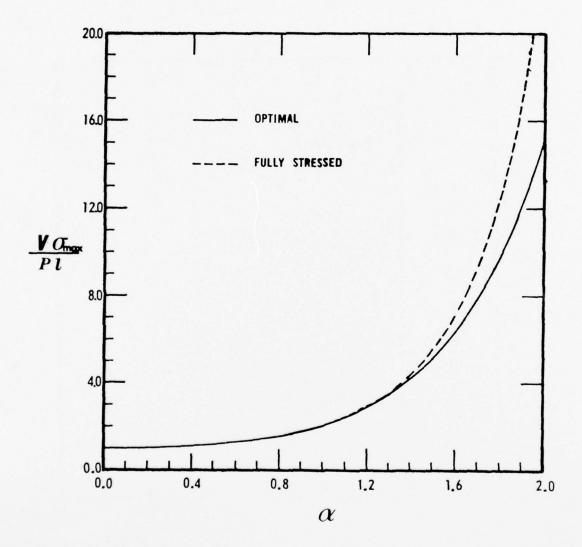


Fig. 32 Dimensional total weight (or volume) of the first-mode optimal design as a function of α . Above α = 1.0908, the fully-stressed design is shown for comparison.

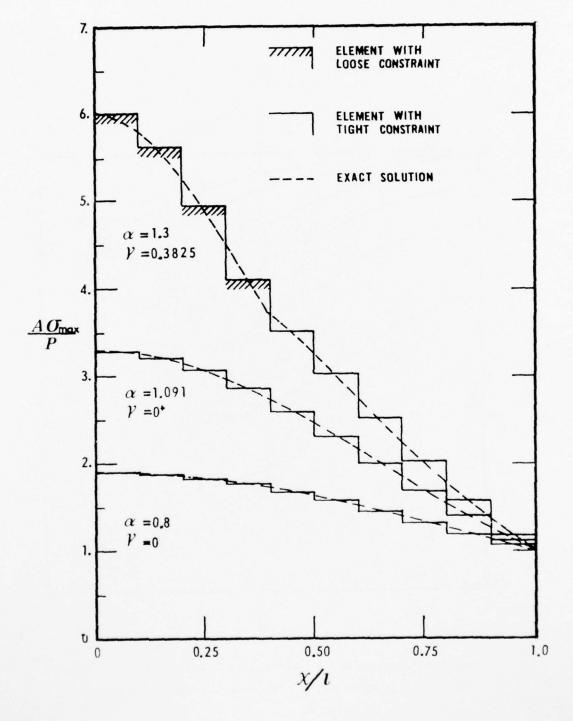


Fig. 33 Dimensionless cross-sectional area distributions of the first-mode optimal designs, plotted as a function of the distance along the bar for three values of the frequency parameter α . The corresponding finite-element solutions are also shown.

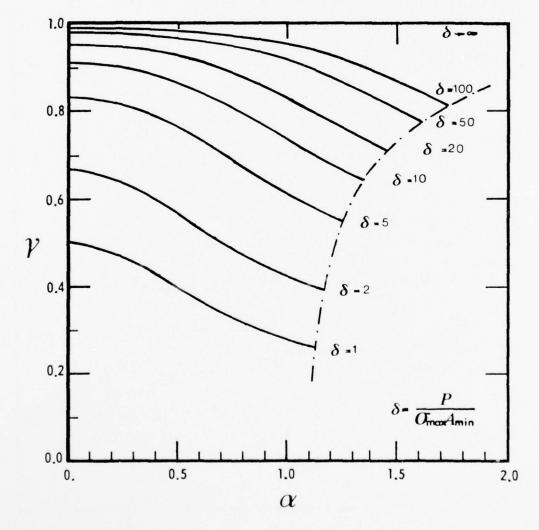
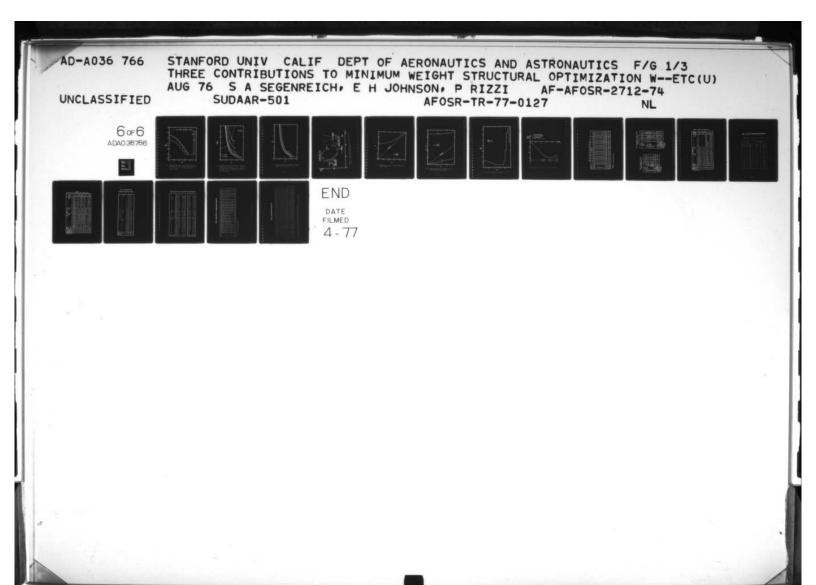


Fig. 34 Matching point $s=\gamma$ between the stressed and minimum-area arcs, plotted vs. α for second-mode designs at eight values of parameter δ .



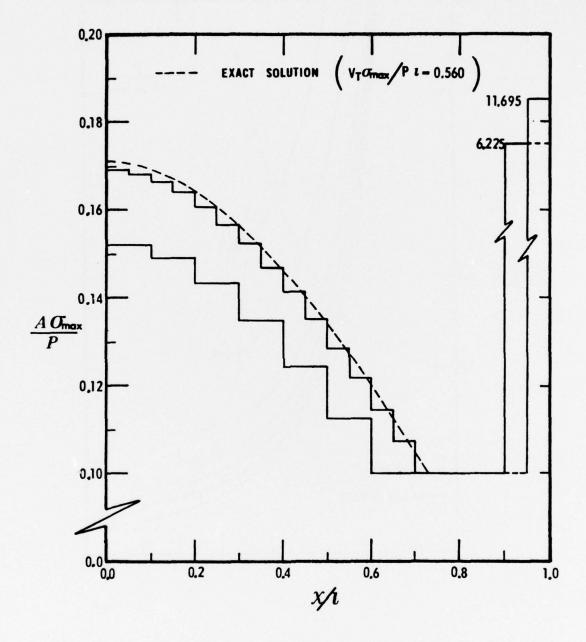


Fig. 35 Dimensionless cross-sectional area distributions of the second-mode optimal design, plotted vs. distance along the bar when α = 1.0 and δ = 10. Continuous and two finite-element solutions.

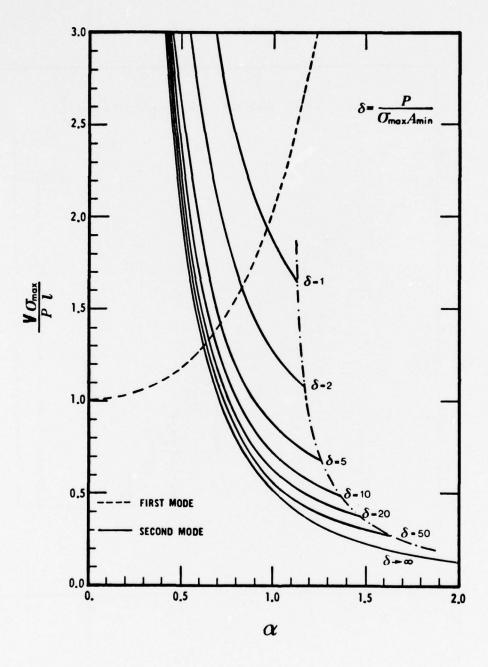


Fig. 36 Dimensionless total weight (or volume) of the second-mode optimal designs as a function of α and δ . The first-mode curve from Fig. 32 is shown dotted. To the right of the dash-sot line, the two-arc solutions of Section 4.5 are no longer optimal.

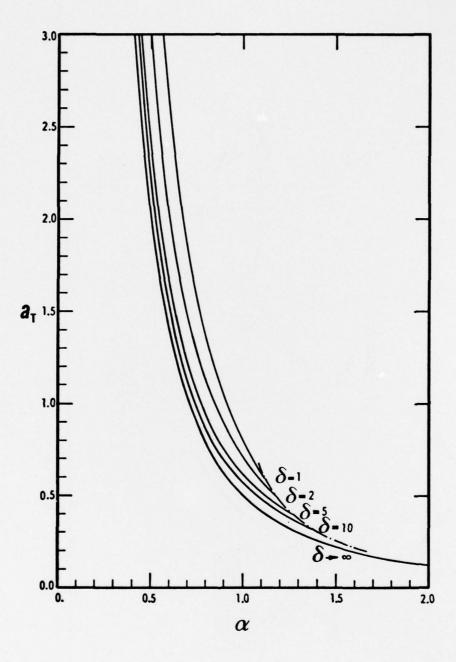


Fig. 37 Dimensionless tip-weight (or volume) of the second-mode optimal designs plotted as a function of α and $\delta.$

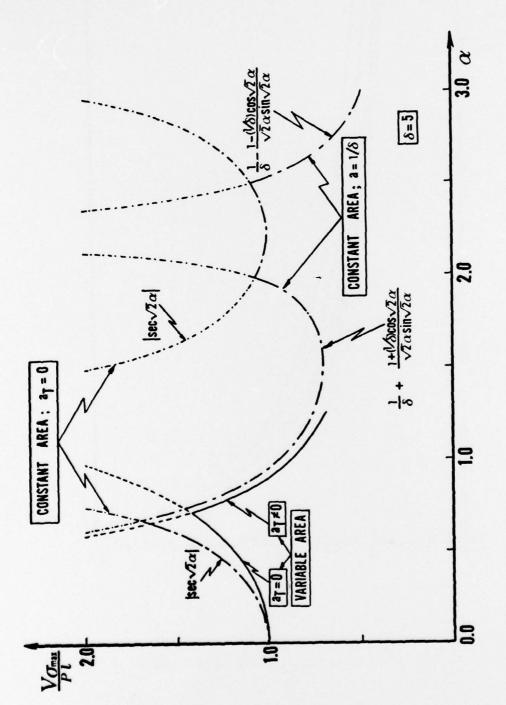


Fig. 38 Comparison of optimal dimensionless weights (or volumes), obtained with variable and constant cross-sectional area, for

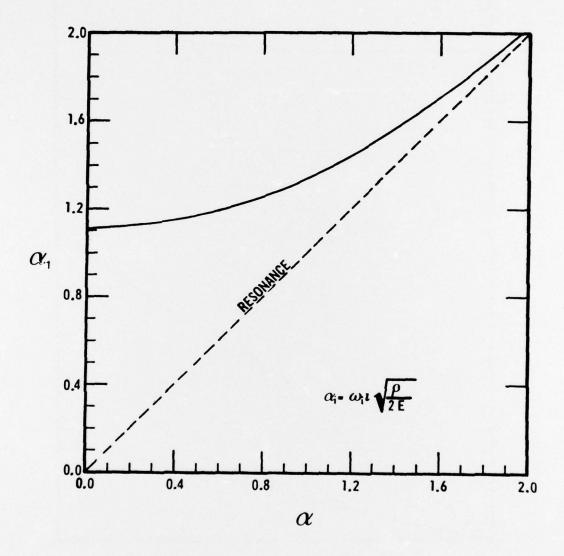


Fig. 39 Fundamental natural frequency of the first-mode optimal designs, plotted vs. α .

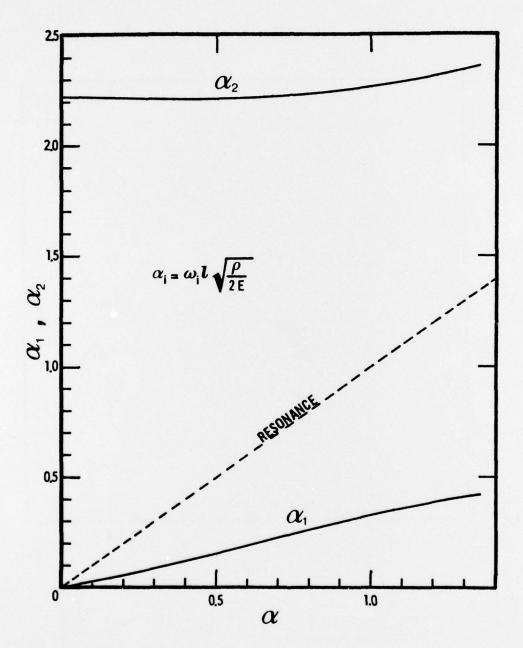


Fig. 40 First two dimensionless natural frequencies of the second-mode optimal designs, plotted vs. α .

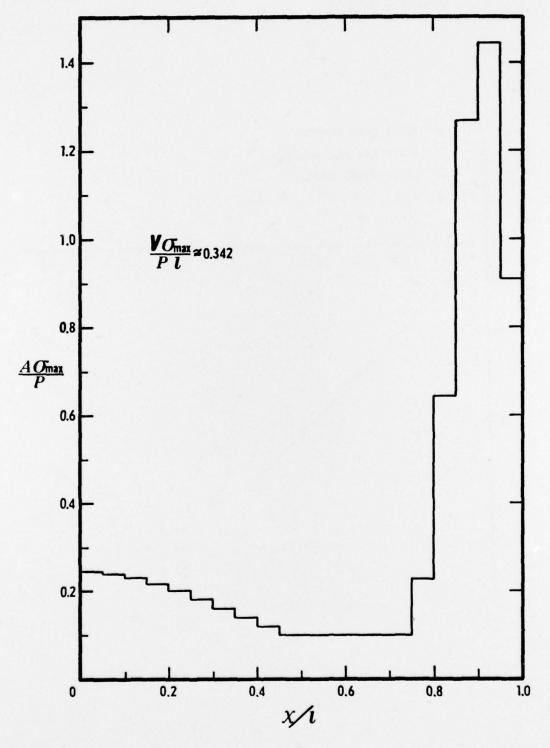


Fig. 41 Finite-element optimal solution for n=20, $\alpha=2.0$, and $\delta=10$.

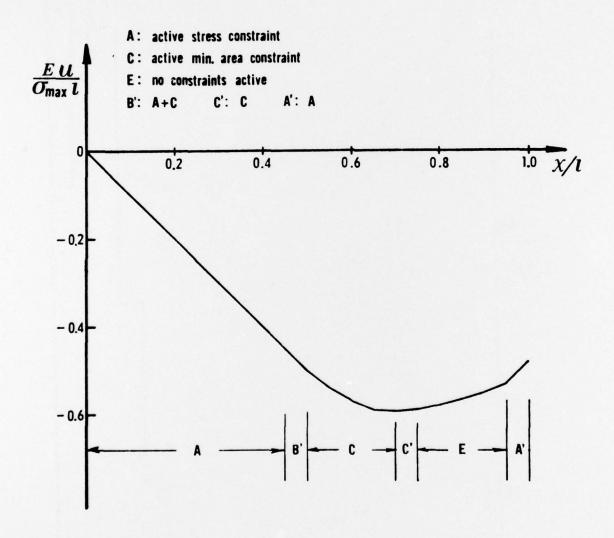


Fig. 42 Mode shape of forced response for the Fig. 41 design.

Table 1. Final designs for the ten bar planar truss.

PROBLEM	1,	A 25 ksi	1 B 05 = 30 ksl	B 0 ksi	1C and 1D 09 - 50 & 70 ksi	ld 1D 8.70 ksi	7		•			
METHOD	Present	Ref. 20	Present	Ref. 20	Present	Ref. 20	Present	Ref. 20	Present	Ref. 20	Present	Ref. 20
اح (کا	7,9379	7.938	7,9296	7.930	7.9000	7.900	5.9478	5.948	30.731	30.67	23.533	23.52
	0.1000	0010	0.1000	0.100	0.1000	0.100	0.1000	0.100	0.1000	0.100	0.1000	0.100
	8.0621	8.062	8.0704	8071	8.1000	8.100	10.052	10.05	23.934	23.76	25.291	25.28
A JI TH3	3.9379	3.930	3.9296	3,930	3,9000	3.900	3.9478	3.948	14.733	14.59	14.374	14.38
	0.1000	0.100	0.1000	0.100	0.1000	0.100	0.1000	0.100	0.1000	0.100	0.1000	0.100
-	0.1000	0.100	0.1000	001.0	0.1000	0.100	20522	2.052	0.1000	0.100	1,9697	1.97
NO 82	5.7447	5.745	5.7565	5.757	5.7983	5.798	8.5592	8.559	8.5416	8.578	12.389	12.39
	5.5690	5.569	5.5572	5.557	5.5154	5.516	2.7545	2.755	20.954	21.07	12.825	12.83
ער כ	5.5690	5.569	4.6310	4.631	3.6769	3.677	5.5830	5.583	20.836	20.96	20.328	20.32
FIN	0.1000	0.100	0.1000	0.100	0.1414	0.142	0.1000	0.100	0.1000	0.100	0.1000	Q. 100
WEIGHT (lbs)	1593.18	1593.23	1545.13	1545.17	1497.60	1497.65	1664.53	1664.55	99.9205	5076.85	4676.92	4676.93
ITERATIONS	15	15	15	15	15	15	12	10	II.	12	21	10
CPU TIME FOR REDESIGN (SeC)	2112	1,624	0.104	1.685	0,136	1,710 [†]	0.092	1375	0.076	1,345	0.081	1.320 [†]

CDC 7600. IBM 360/91. For comparison, time should be divided by 5.

c - 164 -

Table 2. Final Designs for Problem 5. Twenty Five Bar Space Truss.

Table 3. Final Designs for Problem 6. Eighteen Element Wing Box Beam.

Σ	METHOD	Present	Ref. 20
SEZ	Truss 1		0.010
IS 8	(in ²) 2, 3, 4, 3 6, 7, 8, 9	1.9884	1.985 2.996
38	10,11		0.010
EW	12,13	0.010	0.010
W	14,15,16,17		0.684
JA	18,19,20,21	1.6767	1.677
FIN	22,23,24,25		2.662
WE	WEIGHT (lbs)	545.163	545.172
11	TERATIONS	10	6
CPU	CPU TIME FOR REDESIGN (sec)	0.112 *	1.018

* CDC 7600. T IBM 360/91.

	METHOD	0	Present	Ref. 20
	Truss	-	4.0800	4.045
	(in ²)	7	0.10	0.1001
		e	0.10	0.1001
		-	0.10	0.1330
EZ		S	0.10	0.1002
ZIS	CST	1,2	0.082450	0.08286
8 8	(II)	3,4	0.054059	0.05363
138		5	0.037920	0.03786
IM	SSP	_	0.36275	0.3636
3W	(II)	7	0.22277	
1		~	0.13123	
AN		-	0.11496	0.1156
13		S	0.091432	
		9	0.020	
		_	0.020	0.020
		•	0.031028	
WE	WEIGHT	(lbs)	402.744	402.97
11	ITERATIONS	NS	15	8
CPU	CPU TIME	FOR	0.205	1.802
		(200)		

* C D C 7600. † I B M 360/91.

Table 4. Final Designs for the Swept Wing.

P	ROBLEN	4	7A (no	spar caps)	71	В
N	AETHOD		present	Ref. 20	present	Ref. 20
	Truss	1			0.01	0.01202
	(in2)				0.01	0.01349
	(111-)	3			0.01	0.05149
		4			0.01	0.05147
		5,6			0.01	0,03432
		7,8			0.01	0.04857
		9,10			0.01	0.01004
	111111	11			1.50	1.50
		12			0.030895	0.02430
		13			0.024106	0.02055
		14			0.039797	0.03035
		15,16			0.097282	0.04684
		17,18			0.019079	0.01781
0		19.20			0.01	0.01004
MEMBER SIZE	CST	1~6	0.20342	0.2034	0.19139	0.1925
S	(in)	5~12	0.17731	0, 1775	0.17471	0.1747
2		13~18	0.15627	0.1563	0.15594	0.1555
8		19~24	0.12925	0.1292	0.12893	0.1277
W		25 ~36	Q 11098	0.1093	0.11032	0.1095
12		37~48	0.095414	0. 09171	0.096129	0.09710
FINAL	000	49~60	0.02	0. 02001	0.02	0.02001
=	SSP	1~ 4	0.032226	0.03070	0.032391	0.03093
	(in)	5~10	0.02 0.034553	0,02 0,04122	0.02	0.02003
		11~14	0.034553	0.04122	0.032342	0.03740
		15 ~ 20 21 ~ 24	0.043633	0.03398	0.043971	0.2222
		25~30	0.095297	0.2136	0.094101	0.08392
		31 - 34	0.089007	0.08902	0.085855	0.08631
		35~40	0.059588	0. 05470	0.059535	0.06598
		41~49	0.037300	0.03343	0.036159	0.03502
		50~58	0.060363	0.06894	0,058881	0.05737
		59 ~ 70	0.10136	0.1330	0.094286	0.07651
WE	IGHT	(lbs)	2461.76	2466.40	2445.76	2463.96
1	TERATI	ONS	16	12	16	15
	TIME ESIGN (FOR (sec)	0.443	4.007	0.694	14.91

^{+, †} see notes for table 1.

Table 5. Load Data for 33-Design Variable Rectangular Wing.

For all nodes, $P_x = 0.0$ and $P_y = 0.0$

Load Coi	ndition l	Load Co	ndition 2
Node No.	P _z (1bs)	Node No.	P _Z (1bs)
3	165.8	3	299.6
4	414.4	4	374.5
5	142.6	5	257.6
6	356.4	6	322.1
7	131.1	7	236.7
8	327.4	8	295.8
9	117.7	9	212.7
10	294.3	10	265.9
11	97.8	11	176.8
12	244.5	12	220.9
13	38.1	13	68.9
14	95.3	14	86.1

Table 6. Final designs for the 33-design variable rectangular wing.

			8A	8 B	8 C	8 D	8 E
	PROBLE	M			static &		static &
	RUDLL	. m	static constraints	frequency	frequency constraints	flutter	flutter
	_						constraints
	Truss	1	1.8073	1.9971	2.0899	0.10	1.4764
	(in ²)	2	2.3289	1.8702	2.0088	0.10	1.9448
		3	1. 4638	1.7599	1.7372	0.10	1.1797
		4	1.9431	1.7725	1.7573	0.10	1.6599
		5	0.97611	1.3218	1,3081	0.10	0.68860
		6	1.2840	1.3314	1.3207	0.10	0.99601
		7	0.57565	0.88362	0.87591	0.10	0.33840
		8	0.73806	0.88714	0.88123	0.10	0.50367
		9	0.21471	0.46358	0.46026	0.10	0.19481
		10	0.28167	0.46567	0.46333	0.10	0.26517
		11	0.10000	0.10	0.10	0.10	0.10
		12	0.10000	0.10	0.10	0,10	0.10
8	CST	1, 2	0.069509	0.064166	0.054284	0.036997	0.097172
SIZES	(in)	3,4	0.033864	0.035428	0.035121	0.033701	0.056273
S		5,6	0.023125	0.026562	0.026320	0.042768	0.046007
œ		7,8	0.013808	0.017747	0.017609	0.043567	0.032592
18		9,10	0.010088	0.010095	0.010137	0.010	0.011505
MEMBER		11,12	0.010000	0.010	0.010	0.011260	0.010
	SSP	1	0.058995	0.035369	0.064314	0.071632	0.058782
AL	(in)	2	0.073949	0.035585	0.078993	0.12388	0.073896
FINAL		3	0.041397	0.035046	0.042309	0.010	0.041304
-		4	0.052963	0.035323	0.049823	0.010	0.053705
		5	0.034875	0.033731	0.033375	0.010	0.034341
		6	0.045258	0.033974	0.033632	0.10765	0.045681
		7	0.028300	0.031124	0.030850	0.060765	0.027885
		8	0.036780	0.031370	0.031120	0.010	0.037102
		9	0.021156	0.027447	0.027328	0.011735	0.020783
		10	0.026477	0.027507	0.027401	0.010	0.026781
		11	0.010000	0.019358	0.018972	0.020707	0.010
		12	0.011733	0.019698	0.019271	0.010	0.011854
		13	0.010000	0.010	0.010	0.010	0.010
		14	0.010000	0.010	0.010	0.031000	0.010
		15	0.010000	0.010	0.010	0.011397	0.010
WEIG	GHT (ibs)	100-542	107.004	107.426	39.934	100.322
IT	ERATIO	ONS	15	15	10	16	15
	TIME ESIGN	FOR * (sec)	0.268	0.118	0.172	0.129	0.270

CDC 7600 computer.

Table 7. Final Design for Problem 9.

Swept Wing under Static and Flutter Constraints.

	TRUSS	1	0.010
	(in ²)	2	0.010
		3	0.010
		4	0.010
		5,6	0.010
		7,8	0.010
		9,10	0.010
		11	0.46182
		12	0.010
		13	0.010
		14	0.010
S		15,16	0.010
3 E		17,18	0.010
н		19,20	0.010
S	CST	1∿ 6	0.19807
EI KI	(in)	5∿12	0.17508
e e		13∿18	0.15536
Σ N		19∿24	0.12626
E		25∿36	0.17367
1		37∿48	0.089077
<		49~60	0.058249
N	SSP	1~ 4	0.067142
124	(in)	5∿10	0.10460
		11~14	0.033917
		15∿20	0.042425
		21~24	0.20919
		25∿30	0.020
		31∿34	0.13091
		35∿40	0.13752
		41~49	0.033428
		50 ∿58	0.21457
		59∿70	0.19635
WEIGHT (1	.bs)		2692.10
ITERATIONS			16

Table 8. Designs Obtained after 15 and 50 Iterations, for Problems 8A and 8E.

			1				
				PROBL	EM 8A	PROBL	EM 8E
				15 ITER.	50 ITER.	15 ITER.	50 ITER.
	TRUSS	1		1.8073	0.46269	1.4764	1.0818
	(in ²)	2		2.3289	0.71095	1.9448	1.4761
		3		1.4638	1.1738	1.1797	1.1726
		4		1.9431	1.6642	1.6599	1.6680
		5		0.97611	0.68575	0.68860	0.68257
		6		1.2840	1.0112	0.99601	1.0070
		7		0.57565	0.33870	0.33840	0.33641
		8		0.73806	0.51474	0.50367	0.50981
		9		0.21471	0.18778	0.19481	0.19149
		10		0.28167	0.26312	0.26517	0.26444
		11		0.10	0.10	0.10	0.10
		12		0.10	0.10	0.10	0.10
ES	CST	1, 2		0.069509	0.18396	0.097172	0.13052
2	(in)	3, 4		0.033864	0.055648	0.056273	0.055969
SI		5, 6		0.023125	0.045092	0.046007	0.045651
pr.		7, 8		0.013808	0.031898	0.032592	0.032339
μ. μ.		9,10		0.010088	0.011756	0.011505	0.011624
E E		11,12		0.010	0.010	0.010	0.010
μ Σ	SSP	1		0.058995	0.058521	0.958782	0.058661
Σ	(in)	2		0.073949	0.073425	0.073896	0.073727
1		3		0.041397	0.041574	0.041304	0.041400
Y Z		4		0.052963	0.053036	0.053765	0.053056
н		5		0.034875	0.034267	0.034341	0.034500
Ex.		6		0.045258	0.045460	0.045681	0.045419
		7		0.028300	0.027800	0.027885	0.027987
		8		0.036780	0.036949	0.037102	0.036918
		9		0.021156	0.027440	0.020783	0.020935
		10		0.026477	0.026650	0.026781	0.026573
		11		0.010	0.010	0.010	0.010
		12		0.011733	0.011842	0.11854	0.011796
		13		0.010	0.010	0.010	0.010
		14		0.010	0.010	0.010	0.010
		15		0.010	0.010	0.010	0.010
FIN	AL WEIG	нт		100.542	99.614	100.322	100.048

Table 9. Iteration Histories for Examples Studied in Chapter ${\rm I\hspace{-.1em}I\hspace{-.1em}I}$.

PROBLEY	14	13	1C/1D	2	3	,	2	9	٧٧	7.8	8	88	80	8	38	6
-	4100.29	4100.29	4100.29	4111.87	4947.83	4993.21	674.443	848.872	2873.48	2871.14	164.538	147.721	177.769	151.455	144.248	2593.22
2	3237.58	3237.58	3237.58	3245.37	16.1778	5856.56	630.724	920.029	2681.32	2682.60	137.713	116.116	147.492	105.122	120.855	2833.04
6	2307.14	2307.14	2307.14	2306.88	6052.86	6052.11	585.163	508.070	2563.12	2566.88	118.908	105.608	117.949	82.593	107.392	2768.00
X :	1868.09	1868.09	1868.09	1916.77	5917.43	5707.82	559.350	429.680	2486.30	2487.40	105.967	106.891	105.600	59.729	109.957	2715.34
· ·	1662.83	1624.45	1526.04	1892.31	5735.47	5320.49	962.188	413.334	24.59.52	2460.44	101.756	107.130	107.130 107.206*	45.744	100.520	2684.66
H	1648.97	1648.97 1561.40	1509.23	1805.65	1805.65 5580.84 4995.30		548.124 413.470	413.470	2464.40 2463.10	2463.10	100.564	107.128	107.128 107.472	40.932	100.535	2690.86
N	1649.28	1594.03	1542.45	1721.05	5432.14 4712.04		546.089 413.896		2464.38	2646.84" 100.667" 107.229" 107.466	100.667	107.229	107.466	40.189	100.503	2695.34
00	1640.56	1587.02	1531.57	1684.83	\$261.89	4645.07	545.332	411.230	545.332 411.230 2463.70 2463.82 100.661 107.108 107.456*	2463.82	100.661	107.108	107.456	40.047	100.471	2655.30
0	1628.84	1574.18	1522.08	1670.96	\$114.68	4659.74	545.171	545.171* 407.374* 2463.18*	2463.18	2462.80 100.645 107.096 107.441*	100.645	107.096	107.441	39.970	:00.445	2695.05
01	1616.96	1564.37	1514.05	1666.36	16.5705	4672.82	545.163 404.010		2462.78 2461.70 100.631	2461.70	100.631	107.083	107.426	39.948	100.423	2694.84
= v	1607.66	1556.64	1507.51	1664.43	\$976.66	4676.68		402.878	2462.50*	2460.42*	100.615	107.069		39.939*	150.402	2695.40
8 8 12	1660.83	1550.92	1506.09	1664.53		4676.92		402.926	2462.23*	2458.78*	100.600	107.055		39.933*	100.382	2694.32
2	1596.07	1546.90	1498.85		_			402.798	2462.20*	2456.56 100.580	100.580	107.039*		39.931	190.362	2693.58
72	1593.38		1497.60					402.744	2461.96	2453.46 100.561	100.561	107.022		39.931	100.342	2693.50
15		1593.18 1545.13	1497.60					402.746	2461.86*	2449.10 100.542	100.542	107.004		39.933	100.322	2692, 50
16									2461.76	2445.76*				39.934		2652.13
TEASIBILITY	6.5*10-	4.5×10-6	1.5×10-5	4.5×10-7	2.0×10-6	4.0×10-5	8.0×10-7	4.5×10-6	3.5×10-5	2.0×10-5	3.0×10-6	4.0×10 ⁻ 5	6.0×10-5	6.0×10-5	2.04107	5 167-
INTENSIBILITY	6.5×10-	4.5×10-6	1.5×10-5		2.0×10-6		8.0×10	12		4.5×10-6	4.5×10 ⁻⁶ 3.5×10 ⁻⁵ 2.0×10 ⁻⁵	4.5×10 ⁻⁶ 3.5×10 ⁻⁵ 2.0×10 ⁻⁵	4.5×10 ⁻⁶ 3.5×10 ⁻⁵ 2.0×10 ⁻⁵ 3.0×10 ⁻⁶	4.5×10 ⁻⁶ 3.5×10 ⁻⁵ 2.0×10 ⁻⁵ 3.0×10 ⁻⁶ 4.0×10 ⁻⁵	4.5×10 ⁻⁵ 3.5×10 ⁻⁵ 2.0×10 ⁻⁵ 3.0×10 ⁻⁶ 4.0×10 ⁻⁵ 6.0×10 ⁻⁵	4.5×10 ⁻⁶ 3.5×10 ⁻⁵ 2.0×10 ⁻⁵ 3.0×10 ⁻⁶ 4.0×10 ⁻⁷ 6.0×10 ⁻⁷ 6.0×10 ⁻⁷

Usable designs (amount of infeasibility is less than 0.2%).

Final designs are feasible within amount indicated.

Table 10. Summary of Results of Chapter III.

833 X 2 7 3 3 3 3 3 3 3 3 3 3 3 3 3 3 3 3 3 3	Y1 .	831	10/10	2	3	7	5	9	7.4	7.8	8.4	88	BC.	8.0	L. S.	0
\$1:5×212 ± 0 ± 5× ×	10	10	10	10	10	10	25	18	130	150	39	39	39	39	39	150
STATES OF PERSONS OF FREEDOM	80	80	80	80	00	œ	18	15	120	120	36	36	36	36	3.6	120
A THES OF DESIGN CARIABLES	10	10	10	10	10	10	œ	16	18	32	33	33	33	33	33	32
THE K P. LOWERS, GANDLIESS			-	1	-	-	2	2	2	2	2	0	2	0	2	. 2
STATE CONSTANTS	10	10	10	10	10	10	25	16	18	97	33	33	33	33	33	9.7
N. YEEFS OF BENATIONAL CONSTRAINTS	20	20	20	20	28	28	124	99	268	348	110	4	1111	-	111	57.5
ANDRESS NO. OF ACTIVE CONSTRUINS	5	5	9	5	2	3	9	00	12	13	7	1	6	-	œ	17
(SZI) ZEDET (ZS)	4196.47	4196.47	4196.47	4196.47	4196.47	4196.47	661.441	936.098	3277.70	3282.60	192.720	192.720	192.720	192.720	192.720	3252.40
LET -7 DE 181 (* BLE DESIGN (LBS)	1628.85	1574.18	1522.08	1805.65	5580.84	4676.68	\$45.332 (8)	407.374	2464.38	2464.84	100.666	107.130	107,472 (5)	(6)	100.535	2645.30
BLIAN ALTHI (LAS)	1593.18	1545.13	1497.60	1664.53	5076.66	4676.92	545.163	402.744	2461.76	2445.76	100.542	107,004	107.426	36.938	100.322	2602.10
STATE OF FISH DESIGN	6.5-10-7	4.5×10-5	1.5×10-5	4.5×10-7	2.0-10-6	4.0×10-6	8.0×10-7	4.5×10-6	3.5×10-5	2.0×10-5	3.0×10-6	4.0110-5	5.0×10-5	6.0.10-5	2.0.10-f	1.5.10
	16	16	16	13	12	13		16	17	17	16	16	11	1.7	91	1.1
1325 13 15 15 15 15 15 15 15 15 15 15 15 15 15	0.050	0.050	0.050	0.051	0.053	0.056	0.091	0.092	0.504	0.551	0.123	0.154	0.205	0.350	0.418	1.877
THE THE ANALYSIS BLOCK (SEC)	0.035	0.036	0.037	0.029	0.027	0.029	0.094	0.138	2.942	3.025	0.352	0.782	0.639	1.367	1.612	10.580
THE TH SENS, ATAL, BLOCK (SEC)	611.0	0.118	0.127	0.099	0.066	0.077	0.197	0.538	9.305	15.938	2,299	0.325	1.690	0.379	2.535	17.073
TIME IN OPTIMIZATION BLOCK (SEC)	0.112	0.104	0.136	0.092	0.076	0.081	0.112	0.205	0.443	0.694	0.268	0.118	0.172	0.129	0.270	0.745
TOTAL TITE FTR DESIGN (SEC)	0.316	0.308	0.349	0.271	0.222	0.241	0.494	0.973	13.194	20.208	3.142	1.379	2.706	2.231	4.835	30.375

Lisplacement degrees-of-freedom. For problems with dynamic constraints there are also six modal degrees-of-freedom.

This is the average number of behavioral constraints that are left after the constraint reduction. It gives a measure of the size of the Gauss-Seidel problem.